

| | | | |
|--|--|--|--|
| 1. Report No. CFHR 3-5-69-121-5 | 2. Government Accession No. | 3. Recipient's Catalog No. | |
| 4. Title and Subtitle CONSTRUCTION AND LOAD TESTS OF A SEGMENTAL PRECAST BOX GIRDER BRIDGE MODEL | | 5. Report Date February 1975 | 6. Performing Organization Code |
| 7. Author(s) S. Kashima and J. E. Breen | | 8. Performing Organization Report No. Research Report 121-5 | |
| 9. Performing Organization Name and Address Center for Highway Research The University of Texas at Austin Austin, Texas 78712 | | 10. Work Unit No. | 11. Contract or Grant No. Research Study 3-5-69-121 |
| 12. Sponsoring Agency Name and Address Texas State Department of Highways and Public Transportation Transportation Planning Division P. O. Box 5051 Austin, Texas 78763 | | 13. Type of Report and Period Covered Interim | |
| 15. Supplementary Notes Study conducted in cooperation with the U.S. Department of Transportation, Federal Highway Administration. Research Study Title: "Design Procedures for Long Span Prestressed Concrete Bridges of Segmental Construction" | | 14. Sponsoring Agency Code | |
| 16. Abstract <p>The cantilever construction of the first segmental precast prestressed concrete box girder bridge in the United States has been recently completed on the John F. Kennedy Memorial Causeway, Corpus Christi, Texas. The segments were precast, transported to the site, and erected by the balanced cantilever method of post-tensioned construction, using epoxy resin as a jointing material.</p> <p>In order to check the applicability and accuracy of the design criteria, analytical methods, construction techniques, and the shear performance of the epoxy joints, an accurate one-sixth scale model of the three-span continuous bridge was built at the Civil Engineering Structures Research Laboratory of The University of Texas Balcones Research Center.</p> <p>This report documents the construction and load testing of the bridge. Experimental results are compared with analytical values for the various stages of construction, service loadings, ultimate proof loadings, and final failure tests. During the cantilever construction and under service level loadings after completion, experimental results generally agreed with the computerized theoretical analyses. Because of the general absence of warping, a beam theory analysis reasonably predicted behavior of the bridge during the cantilever construction and under uniform service level loading. However, a folded plate theory analysis was required to predict distribution for nonuniform loadings and transverse moment distribution for wheel loadings. Ultimate load theories correctly indicated the load capacity of the structure when all loading and structural configurations were considered.</p> | | | |
| 17. Key Words segmental, precast, box girder, bridge model, construction, load tests, cantilever | | 18. Distribution Statement No restrictions. This document is available to the public through the National Technical Information Service, Springfield, Virginia 22161. | |
| 19. Security Classif. (of this report) Unclassified | 20. Security Classif. (of this page) Unclassified | 21. No. of Pages 284 | 22. Price |

CONSTRUCTION AND LOAD TESTS OF A SEGMENTAL PRECAST
BOX GIRDER BRIDGE MODEL

by

S. Kashima

and

J. E. Breen

Research Report No. 121-5

Research Project No. 3-5-69-121

"Design Procedures for Long Span Prestressed Concrete
Bridges of Segmental Construction"

Conducted for

The Texas Highway Department
In Cooperation with the
U. S. Department of Transportation
Federal Highway Administration

by

CENTER FOR HIGHWAY RESEARCH
THE UNIVERSITY OF TEXAS AT AUSTIN

February 1975

The contents of this report reflect the views of the authors, who are responsible for the facts and the accuracy of the data presented herein. The contents do not necessarily reflect the official views or policies of the Federal Highway Administration. This report does not constitute a standard, specification, or regulation.

P R E F A C E

This report is the fifth in a series which summarizes the detailed investigation of the various problems associated with design and construction of long span prestressed concrete bridges of precast segmental construction. An initial report in this series summarized the general state of the art for design and construction of this type bridge as of 1969. The second report outlined requirements for and reported test results of epoxy resin materials for joining large precast segments. The third report summarized design criteria and procedures for bridges of this type and included two design examples. One of these examples was the three-span segmental bridge constructed in Corpus Christi, Texas, during 1972-73. The fourth report summarized the development of an incremental analysis procedure and computer program to analyze segmentally erected box girder bridges. This report summarizes structural performance data obtained from a realistic one-sixth scale model of the structure and compares these data with analytic results from several computer analyses.

This work is a part of Research Project 3-5-69-121, entitled "Design Procedures for Long Span Prestressed Concrete Bridges of Segmental Construction." The studies described were conducted as a part of the overall research program at The University of Texas at Austin, Center for Highway Research. The work was sponsored jointly by the Texas Highway Department and the Federal Highway Administration under an agreement with The University of Texas at Austin and the Texas Highway Department.

Liaison with the Texas Highway Department was maintained through the contact representative, Mr. Robert L. Reed, and the State Bridge Engineer, Mr. Wayne Henneberger; Mr. D. E. Hartley and Mr. Robert E. Stanford were the contact representatives for the Federal Highway Administration. Special thanks are due to Messrs. Thomas Gallaway,

Lawrence G. Griffis, and John T. Wall, all assistant research engineers at the Civil Engineering Structures Research Laboratory at The University of Texas at Austin's Balcones Research Center. These gentlemen played key roles in the development of model techniques, fabrication procedures, erection methods, and instrumentation systems, and were responsible for various stages of construction operations. The Laboratory staff all contributed significantly to this project with their untiring willingness to work long hours and make an extra effort throughout this project.

The overall study was directed by Dr. John E. Breen, Professor of Civil Engineering. Dr. Ned H. Burns, Professor of Civil Engineering, acted as an advisor on many questions concerning prestressing systems. The erecting and testing was under the immediate supervision of Dr. Satoshi Kashima, research engineer, Center for Highway Research.

S U M M A R Y

The cantilever construction of the first segmental precast prestressed concrete box girder bridge in the United States has been recently completed on the John F. Kennedy Memorial Causeway, Corpus Christi, Texas. The segments were precast, transported to the site, and erected by the balanced cantilever method of post-tensioned construction, using epoxy resin as a jointing material.

In order to check the applicability and accuracy of the design criteria, analytical methods, construction techniques, and the shear performance of the epoxy joints, an accurate one-sixth scale model of the three-span continuous bridge was built previously at the Civil Engineering Structures Research Laboratory of The University of Texas Balcones Research Center.

This report documents the construction and load testing of the bridge. Experimental results are compared with analytical values for the various stages of construction, service loadings, ultimate proof loadings, and final failure tests. During the cantilever construction and under service level loadings after completion, experimental results generally agreed with the computerized theoretical analyses. Because of the general absence of warping, a beam theory analysis reasonably predicted behavior of the bridge during the cantilever construction and under uniform service level loading. However, a folded plate theory analysis was required to predict distribution for nonuniform loadings and transverse moment distribution for wheel loadings. Ultimate load theories correctly indicated the load capacity of the structure when all loading and structural configurations were considered.

The model bridge carried the ultimate proof loads [1.35 dead load + 2.25(live load + impact load)] specified by the 1969 Bureau of Public Roads' criteria for all critical conditions. During tests to failure, the epoxy joints performed very well and there was no evidence of epoxy

separation at the joints. The theoretical calculation for the failure load agreed very well with the experimental results and indicated the necessity for change in the conventional procedure for computing ultimate design load for this type of bridge. Since the structural configuration changes from a simple cantilever to a multispan continuous structure during construction of the bridge, the ultimate design load for computation of shears and bending moments for the bridge should be specified as two values, each which must be satisfied as follows:

$$U = U_1$$

and

$$U = U_2 + U_3$$

$$U_1 = 1.35 DL_1 + 2.25(LL_1 + IL_1) \text{--to be computed for a balanced cantilever}$$

$$U_2 = 1.35 DL, \text{ for negative moments, and } 0.90 DL \text{ for positive moments, to be computed for a balanced cantilever}$$

$$U_3 = 1.35 DL_3 + 2.25(LL_3 + IL_3) + SL \text{--to be computed for the completed continuous structure}$$

where

DL_1 = dead load during cantilevering

DL_3 = dead load added after completion of closure (roadway surfacing, hand rails, etc.)

LL_1 = live load due to construction operations

LL_3 = design live load

IL_1 = impact load of construction operations

IL_3 = design impact load

SL = resultant reactions due to prestressing of tendons and seating forces at outer supports

I M P L E M E N T A T I O N

This report presents the details of a comprehensive model test program of a segmental prestressed concrete box girder bridge. This type of construction is becoming increasingly popular in the United States and this test represents a comprehensive check of the design procedures used for proportioning of such a structure and documents the performance of the structure at various stages of development during the cantilever erection procedure, as well as under test loads at the completion of the entire structure.

The test program validates the general design procedures and is particularly important in verifying the adequacy of the epoxy jointing procedures used in this type of construction. The model used was a one-sixth scale representation of the box girder bridge erected over the Intracoastal Waterway at Corpus Christi, Texas, and was valuable in acquainting design, construction, and contractor personnel with the type of problems which are encountered in this type of construction. In itself the model had a high educational benefit.

Results of the test program indicated that this type of construction is both safe and dependable. A very adequate factor of safety was demonstrated and minor difficulties encountered in the field were satisfactorily explained as a result of additional model tests. As a result of the tests several specific recommendations are made for development of more accurate design procedures and criteria. Implementation of these recommendations should result in economic cost savings in future projects of this type and a more realistic assessment of the strength of such bridges. A number of construction procedures high-lighted during the model tests were carried out in the prototype erection and additional changes are being made in future bridges of this type, based on the test program.

C O N T E N T S

| Chapter | | Page |
|---------|--|------|
| 1 | INTRODUCTION | 1 |
| | 1.1 General | 1 |
| | 1.2 Related Research | 4 |
| | 1.3 Objective and Scope of the Model Study | 5 |
| | 1.4 Report Contents | 6 |
| 2 | SCALE FACTORS FOR THE BRIDGE MODEL | |
| | 2.1 Factors Affecting Scale Selection | 9 |
| | 2.2 Dimensions of Prototype and Model Bridge | 9 |
| | 2.2.1 Longitudinal Dimensions | 9 |
| | 2.2.2 Transverse Dimensions | 9 |
| | 2.3 Choice of Materials | 9 |
| | 2.3.1 Concrete | 9 |
| | 2.3.2 Prestressing Steel | 11 |
| | 2.3.3 Reinforcing Bars | 11 |
| 3 | MATERIAL PROPERTIES | 15 |
| | 3.1 Concrete | 15 |
| | 3.1.1 Concrete Mix Design | 15 |
| | 3.1.2 Strength of Concrete | 15 |
| | 3.1.3 Modulus of Elasticity | 17 |
| | 3.1.4 Poisson's Ratio | 17 |
| | 3.2 Steel | 18 |
| | 3.2.1 Prestressing Strands and Wire | 18 |
| | 3.2.1.1 Ultimate Strength | 18 |
| | 3.2.1.2 Modulus of Elasticity | 18 |
| | 3.2.2 Reinforcing Wire | 18 |
| | 3.2.3 Strength of Bolts at Main Piers | 20 |
| | 3.3 Epoxy Resin as a Jointing Material | 20 |
| | 3.3.1 General | 20 |
| 4 | SEGMENT DETAILS | 23 |
| | 4.1 Reinforcing Cage for Precast Segments | 23 |
| | 4.1.1 Reinforcement | 23 |
| | 4.1.2 Anchorages | 23 |
| | 4.1.3 Tendon Duct | 29 |

| Chapter | Page | |
|---------|---|-----|
| 4.2 | Forms | 31 |
| 4.3 | Strain Instrumentation in Segment Reinforcing Cages | 36 |
| 4.4 | Casting Procedure | 37 |
| 4.5 | Curing of Segments | 40 |
| 4.6 | Surface Preparation of Segments | 41 |
| 4.7 | Compensation Dead Load for Model Bridge | 41 |
| 4.8 | Actual Properties of the Model Bridge | 43 |
| 5 | INSTRUMENTATION AND DATA REDUCTION | 45 |
| 5.1 | General | 45 |
| 5.2 | Load Cells and Pressure Gages | 45 |
| 5.3 | Strain Gage Instrumentation and Data Reduction | 45 |
| 5.4 | Surveyor's Level and Dial Gages | 46 |
| 6 | CONSTRUCTION OPERATIONS AND OBSERVATIONS | 49 |
| 6.1 | Construction Procedure | 49 |
| 6.1.1 | General | 49 |
| 6.1.2 | Construction of Piers | 50 |
| 6.1.3 | Erection of Pier Segments | 52 |
| 6.1.4 | Erection of Segments during Cantilever Stages | 52 |
| 6.1.4.1 | General | 52 |
| 6.1.4.2 | Details of Segment Erection | 53 |
| 6.1.5 | Correction of Horizontal and Vertical Alignment | 61 |
| 6.1.6 | Casting of the Closure Segment | 65 |
| 6.1.7 | Prestressing of the Positive Tendons | 67 |
| 6.1.8 | Grouting of Tendons | 69 |
| 6.1.9 | Casting of the Midstrip Closure between the Two Box Units | 73 |
| 6.2 | Behavior of the Bridge during Construction | 73 |
| 6.2.1 | Rotation Stiffness at the Main Pier | 73 |
| 6.2.2 | Prestressing Force | 78 |
| 6.2.3 | Deflections | 80 |
| 6.2.4 | Strains | 84 |
| 6.2.5 | Reaction at Outer Supports during Positive Tendon Operations | 95 |
| 7 | DESIGN SERVICE AND ULTIMATE LOAD TESTS | 99 |
| 7.1 | General | 99 |
| 7.2 | Test Procedures | 100 |
| 7.2.1 | Simulation of Loading | 100 |
| 7.2.1.1 | Truck Loading | 100 |
| 7.2.1.2 | Lane Loading | 100 |

| Chapter | Page |
|--|---------|
| 7.2.2 Loading System and Instrumentation | 103 |
| 7.2.2.1 Loading System | 103 |
| 7.2.2.2 Instrumentation and Observation | 103 |
| 7.3 Test Results and Interpretations | 108 |
| 7.3.1 General | 108 |
| 7.3.2 Service Loading | 109 |
| 7.3.2.1 Four Lane Loadings | 109 |
| 7.3.2.2 Two Lane Loadings | 117 |
| 7.3.3 Ultimate Design Loading Specified by BPR | 123 |
| 7.3.3.1 Additional 0.35 DL | 123 |
| 7.3.3.2 Maximum Positive Moment, Main Span | 123 |
| 7.3.3.3 Maximum Negative Moment at the Main Pier | 134 |
| 7.3.3.4 Maximum Shear Loading Adjacent to the Main Pier | 139 |
| 7.3.3.5 Maximum Positive Moment in the Side Span | 140 |
| 7.3.4 Study of Transverse Moment | 140 |
| 7.4 Summary | 148 |
| 8 FAILURE LOAD TESTS | 149 |
| 8.1 General | 149 |
| 8.2 Side Span Failure Load Test | 149 |
| 8.2.1 General | 149 |
| 8.2.2 Test Results | 151 |
| 8.2.3 Calculation of Side Span Live Load Capacity | 159 |
| 8.3 Failure in the Main Span | 180 |
| 8.3.1 General | 180 |
| 8.3.2 Test Results | 181 |
| 8.3.3 Determination of the Main Span Live Load Capacity | 192 |
| 8.3.3.1 Flexure | 192 |
| 8.3.3.2 Shear | 204 |
| 8.4 Punching Shear Tests | 206 |
| 9 SPECIAL MEASUREMENTS | 209 |
| 9.1 General | 209 |
| 9.2 Prototype Instrumentation | 209 |
| 9.3 Measurements during Construction | 211 |
| 9.3.1 Strains during Balanced Cantilever Construction | 211 |
| 9.3.2 Closure Operations | 213 |
| 9.4 Prototype Load Testing | 216 |
| 9.5 Ultimate Shear Test | 223 |

| Chapter | Page |
|--|------|
| 10 CONCLUSIONS AND RECOMMENDATIONS | 229 |
| 10.1 Conclusions | 229 |
| 10.1.1 Primary Conclusions | 229 |
| 10.1.2 Secondary Conclusions | 230 |
| 10.2 Recommendations | 232 |
| 10.2.1 Design Recommendations | 232 |
| 10.2.2 Construction Recommendations | 233 |
| REFERENCES | 235 |
| APPENDIX A PROTOTYPE BRIDGE PLANS | 239 |
| APPENDIX B SPECIFICATION FOR EPOXY BONDING AGENT | 251 |
| APPENDIX C NOTATION | 255 |

L I S T O F T A B L E S

| Table | | Page |
|-------|---|------|
| 2.1 | Choice of Strands and Wire for the Model Bridge | 12 |
| 2.1 | Choice of Reinforcing Bars for the Model Bridge | 12 |
| 3.1 | Concrete Mix Design | 15 |
| 3.2 | Compressive Strength of Concrete | 16 |
| 3.3 | Splitting Tensile Strength of Concrete | 16 |
| 3.4 | Modulus of Elasticity of Concrete | 17 |
| 3.5 | Ultimate Strength of Prestressing Strands and Wire . . . | 18 |
| 3.6 | Modulus of Elasticity of Wire and Strands | 19 |
| 3.7 | Test Results of Reinforcing Wire of Precast Segments . . | 19 |
| 3.8 | Tensile Strength of Bolts at Main Piers | 20 |
| 3.9 | Epoxy E Flexure Test Results | 21 |
| 3.10 | Epoxy E Shear Test Results | 21 |
| 4.1 | Dimensions of Anchorage Bearing Plates | 29 |
| 4.2 | Material Properties and Section Properties of the Model Bridge | 44 |
| 6.1 | Friction Loss Test Results | 79 |
| 6.2 | Elongation of Prestressing Cables in Several Stages . . | 80 |
| 6.3 | Details at Each Stage of Construction | 85 |
| 6.4 | Reaction at Outer Support during Prestressing in Main Span | 96 |
| 7.1 | Critical Loading Conditions in Longitudinal Direction . | 99 |
| 7.2 | Moment or Shear for Each Loading Case | 105 |

| Table | | Page |
|-------|---|------|
| 7.3 | Comparison of Experimental and Theoretical Transverse Strains | 146 |
| 8.1 | LF of (LL + IL) for the First Plastic Hinge at Each Joint | 198 |
| 8.2 | Punching Shear Test Results | 208 |

L I S T O F F I G U R E S

| Figure | | Page |
|--------|---|------|
| 1.1 | Typical balanced cantilever construction | 2 |
| 2.1 | Longitudinal dimensions of bridge | 10 |
| 2.2 | Cross section of bridge | 10 |
| 2.3 | Details of prestressing strands and wire | 13 |
| 2.4 | Details of reinforcing bars in segment | 14 |
| 3.1 | Testing of reinforcing wire | 19 |
| 4.1 | Individual mats for a cage | 24 |
| 4.2 | Cage for a segment | 24 |
| 4.3 | Details of reinforcing mats | 25 |
| 4.4 | Details of web reinforcement modification | 27 |
| 4.5 | Reinforcement for the main pier segment model | 28 |
| 4.6 | Details of anchorage and spiral reinforcement | 30 |
| 4.7 | Typical arrangement of tendon duct near anchorage | 31 |
| 4.8 | Tendon duct profiles in main span | 32 |
| 4.9 | Tendon duct profiles in side span | 33 |
| 4.10 | Details of tendon profiles | 34 |
| 4.11 | General view of soffit forms | 35 |
| 4.12 | Details of forms for segment | 35 |
| 4.13 | General view of assembled forms | 37 |
| 4.14 | Position of strain gages in segments | 38 |
| 4.15. | Sequence of casting segments | 39 |

| Figure | Page | |
|--------|---|----|
| 4.16 | Position of rams for separation of segment | 40 |
| 4.17 | Tools used for surface preparation | 42 |
| 4.18 | Compensating dead loads for the model bridge | 42 |
| 5.1 | Strain gage instrumentation | 46 |
| 5.2 | VIDAR system and teletype | 47 |
| 6.1 | Reinforcement of the main pier | 50 |
| 6.2 | Connection of pier to the testing floor | 51 |
| 6.3 | Detail of support at main pier | 51 |
| 6.4 | General view of the pier segment on the main pier . . . | 53 |
| 6.5 | Typical independent crane used for erection of segments | 54 |
| 6.6 | Mechanical device for temporary joining | 55 |
| 6.7 | Typical structure supported cranes used in some cases . | 55 |
| 6.8 | Insertion of prestressing cable | 57 |
| 6.9 | Adjustment of level | 58 |
| 6.10 | Application of the epoxy resin on the joining surface . | 58 |
| 6.11 | General view of prestressing system for negative tendons | 59 |
| 6.12 | Details of prestressing system | 60 |
| 6.13 | Errors of horizontal alignment | 61 |
| 6.14 | Adjustment of horizontal alignment | 63 |
| 6.15 | Accumulation of joining error | 64 |
| 6.16 | Correction of the vertical alignment | 65 |
| 6.17 | Connection of tendon duct at the closure | 66 |
| 6.18 | Simulation of the closure | 66 |
| 6.19 | Setup for prestressing of positive tendons | 68 |

| Figure | Page |
|--------|--|
| 6.20 | Order of grouting for each tendon group 70 |
| 6.21 | Examples of tendon arrangement 70 |
| 6.22 | Connection of injection pipes and inlets of tendons . . 72 |
| 6.23 | Deflection at unbalanced loading 74 |
| 6.24 | Individual factors affecting the deflection 76 |
| 6.25 | Suggested improvement for temporary support 78 |
| 6.26 | Deflection predicted by SIMPLA2 for cantilever erection 82 |
| 6.27 | Typical measured deflection during cantilever erection . 82 |
| 6.28 | Deflection relative to the center of 6th segment 83 |
| 6.29 | Deflection at the center in main span during positive tendon operations 83 |
| 6.30 | Strain in M1 and S1 segments during balanced cantilever construction 86 |
| 6.31 | Strains in M1 and S1 segments during erection of half segments 87 |
| 6.32 | Strains in M1 segments during closure operation 88 |
| 6.33 | Strains in the top slab of M1 segments during construction 89 |
| 6.34 | Strains in the bottom slab of M1 segments during construction 90 |
| 6.35 | Strains in the M6 and S6 segments at erection of the 6th segment 91 |
| 6.36 | Strains in the M9 segment during closure operations . . 92 |
| 6.37 | Strains in the top slab around the center of the main span 93 |
| 6.38 | Strains in the bottom slab around the center of the main span 93 |
| 6.39 | Calculation of end reaction due to positive tendons . . 96 |

| Figure | Page |
|--|------|
| 7.1 Dimensions of full size and 1/6 scale model AASHO HS20-S16 truck | 101 |
| 7.2 Scaled wheels and AASHO HS20-S16 truck | 102 |
| 7.3 Application of concentrated loads above the webs (in each lane) | 103 |
| 7.4 Lane loads and equivalent concentrated loads for four lanes with impact allowances | 104 |
| 7.5 Application of lane load | 106 |
| 7.6 Locations of dial gage readings | 107 |
| 7.7 Position of truck loading | 109 |
| 7.8 Deflections for truck loadings (four lanes) in side span | 110 |
| 7.9 Reactions at outer supports for truck loadings (four lanes) in side span | 111 |
| 7.10 Longitudinal strains along SS7 and SS6 for truck loadings (four lanes) in side span | 112 |
| 7.11 Deflections for lane loadings (four lanes) in main span | 113 |
| 7.12 Reactions at outer supports for lane loadings (four lanes) in main span | 113 |
| 7.13 Longitudinal strains along NM9 for lane loadings (four lanes) in main span | 114 |
| 7.14 Deflections for lane loadings (four lanes) in main and one side span | 115 |
| 7.15 Reactions at outer supports for lane loadings in main and one side span | 115 |
| 7.16 Longitudinal strains for lane loadings (four lanes) in main and one side span | 116 |
| 7.17 Deflections for lane loadings (two lanes) in main span . | 118 |
| 7.18 Longitudinal strains along NM9 for lane loadings (two lanes) in main span | 119 |
| 7.19 Reactions at outer supports for lane loadings (two lanes) in main span | 119 |

| Figure | | Page |
|--------|--|------|
| 7.20 | Deflections for lane loadings (two lanes) in main and one side span | 120 |
| 7.21 | Longitudinal strains for lane loadings (two lanes) in main and one side span | 121 |
| 7.22 | Reactions at outer supports for lane loadings (two lanes) in main and one side span | 122 |
| 7.23 | Concrete blocks for 0.35 DL | 124 |
| 7.24 | Deflections for 0.35 DL | 125 |
| 7.25 | Reactions at outer supports for 0.35 DL | 125 |
| 7.26 | Longitudinal strains along NM9, NM1 and NS1 for 0.35 DL | 126 |
| 7.27 | Deflections at SM10 for lane loadings (four lanes) in main span (design ultimate) | 127 |
| 7.28 | Deflections for lane loadings (four lanes) in main span (design ultimate) | 129 |
| 7.29 | Reactions at outer supports for lane loadings (four lanes) in main span (design ultimate) | 130 |
| 7.30 | Longitudinal strains along NM9 for lane loadings (four lanes) in main span (design ultimate) | 130 |
| 7.31 | Development of cracks for lane loadings (four lanes) in main span (design ultimate) | 131 |
| 7.32 | Relation between the end reaction and cracking moment . | 133 |
| 7.33 | Deflections at SM10 for lane loadings (four lanes) in the main and one side span (design ultimate) | 133 |
| 7.34 | Deflections for lane loadings (four lanes) in the main and one side span (design ultimate) | 135 |
| 7.35 | Longitudinal strains at NM9 for lane loadings (four lanes) in the main and one side span (design ultimate) . | 136 |
| 7.36 | Longitudinal strains at NM1 for lane loadings (four lanes) in the main and one side span (design ultimate) . | 136 |
| 7.37 | Reactions at outer supports for lane loadings (four lanes) in the main and one side span (design ultimate) . | 137 |

| Figure | Page |
|---|------|
| 7.38 Development of cracks for lane loadings (four lanes) in the main and one side span (design ultimate) | 138 |
| 7.39 Arrangement of slip gage at the first joint | 139 |
| 7.40 Position of truck loadings (design ultimate) | 141 |
| 7.41 Deflections at SS7 for truck loadings (four lanes) in side span (design ultimate) | 141 |
| 7.42 Deflections for truck loadings (four lanes) in side span (design ultimate) | 142 |
| 7.43 Longitudinal strains at SS7 for truck loadings (four lanes) in side span (design ultimate) | 143 |
| 7.44 Longitudinal strains at SS6 for truck loadings (four lanes) in side span (design ultimate) | 143 |
| 7.45 Reactions at outer supports for truck loadings (four lanes) in side span (design ultimate) | 144 |
| 7.46 Transverse strain at SS7 R for truck loadings (four lanes) in side span (design ultimate) | 144 |
| 7.47 Transverse slab moment (M_y) diagram for different loading cases by MUPDI | 145 |
| 7.48 Typical strain readings in punching shear tests | 147 |
| 8.1 Bridge failure loading | 150 |
| 8.2 Truck loadings at 1.0(LL + IL) for maximum positive moment in the side span | 150 |
| 8.3 Deflections at the center of the SS7 segment in side span | 152 |
| 8.4 Longitudinal strains at the center of the SS6L moment | 153 |
| 8.5 Longitudinal strains at the center of the SS7R segment | 153 |
| 8.6 Development of cracks during loading | 154 |
| 8.7 Longitudinal strains at the center of the SS1 segment | 155 |
| 8.8 Reactions at the outer supports | 156 |
| 8.9 Failure mechanism for truck loadings in the side span | 157 |

| Figure | | Page |
|--------|---|------|
| 8.10 | Horizontal force on the top of the outer pier | 158 |
| 8.11 | Deflections along the center of the SS7 segment in side span | 160 |
| 8.12 | Transverse strains at the center of the SS7 segment . . | 161 |
| 8.13 | Forces and moments acting on the bridge for a typical cantilever stage | 162 |
| 8.14 | Horizontal forces and moments at completion of cantilever erection | 163 |
| 8.15 | Horizontal forces and moments due to prestressing in side span | 165 |
| 8.16 | Horizontal forces and moments due to prestressing in main span | 166 |
| 8.17 | Horizontal forces and moments at completion of all prestressing operations | 167 |
| 8.18 | Moment diagram for 0.35 DL (M_{E3}) | 170 |
| 8.19 | Moment diagram for truck loads in side span (M_{E4}) . . . | 170 |
| 8.20 | Ultimate force at a certain section | 171 |
| 8.21 | Stress-strain curves of prestressing cables | 172 |
| 8.22 | Calculation of T_i for different strain profiles | 173 |
| 8.23 | Calculation of ultimate internal moment | 174 |
| 8.24 | Calculation of ultimate internal moment at pier section | 177 |
| 8.25 | Plastic hinges and moment diagram | 178 |
| 8.26 | 1.0(LL + IL) loading for maximum shear at the NM pier . | 181 |
| 8.27 | Reaction at outer supports during loading to failure . . | 182 |
| 8.28 | Longitudinal strains at SS7R and SS6L during loading to failure | 182 |
| 8.29 | Longitudinal strains at SS1 during loading to failure . | 183 |
| 8.30 | Longitudinal strains at SM1 during loading to failure . | 183 |

| Figure | Page |
|--------|---|
| 8.31 | Longitudinal strains at NS6 during loading to failure 184 |
| 8.32 | Longitudinal strains at NM6 during loading to failure 184 |
| 8.33 | Deflections at SM10 during loading to failure 186 |
| 8.34 | Development of cracks around NM pier during loading to failure 187 |
| 8.35 | Development of cracks around the center of main span during loading to failure 188 |
| 8.36 | Typical crack around the joint (after failure) 189 |
| 8.37 | Longitudinal strains at NM9 during loading to failure 190 |
| 8.38 | Longitudinal strains at NM1 during loading to failure 191 |
| 8.39 | Longitudinal strains at NS1 during loading to failure 191 |
| 8.40 | General view of the bridge after failure 193 |
| 8.41 | Deflections along the bridge during loading to failure 194 |
| 8.43 | Moment diagram for 0.35 DL for three different conditions (M_{E3}) 196 |
| 8.44 | Moment diagram for 1.0(LL + IL) for three different conditions (M_{E4}) 197 |
| 8.45 | Failure loading at the center of the main span 202 |
| 9.1 | Location of strain gages in prototype bridge 210 |
| 9.2 | Measured strain in M1 and S1 segments during several stages of balanced cantilever construction 212 |
| 9.3 | Measured strains in M1 segments during closure operation 214 |
| 9.4 | Measured strains in the model M9 segment and prototype M10 during closure operations 215 |
| 9.5 | (a) Truck loading tests (b) Average truck properties 217 |
| 9.6 | Influence line for bottom flange strain, Station SS1 219 |

| Figure | | Page |
|--------|--|------|
| 9.7 | Influence line for bottom flange strain, Station MS1 . . | 220 |
| 9.8 | Influence line for bottom flange strain, Station SS7 . . | 221 |
| 9.9 | Influence line for bottom flange strain, Station MS10 . | 222 |
| 9.10 | Test arrangement--ultimate shear test | 225 |

C H A P T E R 1

INTRODUCTION

1.1 General

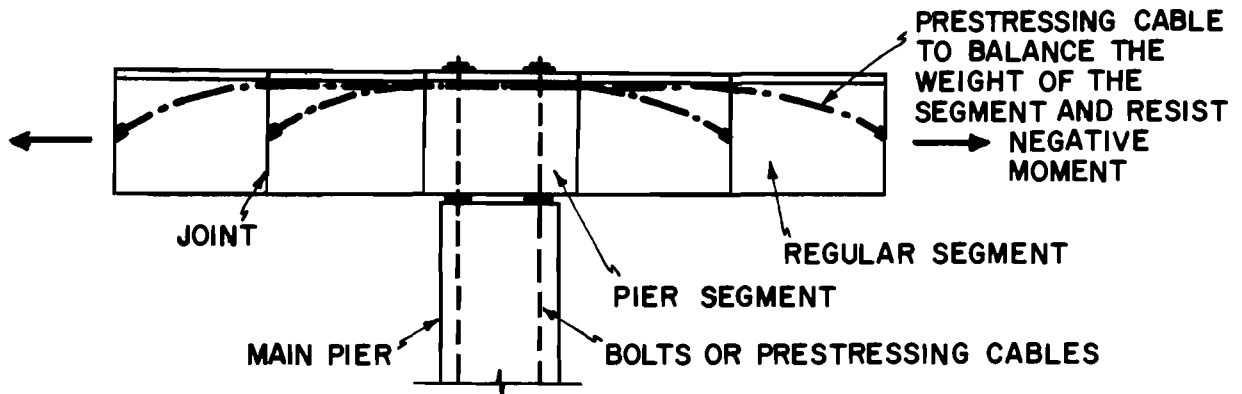
Construction of longer span bridges is increasing in the United States to satisfy requirements of function, economics, safety, and aesthetics. The long span potential of prestressed concrete cannot be fully developed in pretensioned I-girder and composite slab systems. These systems have practical limits in the 120 ft. span range. However, substantially longer span prestressed concrete bridges have been built in several countries by utilizing precast and cast-in-place box girder bridges erected using cantilevering techniques.³² This study will treat only the segmental precast prestressed concrete box girder bridge erected by the cantilever method.

In this construction method, precast segments [Fig. 1.1(a)] are cast and transported to the bridge site. The precast segments are erected, as shown in Fig. 1.1(b), as balanced cantilevers from the pier segment which is rigidly connected to the pier either temporarily or permanently. In some applications temporary props are used to provide the cantilever moment capacity. In the first applications of this construction technique, concrete or mortar was used as a jointing material between segments. However, the French used epoxy resin successfully as a jointing material in 1964.³⁰ Because of the rapid setting of the epoxy resin, this type of jointing shortened the construction period appreciably and became widely accepted. As each pair of segments is positioned at the ends of the balanced cantilever, negative moment tendons are inserted and tensioned. These tendons must provide moment capacity for the full cantilever moment. Erection continues until the last cantilevered sections are placed at the center of the span and at the end supports, as shown in

(a) TYPICAL CROSS SECTION OF BOX GIRDER



(b) CANTILEVER ERECTION OF PRECAST SEGMENTS



(c) COMPLETION OF CANTILEVER CONSTRUCTION

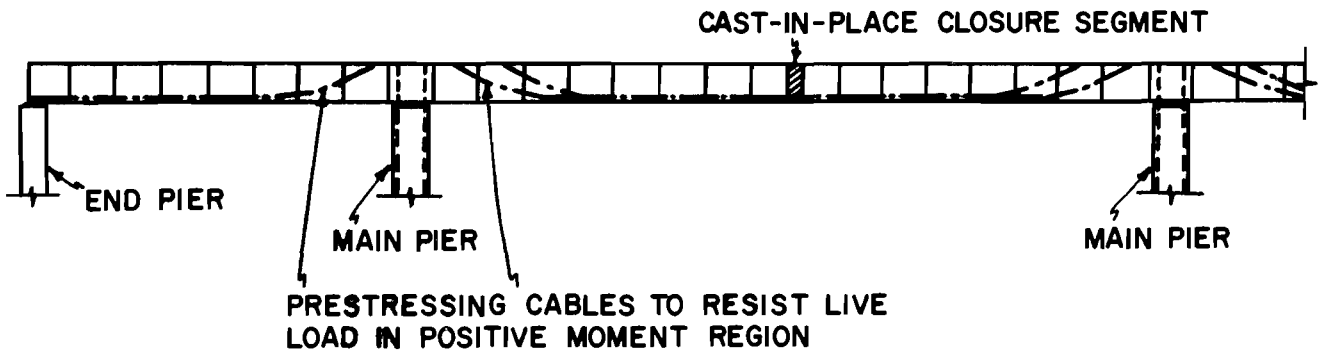


Fig. 1.1. Typical balanced cantilever construction

Fig. 1.1(c). The positive moment tendons in the end span are prestressed and the end segments are seated on their supports prior to or during stressing of prestressing cables in the main span positive moment region. At midspan, the gap between the two cantilever arms is closed with cast-in-place concrete. Prestressing cables to resist live load in the central span positive moment region are inserted and stressed. Reactions in the end spans are adjusted as required.

The use of such precasting and cantilevering techniques has the following advantages:^{16,30}

- (1) Maintenance of navigational or traffic clearance during construction.
- (2) High quality control of segments and control of deflection.
- (3) Flexible choice of the segment length depending on the capacity of transportation and lifting equipment.
- (4) Simultaneous start of segment casting and pier construction.
- (5) Significantly reduced erection time at the site.
- (6) Highly efficient use of forms.

Because this type of bridge had never been built in the United States, a cooperative research project with the Texas Highway Department and the Federal Highway Administration to investigate the various problems associated with design and construction procedures for long span precast prestressed concrete box girder bridges of segmental construction was undertaken by The University of Texas at Austin, Center for Highway Research, in 1968.⁹

The Texas Highway Department utilized a preliminary design developed as part of the project by The University of Texas at Austin researchers in developing plans for a long span bridge on the John F. Kennedy Memorial Causeway, Park Road 22, Corpus Christi, Texas. The requirement to maintain navigational clearance during construction as well as the highly corrosive environment on the Texas coast led to the choice of a precast prestressed concrete box girder bridge built in cantilever.

In order to study the applicability and accuracy of the design criteria, analytical methods, construction techniques, and shear

performance of the epoxy resin joints, an accurate one-sixth scale model of the three-span continuous bridge was built and tested at the Civil Engineering Structures Research Laboratory of The University of Texas at Austin's Balcones Research Center. This report summarizes the construction and testing of the model. Complete details are available in Ref. 18.

1.2 Related Research

This model test was only one element in a comprehensive investigation. Related research which has been completed includes:

(1) State-of-the-Art-Survey.^{20,22} In the initial stages of the research program, a comprehensive literature survey was completed.

(2) Design and Optimization.^{21,23} Criteria were developed for design procedures and preliminary designs of several example structures were made. The Texas Highway Department adopted one of these preliminary designs for the Corpus Christi structure and developed final plans. The bridge was largely designed by the Ultimate Strength Design method assuming that beam theory was applicable. Allowable stresses during construction and under service loads were also checked using beam theory. Service load behavior of the completed structure was then checked using folded plate theory to determine the effect of warping. Optimization of the cross section was studied by unconstrained nonlinear programming, although the optimal cross section was not used in the final design.

(3) Segmental Analysis.^{10,11} In order to investigate the various critical stages during the cantilevering procedures, an incremental box girder analysis computer program utilizing the Finite Segment Method was developed by Brown. This program (SIMPLA2) treats staged construction with realistic prestressing forces and determines effects in both longitudinal and transverse directions.

(4) Experimental Study of Epoxy Resin Jointing.^{17,19} While epoxy resins have been widely used with concrete as coating or patching materials and although a guide⁴ existed for the general use of epoxy resin with concrete, at the inception of the study there was no U.S. specification for

the specific use of epoxy resins in jointing a segmental precast prestressed concrete box girder bridge. A program of evaluations of various epoxy resin properties and requirements was undertaken which resulted in development of a Texas Highway Department tentative specification. Prior to the model bridge construction, a number of different epoxy resins were evaluated and the epoxy resin which came closest to meeting the specifications was selected for construction of the model. A revised specification has been suggested in Ref. 19.

(5) Field Study. The Corpus Christi bridge was instrumented with strain gages which were mounted on the reinforcement in various segments. Readings were taken at the time of cantilever erection. Structural behavior under actual service loads was observed for various loading conditions upon completion of the prototype construction. A summary of the field observations and a comparison with the model test results will be given in this report.

1.3 Objective and Scope of the Model Study

Tests of model structures can be very powerful tools to check the adaptability or accuracy of design procedures and to verify analytical assumptions and procedures.

In utilizing precast segments in construction of a bridge, continuity of the structure at the joints is a very important problem. Several concrete box girder bridge models have been tested in various laboratories.^{12,16,35,36} All of the model bridges, except for a two-span (72 ft. long) four-cell reinforced concrete box girder model tested in California,³⁵ were precast prestressed microconcrete box segments joined with mortar. One of the models¹² had continuous reinforcement across all the joints. The 1/12th scale Mancunian Highway microconcrete model¹⁶ (16 ft., 10 in. long) and the 1/16th scale three-cell box beam tested by Swann³⁶ proved the strength adequacy of the mortar joint in failure tests.

Some French tests have been reported¹⁶ which demonstrated the structural continuity of epoxy joints in continuous slabs (1/4.64th scale, 50 ft. long). An investigation of the shear capacity of precast segments joined with epoxy resin has been reported in Japan.¹⁶

However, to the authors' knowledge there has not been another test program in which a precast prestressed concrete segmental bridge model with epoxy resin joints has been built with accurate simulation of the construction procedure and then loaded to failure. Since this model of a three-span precast prestressed concrete segmental twin box girder bridge is a one-sixth scale "direct" model,^{1,29} and was built in full conformance with prototype construction procedures, it closely simulates the behavior of the prototype both in the elastic and inelastic range.

The objectives of this model study included the following:

- (1) Determination of strain distribution due to prestressing and of deflections during cantilever construction and during closure operations.
- (2) Documentation of bridge behavior under service level loading for the various design loading conditions.
- (3) Comparison of analytical results from beam theory and folded plate theory with the construction and service level loading experimental results.
- (4) Determination of bridge behavior under ultimate proof loading (1.35 DL + 2.25 (LL + IL)) for the various design loading conditions.
- (5) Determination of final failure mechanisms with special attention to any adverse effect of the epoxy resin on the shear or flexural capacity of the bridge. Determination of the punching shear capacity of the top slab and evaluation of any adverse effect of the epoxy resin on such capacity.
- (6) Assessment of the applicability of the Ultimate Strength Design criteria proposed for this type bridge.
- (7) Determination of any improvements of design details which might minimize field construction problems prior to the prototype bridge construction.
- (8) Provision of a meaningful demonstration to prospective contractors to assist them in the visualization of the construction technique so as to reduce uncertainty and encourage bidding for the prototype construction.

1.4 Report Contents

Details of modeling procedures used are given in Chapter 2. Test results of materials used for the model are discussed in Chapter 3. Details of the segments, casting procedures, and segment preparation are

illustrated in Chapter 4. The instrumentation used in the model bridge tests and the procedures for data reduction are briefly explained in Chapter 5. Chapter 6 illustrates all construction procedures for the model bridge and discusses the behavior of the bridge during construction. After completion of construction, a wide variety of service level loadings were applied to the bridge and then various design ultimate loads specified by the 1969 Bureau of Public Roads criteria were applied to prove the safety of the structure. Results from these tests are discussed in Chapter 7.

Finally, the bridge model was loaded to complete failure. The behavior during failure loadings is documented and comparisons of the theoretical and experimental values for the ultimate strength of the bridge are discussed in Chapter 8. A brief comparison of model test results with field measurements and description of a special test of the shear capacity of a reduced model consisting of several segments is given in Chapter 9. Chapter 10 gives the conclusions determined from the model study and recommendations for improvements in design and construction criteria.

This page replaces an intentionally blank page in the original.

-- CTR Library Digitization Team

C H A P T E R 2

SCALE FACTORS FOR THE BRIDGE MODEL

2.1 Factors Affecting Scale Selection

Selection of the scale factor for the model bridge was primarily governed by availability of materials and loading facilities. Consideration of dependability of results, costs, and construction times were additional important factors.

The one-sixth scale factor was dictated by availability of model materials (mainly prestressing cable).¹⁴ At this scale, all prestressing strands and reinforcing bars could be modeled very closely with a maximum 9 percent deviation. Although deformed bars were not available for these small sizes, bonding of the rebar wires was not a critical problem in this study. After tentative selection of the one-sixth scale factor, testing facility and loading equipment availability were not found to be controlling factors.

2.2 Dimensions of Prototype and Model Bridge

2.2.1 Longitudinal Dimensions. The 200 ft. main span and balancing 100 ft. side spans of the prototype bridge were modeled in one-sixth scale, as shown in Fig. 2.1.

2.2.2 Transverse Dimensions. Details of the transverse cross section are shown in Fig. 2.2.

2.3 Choice of Materials

2.3.1 Concrete. At The University of Texas at Austin, a 1/5.5 scale microconcrete²⁴ (reduced aggregate which has a gradation similar to ordinary aggregate gradation) has been used for a number of model studies. This microconcrete is designed to closely match the critical properties (E_c and f'_c) of the prototype concrete. It was decided to use this type

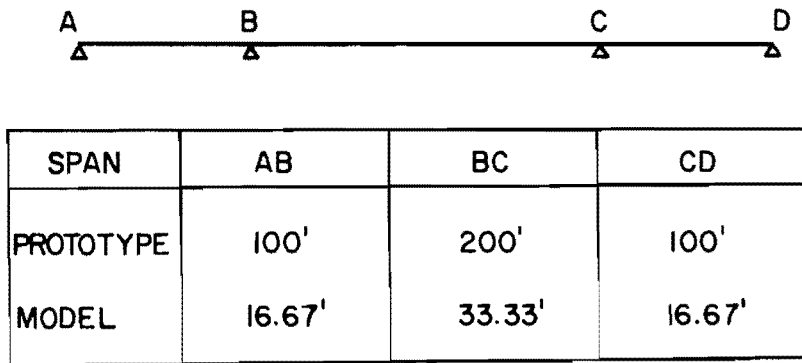
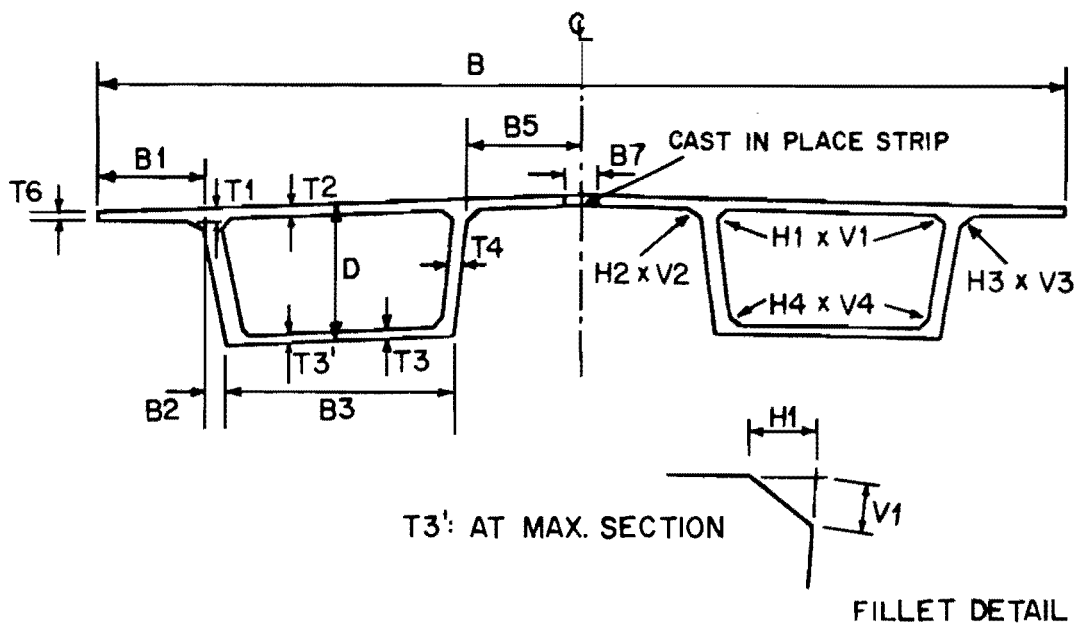


Fig. 2.1. Longitudinal dimensions of bridge



| | B | B1 | B2 | B3 | B5 | B7 | T1 | T2 | T3 | T3' | T4 | T6 | D | H1 | V1 | H2 | V2 | H3 | V3 | H4 | V4 |
|------------|------|-------|------|------|-------|-----|-------|-------|----|-------|-----|----|-----|-------|----|-------|----|-------|----|-------|-------|
| PROTO-TYPE | 671" | 71.5" | 14" | 156" | 80" | 24" | 8" | 7" | 6" | 10" | 12" | 6" | 96" | 8" | 6" | 8" | 6" | 8" | 6" | 4" | 4" |
| MODEL | 112" | 11.9" | 2.3" | 26" | 13.3" | 4" | 1.33" | 1.17" | 1" | 1.67" | 2" | 1" | 16" | 1.33" | 1" | 1.33" | 1" | 1.33" | 1" | 0.67" | 0.67" |

Fig. 2.2. Cross section of bridge

concrete after trial mixes indicated it possible to attain the minimum $f'_c = 6000$ psi. Details of the scaled microconcrete are described in Sec. 3.1.

2.3.2 Prestressing Steel. Four groups of strands were used in the original design of the prototype. Minor changes were made in the tendon groups actually used in the prototype construction. The scale reduction for the model tendons is shown in Table 2.1. All tendons were scaled down to match the ultimate strength requirements. Therefore, the type and grades of steel for the prototype and the model were not always the same. Figure 2.3 shows the position of each tendon.

2.3.3 Reinforcing Bars. Three different reinforcing bar sizes were used in each segment and another bar size was used for the longitudinal cast-in-place joint. These bars were specified as Grade 60 in the prototype. The reduction to one-sixth scale for these bars is described in Table 2.2. The reinforcing bars used for the model were C-1018 wire. These wires were not deformed but the bond strength of wire to microconcrete has been shown to be adequate in other tests.¹ In order to obtain a distinct yield plateau in the wires to match the reinforcing bars of the prototype, wires for the cages were annealed by a commercial firm in a controlled temperature oven. Then the reinforcing cages were assembled. Details of the reinforcement are shown in Fig. 2.4. All details matched those of the prototype units.

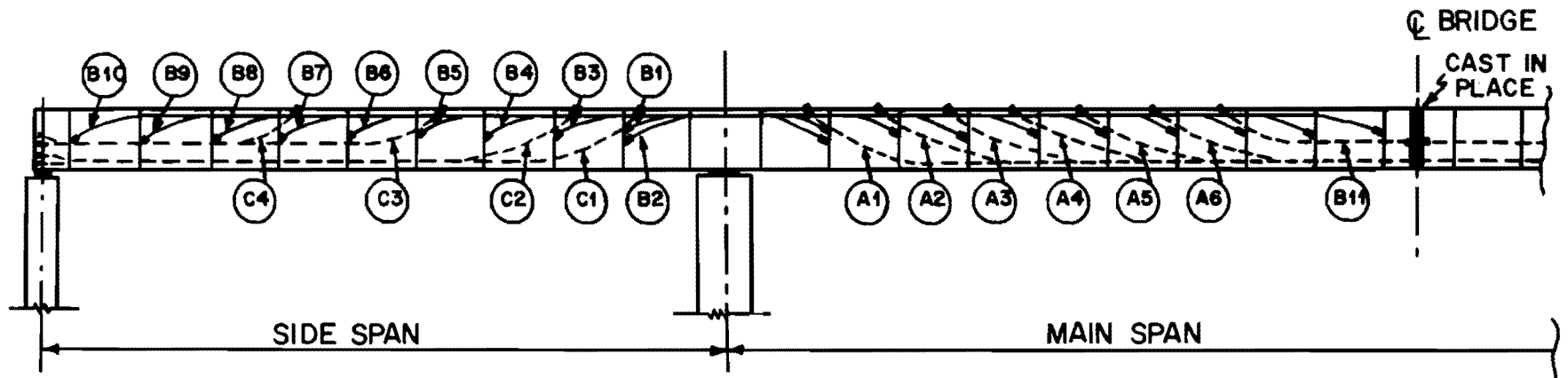
Details of individual bars and some modifications (such as spirals and anchorages) are shown in Sec. 4.1.

TABLE 2.1. CHOICE OF STRANDS AND WIRE FOR THE MODEL BRIDGE

| Prototype | | Model | | |
|------------------------------------|-------------------------------|--|------------------------------|---|
| No. of 1/2" ϕ 270K Strands | Ultimate Strength (kip) | Required Ultimate Strength (kip) | Selected Wires or Strands | Strength of Selected Material (kip) |
| 20 | 825 | 22.9 | 3/8 in. Strands | 23.0 |
| 13 | 537 | 14.9 | 7 mm Wire | 14.7 |
| 8 | 329 | 9.1 | 1/4 in. Strands | 9.0 |
| 6 | 248 | 6.9 | 6 ga. Wire | 7.2 |

TABLE 2.2. CHOICE OF REINFORCING BARS FOR THE MODEL BRIDGE

| Prototype | | Model | | |
|-----------|-------------------|----------------------------|--------------|----------------------------------|
| Bar | Area (sq. in.) | Required Area (sq. in.) | Chosen Wire | Area of Chosen Wire (sq. in.) |
| #8 | 0.79 | 0.0220 | 8 ga. Wire | 0.0206 |
| #6 | 0.44 | 0.0122 | 1/8 in. Wire | 0.0122 |
| #5 | 0.31 | 0.0086 | 12 ga. Wire | 0.0087 |
| #4 | 0.20 | 0.0056 | 14 ga. Wire | 0.0050 |

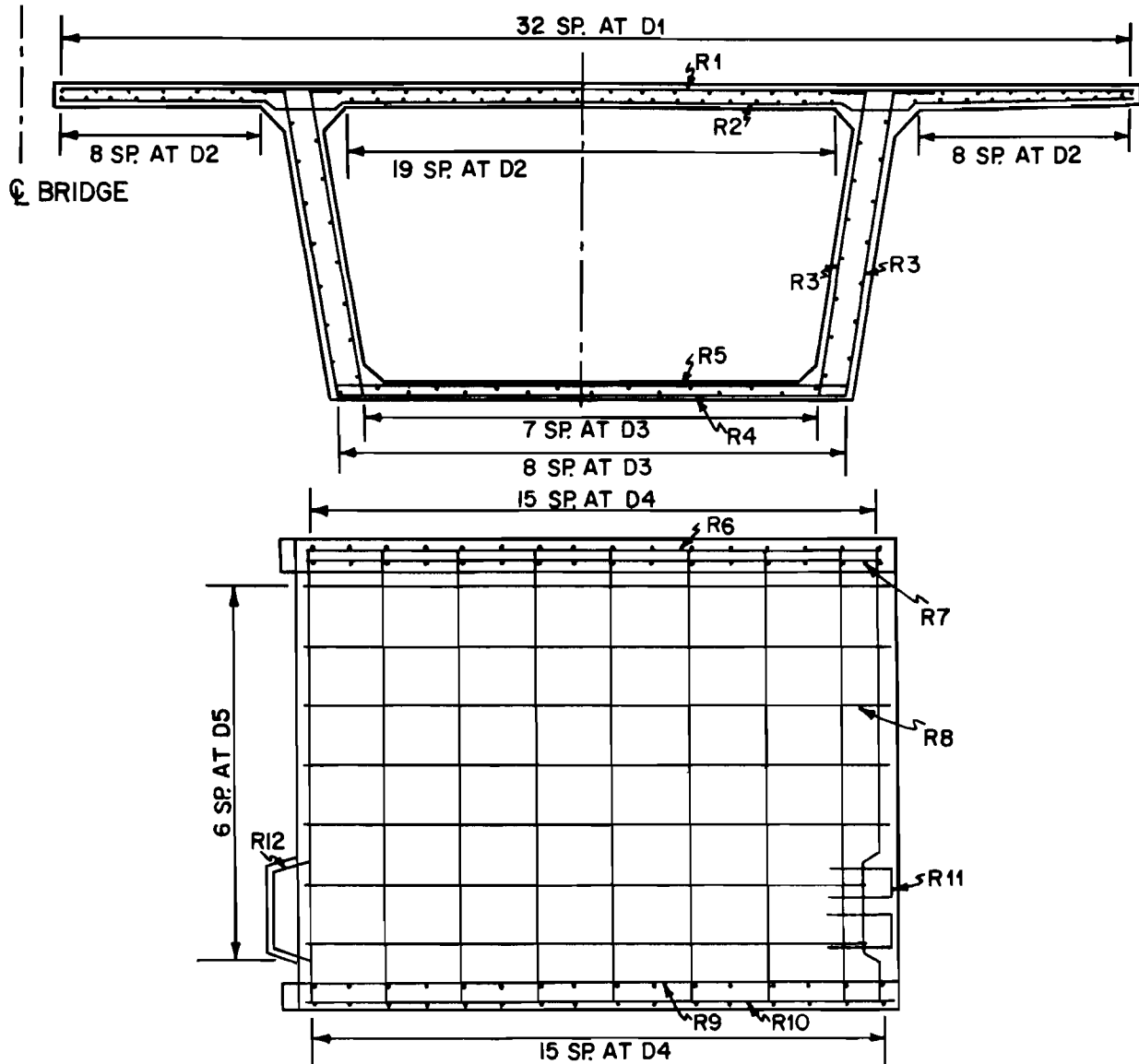


| | PROTOTYPE * | MODEL |
|-----|-------------|---------------------------|
| B1 | 13 STRANDS | 7 MM. WIRE |
| B2 | 13 STRANDS | 7 MM. WIRE |
| B3 | 20 STRANDS | $\frac{3}{8}$ IN. STRANDS |
| B4 | 20 STRANDS | $\frac{3}{8}$ IN STRANDS |
| B5 | 13 STRANDS | 7 MM. WIRE |
| B6 | 13 STRANDS | 7 MM. WIRE |
| B7 | 13 STRANDS | 7 MM. WIRE |
| B8 | 6 STRANDS | 6 GA. WIRE |
| B9 | 6 STRANDS | 6 GA. WIRE |
| B10 | 6 STRANDS | 6 GA. WIRE |
| B11 | 6 STRANDS | 6 GA. WIRE |

| | PROTOTYPE | MODEL |
|----|-----------|---------------------------|
| A1 | 8 STRANDS | $\frac{1}{4}$ IN. STRANDS |
| A2 | 8 STRANDS | $\frac{1}{4}$ IN. STRANDS |
| A3 | 8 STRANDS | $\frac{1}{4}$ IN. STRANDS |
| A4 | 8 STRANDS | $\frac{1}{4}$ IN. STRANDS |
| A5 | 8 STRANDS | $\frac{1}{4}$ IN. STRANDS |
| A6 | 8 STRANDS | $\frac{1}{4}$ IN. STRANDS |
| C1 | 6 STRANDS | 6 GA. WIRE |
| C2 | 6 STRANDS | 6 GA. WIRE |
| C3 | 6 STRANDS | 6 GA. WIRE |
| C4 | 6 STRANDS | 6 GA. WIRE |

* AS ORIGINALLY DESIGNED

Fig. 2.3. Details of prestressing strands and wire



| REINFORCEMENT | PROTOTYPE | MODEL |
|---------------|-----------|--------------|
| R1 | #8 | 8 GA. WIRE |
| R2 | #8 | 8 GA. WIRE |
| R3 | #8 | 8 GA. WIRE |
| R4 | #4 | 14 GA. WIRE |
| R5 | #4 | 14 GA. WIRE |
| R6 | #4 | 14 GA. WIRE |
| R7 | #6 | 1/8 IN. WIRE |
| R8 | #4 | 14 GA. WIRE |
| R9 | #4 | 14 GA. WIRE |
| R10 | #4 | 14 GA. WIRE |
| R11 | #4 | 14 GA. WIRE |
| R12 | #3 | 16 GA. WIRE |

| SPACING | PROTOTYPE | MODEL |
|---------|-----------|----------|
| D1 | 10 IN. | 1.67 IN. |
| D2 | 7 IN. | 1.17 IN. |
| D3 | 18 IN. | 3 IN. |
| D4 | 7 1/2 IN. | 1.25 IN. |
| D5 | 12 IN. | 2 IN. |

Fig. 2.4. Details of reinforcing bars in segment

C H A P T E R 3

MATERIAL PROPERTIES

3.1 Concrete

3.1.1 Concrete Mix Design. After several trial mixes, the mix of Table 3.1 was used for segment casting. Consistency of the micro-concrete was judged by visual inspection. The workability was good even though the mixes appeared somewhat dry and harsh.

TABLE 3.1. CONCRETE MIX DESIGN
(2.4 cu. ft.)

| | |
|-----------------------------------|-----------|
| Design strength | 6000 psi |
| W/C (lb/lb) | 51.6% |
| Water | 41.5 lbs. |
| Cement (Type III portland cement) | 80.5 lbs. |
| TCM 154 (Aggregate) | 61.2 lbs. |
| Ottawa Sand | 70.9 lbs. |
| Blast sand No. 1 | 65.4 lbs. |
| Blast sand No. 2 | 18.9 lbs. |
| Colorado River red sand | 18.9 lbs. |
| Airsene L (Retarder) | 94.8 cc |

3.1.2 Strength of Concrete. One or two cylinders (3 x 6 in. or 2 x 4 in.) were cast with each segment. Several cylinders were tested at the time of erection and the remainder were tested at the time of loading tests. Compressive strength of the closure segment was tested one week after casting but prior to positive tendon operation. Test results are summarized in Table 3.2 and Table 3.3.

TABLE 3.2. COMPRESSIVE STRENGTH OF CONCRETE

| Type of Cylinder | No. of Cylinders Tested | Average Compressive Strength (psi) | Standard Deviation (\bar{s}) of Compressive Strength (psi) |
|------------------|-------------------------|------------------------------------|--|
| 3 × 6 in. | 49 | 7090 | 523 |
| 2 × 4 in. | 24 | 7430 | 810 |

TABLE 3.3. SPLITTING TENSILE STRENGTH OF CONCRETE

| Type of Cylinder | No. of Cylinders Tested | Average Tensile Strength (psi) | Standard Deviation (\bar{s}) of Tensile Strength (psi) |
|------------------|-------------------------|--------------------------------|--|
| 3 × 6 in. | 35 | 597 | 31 |
| 2 × 4 in. | 20 | 633 | 71 |

A universal hydraulic testing machine (max. 120 kip) was used for compression and splitting tensile tests of cylinders. Scaled loading heads and caps were necessary to minimize scatter of test results.^{1,31} For the compression test, cylinders were capped on both ends with sulphur capping compound in a scaled capping device and tested by using scaled adjustable spherical load heads on the top of cylinders. For the splitting tensile test, loading bars and wooden strips were scaled down for each size of cylinder. Also, the loading rate was reduced by the appropriate scale.

No cylinder tested had a compressive strength lower than the specified 6000 psi. The strengths of the 2 × 4 in. cylinders were slightly greater and showed higher variations than the 3 × 6 in. cylinders. The values obtained with the 3 × 6 in. cylinders are more reliable than those

of the 2 x 4 in. cylinders because the standard deviation for the 3 x 6 in. cylinders is much less than for the 2 x 4 in. cylinders. Therefore, the values for f'_c of 7090 psi and splitting tensile strength of 597 psi are used in later calculations. F_{sp} for the 3 x 6 in. cylinders is $597/\sqrt{7090} = 7.09$.

3.1.3 Modulus of Elasticity. Four 0.4 in. paper strain gages were mounted vertically in series at the middle of several cylinders. The cylinders were preloaded to about 1/10th of the estimated failure load two or three times prior to taking any strain reading. The strain readings of all four gages were averaged and stress-strain curves were drawn to find E_c . E_c was determined by the slope of the chord up to about $0.5f'_c$ (the secant modulus of elasticity).¹³ Eight cylinders (3 x 6 in.), including one from the closure, were tested and the results are shown in Table 3.4. Although the value obtained from the 3 x 6 in. cylinders is used in all calculations, E_c of the 2 x 4 in. cylinders was also checked by the same procedure.

TABLE 3.4. MODULUS OF ELASTICITY OF CONCRETE

| Type of Cylinder | No. of Cylinders Tested | Average E_c (psi) | Standard Deviation (\bar{s}) of E_c (psi) | Average f'_c (psi) |
|------------------|-------------------------|---------------------|---|----------------------|
| 3 x 6 in. | 8 | 4.56×10^6 | 0.37×10^6 | 7550 |
| 2 x 4 in. | 2 | 4.46×10^6 | 0.24×10^6 | 7190 |

The ACI² formula gives $E_c = w^{1.5} \times 33\sqrt{f'_c}$. Since the unit weight of microconcrete is 133 lb/cu.ft.,^{1,24} $E_c = 133^{1.5} \times \sqrt{7550} = 4.39 \times 10^6$ psi for $f'_c = 7550$ psi. This is in close agreement with the measured values.

3.1.4 Poisson's Ratio. Six 0.4 in. paper strain gages were mounted vertically and horizontally in series at the middle of several test cylinders. Three vertical strain readings and three horizontal strain readings were averaged and Poisson's ratio was calculated. Three

3 x 6 in. cylinders were tested to find Poisson's ratio. The average Poisson's ratio was 0.184 and standard deviation was 0.016.

3.2 Steel

3.2.1 Prestressing Strands and Wire

3.2.1.1 Ultimate Strength. Six to seven specimens of each size were tested. Results are given in Table 3.5.

TABLE 3.5. ULTIMATE STRENGTH OF PRESTRESSING STRANDS AND WIRE

| Type of Cable | No. of Specimens | Average F'_s (kip) | Area (sq. in.) | Average f'_s and (\bar{s}) (ksi) |
|-----------------|------------------|----------------------|----------------|--------------------------------------|
| 6 ga. Wire | 6 | 8.22 | 0.029 | 280 (13) |
| 1/4 in. Strands | 6 | 9.15 | 0.0356 | 257 (8) |
| 7 mm Wire | 6 | 15.3 | 0.0594 | 258 (8) |
| 3/8 in. Strands | 7 | 22.0 | 0.085 | 259 (4) |

3.2.1.2 Modulus of Elasticity. Two strain gages were mounted on opposite faces of the wire and E_s was calculated from stress-strain curves. In an attempt to measure the modulus of strands, epoxy resin coatings were applied to get a smooth surface for strain gages. Two strain gages were then mounted using the same procedure as that for the wire. Since these strains were not measured successfully, E_s values for strands were taken from Ref. 26. E_s values are shown in Table 3.6.

3.2.2 Reinforcing Wire. Samples of all reinforcing wire sizes used in the segments were tested, as shown in Fig. 3.1, without breaking the spot-welded cross wires. Some difference in f_y and f'_s was noticed between sizes of wires. Test results are shown in Table 3.7. All segment reinforcing wires had yield points above Grade 60 minimums. The 12 gage wire which was used in the midstrip closure had $f_y = 45.1$ ksi ($\bar{s} = 3.1$) and $f'_s = 53.6$ ksi ($\bar{s} = 1.8$).

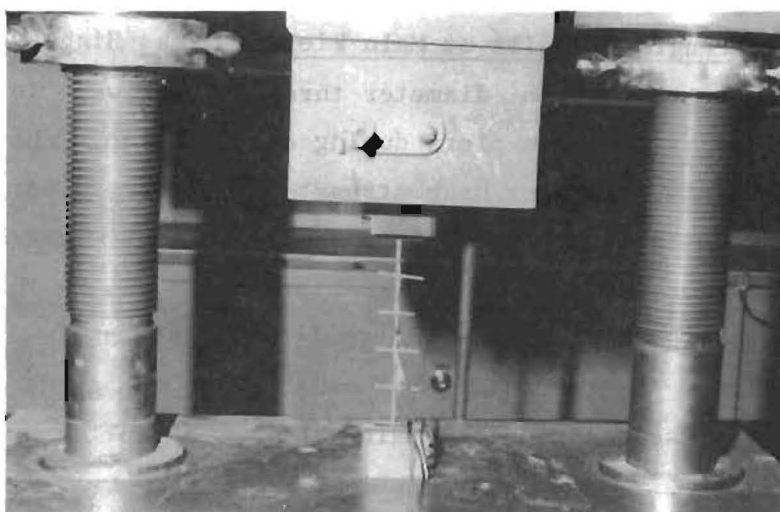


Fig. 3.1. Testing of reinforcing wire

TABLE 3.6. MODULUS OF ELASTICITY OF WIRE AND STRANDS

| Type of Cable | No. of Specimens | Average E_s and (\bar{s}) (psi) | |
|-----------------|------------------|-------------------------------------|----------------------|
| 6 ga. Wire | 4 | 30.9×10^6 | (0.11×10^6) |
| 1/4 in. Strands | — | 27.0×10^6 | (————) |
| 7 mm Wire | 5 | 30.5×10^6 | (0.17×10^6) |
| 3/8 in. Strands | — | 27.0×10^6 | (————) |

TABLE 3.7. TEST RESULTS OF REINFORCING WIRE OF PRECAST SEGMENTS

| Type of Wire | No. of Specimens | Average f_y and (\bar{s}) (ksi) | Average f'_s and (\bar{s}) (ksi) |
|--------------|------------------|-------------------------------------|--------------------------------------|
| 8 ga. Wire | 6 | 70.6 (3.4) | 75.1 (4.2) |
| 1/8 in. Wire | 6 | 79.0 (4.3) | 80.4 (3.0) |
| 14 ga. Wire | 15 | 72.2 (12.1) | 74.6 (11.4) |

3.2.3 Strength of Bolts at Main Piers. Texas Highway Department plans specify that twelve 3-in. diameter threaded rods were to be used for moment connections at the main piers during construction. For the model bridge, twelve 1/2-in. diameter high strength bolts were used at the main piers to hold segments temporarily during construction. Test results of those bolts are shown in Table 3.8. Experimental f'_s was in the range (60-100 ksi) specified by ASTM for the grade bolt originally called for in the bridge plans. Subsequent to the model test, the grade of the bolt material specified was changed to obtain a higher f_y in the prototype.

TABLE 3.8. TENSILE STRENGTH OF BOLTS AT MAIN PIERS

| Type of Bolt | No. of Specimens | Average f_y and (s) (ksi) | Average f'_s and (s) (ksi) |
|------------------|------------------|-----------------------------|------------------------------|
| 1/2-in. diameter | 3 | 75.1 (0.85) | 78.8 (0.9) |

3.3 Epoxy Resin as a Jointing Material

3.3.1 General. The advantage of the epoxy resin as a jointing material as compared to concrete or mortar joints is its quick hardening. The epoxy should seal the joint against corrosion and the epoxy joint should be as strong as concrete in flexure and shear. The epoxy resin joints should increase the cracking moment at joints or shift the cracks to some other position under overloading.

A complete report on the epoxy evaluation program has been presented in Ref. 19. The epoxy used in construction of the model was Epoxy E in that report. It had flexural and shear strengths when jointing hardened concrete, as shown in Tables 3.9 and 3.10.

TABLE 3.9. EPOXY E FLEXURE TEST RESULTS

| Epoxy Resin | Conditions of Specimen | Flexural Strength (psi) | Type of Failure | Percentage of Strength of Monolithic Specimen (%) |
|---|------------------------|-------------------------|----------------------------|---|
| (E) | Dry, No Oil | 733 | Concrete Adjacent to Joint | 100 |
| | Dry, Oil | 742 | Concrete | 102 |
| | Saturated, No Oil | 467 | Concrete Adjacent to Joint | 64 |
| Compressive Strength of Cylinder: | | | | 6760 psi ($\bar{s} = 842$) |
| Splitting Tensile Strength: | | | | 538 psi ($\bar{s} = 73$) |
| Flexural Strength of Monolithic Specimen: | | | | 729 psi ($\bar{s} = 43$) |

TABLE 3.10. EPOXY E SHEAR TEST RESULTS

| Epoxy Resin | Shear Strength (psi) | Type of Failure | Average Shear Strength and (\bar{s}) (psi) | Percentage of Strength of Monolithic Specimen (%) |
|--|----------------------|----------------------------|--|---|
| (E) | 542 | Epoxy Separation | | |
| | 504 | Concrete Adjacent to Joint | 571 (69) | 76 |
| | 666 | Concrete Adjacent to Joint | | |
| Compressive Strength of Cylinder: | | | | 6760 psi ($\bar{s} = 842$) |
| Splitting Tensile Strength: | | | | 538 psi ($\bar{s} = 73$) |
| Shear Strength of Monolithic Specimen: | | | | 753 psi ($\bar{s} = 103$) |

This page replaces an intentionally blank page in the original.

-- CTR Library Digitization Team

CHAPTER 4

SEGMENT DETAILS

4.1 Reinforcing Cage for Precast Segments

4.1.1 Reinforcement. Hand assemblage of each reinforcement cage with individually tied wires would have required excessive time to complete 84 segments. Therefore, the five different wire mats which were required for each segment were lightly spot-welded and were then annealed. These mats were then cut and bent to proper length and shape, as shown in Fig. 4.1. All mats of a segment were assembled as shown in Fig. 4.2, by using a jig. Details of each mat are shown in Fig. 4.3. Development length of web reinforcement spliced into the top slab was longer than that specified by the prototype plan to compensate for the use of plain bars in the model instead of deformed bars.

Modification of the cages was required at the shear key and anchorage points as shown in Fig. 4.4. Whenever a wire was cut, replacement bars were spliced in, or wires were rotated or rerouted as necessary. No bars called for on the plans were ever omitted.

The reinforcement of the pier segments was scaled as shown in Fig. 4.5.

4.1.2 Anchorages. Since it was impossible to exactly model the multiple strand commercial tendons and anchorages used in the prototype, prestressing cables were modeled by selecting for each tendon an equivalent single cable which could produce the correctly scaled tendon force. Normal strand chucks were selected as the basic anchorage device for the single cables. The model was constructed before the prototype bidding and selection of the contractor. At the time of anchorage selection for the model, the prototype plans allowed the contractor to choose bearing or wedge types of anchorage. For the model, the bearing type was chosen.* The dimensions

*The contractor later chose the wedge type for prototype construction.

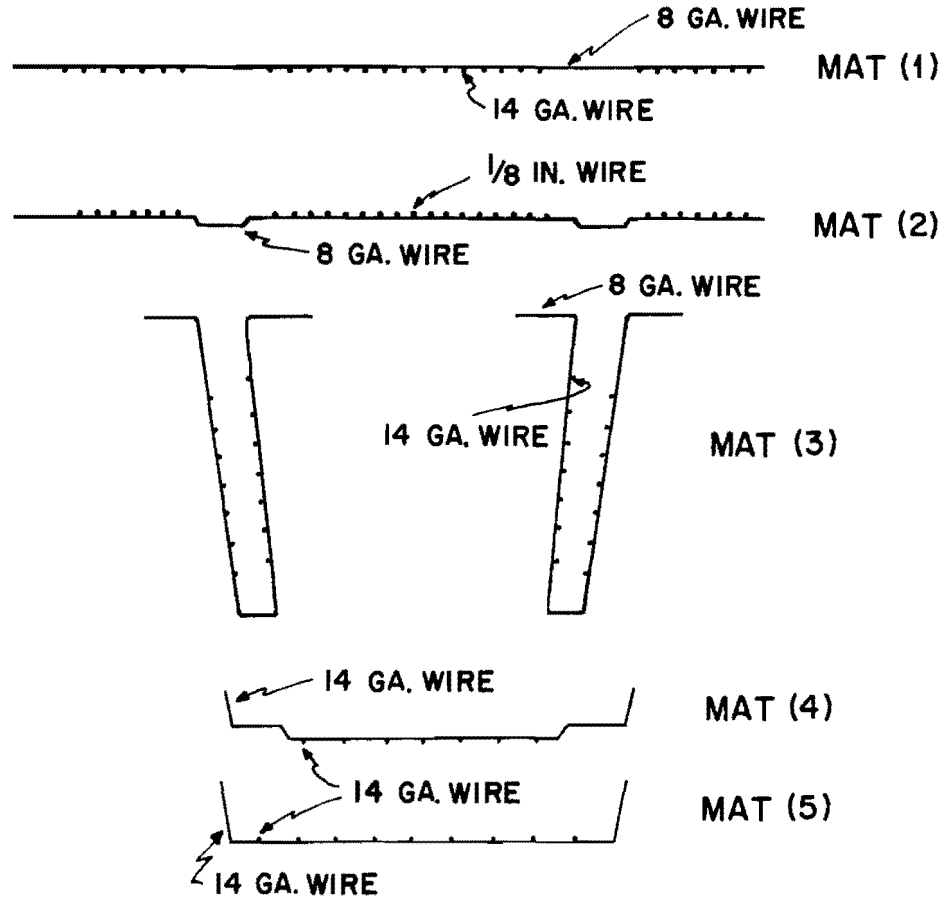


Fig. 4.1. Individual mats for a cage

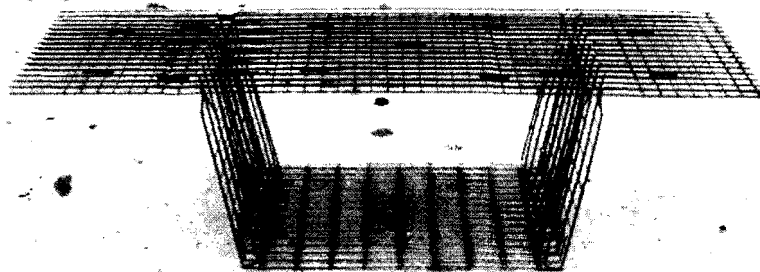


Fig. 4.2. Cage for a segment

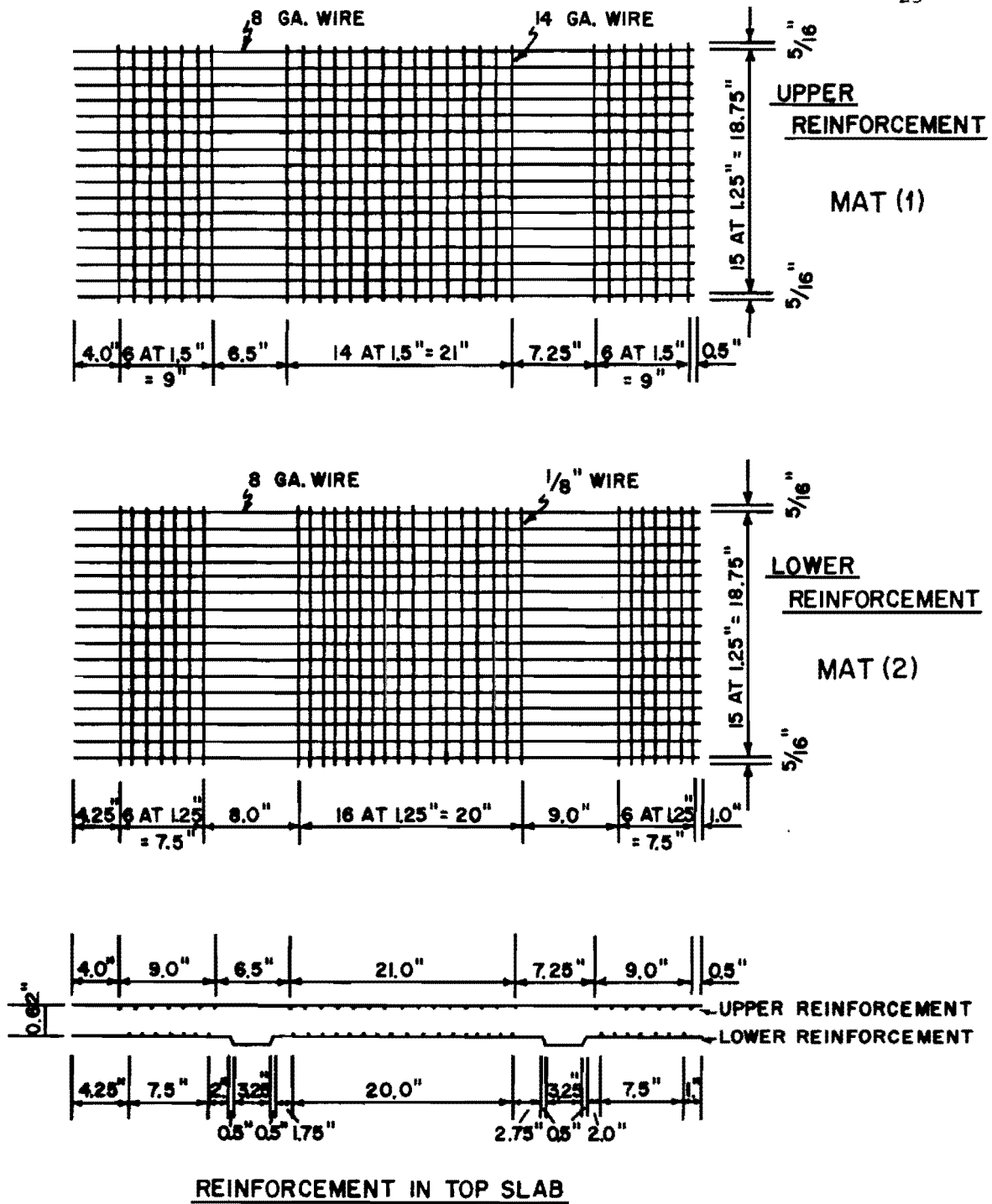
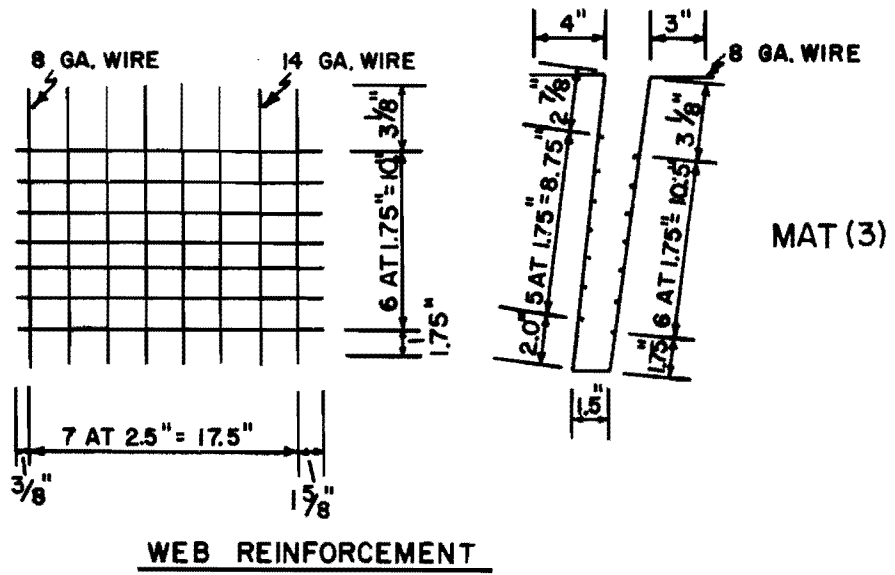
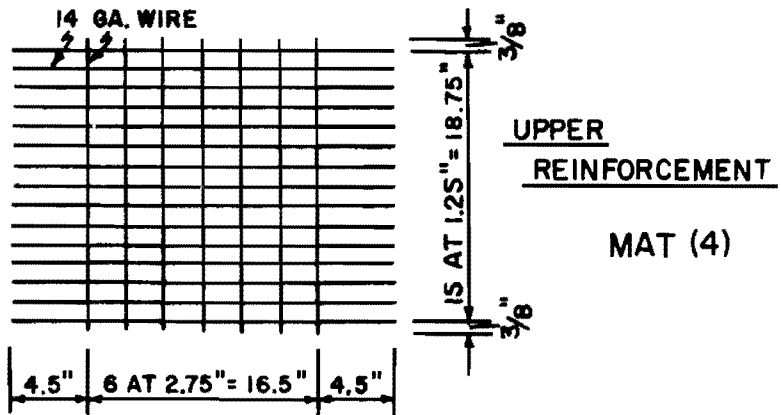


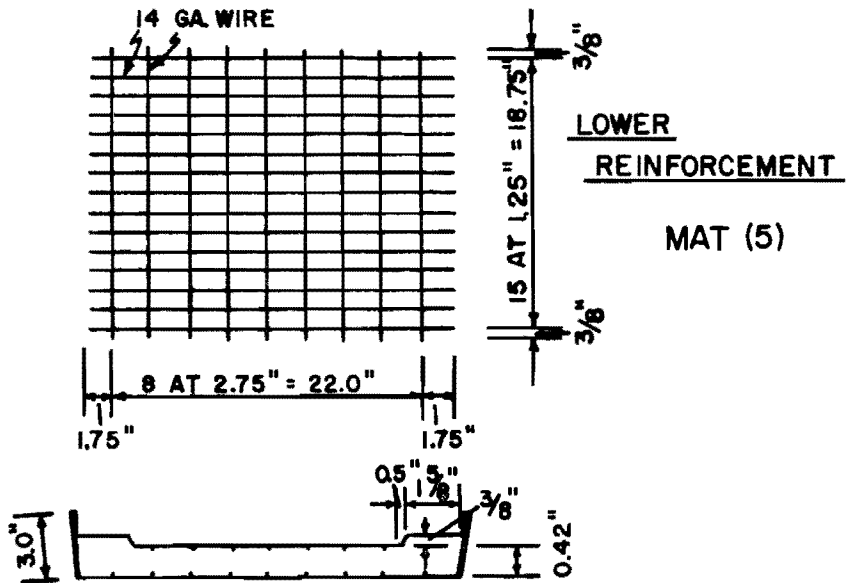
Fig. 4.3(a). Details of reinforcing mats



MAT (3)



MAT (4)



MAT (5)

REINFORCEMENT IN BOTTOM SLAB

Fig. 4.3(b). (Continued)

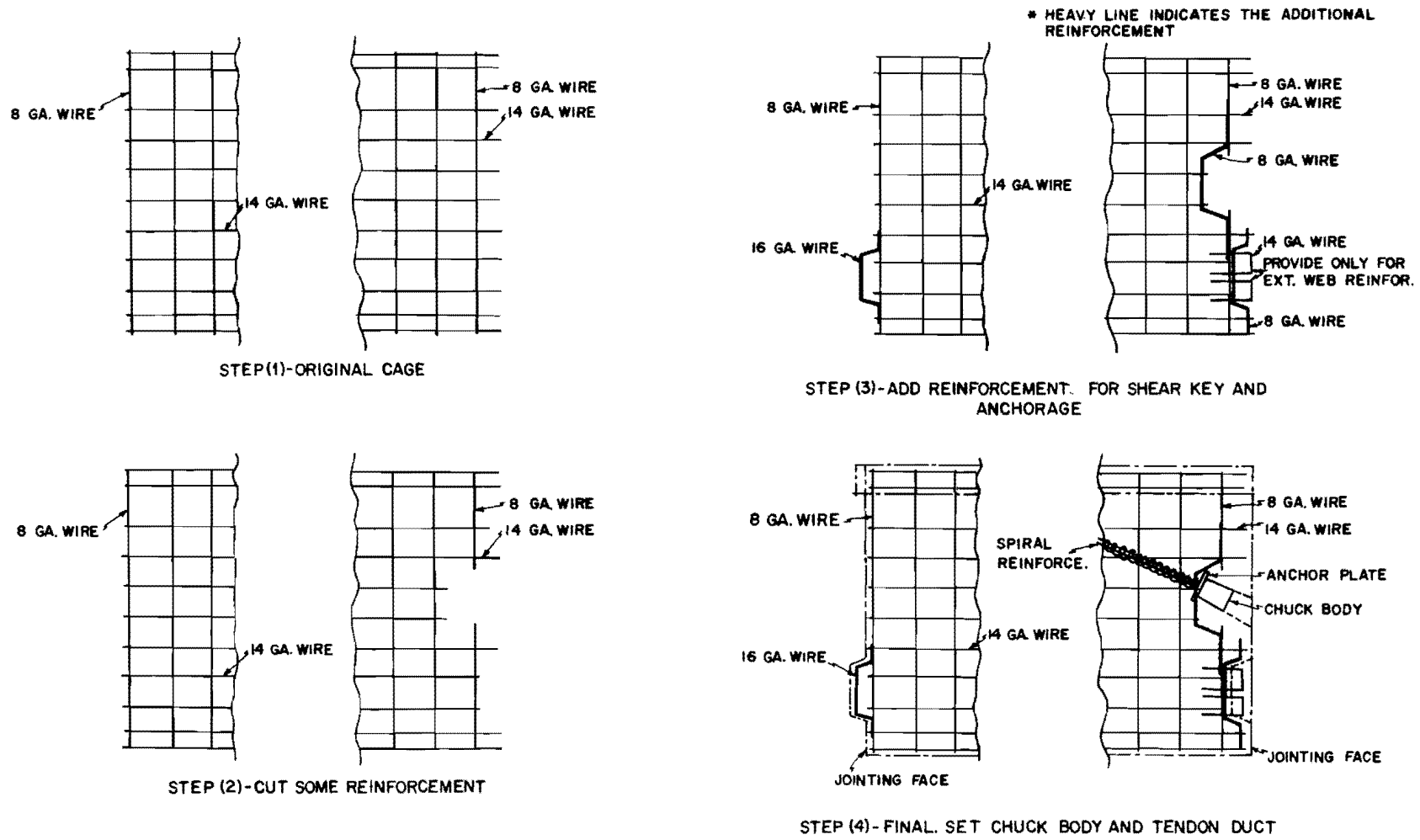
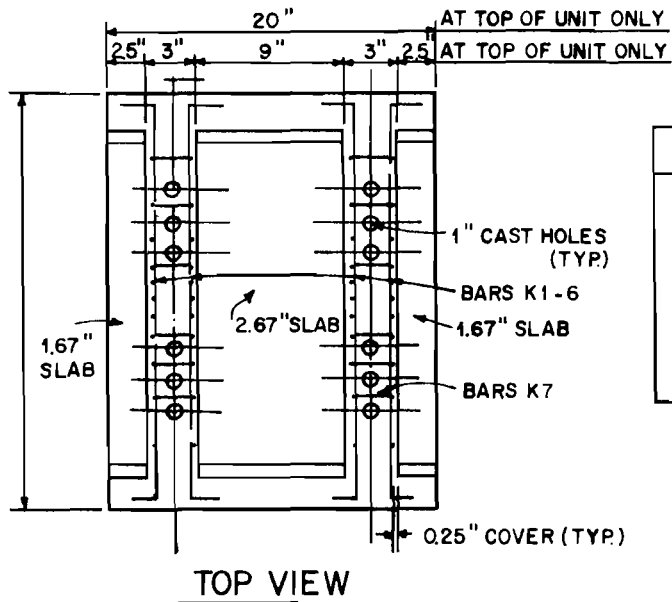
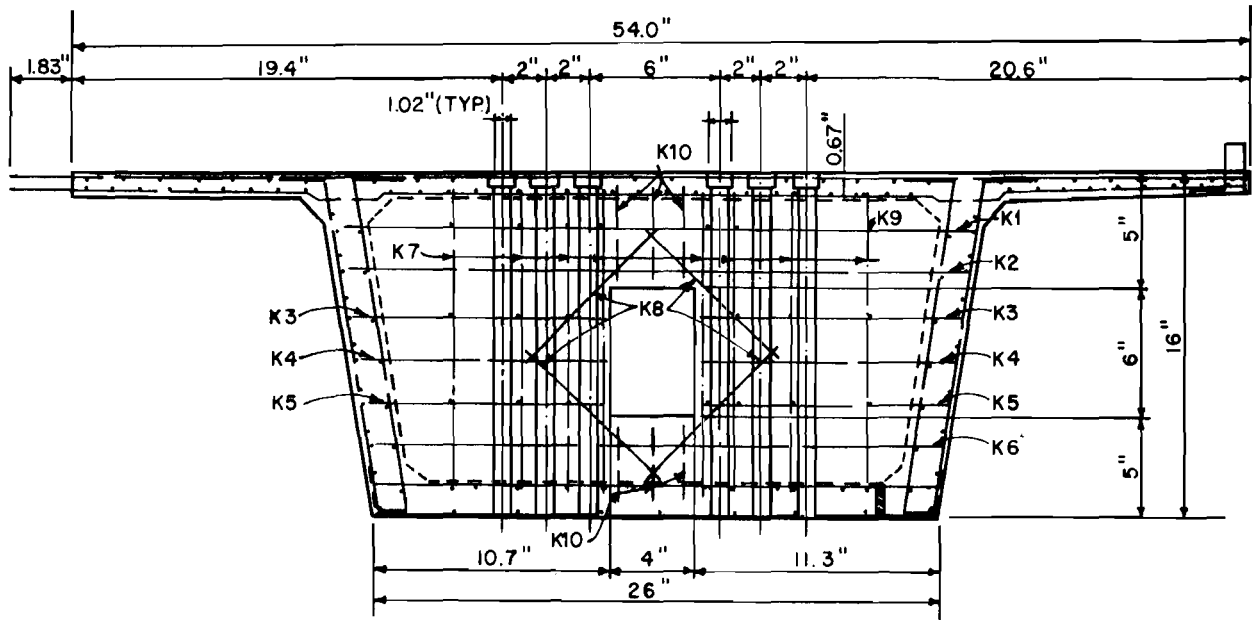


Fig. 4.4. Details of web reinforcement modification



| TYPE OF REINFORCING BAR | |
|-------------------------|--------------|
| K1, K2, K3 | 1/8 IN. WIRE |
| K4, K5 | |
| K6, K8 | 12 GA. WIRE |
| K7, K9, K10 | |

Fig. 4.5. Reinforcement for the main pier segment model

of the anchorage bearing plates shown in Table 4.1 were sized to satisfy the then current ACI² and AASHO⁶ specifications in a preparatory study.¹⁴ The commercial anchorage chuck was welded to the bearing plate as shown in Fig. 4.6. When double tendons in each web were used in the first segments adjacent to the main piers, the area of the bearing plate was doubled and both commercial anchorages were welded to the same plate.

TABLE 4.1. DIMENSIONS OF ANCHORAGE BEARING PLATES

| Cable | Bearing Plate (in. × in. × in.) | Bearing Stress at $0.8f'_s$ (psi) | Allowable f_{cp} (psi) |
|-----------------|------------------------------------|--------------------------------------|-----------------------------|
| 3/8 in. Strands | 1-1/2 × 1/4 × 3 | 4280 | 4390 |
| 7 mm Wire | 1-1/2 × 1/4 × 2 | 4200 | 4410 |
| 1/4 in. Strands | 1-1/2 × 1/4 × 1-1/2 | 3370 | 4390 |
| 6 ga. Wire | 1-1/2 × 1/4 × 1-1/2 | 2700 | 4390 |

During preliminary tests,¹⁴ a tendency for splitting along the tendon was observed, which was restricted by use of a spiral. Even though the bearing plates for the model were conservatively sized and the tendon curvature was not as great as in the preliminary tests, the use of the spiral shown in Fig. 4.6 was adopted as a good detailing practice. Each duct and its spiral were always completely contained inside the reinforcement cages.

4.1.3 Tendon Duct. Polyethelene tubes were used to form the curved ducts in the segments containing the duct anchorages. Steel tubes were used as duct formers in the other straight portions, as shown in Fig. 4.7. Pipes for grouting access were welded to the tendon ducts near the anchorage.

Two different sizes of ducts were used. 7/16-in. diameter (I.D.) was used for the 7 mm wire, 1/4-in. strand and 6 ga. wire tendons, while 9/16-in. diameter (I.D.) was used for the 3/8-in. strand tendons.

* (COMMERCIAL "SUPERIOR"
SINGLE USE)

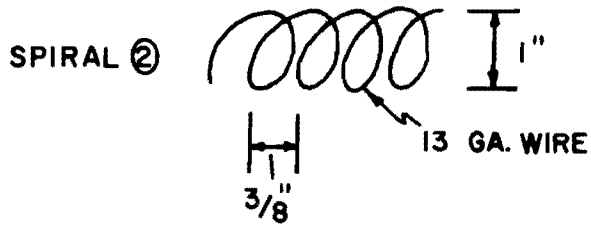
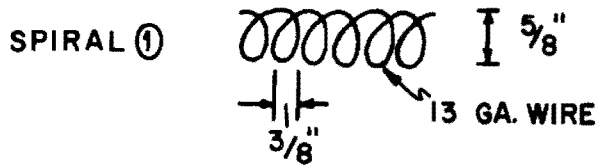
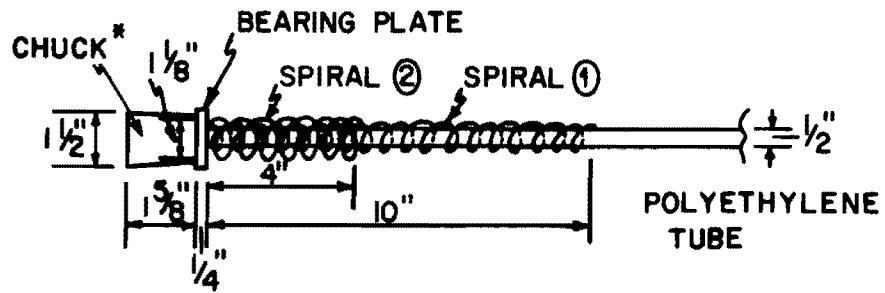


Fig. 4.6. Details of anchorage and spiral reinforcement

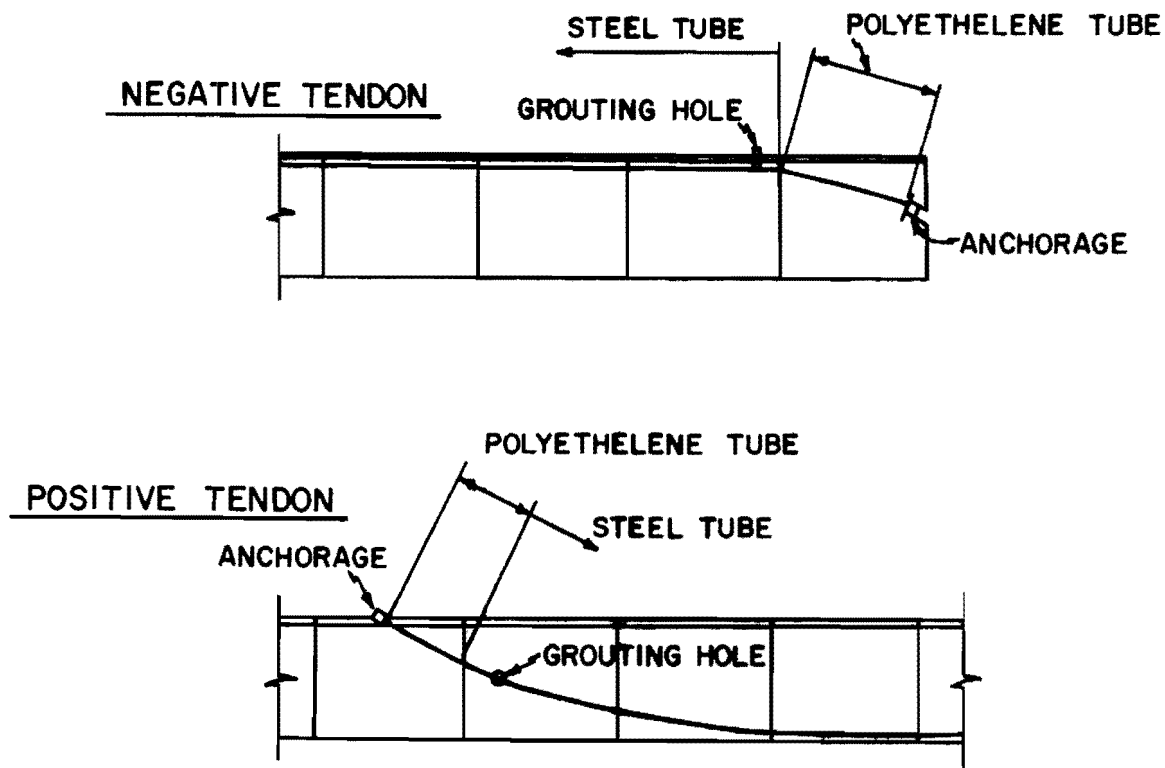


Fig. 4.7. Typical arrangement of tendon duct near anchorage

Figures 4.8 and 4.9 show the profile of the tendon ducts in the main and side spans while Fig. 4.10 shows the detailed profiles of tendon ducts in the curved portions.

4.2 Forms

The accuracy of vertical and horizontal alignment of the segments and the need for segments to fit exactly are key considerations dictating well-controlled match casting. To simplify control, continuous soffit forms were used for the base form and segments were match cast against the segment to which they were going to be joined at the time of construction. Two continuous soffit forms (half the length of the total span of the bridge) were mounted on the test floor, as shown in Fig. 4.11. These soffits were built straight and level within 1/16-in. accuracy.

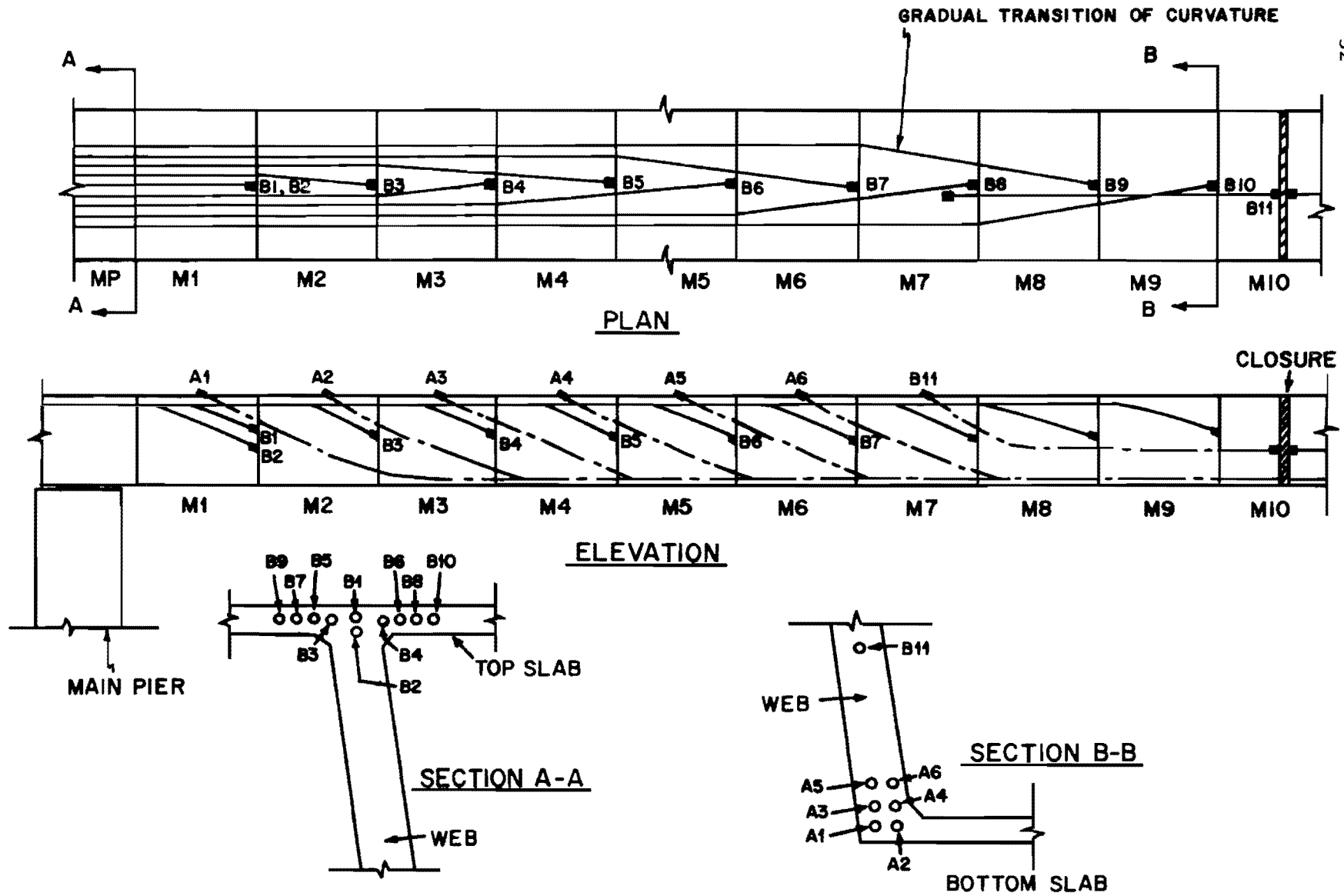


Fig. 4.8. Tendon duct profiles in main span

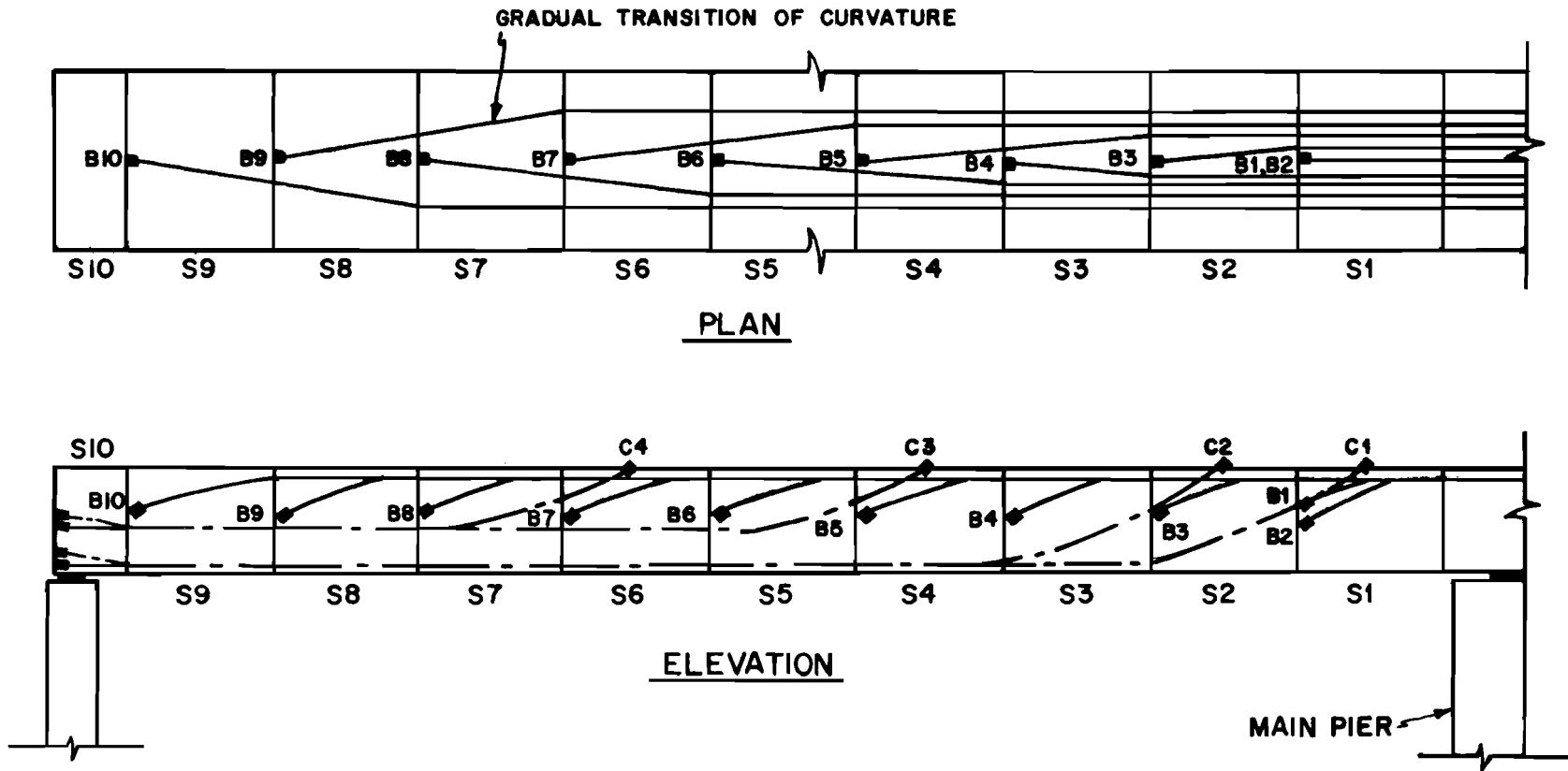


Fig. 4.9. Tendon duct profiles in side span

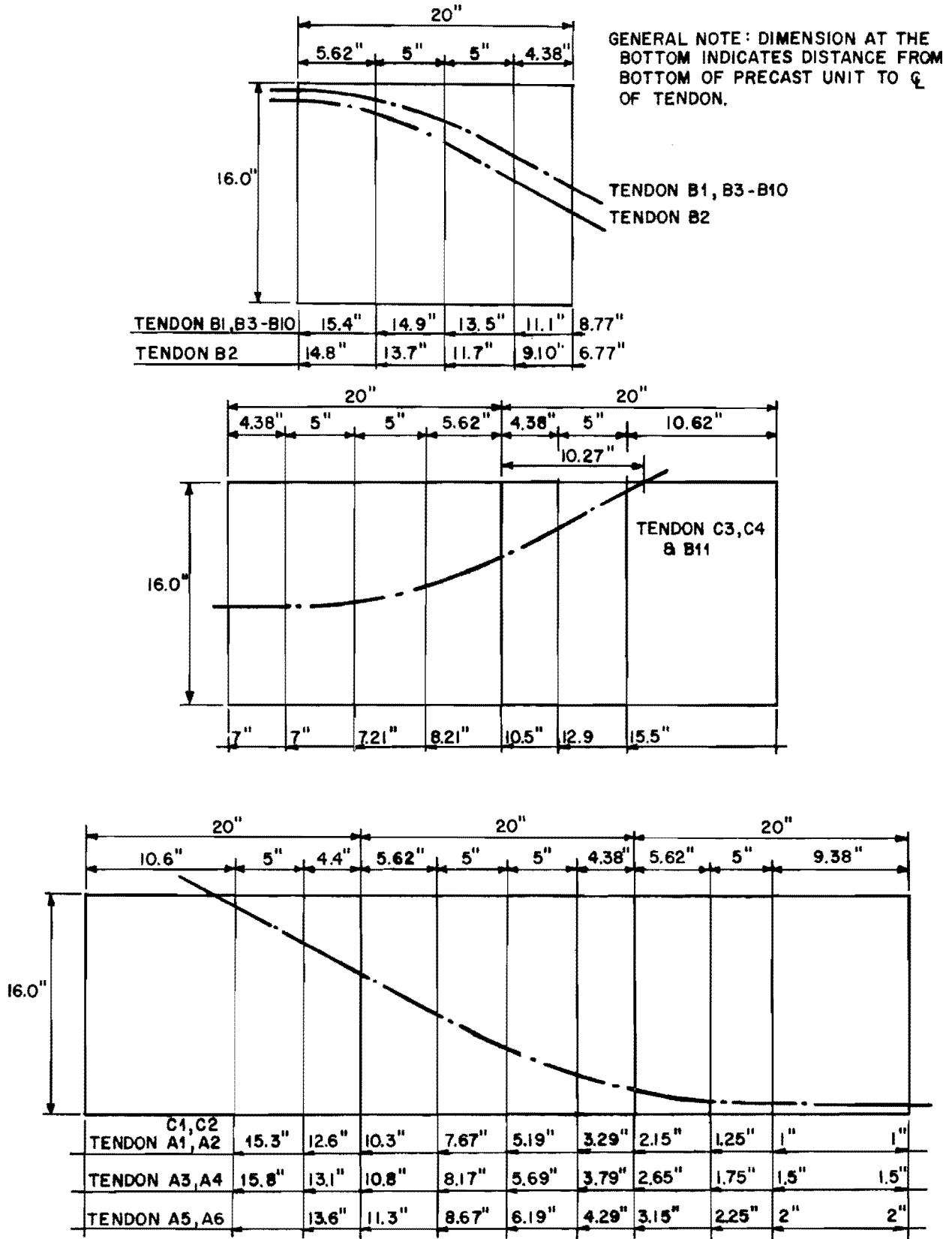


Fig. 4.10. Details of tendon profiles

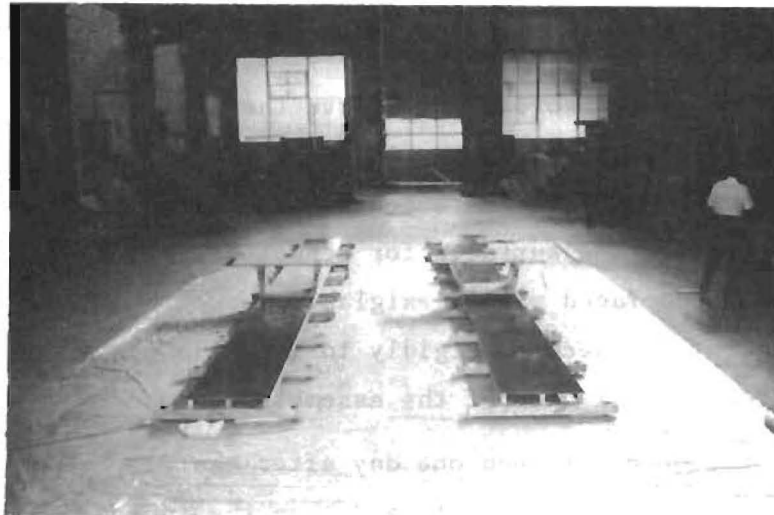


Fig. 4.11. General view of soffit forms

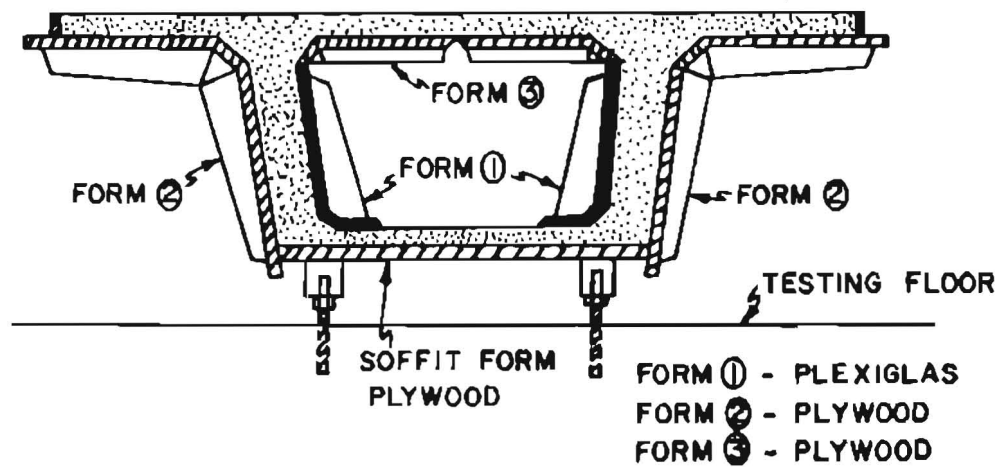


Fig. 4.12. Details of forms for segment

Three materials (steel, plywood, and plexiglas) were considered for segment forms during the planning stage. Steel was abandoned because of high estimated costs. After several trial castings using plexiglas and plywood, stiffened plexiglas (1/4 in. thick) and plywood (1/2 in. thick) were used in combination, as shown in Fig. 4.12. Plywood costs were lowest but the use of plexiglas was desirable for either the interior or exterior side forms in order to observe the flow of concrete in the webs so as to minimize honeycombing in the congested areas around the anchorages. Plywood surfaces were coated with lacquer to simplify stripping and protect the surfaces for repeated use. The end bulkheads were made of plywood faced with plexiglas. These forms were set at the end of the segment and secured rigidly to the side forms with bolts. Figure 4.13 is a general view of the assembled forms.

All forms were stripped one day after casting. End bulkhead and outer sideforms were stripped first and then the inner top form [Form (3) in Fig. 4.12] was stripped by folding the joint at the center. Then the interior side forms were stripped. These forms were moved ahead as each segment was cast against the previous segment. Most segments were not separated until all segments on the soffit were cast in order to simplify maintenance of overall tolerances. A few of the initial segments cast were separated early to check the adequacy of the bond breaking compound.

4.3 Strain Instrumentation in Segment Reinforcing Cages

Since the main purpose of this study was to document the behavior of critical sections during various stages of **construction** as well as during the loading tests, strain gages were primarily placed in the first segments next to the main piers and at the center of the main span.

Although it was possible to mount strain gages directly on the wires of the cage, because of the difficulty of protecting the gages during cage preparation and handling it was decided to mount strain gages on "extensometers" consisting of separate 10 in. lengths of 0.1-in. diameter wire and to connect these to the cages at certain positions.

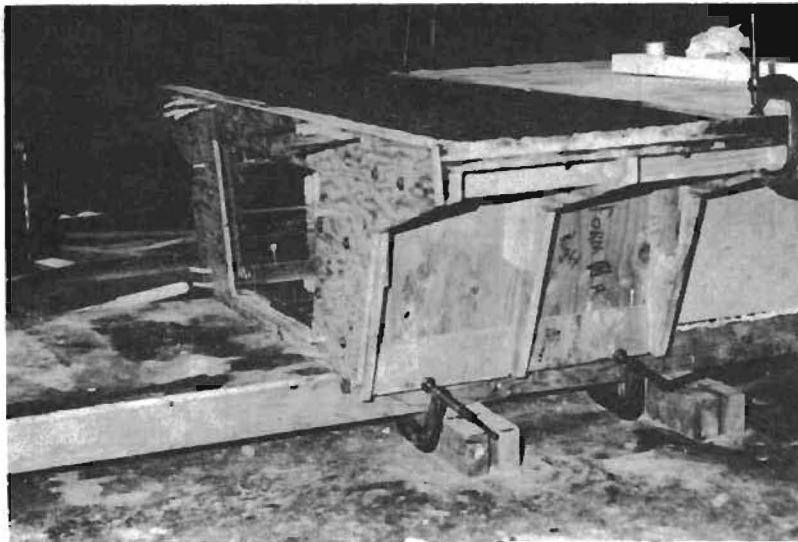


Fig. 4.13. General view of assembled forms

The bars with strain gages were positioned longitudinally underneath the top mat in the upper slab and on top of the bottom mat in the lower slab. Strain gages could not be successfully placed on the transverse bars of the cage to measure transverse behavior in the segments due to the thin cover and difficulty of casting concrete to proper thickness. Transverse paper gages were applied to the concrete surface of the segments at required positions before the loading tests.

Four types of gage installation patterns were used with the segments. The position of strain gages for each pattern and the pattern used in each particular segment location is shown in Fig. 4.14.

4.4 Casting Procedure

Usually four segments were cast per day, with two segments cast on each continuous soffit form. The order of casting on the continuous soffit form is shown in Fig. 4.15.

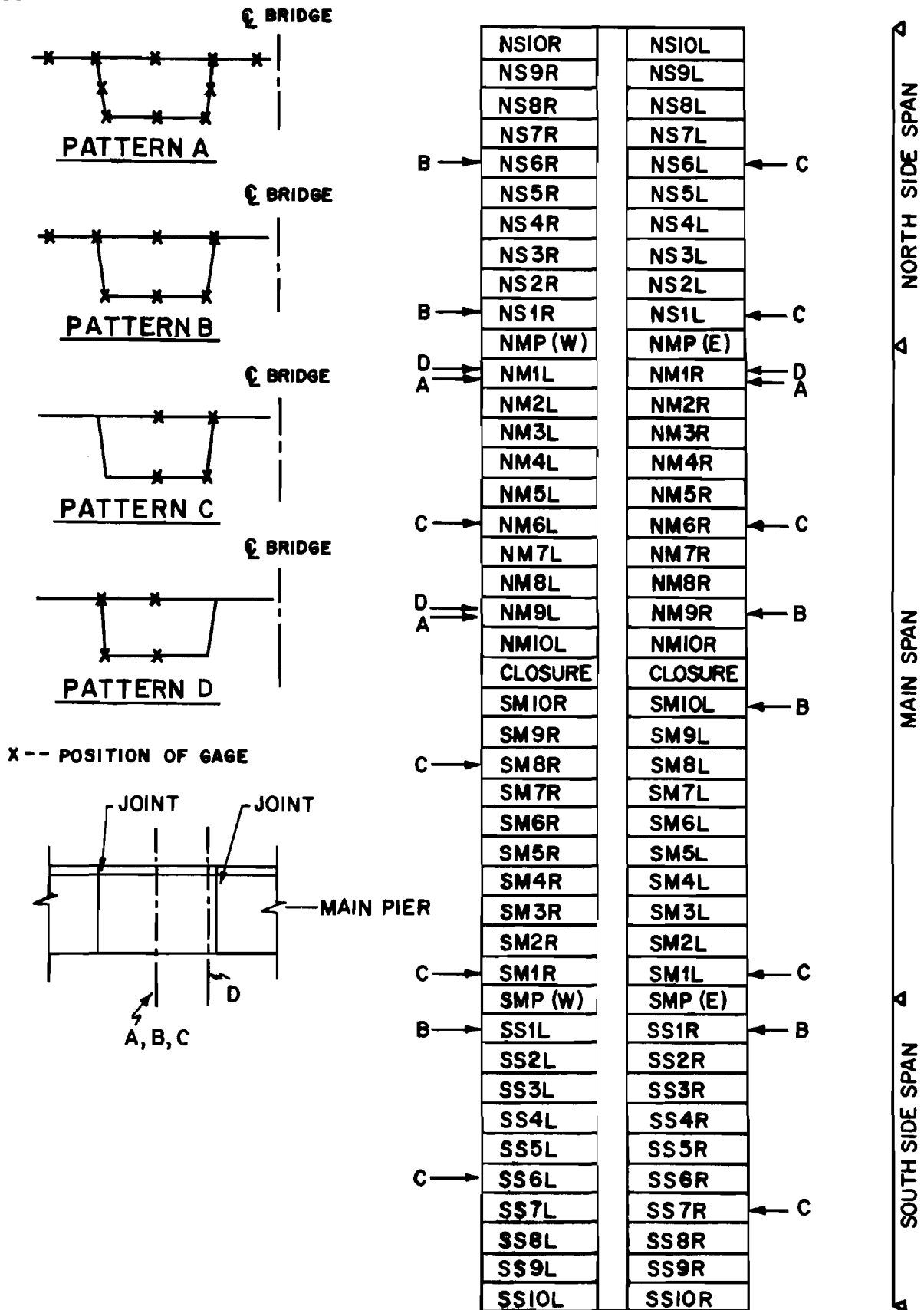


Fig. 4.14. Position of strain gages in segments

| | | | | | | | | | | | | | | | | | | | | |
|-----|----|----|----|----|----|----|----|----|----|----|----|----|----|----|----|----|----|----|----|-----|
| S10 | S9 | S8 | S7 | S6 | S5 | S4 | S3 | S2 | S1 | MP | M1 | M2 | M3 | M4 | M5 | M6 | M7 | M8 | M9 | M10 |
| 10 | 9 | 8 | 7 | 6 | 5 | 4 | 3 | 2 | 1 | 11 | 1 | 2 | 3 | 4 | 5 | 6 | 7 | 8 | 9 | 10 |

Fig. 4.15. Sequence of casting segments

For the first segment, the two bulkheads were set at carefully determined distances. Subsequently the forms were moved ahead, and each segment was cast against the previously cast segment.

The preparation for casting segments after the first segments was as follows:

- (1) Remove all forms.
- (2) Clean the surface of the previous segment and grind off the excess tendon duct. Seal the anchorage holes of previous segment with styrofoam.
- (3) Clean all parts of forms and put on coating of lacquer.
- (4) Put bond breaking compound on the outer face of the hardened segment one day before the next casting.
- (5) Set reinforcing cage on the soffit form adjacent to the previous segments.
- (6) Set chucks and polyethelene duct in curved portion, and set steel duct in straight portion.
- (7) Set the end bulkhead into position and adjust all tendons in the proper holes of the bulkhead.
- (8) Put caulking compound along the joints of forms and set both inner and outer side forms into position. Position the interior form for the top slab. Bolt all side forms to the bulkhead and soffit forms.
- (9) Place polyethelene blockouts for pass through openings for attachment of dead load blocks and for web openings for use in separation and temporary prestressing operations.
- (10) Install bracing for interior side forms.

All web concrete was placed through the top of the web and the side form was filled from bottom to top and consolidated to eliminate any honeycomb effect. A vibrator was used carefully for this consolidation while

the web was observed through the interior plexiglas form. Although many ways of vibrating the web concrete were tried, it was concluded that the most effective way was to vibrate directly on the cage of the top slab over the web. Before casting the web portion, blocks were set between the webs and the bottom slab to prevent the flow of concrete from the web portion to the bottom slab. The bottom slab was cast after completing the casting of the webs and then the blocks between the webs and bottom slab were removed. The top slab was cast last. After casting the entire portion, the top slab was coated with a membrane coating compound to prevent shrinkage cracks.

After completing all casting of 21 segments on a soffit form, each segment was separated by using four small rams. Figure 4.16 shows the position of rams. Although it would be possible to develop the forces to separate the segments by hand, usage of rams to equalize forces minimized local concrete damage at the shear keys on the webs and the guide keys of the top and bottom slabs. In most cases, the force actually applied on each ram was less than 0.4 kips.

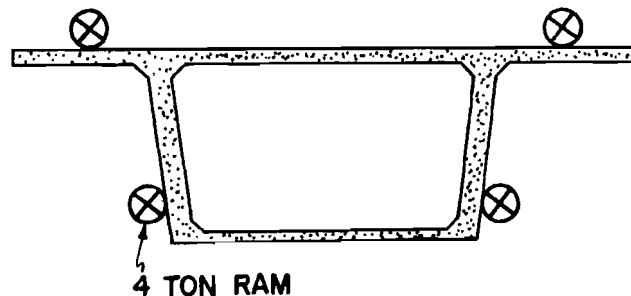


Fig. 4.16. Position of rams for separation of segment

4.5 Curing of Segments

Because the sequence used in casting and construction was the same, all segments except the pier segments were erected five to six months after

casting. The segments were air cured at $75 \pm 3^{\circ}\text{F}$ until they were steam cleaned.

4.6 Surface Preparation of Segments

Surface preparation of the joint faces is necessary to ensure a good epoxy joint between segments. The order of surface preparation was as follows:

- (1) The segments were checked to make sure that the tendon ducts did not extend beyond the joining surface of the segments.
- (2) Excess concrete and sealing material were taken out using a hand grinder (No. 4 in Fig. 4.17).
- (3) Light grinding of the joint faces was accomplished using a small grinder connected to an electric drill (No. 3 in Fig. 4.17) in lieu of sandblasting.
- (4) If the stressing jack seating attachment would not set on the chuck body smoothly, the holes for the seating attachment at the anchorages were enlarged by drilling, using No. 5 shown in Fig. 4.17.
- (5) Chucks were cleaned using a wire brush connected to an electric drill (No. 2 in Fig. 4.17).
- (6) Segments were steam cleaned and rust was removed from chucks and steel ducts. Steam cleaning was used because it was found that form oil had been used in error on the bulkhead before casting for a few of the segments. The effect of oil was eliminated by steam cleaning, as reported in Ref. 19.

4.7 Compensation Dead Load for Model Bridge

To satisfy similitude requirements and to obtain the same dead load stress conditions as the prototype bridge, it is necessary that the density of a one-sixth scale model material be six times that of the prototype bridge. This is impractical to implement.

Compensating dead loads have been added in various ways for model structures.^{1,12} In this case, five times the weight of the model segment was added to the segments using concrete blocks, as shown in Fig. 4.18.

All dead load blocks were distributed to represent the weight of each portion and to give reasonable transverse as well as longitudinal

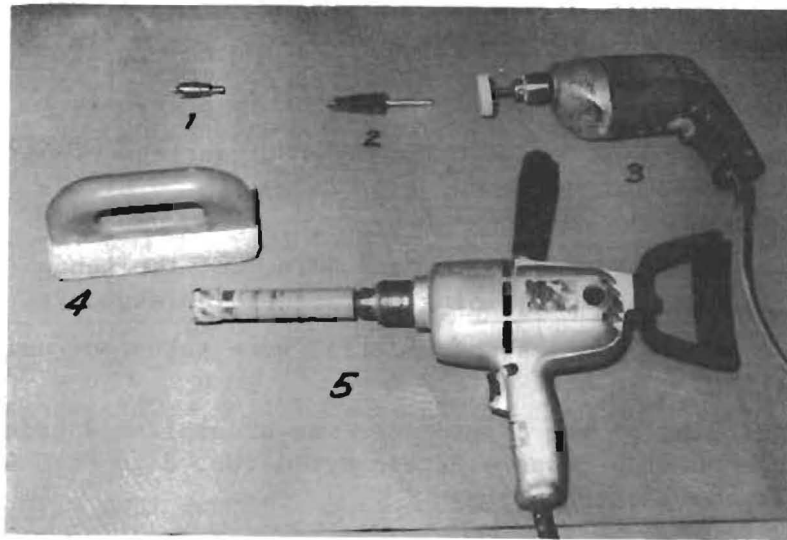


Fig. 4.17. Tools used for surface preparation

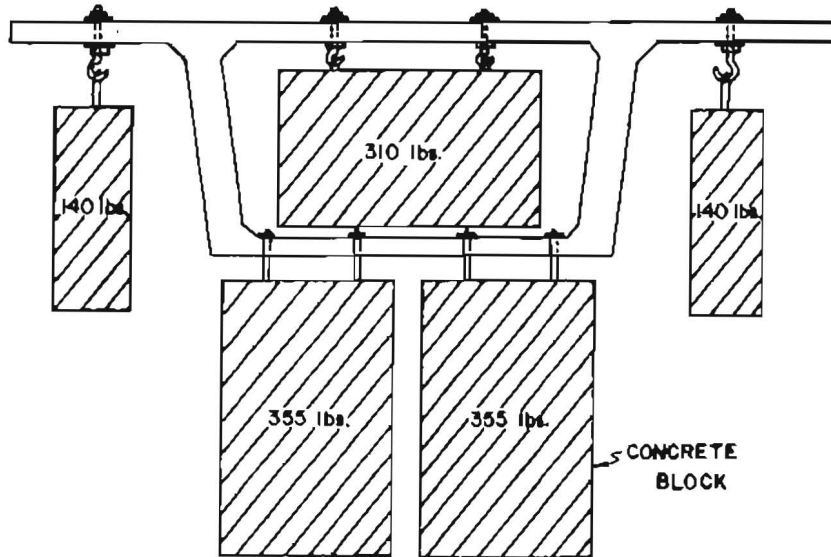


Fig. 4.18. Compensating dead loads for the model bridge

distribution. Two 140 lb. blocks were used for the top slab cantilever portions, a 310 lb. block was used for the interior top slab, and two 355 lb. blocks compensated for the webs and bottom slab, as shown in Fig. 4.18.

Four points were used to support the 310 and 355 lb. dead loads and two points were used for the 140 lb. blocks, since the additional dead weight could not be placed uniformly. The maximum weight on any loading point was less than 90 lbs. This distribution closely simulates the uniform dead load.

Because of the heavier weight of the thicker slabs in the segments adjacent to the main piers, it was theoretically necessary to hang 70 lbs. more weight on them. However, this minor effect was ignored and the same compensating dead weights were hung uniformly on all segments.

4.8 Actual Properties of the Model Bridge

All experimental material properties and measured as built section properties of the model bridge are summarized in Table 4.2. Those values were used in the theoretical calculations.

TABLE 4.2. MATERIAL PROPERTIES AND SECTION PROPERTIES OF THE MODEL BRIDGE

| | HALF SECTION | | FULL SECTION | | | |
|-----------------------------------|---|-------------------------------|------------------------------|--------------------------|-----------------------------|--------------------|
| | MAX. SECT. | MIN. SECT. | MAX. SECT. | MIN. SECT. | | |
| SECTION PROPERTIES OF BOX SECTION | AREA (IN. ²) | 179 | 165 | 363 | 335 | |
| | DIST. FROM TOP TO CENTROID (IN.) | 6.86 | 6.20 | 6.77 | 6.12 | |
| | SECOND MOMENT OF AREA (IN. ⁴) | 6970 | 6060 | 14100 | 12300 | |
| | SECTION MODULUS AT TOP (IN. ³) | 1020 | 977 | 2090 | 2010 | |
| | SECTION MODULUS AT BOT. (IN. ³) | 752 | 611 | 1590 | 1230 | |
| PROPERTIES OF CONCRETE | $E_c = 4.56 \times 10^6 \text{ PSI}$ ($\bar{\sigma} = 0.37 \times 10^6 \text{ PSI}$) $f'_c = 7090 \text{ PSI}$ ($\bar{\sigma} = 523 \text{ PSI}$) $f'_{sp} = 597 \text{ PSI}$ ($\bar{\sigma} = 31 \text{ PSI}$) $\mu = 0.184$ ($\bar{\sigma} = 0.016$) | | | | | |
| PROPERTIES OF PRESTRESSING CABLES | | REQUIRED 0.6 F_s' (KIPS) | EXPERIMNTL. F_s' (KIPS) | A (IN. ²) | EXPERIMNTL. f'_s (KSI) | E_s (PSI) |
| | 3/8 IN. STRANDS | 13.75 | 22.4 | 0.085 | 259 | 27.0×10^6 |
| | 7 MM. WIRE | 8.94 | 15.3 | 0.0594 | 258 | 30.5×10^6 |
| | 1/4 IN. STRANDS | 5.46 | 9.18 | 0.0356 | 257 | 27.0×10^6 |
| | 6 GA. WIRE | 4.13 | 8.12 | 0.029 | 280 | 30.9×10^6 |

CHAPTER 5

INSTRUMENTATION AND DATA REDUCTION

5.1 General

Load cells, pressure gages, strain gages, surveyor's level, and dial gages comprised the instrumentation used for the model study.

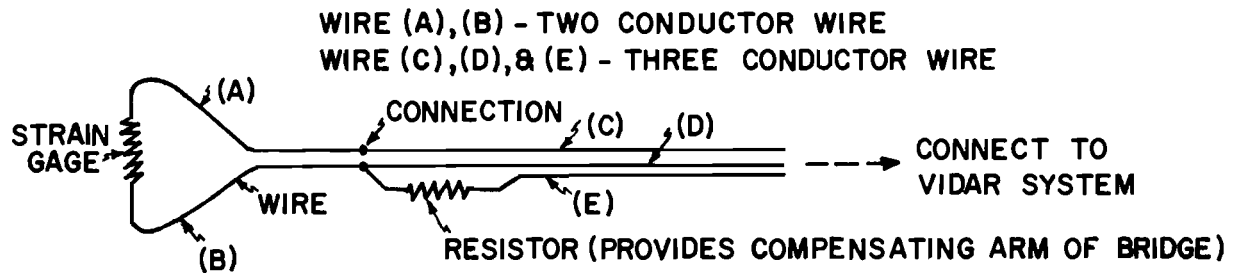
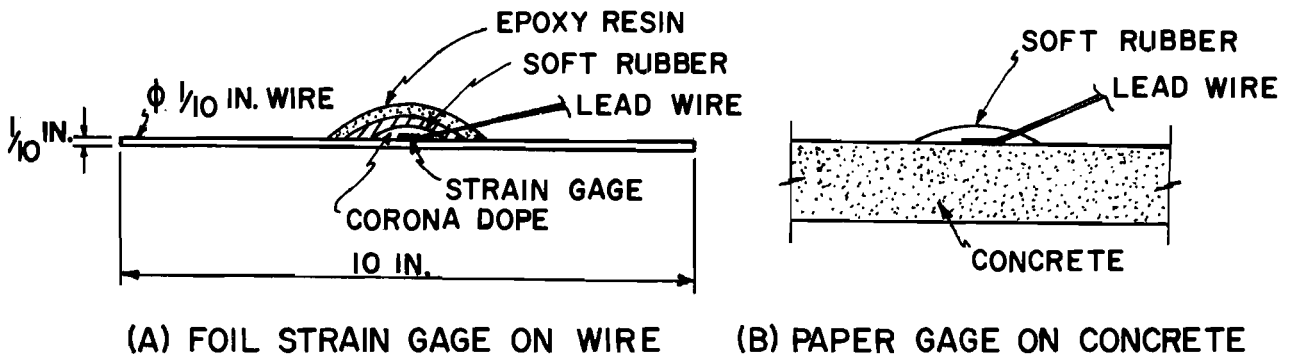
5.2 Load Cells and Pressure Gages

Prestressing forces during construction and live loads for the completed structure were applied by hydraulic rams. Strain indicators connected to load cells were the primary control for forces applied. Calibrated hydraulic pressure gages were used for checks of the applied forces.

5.3 Strain Gage Instrumentation and Data Reduction

Two types of strain gages were used for the model bridge: Foil strain gages were used on the steel wires and paper gages were used on the surface of the concrete (see Sec. 4.3).

One-quarter in. long foil strain gages were mounted on 0.1 in. diameter \times 10 in. long steel wires, as shown in Fig. 5.1(a). These strain gages were waterproofed and rarely failed even if they were kept in a segment more than one year. Eight-tenths in. long paper gages were put on the smooth surface of the concrete prior to loading tests [Fig. 5.1(b)]. Two short wires were connected to the strain gages in the segment. Then three conductor wires were connected to two conductor wires, as shown in Fig. 5.1(c). Because of the use of three conductor wires, the effect of temperature change in the long leadwires was eliminated. These three conductor wires were connected to the VIDAR digital data acquisition system.³⁷ The VIDAR system is able to scan rapidly and autorange with



(C) CONNECTION BETWEEN TWO AND THREE CONDUCTOR WIRE

Fig. 5.1. Strain gage instrumentation

1 microvolt resolution. Output from the system can be either teletype, punch paper tape, or magnetic tape. Figure 5.2 shows the VIDAR system and teletype. Data outputs were put into permanent file in the computation center and were reduced by the data reduction program SPEED.⁸

5.4 Surveyor's Level and Dial Gages

A surveyor's level and dial gages were used to measure deflections during construction and loading tests. Accuracy of the level readings was 0.01 in. and of dial gages within 0.0005 in.



Fig. 5.2. VIDAR system and teletype

This page replaces an intentionally blank page in the original.

-- CTR Library Digitization Team

C H A P T E R 6

CONSTRUCTION OPERATIONS AND OBSERVATIONS

6.1 Construction Procedure

6.1.1 General. The following is an outline of the steps followed in the model bridge erection and closure:

- (1) Pier segments were temporarily fixed to the piers using bolts tightened to a predetermined torque.
- (2) The precast segments were sequentially erected using the cantilever construction method with epoxy joints.
- (3) The bolts at the pier were temporarily slackened and the vertical and horizontal alignment was adjusted after completion of the erection of precast segments 1 through 9. The bolts were then retorqued.
- (4) The outer pier segments (S10) were erected and the positive moment tendons in the side spans were prestressed.
- (5) The half segments (M10) in the main span were erected. The longitudinal reinforcement extending across the midspan gap from each of the half segments was joined and the concrete closure segment was cast.
- (6) The positive tendons in the main span were inserted and tensioned after 7 days of curing of the closure segment. The bolts temporarily fixing the segments to the main piers were released during the positive tendon stressing operation.
- (7) The bridge was lowered to final position on neoprene pads on the piers.
- (8) The correct reactions were jacked into the outer piers.

6.1.2 Construction of Piers. Because the pier height of the prototype bridge was 90 ft. and complete pier similtude was not a requirement of the study, the full height of the pier was not scaled in the model. The reduced pier height for the model bridge was set at 55 in. to allow adequate space below the model for insertion of compensating dead load blocks. However, the general cross section of the prototype piers (see Appendix A) was used at one-sixth scale. Figure 6.1 shows the reinforcing bars for an inner pier model. The piers were carefully set in correct position prior to casting of concrete. In order to prevent overturning of the piers under unbalanced loading, I-beams were welded to the pier base and tied down to the testing floor, as shown in Fig. 6.2.



Fig. 6.1. Reinforcement of the main pier

The completed pier with the bolts for temporary connection of pier segments and the neoprene pads for final bearing is shown in Fig. 6.3. The bolts and neoprene pads were scaled down to one-sixth actual size. The diameter of the bolts in the model was 1/2 in. and the size of the neoprene pad was $4\frac{1}{6} \times 7 \times \frac{1}{4}$ in. Dimensions of the bearing plates used to restrain or support the pier segments at the top and bottom faces for each 6-bolt group were $4 \times 16 \times \frac{1}{2}$ in.



Fig. 6.2. Connection of pier to the testing floor

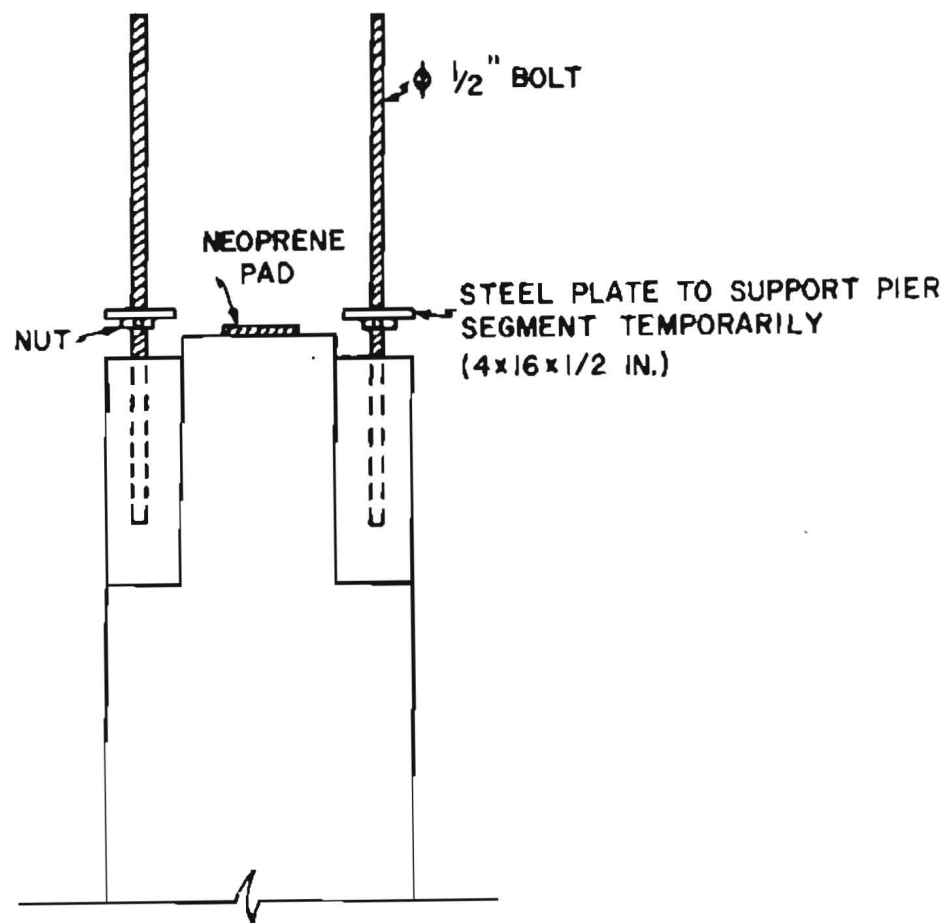


Fig. 6.3. Detail of support at main pier

6.1.3 Erection of Pier Segments. It is very important to set the initial horizontal and vertical alignment of the pier segments as correctly as possible in order to minimize adjustments of the two separate cantilever sections prior to the closure operation. Adjustment of the vertical alignment was made prior to setting the pier segment by turning the nuts under the steel plates shown in Fig. 6.3. For erection of the first half of the bridge, the horizontal alignment of the pier segments was carefully judged by eye and was later considered inaccurate. In erection of the second half, the horizontal alignment of each pier segment was carefully adjusted using a positive reference line formed by a piano wire stretched between each pier segment. This procedure was far more satisfactory.

The mechanism for anchoring each pier segment consisted of 12-1/2 in. diameter bolts and 1/2 in. thick steel bearing plates. The pipes which formed vertical ducts in the pier segments to pass over the 1/2 in. diameter bolts had a 1 in. inner diameter, so that there was adequate play to allow adjustment of the horizontal alignment. After initial alignment of the pier segments, the anchor bolts were tensioned to approximately 1 kip each, using a torque wrench. The gap between the segment and the neoprene pad on the main pier was set at 1/4 in. for the first half of the bridge. However, a gap of 3/4 in. had to be used for the second half to minimize later vertical adjustment in order to match the first half of the bridge. Figure 6.4 shows a general view of the pier segment on the pier

6.1.4 Erection of Segments during the Cantilever Stages.

6.1.4.1 General. Possible erection methods for precast concrete cantilever construction over water may be classified as follows:³⁰

- (1) Segments floated in on barges with barge-mounted crane erection.
- (2) Segments floated in on barges but erected using lifting equipment supported on the previously erected cantilever segments.
- (3) Transportation of segments on the structure itself with a large launching gantry used to place segments.

The cost of erection equipment for method (3) was considered too expensive and not necessary for the prototype bridge. Erection methods

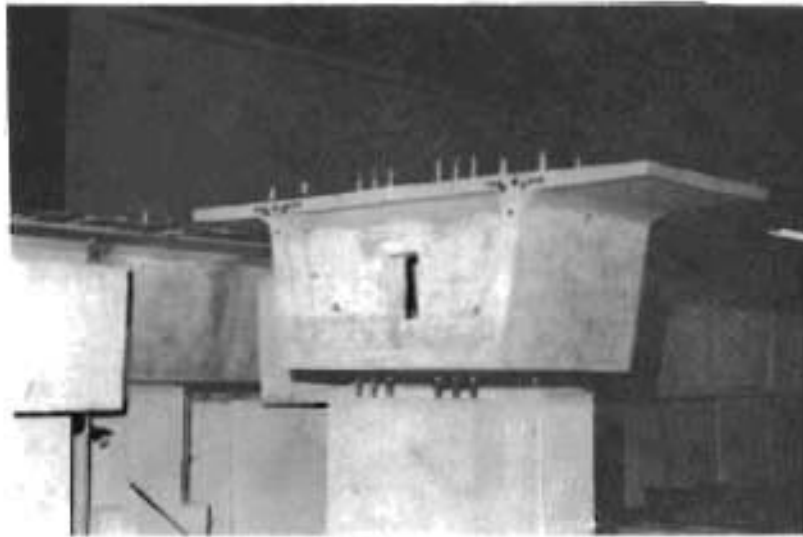


Fig. 6.4. General view of the pier segment on the main pier

(1) and (2) were both considered practical for this prototype. Since contractors had the option to use either method, both were simulated in the model bridge erection. During the majority of the model bridge erection, segments were lifted by various overhead cranes, as shown in Fig. 6.5. These cranes were not supported on previously erected segments. The units were connected temporarily by mechanical devices (Fig. 6.6) to ensure correct seating and were then prestressed. This mechanical device was designed to prevent any movement at the joint until stressing started and could not affect the prestressing force applied by the cables. However, in a number of cases, lifting equipment was used which simulated light cranes mounted on the previously erected cantilever structure (Fig. 6.7). The weight of a crane was about 370 lbs. (13.3 kips in the prototype).

6.1.4.2 Details of Segment Erection. Two segments were usually erected per day. However, it was not difficult to erect four segments per day with proper preparation and adequate labor availability. All erection work was done in the afternoon to minimize the effect of temperature change on instrumentation. Temperature and humidity during the time of erection

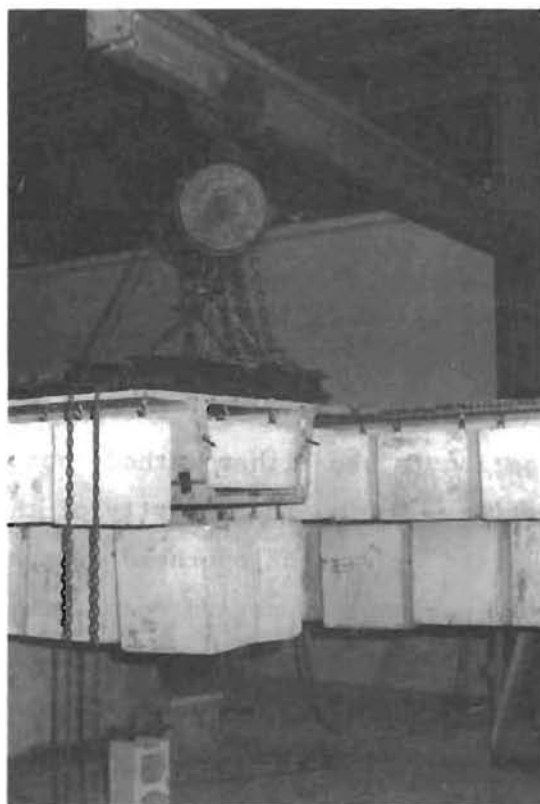


Fig. 6.5. Typical independent crane used for erection of segments

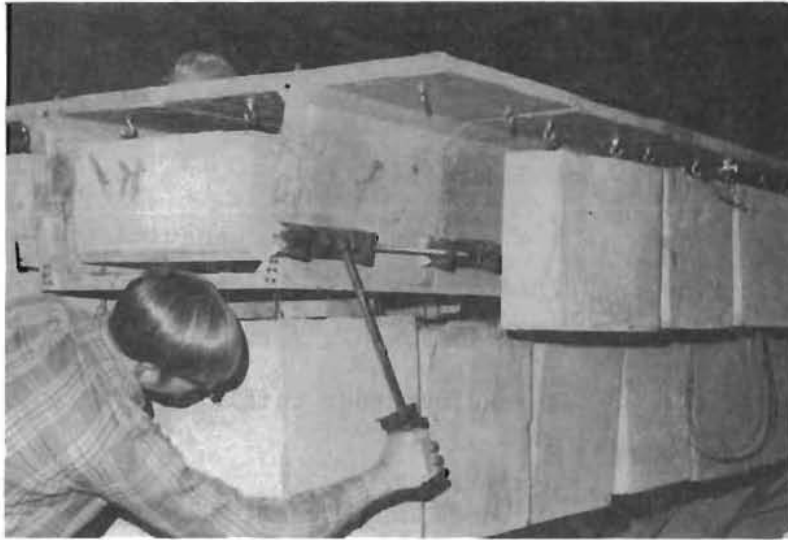


Fig. 6.6. Mechanical device for temporary joining

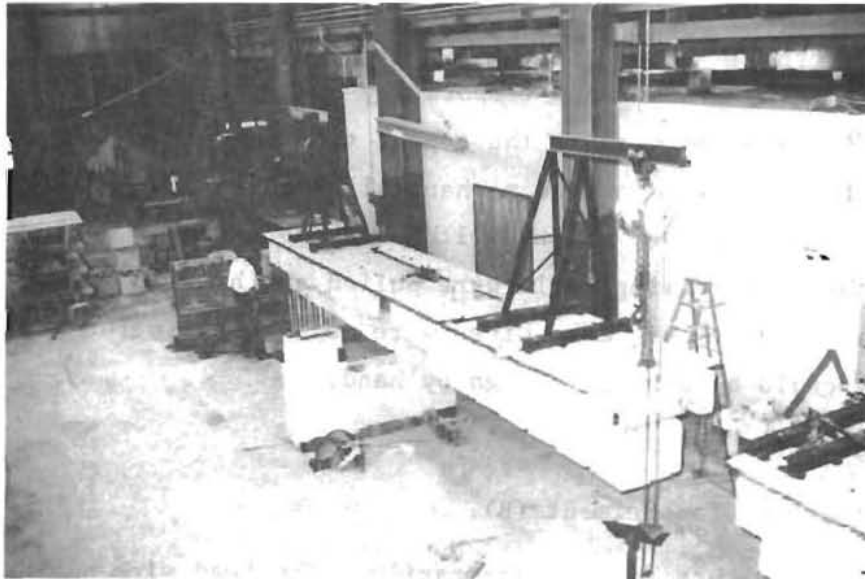


Fig. 6.7. Typical structure supported cranes used in some cases

varied between 75 - 90°F and 50 - 70 percent RH, respectively. All segments of one longitudinal box girder were erected completely before cantilevering started on the other box girder.

Details of the erection procedure were as follows:

- (1) Lead wires of any implanted strain gages in the unit to be erected were connected to the VIDAR system.
- (2) Two wide flanges (4 x 4 x 50 in.) were connected to the bolts used to support the dead load blocks which pierced the top slab of each segment, as shown in Fig. 6.5.
- (3) Preweighed epoxy resin and hardener sufficient for joining two segments was mixed.
- (4) Prestressing wire or strands were inserted in the straight portion of the tendon ducts (Stage 1 in Fig. 6.8).
- (5) Segment (A) was lifted, the height adjusted and leveled by turn buckles, as shown in Fig. 6.9 (Stage 2 in Fig. 6.8).
- (6) Segment (A) was separated after this adjustment. The joining surfaces were cleaned with acetone and the epoxy resin was spread on both joining surfaces, as shown in Fig. 6.10.
- (7) Segment (A) was clamped temporarily near the lower flange as shown in Fig. 6.6 and also at the top of the segments (Stage 3 in Fig. 6.8). The force applied on the mechanical clamping device was approximately 1 kip each and was checked with a torque wrench. Lead wires connected to the prestressing cable were pulled south until the end of the straight portion. Lead wires were not necessary for the strands as they could be pushed through by hand.
- (8) Same as (5) for Segment (B).
- (9) Same as (6) for Segment (B).
- (10) Segment (B) was joined temporarily. The lead wire was pulled north until the prestressing cable was extended just enough for seating (Stage 4 in Fig. 6.8).

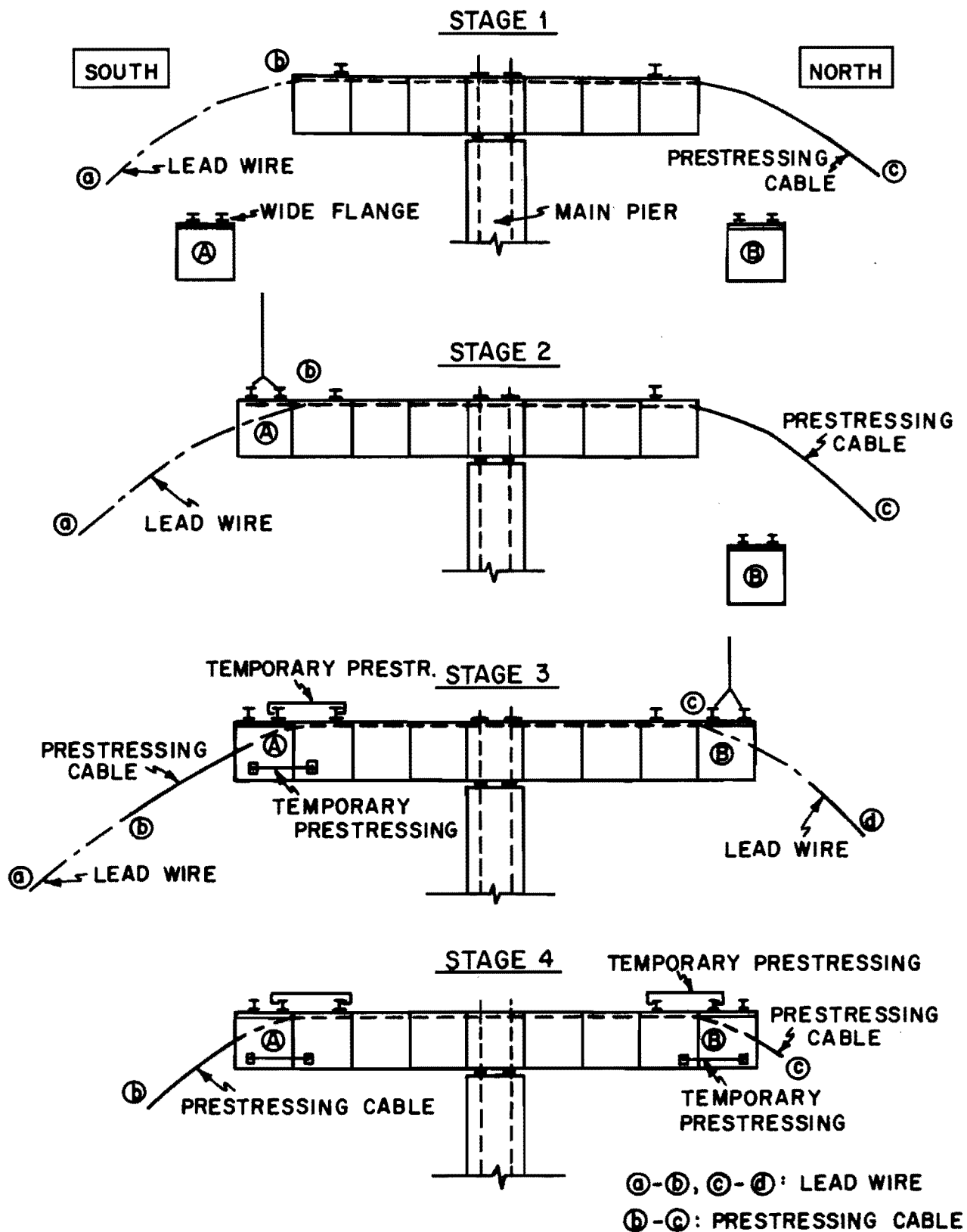


Fig. 6.8. Insertion of prestressing cable

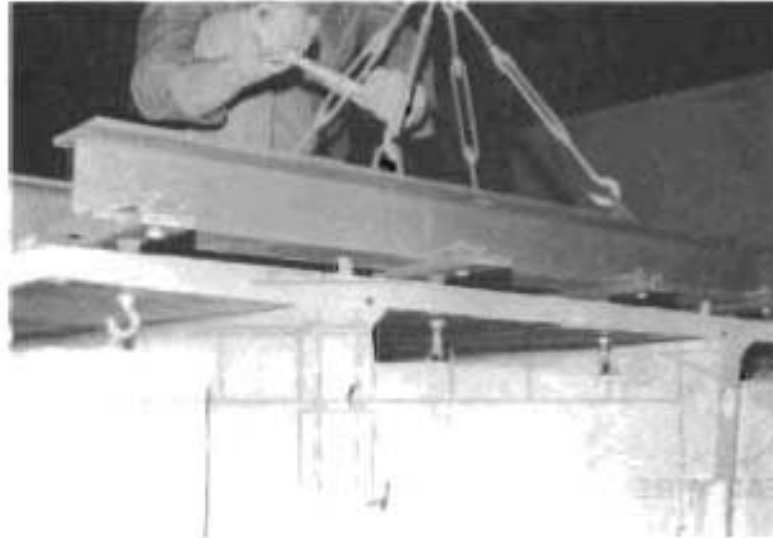


Fig. 6.9. Adjustment of level



Fig. 6.10. Application of the epoxy resin on the joining surface

- (11) The prestressing equipment was set on one end (Fig. 6.11). Details of the prestressing system are shown in Fig. 6.12. Prestressing force was applied using 30 ton hydraulic rams. The amount of force applied was controlled by a load cell. In addition, the prestressing force applied was checked approximately with a pressure gage.
- (12) A prestressing force of $0.8f'_s$ was applied in order to overcome the friction loss and then was dropped to $0.65f'_s$ for seating. Although the prestressing operations must be performed at both ends in the prototype, prestressing force was applied only from one end for the model because of the shorter lengths involved. However, prestressing operations were done alternately at each end. Friction loss tests were performed at various stages, as reported in Sec. 6.2.2.

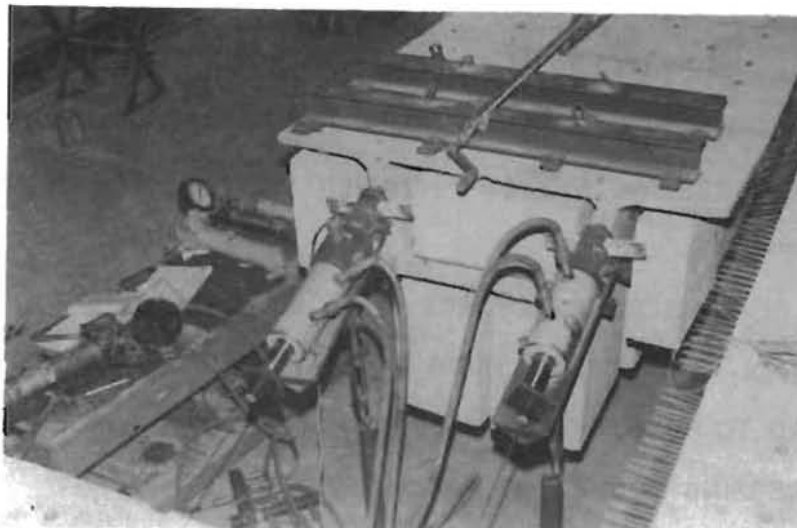
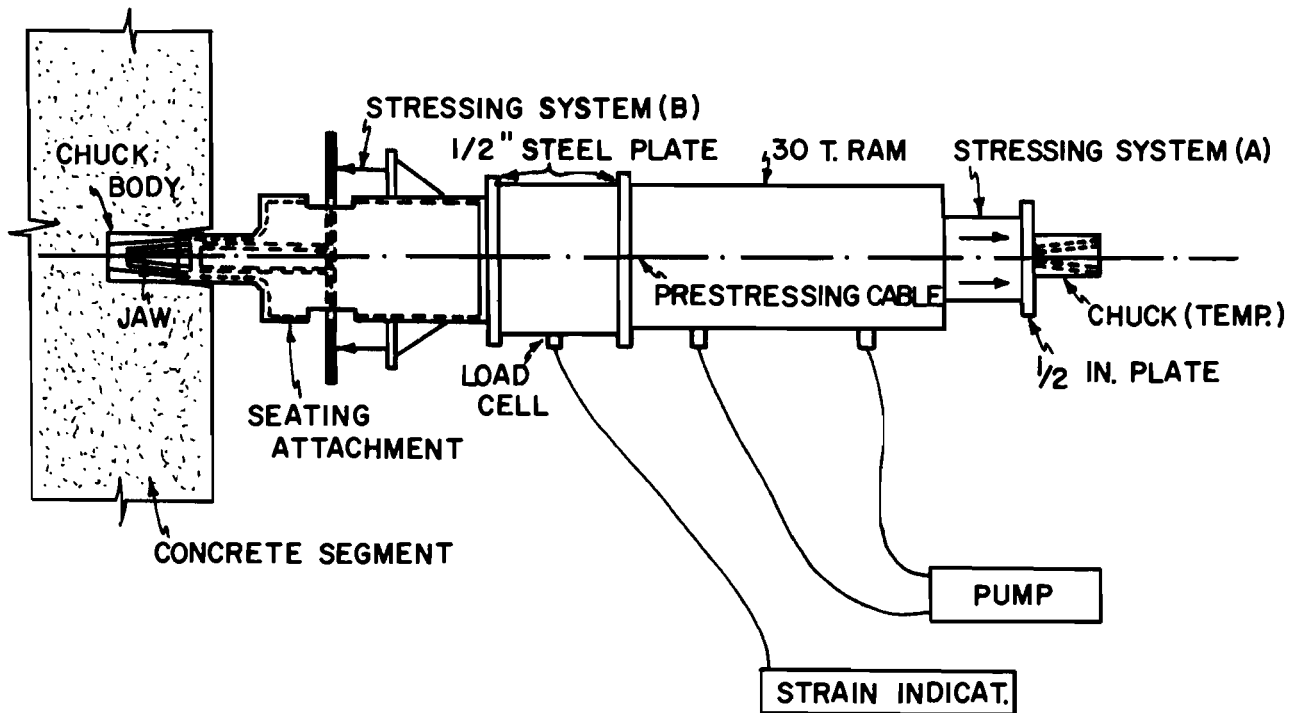


Fig. 6.11. General view of prestressing system for negative tendons



PRESTRESSING PROCEDURES:

- (1) INSERT PRESTRESSING CABLE.
- (2) PUT JAW INTO CHUCK BODY.
- (3) SET SEATING ATTACHMENT, LOAD CELL AND 30 TON RAM.
- (4) INSERT TEMPORARY CHUCK AT THE END OF RAM AND HOLD IN POSITION.
- (5) EXTEND STRESSING SYSTEM (A) UNTIL $0.8 f_s'$ IS REACHED IN PRESTRESSING CABLE.
- (6) DROP THE PRESTRESSING FORCE FROM $0.8 f_s'$ TO $0.65 f_s'$.
- (7) SET SMALL RAMS AT STRESSING SYSTEM (B) AND APPLY 2 TO 3 KIPS OF LOAD TO PUSH THE JAWS INTO CHUCK BODY IN ORDER TO SEAT THE PRESTRESSING CABLE. RELEASE SYSTEM (B).
- (8) RELEASE SYSTEM (A), AND REMOVE SEATING ATTACHMENT, LOAD CELL AND 30 TON RAM.

Fig. 6.12. Details of prestressing system

- (13) Excess prestressing wire or strands protruding from anchors were cut with an electric grinder after seating of the jaws into the chuck bodies. Anchorage holes were filled with epoxy mortar [(Epoxy Resin): (Sand + Aggregate) = 1:1]. These surfaces were ground smooth on the next day.

6.1.5 Correction of Horizontal and Vertical Alignment. Correction of horizontal and vertical alignment was performed after the 9th segment out from each pier was erected because the balanced cantilever sections were still symmetrical and easy to adjust.

The following are the correction procedure steps used:

(a) Horizontal Alignment. There are two possible errors in horizontal alignment which may occur in (twin box) precast segmental cantilever construction, as shown in Fig. 6.13. Points a, b, c, and d in Fig. 6.13 are the center points of the pier segments.

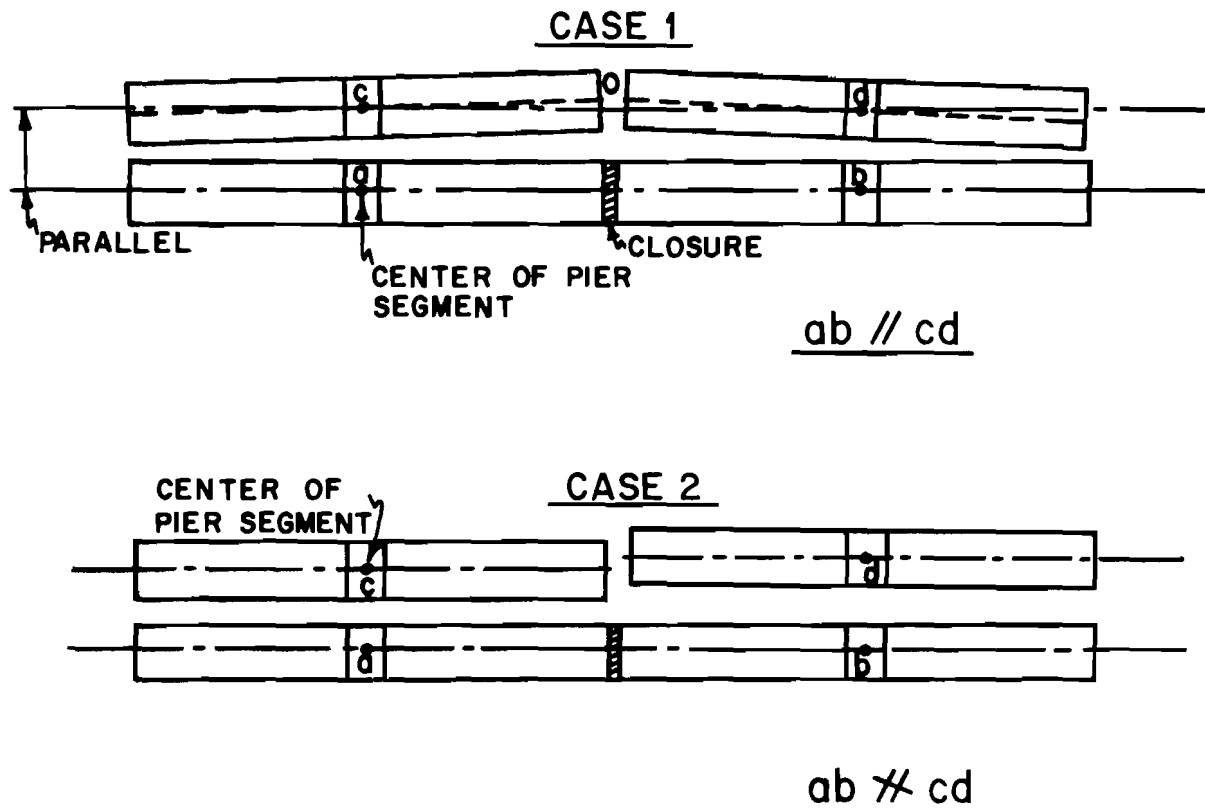


Fig. 6.13. Errors of horizontal alignment

In case (1), lines ab and cd are parallel, but the cantilever sections co and do extending from piers c and d are not in correct horizontal alignment.

In case (2), piers are not correctly positioned and the distances between ac and bd are not equal so that ab and cd are not parallel.

The anchor bolts in the piers were carefully set so that there was no error of the case (2) type in the model.

There was about 3/4 in. of correction for case (1) required at the closure of the two cantilever sections during erection of the first half of the bridge. During the construction of the second half, a piano wire was stretched between the points c and d (in Fig. 6.13) in order to provide a base line for setting the two pier sections. This provided much finer alignment. Less than 1/4 in. of correction was required for the second half of the bridge.

Each cantilever section was adjusted after erection of nine segments so that the center line of each cantilever tip would meet on the base line. In order to adjust the cantilever sections with equipment which could be practically scaled up for the prototype construction, a small channel was connected to the webs of the 8th and 9th segments and was pulled laterally by a ratchet hoist attached to the end pier, as shown in Fig. 6.14. The maximum capacity of the ratchet hoist was 4 kips.

(b) Vertical Alignment. There are three possible errors in vertical alignment at the closure of the two cantilever sections. They are:

- (1) Errors due to incorrect initial adjustment of the nuts supporting the pier segments.
- (2) Errors due to variations in height of the soffit at the time of casting.
- (3) Errors in joint widths at the time of cantilever erection.

It had been predicted in the design²¹ that a small tensile stress would occur on the bottom fiber at a distance of 30 in. from the pier center (at the joint between the 1st and 2nd cantilevered segments), when

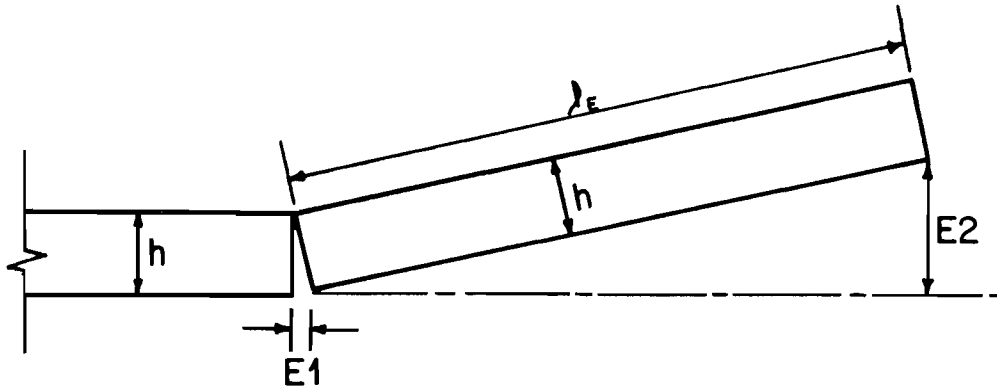


Fig. 6.14. Adjustment of horizontal alignment

the cantilever arm length was 50 in. and 70 in. In the erection of the first half of the bridge, definite jointing errors occurred because of omission of the temporary prestressing system at the bottom of the segment to counteract these tensile forces during erection of the first several segments. Design and construction procedures should ensure that there is no tension on any epoxy joints during the cantilever erection. There were other probable minor errors in the first few joints before crew experience was obtained as well as possible errors due to variation in the height of the soffit. Therefore, substantial vertical adjustment had to be done at the end of the cantilever erection.

Jointing errors in the early stages of cantilever erection accumulate and are magnified at the end of the cantilever, as shown in Fig. 6.15.

Although the second box of the bridge was constructed with almost no vertical error, adjustment of vertical alignment was necessary to provide a way to cast the longitudinal closure with the previously constructed box.



$$E2 = \frac{\lambda_E}{h} \times E1$$

where,

h = Depth of segment

λ_E = Distance from the joint with the erection error

$E1$ = Thickness of error in joint at bottom

$E2$ = Accumulated error in height at the distance λ_E

Fig. 6.15. Accumulation of joining error

Using procedures possible in the field, to correct the vertical alignment the nuts at D in Fig. 6.16 were loosened slightly and about 600 lbs. of unbalanced weight was put on the top of the M9 segment. The nuts at B were then backed down in small increments. If the nuts at B were turned down one turn, then the outer end of the S9 segment dropped 1-1/4 in. $[(1/13) \times (196/12)]$ when the weight was removed from M9.

In the erection of the first box of the bridge, the two cantilver sections were adjusted to the correct vertical alignment prior to the closure operation, but were not lowered to the neoprene pads until after

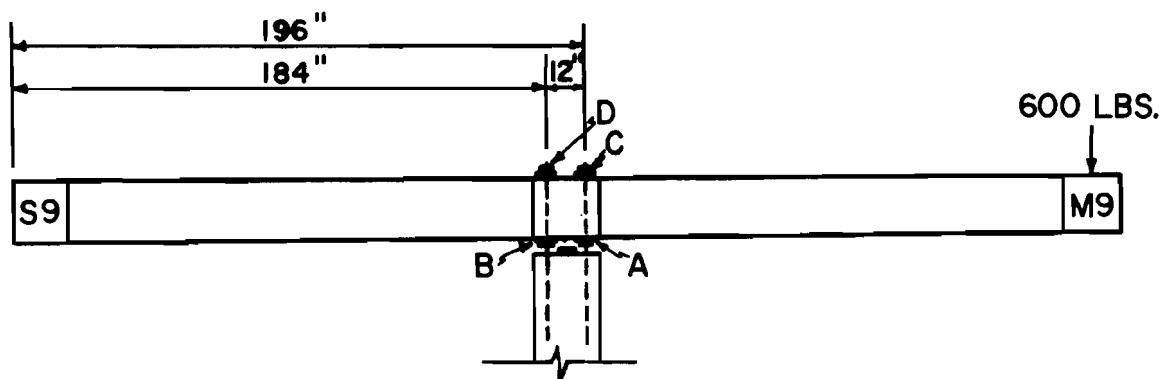


Fig. 6.16. Correction of the vertical alignment

the positive tendons had been stressed. However, for the second half (box) of the bridge, the two cantilever sections were separately lowered to their final position on shims on the neoprene pads prior to the closure operation. It was easier to lower the balanced sections onto the neoprene pads prior to the closure operation and it simplified the positive tendon operation. All lowering was done by unbalancing the overhangs and backing the plate support nuts down in small increments.

6.1.6 Casting of the Closure Segment. After adjusting the vertical and horizontal alignments, the half segments with diaphragms were erected over the end piers and the positive tendons in the side span were prestressed (details are in Sec. 6.1.7). Half segments (8.5 in. long) were erected for each cantilever in the main span, and the overlapping reinforcement extending from each half segment was joined by tie wires. In addition, the tendon ducts extending from each midspan half segment were connected by polyethylene tubes at the closure and sealed by epoxy resin, as shown in Fig. 6.17. The positive tendons for the main span were inserted immediately after the above operation was completed and before concreting of the closure.

Figure 6.18 shows the simulation of the closure prior to the construction of the half segments. Since there was no space to work

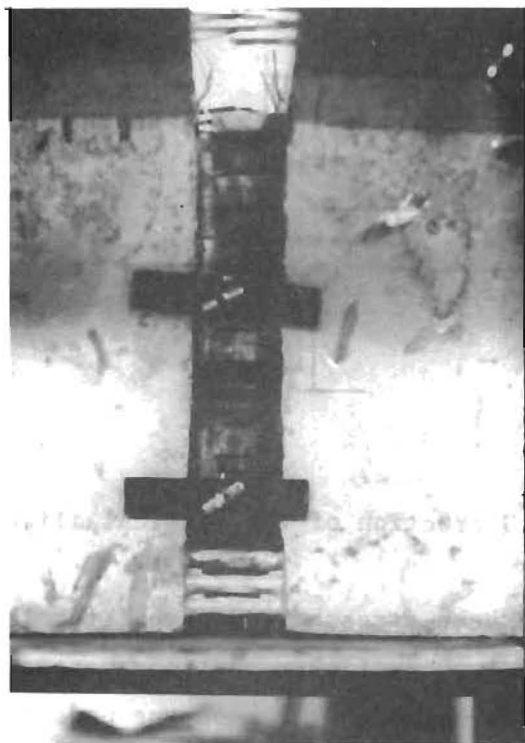


Fig. 6.17. Connection of tendon duct at the closure

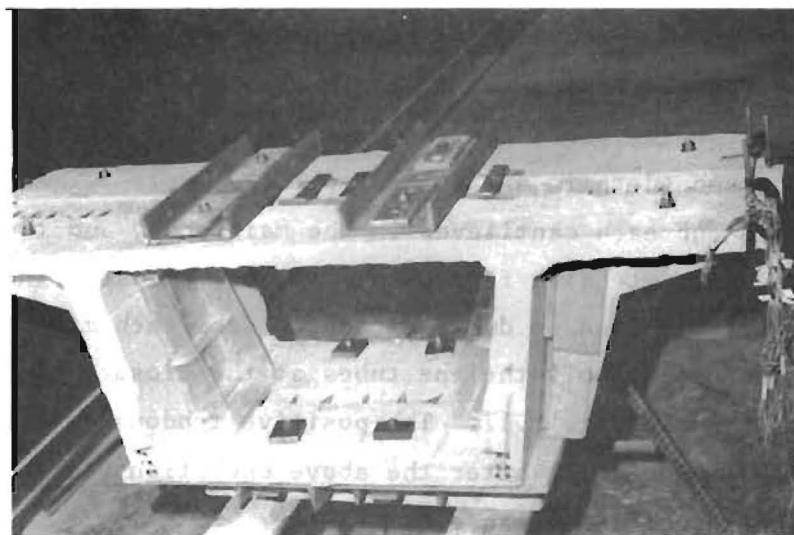


Fig. 6.18. Simulation of the closure

inside the model segments, interior side and top slab forms were set in place prior to joining the reinforcement at the closure and the top slab forms were supported using the holes made for dead load blocks. Plexiglas windows were provided in the bottom of the exterior side forms, in order to observe any tendency for honeycombing around the tendon ducts. Also, temporary bracing channels were rigidly attached to the top and bottom slabs of the half segments, as shown in Fig. 6.18. These channels were intended to provide temporary flexural stiffness across the closure equivalent to half of the flexural stiffness of the finished concrete box section and were kept in place until the concrete had cured.

In order to cast concrete in the bottom slab at the closure, the concrete was placed through the gap between the top slabs and vibrated from outside the bottom form. The form for the top slab was then set in place prior to casting the web and top slab. Concrete in the closure was cured for a week until the positive tendon stressing operation was performed.

6.1.7 Prestressing of the Positive Tendons. In order to minimize the effects of the secondary moments due to prestressing which occur in indeterminate structures, the prestressing operation for the positive moment tendons in the side spans was completed prior to the closure operation. The C3 and C4 tendons, as shown in Fig. 2.3, were also intended to prevent tensile cracking in the top slab due to prestressing of the C1 and C2 tendons. The order of the prestressing operation was tendons C4, C3, C2, and C1, as designated in Fig. 2.3. All tendons were prestressed from the anchorages in the top slab, as shown in Fig. 6.19. Details of the prestressing equipment were the same as reported in Sec. 6.1.4.2.

The procedure for the positive tendon operations in the main span was specified in the Texas Highway Department plans as follows:

- (1) Set jacks at end supports.
- (2) Stress tendons A1, A2, A3, and A4, in that order.
- (3) Lower restraining nuts at pier units PS and transfer load to bearing pads.
- (4) Adjust jacks at outer supports for a reaction of 15 kips (0.417 kips for the model) for each segment at each support.

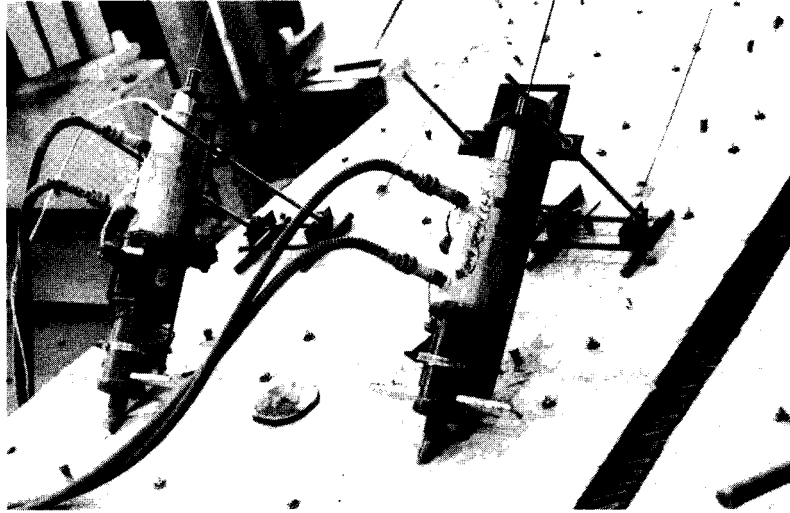


Fig. 6.19. Setup for prestressing of positive tendons

- (5) Stress tendon A5, then A6.
- (6) Increase jacking reactions at outer supports to 92 kips (2.56 kips for the model) at each segment, at each support. Set bearing pads and shim to maintain this reaction.

This procedure was used as a guide for the model bridge construction. For the model box girder bridge construction, the procedure indicated in the Texas Highway Department plans was followed, except for step (3) and the amount of reaction in step (4). Step (3) was done after stressing tendons A5 and A6. The reaction of 15 kips in step (4) (0.417 kips for the model) was very small and was already produced by stressing A1, A2, A3, and A4 tendons. Therefore, the reaction was increased by 0.28 kips (10.1 kips for the prototype) according to Lacey's preliminary design recommendation.²¹

The reaction at the ends was measured using load cells, while the deflections at the ends and at the center of the main span were measured with dial gages. Detailed results are given in Sec. 6.2.3 and 6.2.5. Details of the prestressing system were the same as in Sec. 6.1.4.2. Prestressing was performed from each end alternately.

In view of the experience gained in this erection sequence, recommended procedures for the prototype bridge construction were as follows:

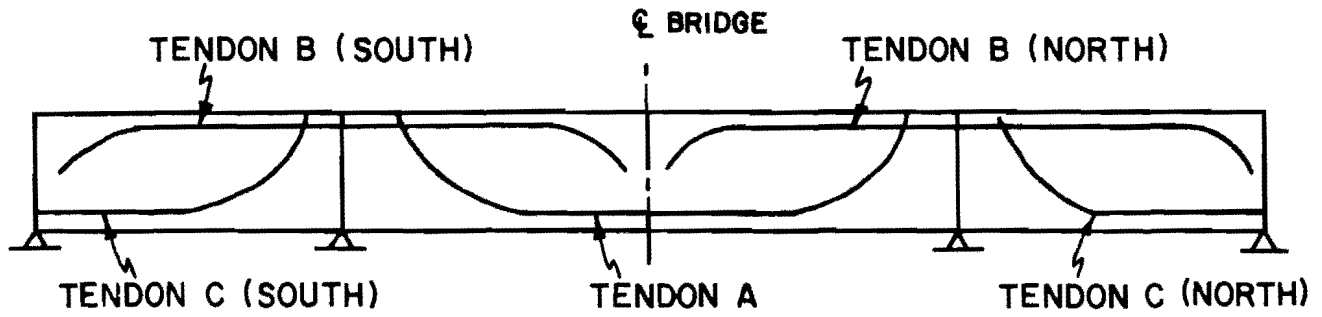
- (1) Lower the S9-M9 completed sections to their final position over the main pier at the symmetrical cantilever stage.
- (2) Attach the end segments and prestress positive tendons in the side spans.
- (3) Erect the midspan half segments and insert the positive tendons in the main span, prior to casting the closure segment.
- (4) Cast the closure segment.
- (5) Set jacks at outer supports and stress tendon A1.
- (6) Release restraining nuts at the main piers and temporary stiffness at the closure.
- (7)-(9) Stress tendons A2-A4.
- (10) Increase jacking reaction by 10 kips.
- (11)-(12) Stress tendons A5-A6.
- (13) Adjust elevation of the end segments to the optimum amount of reaction (see Sec. 7.3.3.2).

6.1.8 Grouting of Tendons. There were two options for grouting the tendons of the model bridge.

- (1) After prestressing each tendon.
- (2) After prestressing all tendons.

Procedure (1) was required in the prototype structure to minimize corrosion hazards. However, grouting after each stressing was considered too time-consuming and too prone to the hazard of possible leakage of grout into the adjacent tendon ducts due to possible honeycombing in the concrete or if sufficient epoxy resin was not spread between the tendon ducts at the joints. Therefore, procedure (2) was used in the model bridge. Grouting was done separately for five groups of tendons, as shown in Fig. 6.20. The grout pump and hoses were washed with clean water after grouting each group of tendons.

Tendons in each group were located close to each other, as shown in Fig. 6.21. When the B9 tendon was grouted, grout came out from the outlets of both the B9 and B7 tendons simultaneously. This happened



- ORDER OF GROUTING:
- 1) TENDON B (NORTH)
 - 2) TENDON B (SOUTH)
 - 3) TENDON C (NORTH)
 - 4) TENDON C (SOUTH)
 - 5) TENDON A

Fig. 6.20. Order of grouting for each tendon group

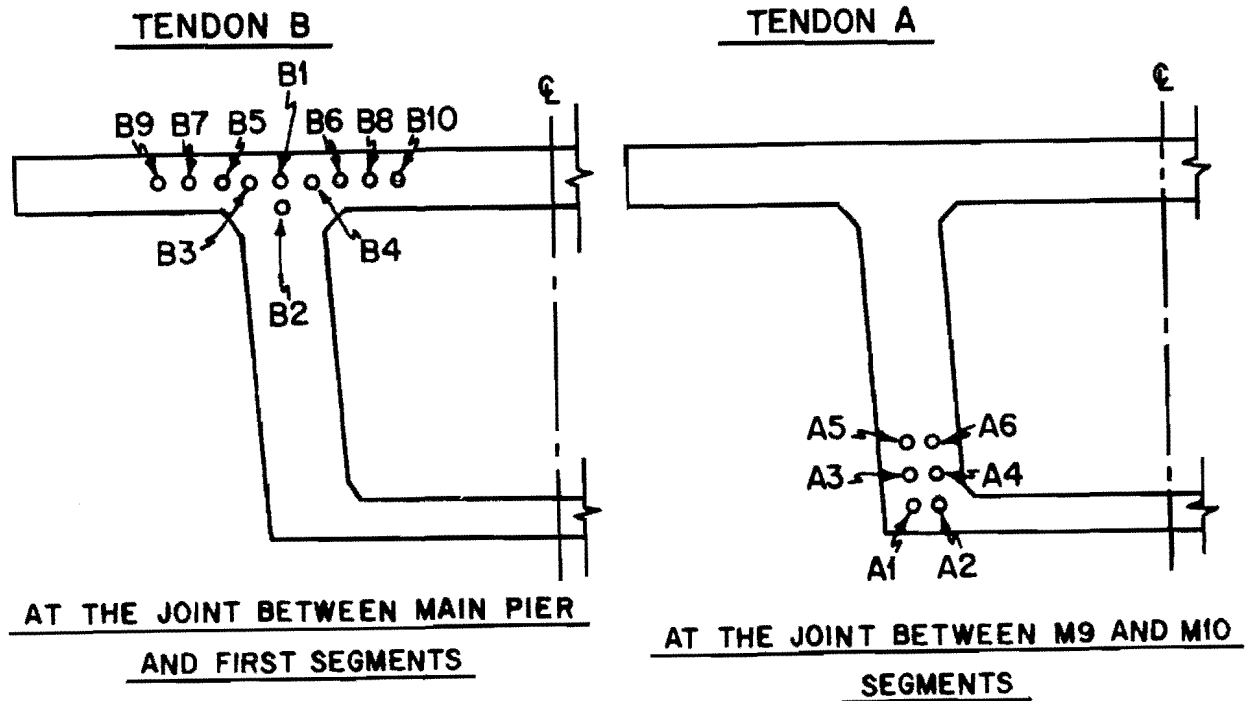


Fig. 6.21. Examples of tendon arrangement

because the distance between the B7 and B9 tendons was very small and epoxy resin was apparently not spread fully between the tendon ducts at some joint. However, it was not critical since grouting of the B7 tendon was completed immediately after grouting the B9 tendon. It could have had very serious consequences in the prototype with sequenced grouting. Grout also came out from a joint which had marked damage on the concrete face near a tendon duct.

Grouting mix and grouting procedures were in accord with Ref. 33.

The grouting mix used was:

| | |
|---------------------------------|---------|
| Type III portland cement: | 94 lbs. |
| Water: | 42 lbs. |
| Admixture (INTRAPLAST C, SIKA): | 1 lb. |

In the first half of the bridge all tendon ducts were flushed with clean water under pressure immediately before grouting. For the second half, all tendons were blown out with air pressure immediately prior to grouting and not flushed.

The following grouting procedure was used:

- (1) Grouting injection pipes were screwed into the inlets of tendons as shown in Fig. 6.22
- (2) Grout was pumped through the ducts and permitted to flow from the outlet until no visible slag of water or air was ejected.
- (3) The valves of the injection pipes were closed while maintaining pressure and the outlets were closed.
- (4) The injection pipes were removed from the inlets of the tendons and the inlets were closed.

The B series tendons were grouted completely in both the first and second half of the bridge. It was initially felt that the A and C series tendons were only grouted with about 70 percent effectiveness because of some signs that grout might have leaked at some joints due to honeycombing of concrete around the joints. However, by cutting segments at several points after the failure of the bridge, it was determined that the grouting for A and C series tendons was also virtually fully effective.



Fig. 6.22. Connection of injection pipes and inlets of tendons

6.1.9 Casting of the Midstrip Closure between the Two Box Units.

It was necessary to connect the two box girder bridges along the longitudinal midstrip closure after completing all prestressing and grouting work for both boxes. If the reinforcement splices in the midstrip closure had followed the prototype plan, the transverse reinforcement would have extended past the concrete 1.8 in. and been spliced by welding a 2 in. long bar to both protruding transverse bars (see Appendix A). Because space limitations made it extremely difficult to weld splice bars on the model, the transverse reinforcement in the top slab was extended about 3 in. at the time of casting so that the bars overlapped. Thus the connection was developed by lap splicing of the transverse reinforcement. Twelve ga. wires were inserted between and tied to the transverse reinforcement at each connection to serve as longitudinal and distribution reinforcement in the closure strip.

A continuous form was set under the top slab of the cantilever portion and sealed to prevent the flow of concrete. Since the vertical surface of the top slab at the midstrip closure was not rough, water was sprayed on the surface, and a light coating of cement mixed with water was placed on the surfaces just prior to casting. Concrete (same mix as used in the precast segments) was cast and the surface was coated to prevent shrinkage cracks in the midstrip closure.

6.2 Behavior of the Bridge during Construction

6.2.1 Rotational Stiffness at the Main Pier. Unbalanced loading tests were performed at various stages of construction in order to check the performance of the temporary anchor bolts. These results are shown in Fig. 6.23.

After each unbalanced loading test was completed, the balancing segment was erected. Although the bolts behaved elastically during the test of the 7th segment, there was noticeable residual deflection after the test of the 9th segment. When the structure was brought to a balanced configuration after the unbalanced loading experiment with the 9th segment,

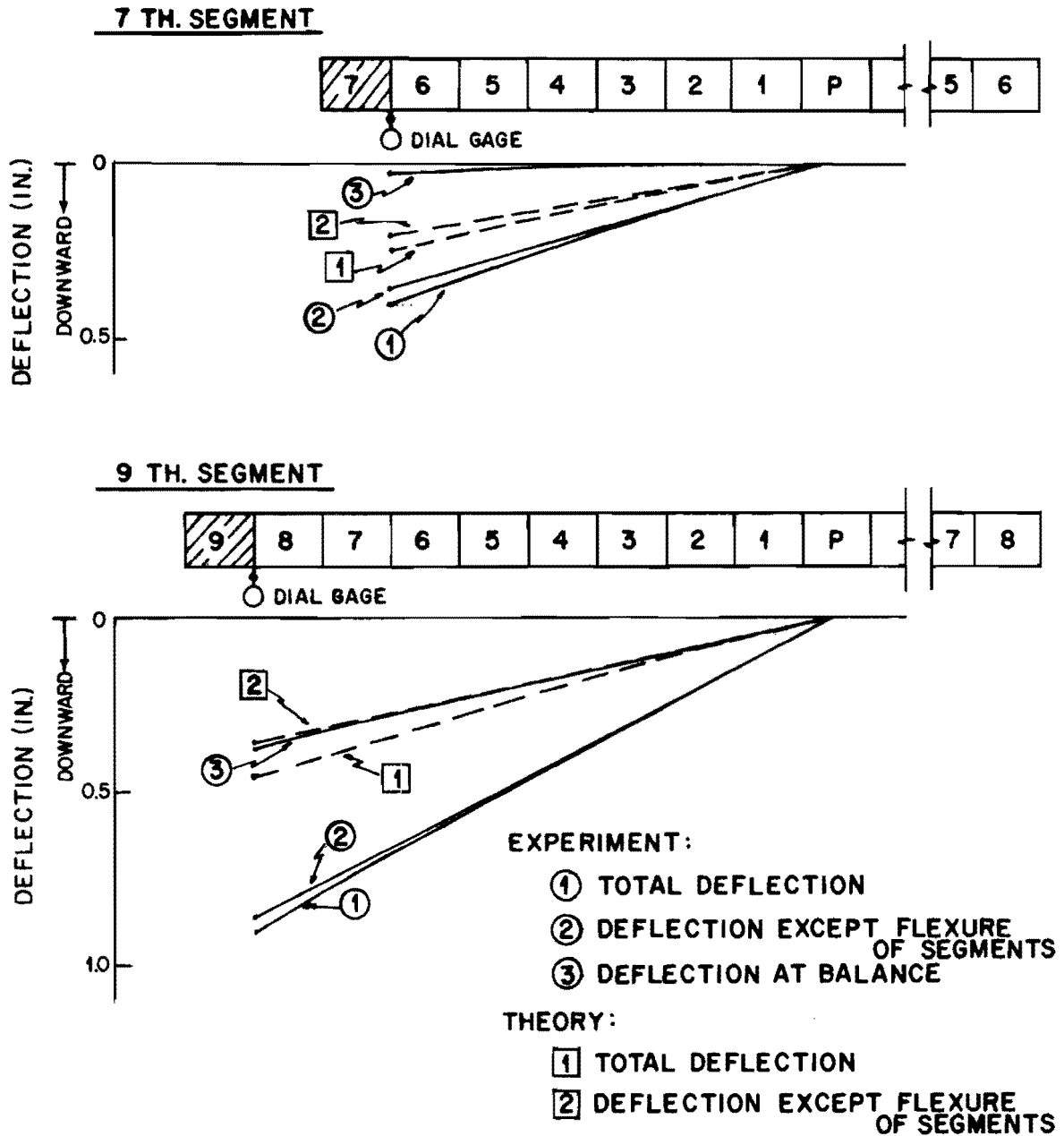


Fig. 6.23. Deflection at unbalanced loading

the bolts under the pier segments were carefully examined and it was found that the bolts on the compression side had deformed and showed evidence of yielding. Although the calculated direct compressive stress was less than the bolt yield strength, yielding was apparently influenced by the large gap between the pier segments and the pier, with consequent local bending and accentuated by the stress concentration in the threads.

Experimental and theoretical values for deflection under unbalanced loading are compared in Fig. 6.23. In both cases, the experimental deflection was appreciably larger than the theoretical value. Several factors which affect the deflection under unbalanced loading are:

- (1) Flexure of segments [see Fig. 6.24, Case (1)].
- (2) Elongation of the pier bolts [see Fig. 6.24, Case (2)]
- (3) Bending of the pier [see Fig. 6.24, Case (3)]
- (4) Moment connection of the pier to the test floor.
- (5) Slippage of bolts with respect to the pier concrete.

All cases except (4) and (5) were considered in the calculation of the theoretical deflection.

For the 7th segment, deflections were calculated as follows:

Deflection due to flexure of segments [Fig. 6.24 (1)]:

$$\delta_1 = Pl^3/3EI = 1.56 \times 140^3 / (3 \times 4.56 \times 10^3 \times 6060) = 0.052 \text{ in.}$$

Deflection due to elongation of bolts [Fig. 6.24 (2)]:

$$\begin{aligned} \Delta_1 &= S_1 \ell_c / AE_s = (19.0 \times 1.5) / (6 \times 0.142 \times 29 \times 10^3) \\ &= 1.15 \times 10^{-3} \text{ in.} \end{aligned}$$

$$\begin{aligned} \Delta_2 &= S_2 \ell_t / AE_s = (17.4 \times 19.0) / (6 \times 0.142 \times 29 \times 10^3) \\ &= 13.4 \times 10^{-3} \text{ in.} \end{aligned}$$

$$\theta_2 = (1.15 + 13.4) \times 10^{-3} / 12 = 1.21 \times 10^{-3} \text{ radian.}$$

$$\delta_2 = 1.21 \times 10^{-3} \times 125 = 0.151 \text{ in.}$$

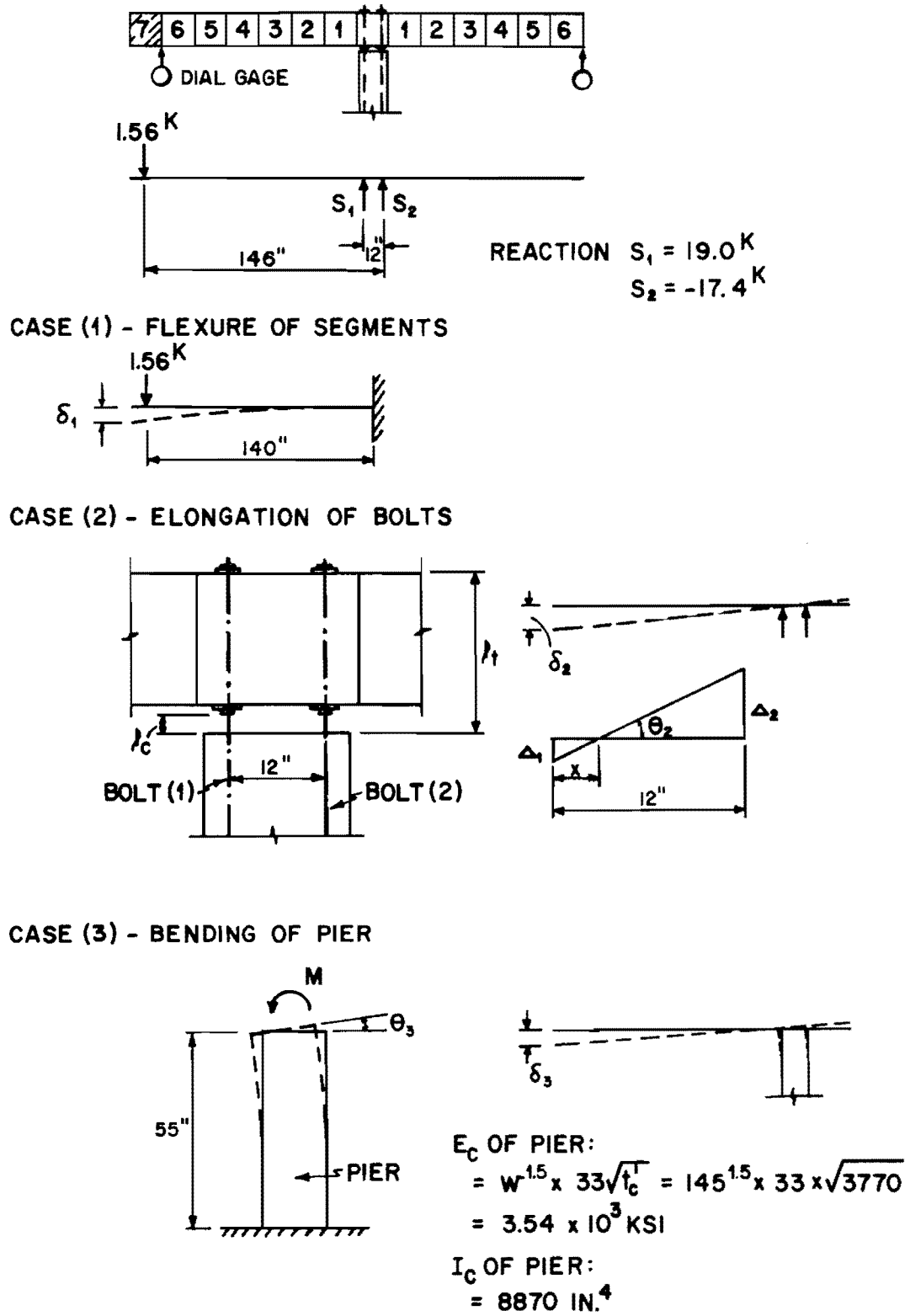


Fig. 6.24. Individual factors affecting the deflection

Deflection due to bending of pier [Fig. 6.24 (3)]:

$$\begin{aligned}\theta_3 &= Mh/E_c I = 218 \times 55 / (3.51 \times 10^3 \times 8870) \\ &= 0.382 \times 10^{-3} \text{ radian.}\end{aligned}$$

$$\delta_3 = 0.382 \times 10^{-3} \times 130 = 0.050 \text{ in.}$$

Therefore

$$\delta_2 + \delta_3 = 0.151 + 0.050 = 0.201 \text{ in.}$$

$$\delta_1 + \delta_2 + \delta_3 = 0.253 \text{ in.}$$

While it is not possible to quantify the exact length of bolt embedment required for full development of bond and prevention of any slip with reference to the concrete, if this length is as much as 33 percent of the development length specified for an equivalent deformed bar under the 1971 ACI Code,³ the calculated deflection would increase by almost 33 percent and be in much better agreement with the observed values. A substantial part of the deflection discrepancy is believed due to the uncertainty of effective bolt imbedment.

Deflection for the 9th segment (unbalanced) was calculated in the same manner as follows:

$$\delta_1 = 0.110 \text{ in.} \quad \delta_2 = 0.259 \text{ in.} \quad \delta_3 = 0.084 \text{ in.}$$

$$\delta_2 + \delta_3 = 0.343 \text{ in.}$$

$$\delta_1 + \delta_2 + \delta_3 = 0.453 \text{ in.}$$

Although there are many ways to connect the pier segment to the pier temporarily or permanently, it is not recommended that the same method used in this model bridge be used in future bridges, because of the high compressive force applied to the bolts and the lack of stiffness in the connection. If the same general type of moment connection is to

be used, as shown in Fig. 6.25, it should provide for temporary compression support blocks to carry the compression and require the bolts to be prestressed so that the large deflection component (δ_2) due to bolt elongation would be eliminated.

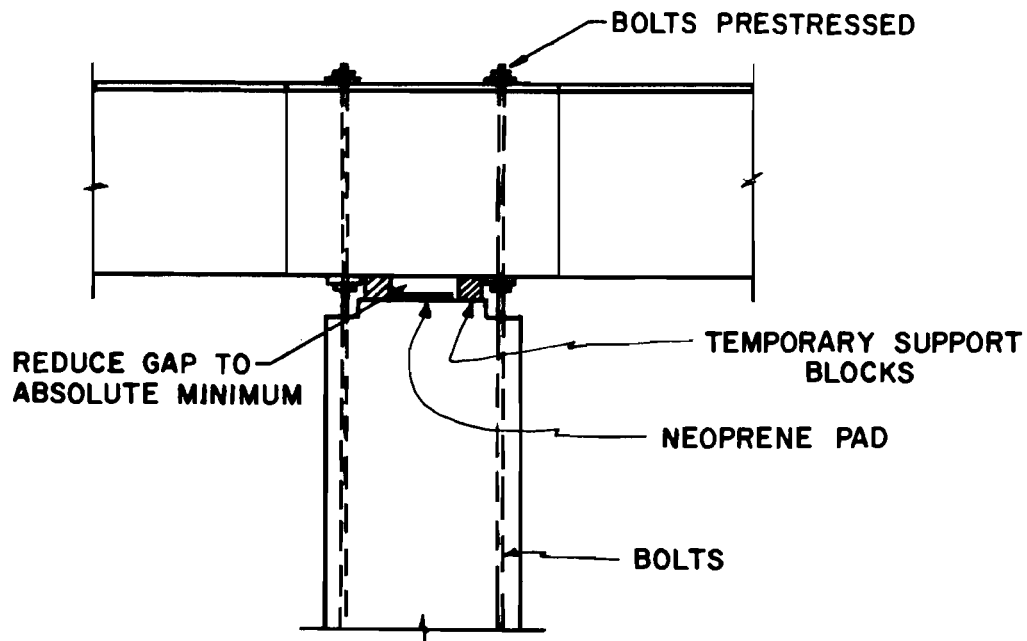


Fig. 6.25. Suggested improvement for temporary support

6.2.2 Prestressing Force. In Brown's incremental analysis,¹⁰ he recommended that an initial $0.8f'_s$ overstress be applied and then be reduced prior to seating to about $0.65f'_s$, so that after losses the tendon force would be $0.6f'_s$ in the straight portion of the prestressing cables. In the analysis of the bridge (using SIMPLA2 as explained in Sec. 6.2.3), the friction coefficient (μ) and the wobble coefficient (λ) were assumed as 0.25/radian and 0.000017/in., respectively.

Friction loss tests were performed during stressing of three different cables (B6, A1, and A4 in the second half of construction). Prestressing force was applied at one end and the resulting force at the far end was measured using a load cell at that point. Prestressing

force was applied up to the specified $0.8f'_s$ and the elongation of the prestressing cables was also measured.

The generally accepted equation²⁶ to find prestressing force at any location after friction and wobble loss is given as follows:

$$P_{ij} = P_{io} e^{-(\mu\alpha + \lambda\ell_p)}$$

where

- P_{ij} = prestressing force at a certain point (kip)
- P_{io} = prestressing force applied at the end (kip)
- μ = friction coefficient (per radian)
- α = angle change of tendon (radian)
- λ = wobble coefficient (per in.)
- ℓ_p = length of cables from the end to the point considered (in.)

Theoretical total elongation may be calculated by the follow equation:

$$\Delta\ell_p = \Sigma(P_{ij}/E_s A_p) d\ell_p$$

where

- P_{ij} = prestressing force at the certain point (kip)
- E_s = modulus of elasticity of prestressing cable (ksi)
- A_p = area of prestressing cable (in.²)
- ℓ_p = length of prestressing cable (in.)

Experimental results were compared with the theoretical values, as shown in Tables 6.1 and 6.2. Tendon profiles used in the theoretical calculations were taken from the plans.

TABLE 6.1. FRICTION LOSS TEST RESULTS

| Tendon | Force (0.8f' _s) Applied (kip) | Force at the Far End (k) | | (Experiment/Theory) |
|--------|--|--------------------------|--------|---------------------|
| | | Experiment | Theory | |
| B6 | 11.9 | 8.94 | 9.26 | 0.966 |
| A1 | 7.28 | 5.30 | 5.58 | 0.950 |
| A4 | 7.28 | 5.26 | 5.59 | 0.942 |

TABLE 6.2. ELONGATION OF PRESTRESSING CABLES IN SEVERAL STAGES

| Tendon | Experimental Elongation (in.) | Theoretical Elongation | | |
|--------|-------------------------------------|------------------------|--------------------|------------|
| | | E_s (ksi) | ΔC_p (in.) | Exp./Theo. |
| B6 | 1.67 | 27.0×10^3 | 1.65 | 1.01 |
| B7 | 1.99 | | 1.91 | 1.04 |
| B9 | 2.28 | 27.0×10^3 | 2.31 | 0.986 |
| B10 | 2.41 | | 2.55 | 0.945 |
| A1 | 2.46 | 27.0×10^3 | 2.64 | 0.931 |
| A2 | 2.19 | | 2.37 | 0.924 |
| A3 | 2.06 | | 2.11 | 0.975 |
| A4 | 1.78 | | 1.85 | 0.961 |

Table 6.1 indicates that the measured force at the far end was less than the theoretical value by 5 percent. Five percent difference at the far end indicates that there would be about 3 percent difference between the theoretical and experimental values in the straight portion. So a prestressing force of $0.6f'_s$ was assumed in the straight portion in all theoretical calculations.

Table 6.2 lists some measured elongations during various stages of construction, including the friction loss tests. Experimental results are compared with the theoretical calculations. The ratio of measured (experiment) to calculated (theory) elongation of all strands showed the same good accuracy as the results for forces shown in Table 6.1.

When the applied prestressing force was lowered to $0.65f'_s$ for seating, some change in elongation was measured, but no change was noted in the force at the far end.

6.2.3 Deflections. It was difficult to accurately measure the vertical deflection during construction because the deflection was so small in comparison to the span ($L/1800$). Casting and construction of the model

segments required six times the accuracy of the prototype in order to maintain the same relative tolerance as the prototype. This was not completely feasible, so deflections were measured only to see the general trend of cantilever section behavior. Theoretical deflections were calculated using the computer program SIMPLA2¹¹ which provides an analysis at each stage of erection using the finite segment technique.

The theoretical and experimental deflection profiles are shown in Figs. 6.26 and 6.27, respectively, for all stages of erection. Relative deflections for one typical case are compared in Fig. 6.28. There are many factors which affect the vertical deflections, as mentioned in Sec. 6.1.5(b). Therefore, it is very hard to determine the cause of errors in deflection. This is especially difficult since the component of deflection due to dead load is almost completely balanced by the deflection due to the prestressing. Figures 6.26 and 6.27 indicate that the overall trend of the theoretical and experimental results agreed fairly well except that the measured results show a pronounced upward skew. Although the experimental deflection at construction of the 7th segment was still upward at the tip of the last unit, it decreased upon the addition of the 8th and 9th segments, as did the theoretical results.

Experimental deflection measurements shown in Fig. 6.27 are averages at each corresponding point to eliminate the effect of unbalance or bolt bending. Figure 6.27 readily indicates the jointing errors in the initial stages of cantilever erection when temporary tensile stresses at the bottom of initial joints were not controlled and joints widened at the base, causing upward deflections.

During the positive tendon operations in the main span, Fig. 6.29 indicates experimental and theoretical deflections agreed well. The additional theoretical procedure used to calculate these deflections using program BMCOL50²⁸ is explained in Sec. 6.2.5.

Superimposing results from Figs. 6.26 and 6.29 indicates that the relative displacement at the center in the main span should be almost zero upon prestressing of all positive tendons (A1-A6). The center of the main

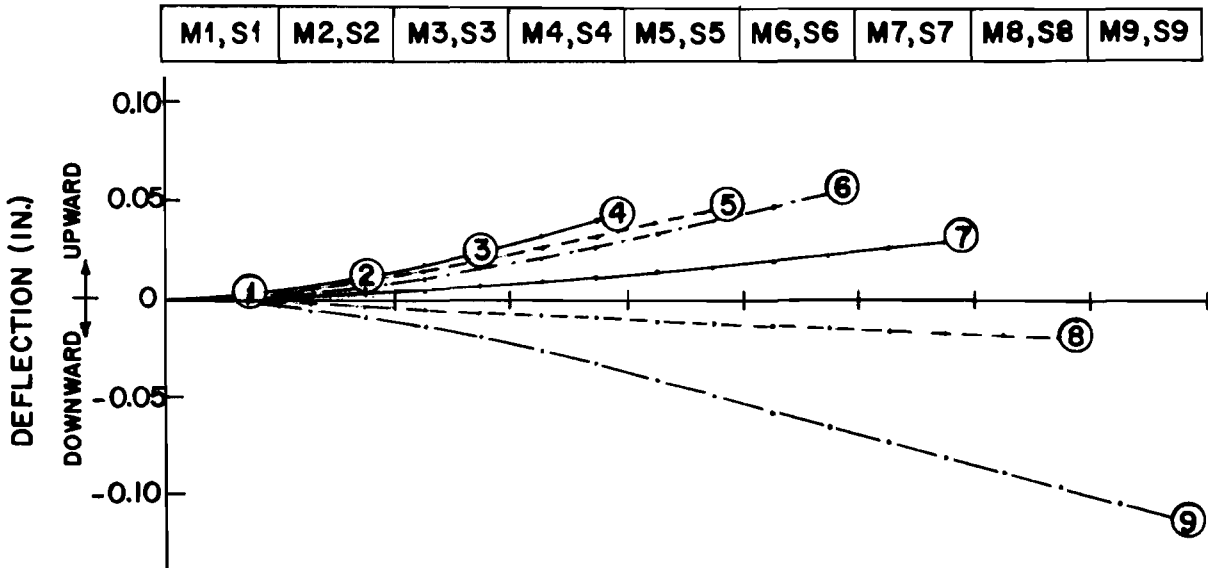


Fig. 6.26. Deflection predicted by SIMPLA2 for cantilever erection

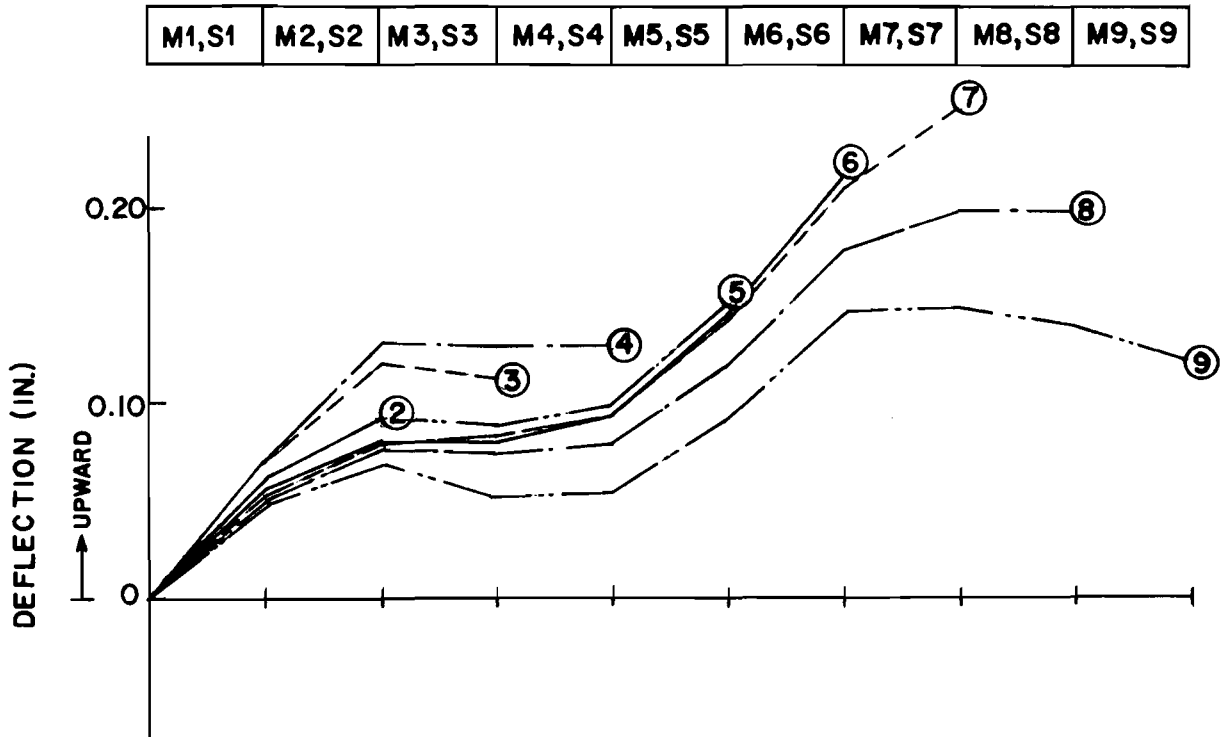


Fig. 6.27. Typical measured deflection during cantilever erection

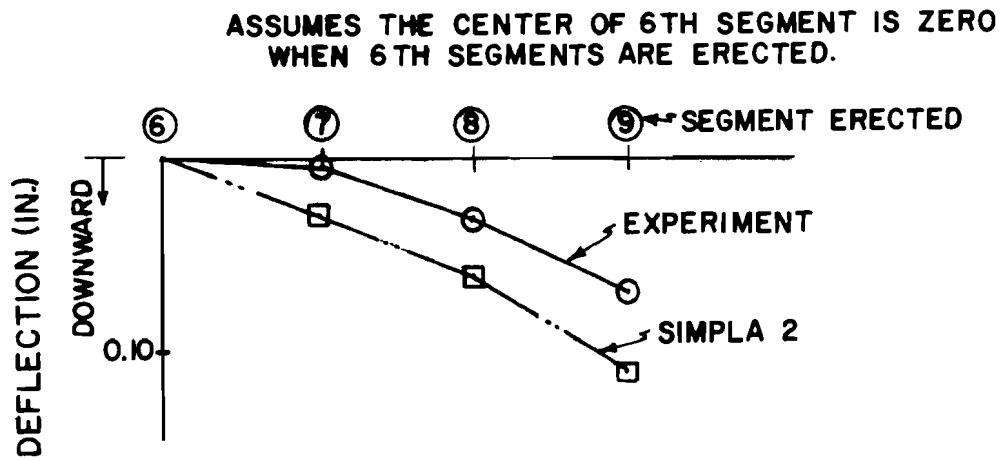


Fig. 6.28. Deflection relative to the center of 6th segment

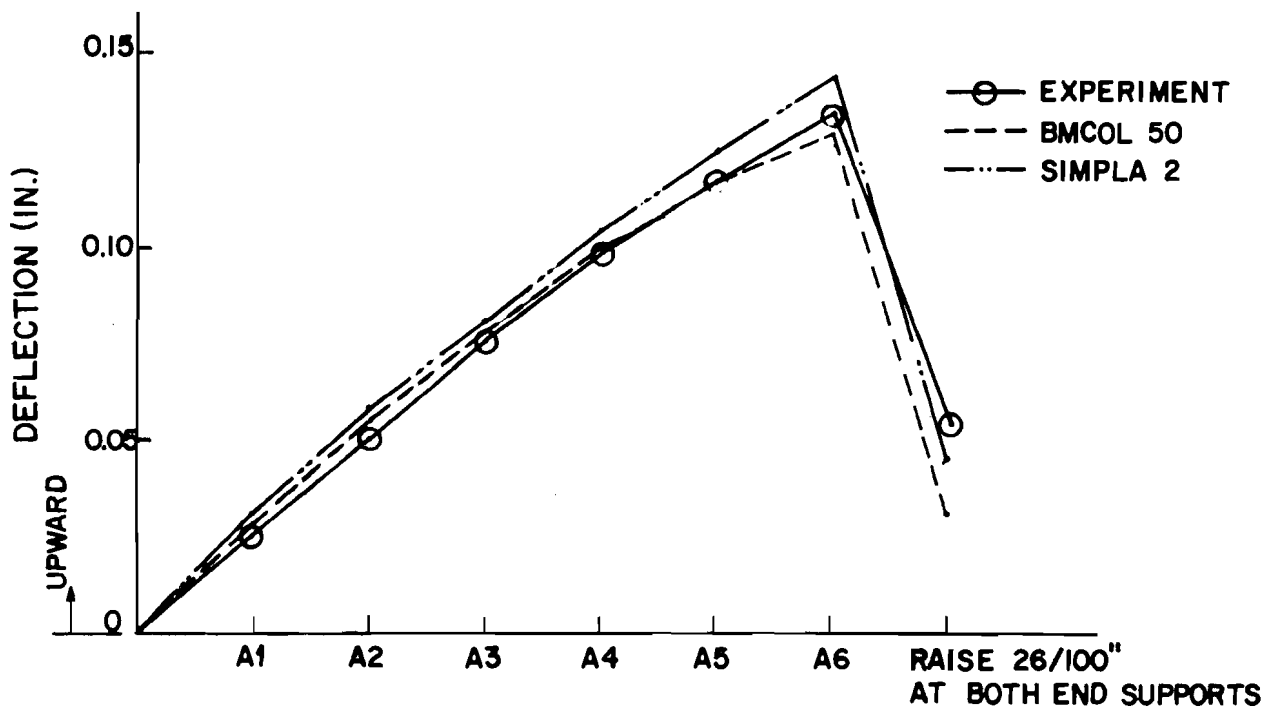


Fig. 6.29. Deflection at the center in main span during positive tendon operations

span was subsequently lowered 0.08 in. (0.48 in. in the prototype) by the jacking at the outer supports

6.2.4 Strains. The sequence of construction stages is listed in Table 6.3. Measured and computed strains are shown in Figs. 6.30 to 6.38.

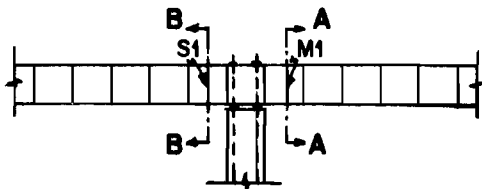
Longitudinal strains plotted are usually averages of duplicate readings at identical positions in similar segments.

Figure 6.30 shows that the experimental strains in the top slab of the M1 and S1 segments varied widely across the cross section during erection of several segments. The measured results are in good agreement with the theoretical calculations for stage 1 and after erection of the 5th segment. Experimental strains were uniform across the cross section and close to the beam analysis values for the erection of the 6th and subsequent segments. Although the longitudinal strains in the top slab of the M1 and S1 segments varied across the cross sections in early erection stages, it is not a serious problem. All strains are in compression across the cross section and are well below the strains which would accompany the maximum allowable compressive stress. The non-uniformity of strain in the top slab over the web was probably greatly influenced by the local concentrated tendon forces. As additional tendons were stressed during the erection of the second through fifth segments, these local effects died out, as shown in Fig. 6.30.

For strains in the M1 and S1 segments, SIMPLA2 gave reasonable predictions of the longitudinal strain distribution at the erection of the first segment, but then showed poorer agreement with the experimental results until the erection of the 6th segments. Since beam theory does not predict any variation in longitudinal strain distribution across a transverse section, the deviation from the experimental values indicated for the first two stages were somewhat expected. For erection of the 3rd through 6th segments, calculation by beam theory was closer to the experimental values. In subsequent stages, beam theory showed excellent agreement with measured values. Deviation of the experimental and beam theory results in the initial stages greatly affects the accumulated values of

TABLE 6.3. DETAILS AT EACH STAGE OF CONSTRUCTION

| Stage | Segment Erected | Prestressing Cable | Amount of Force Per Cable at $0.8f'_s$ (kip) | Amount of Force Per Cable at $0.6f'_s$ (kip) |
|---|-----------------------------------|--------------------|--|--|
| 1 | M1, S1 | B1, B2 | 11.9 | 8.94 |
| 2 | M2, S2 | B3 | 18.3 | 13.8 |
| 3 | M3, S3 | B4 | 18.3 | 13.8 |
| 4 | M4, S4 | B5 | 11.9 | 8.94 |
| 5 | M5, S5 | B6 | 11.9 | 8.94 |
| 6 | M6, S6 | B7 | 11.9 | 8.94 |
| 7 | M7, S7 | B8 | 5.52 | 4.13 |
| 8 | M8, S8 | B9 | 5.52 | 4.13 |
| 9 | M9, S9 | B10 | 5.52 | 4.13 |
| 10 | S10 | C4 | 5.52 | 4.13 |
| 11 | ----- | C3 | 5.52 | 4.13 |
| 12 | ----- | C2 | 5.52 | 4.13 |
| 13 | ----- | C1 | 5.52 | 4.13 |
| 14 | M10 | B11 | 5.52 | 4.13 |
| Closure segment was cast and supported at ends (3 span continuous beam). | | | | |
| 15 | ----- | A1 | 7.28 | 5.46 |
| 16 | ----- | A2 | 7.28 | 5.46 |
| 17 | ----- | A3 | 7.28 | 5.46 |
| 18 | ----- | A4 | 7.28 | 5.46 |
| 19 | ----- | A5 | 7.28 | 5.46 |
| 20 | ----- | A6 | 7.28 | 5.46 |
| 21 | Raise 0.26 in. at outer supports. | | | |



* STRAIN READINGS AT A-A AND B-B WERE AVERAGED.
 ○ - EXPERIMENT
 △ - SIMPLA 2
 --- BM THEORY

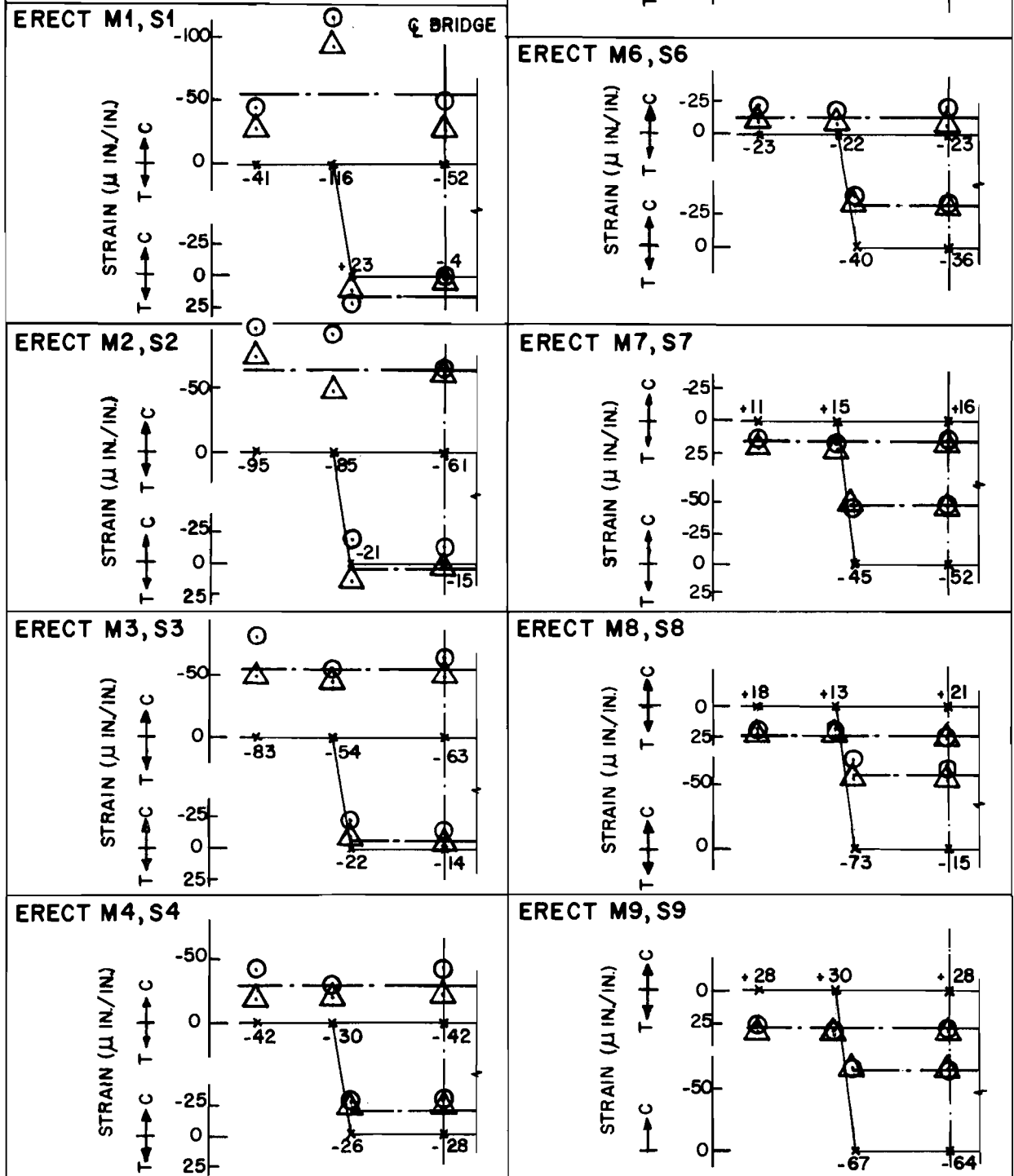
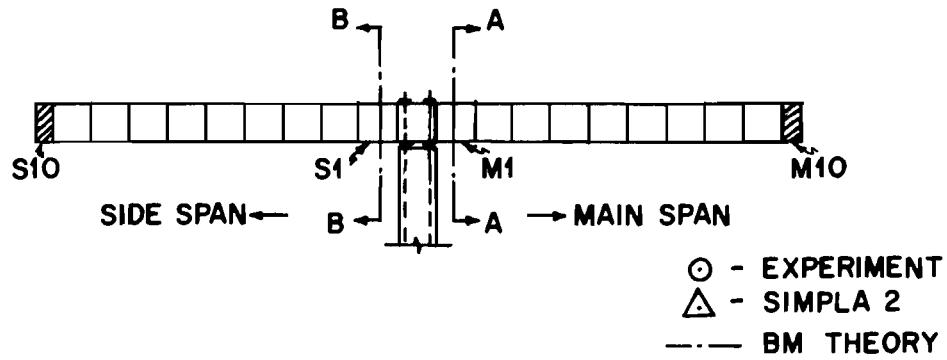


Fig. 6.30. Strain in M1 and S1 segments during balanced cantilever construction



| STAGE | AT SECTION B-B | AT SECTION A-A |
|-------------|---|--|
| (10) → (13) | <p>PRESTRESS C4,C3,C2,C1 ϵ BRIDGE</p> <p>STRAIN (μ IN/IN)</p> <p>Top: +24, +22, +23 Bottom: -27, -23</p> | <p>PRESTRESS C4,C3,C2,C1 ϵ BRIDGE</p> <p>STRAIN (μ IN/IN)</p> <p>Top: +5, +6, -2 Bottom: -3, -1</p> |
| (14) | <p>ERECT M10 ϵ BRIDGE</p> <p>STRAIN (μ IN/IN)</p> <p>Top: -6, -4, -3 Bottom: -5, -4</p> | <p>ERECT M10 ϵ BRIDGE</p> <p>STRAIN (μ IN/IN)</p> <p>Top: +13, +28, +10 Bottom: -38, -15</p> |

Fig. 6.31. Strains in M1 and S1 segments during erection of half segments

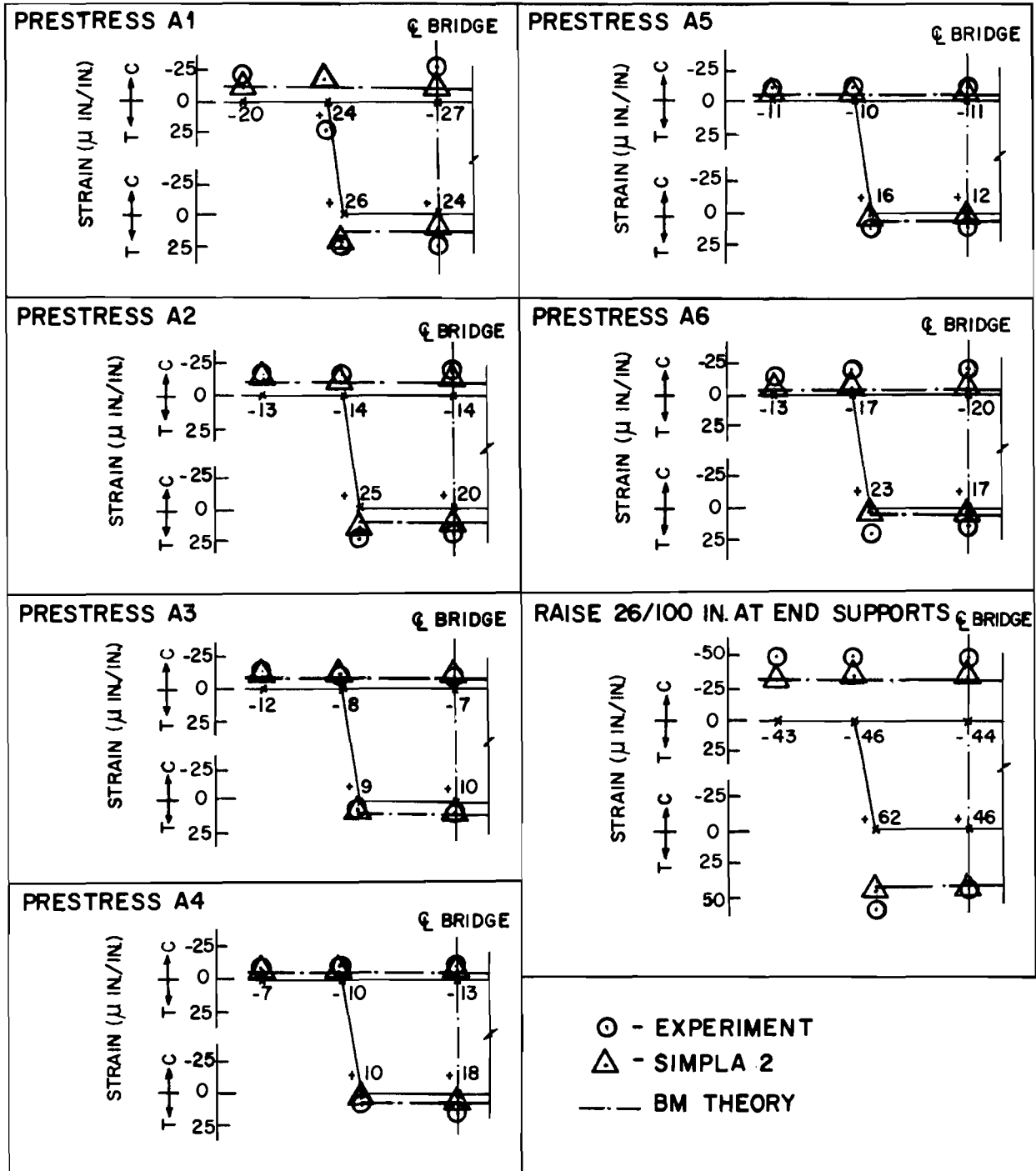
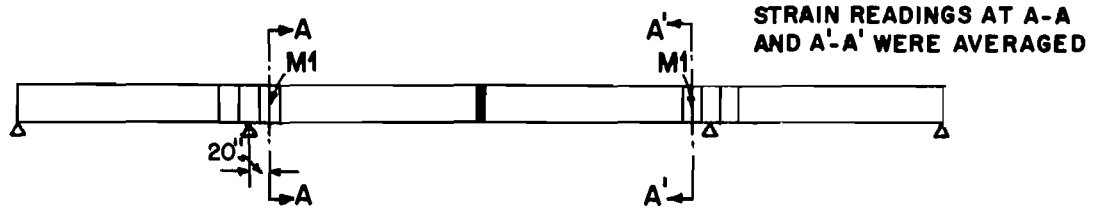


Fig. 6.32. Strains in M1 segments during closure operation

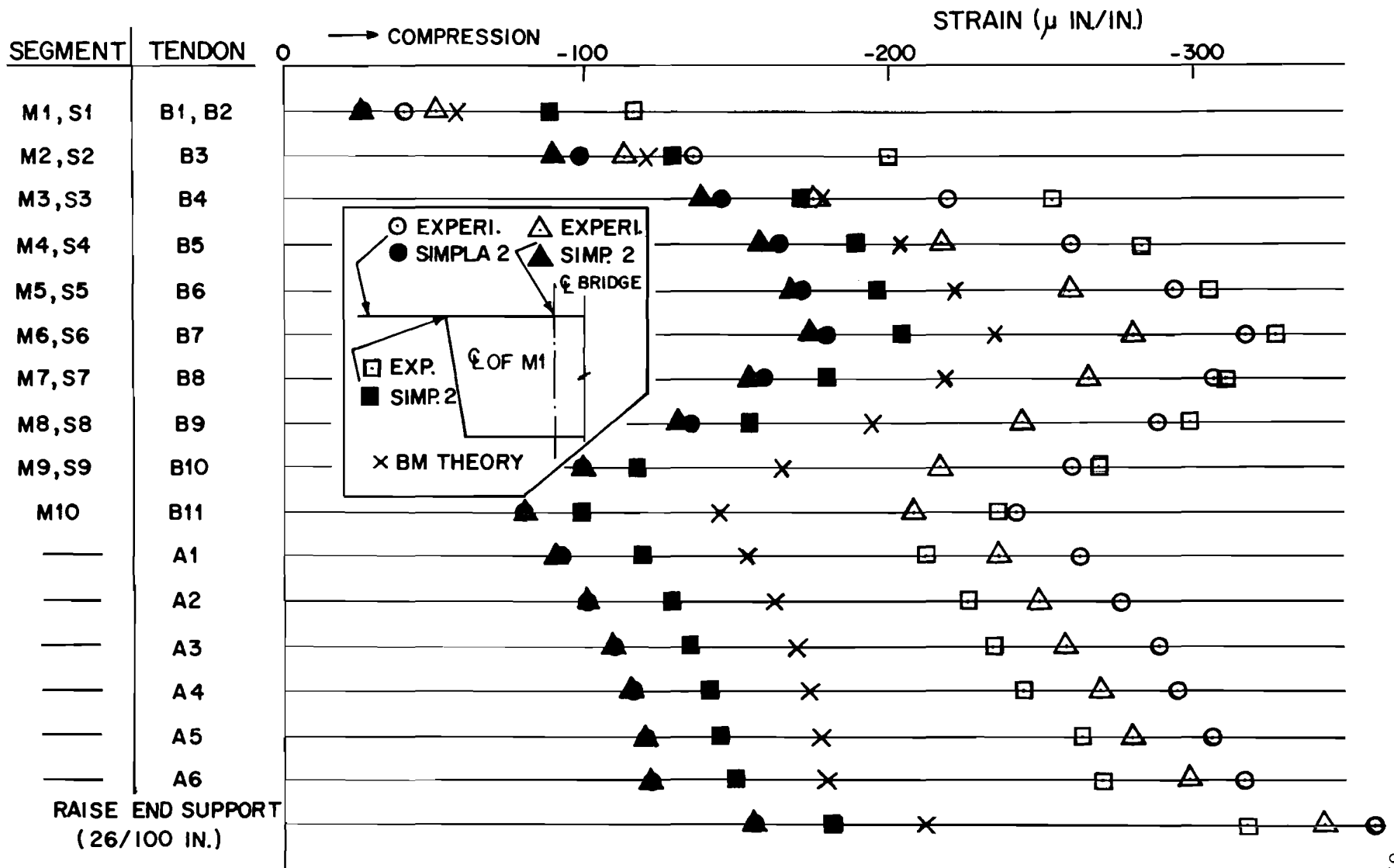


Fig. 6.33. Strains in the top slab of M1 segments during construction

STRAIN (μ IN/IN.)

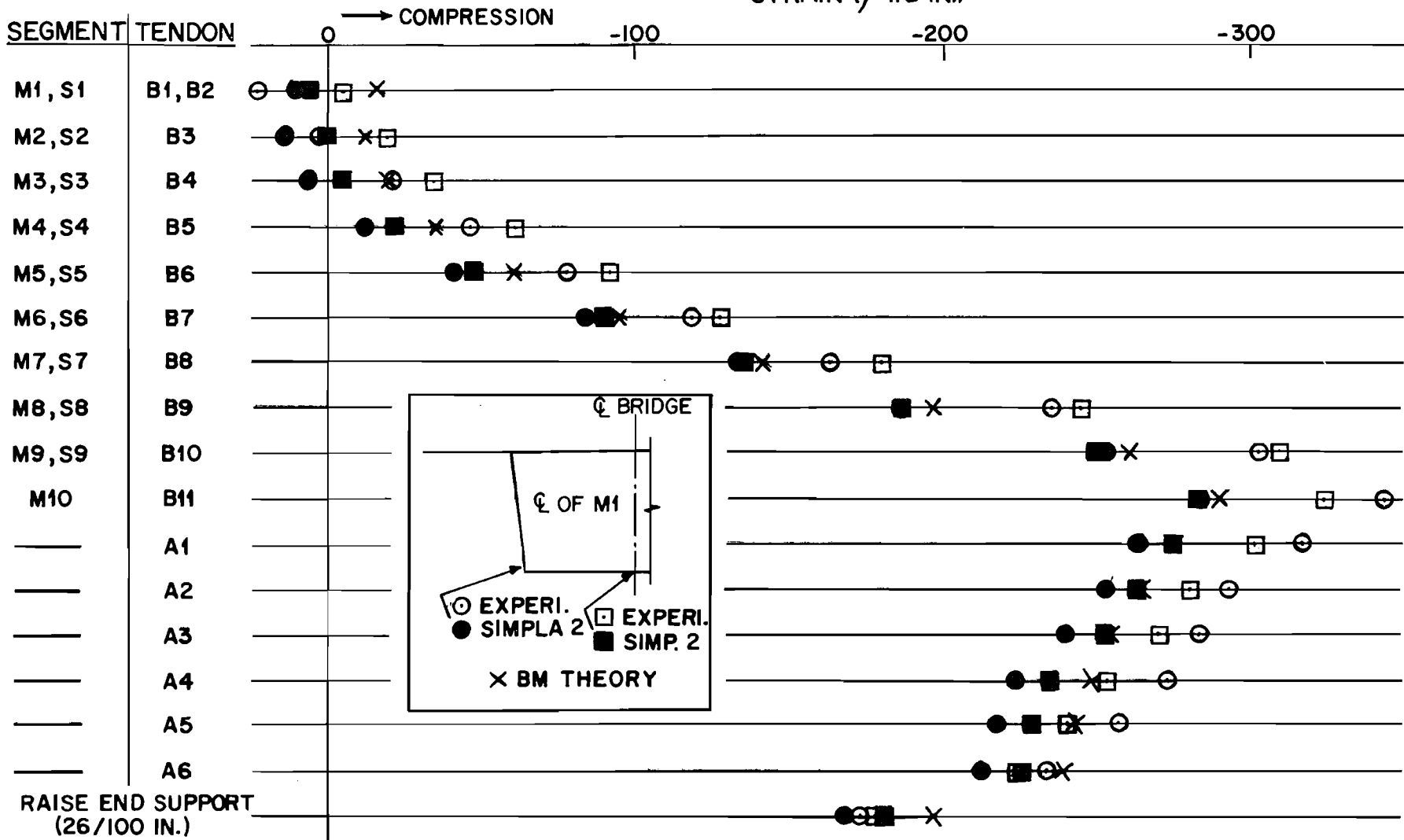


Fig. 6.34. Strains in the bottom slab of M1 segments during construction

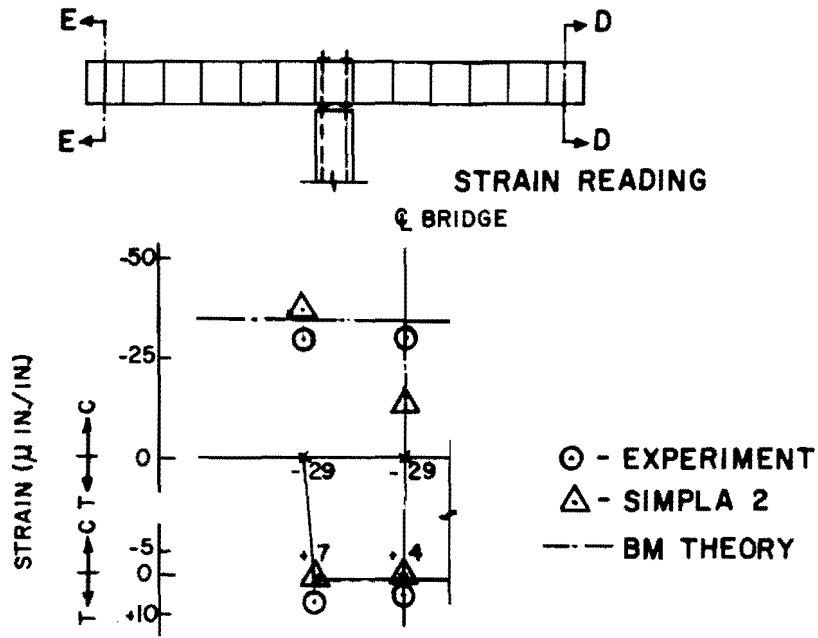


Fig. 6.35. Strains in the M6 and S6 segments at erection of the 6th segment

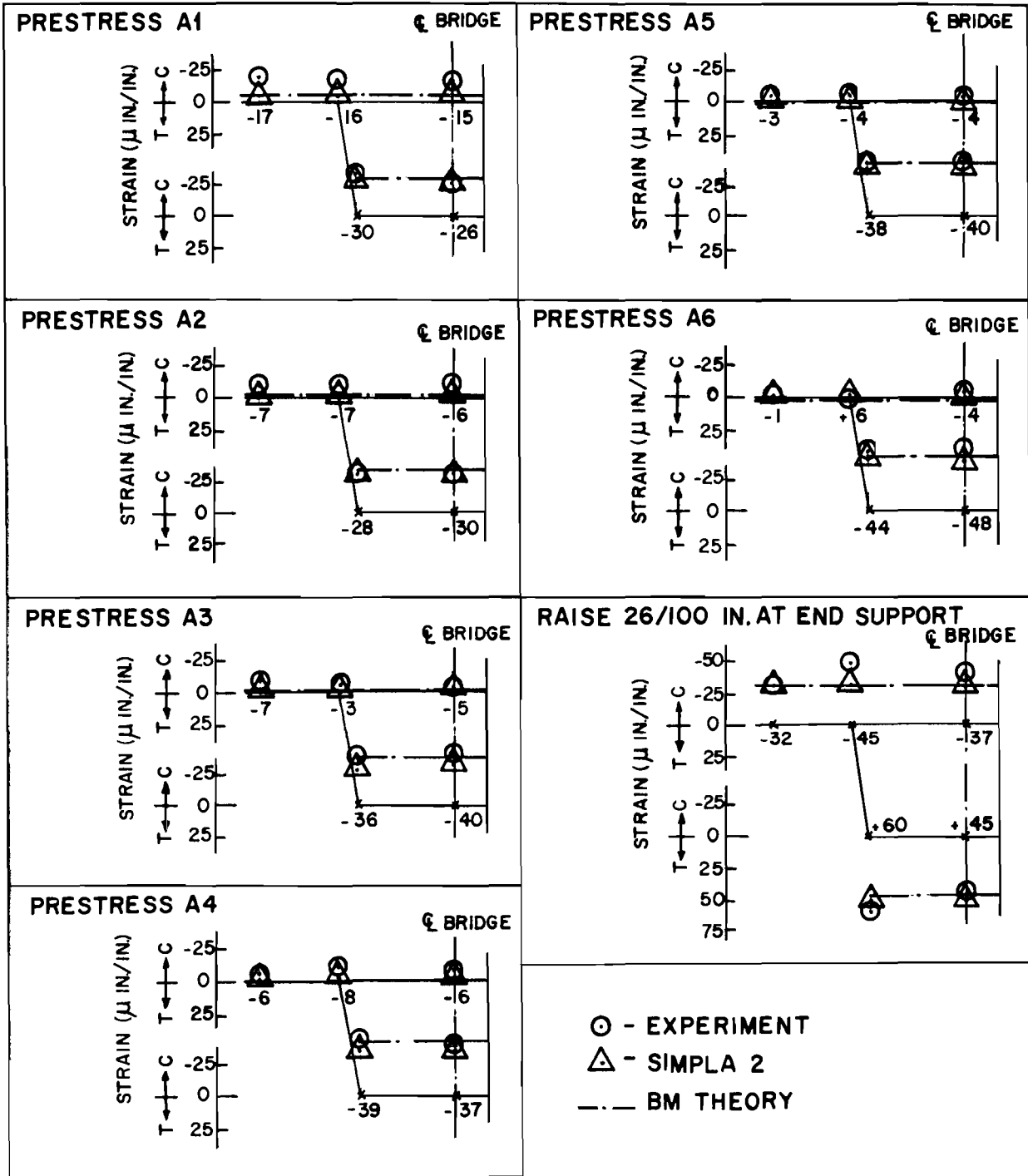
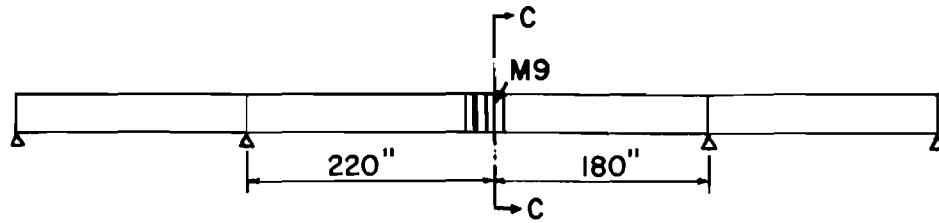


Fig. 6.36. Strains in the M9 segment during closure operations

strain in the top slab of M1 and S1, as shown in Fig. 6.33, even though the subsequent longitudinal strain increments agreed during cantilever erection, as shown in Figs. 6.30 and 6.31. Figure 6.33 gives a distorted feel for the accuracy. The large discrepancies at each stage are almost completely due to the lack of agreement in the first two stages.

Because Figs. 6.30 through 6.34 indicated so much deviation in the longitudinal strains across the cross section for the M1 and S1 segments during erection of the first groups of segments, the longitudinal strains in the 6th segment during its erection are shown in Fig. 6.35. At this stage the experimental strains measured in the top slab were uniform although SIMPLA2 predicted some deviation. The magnitude of this deviation was small in comparison to the first segment because of the lower prestressing force as the cantilever sections extended. Apparently little local compression effect existed.

In the bottom slab the experimental and theoretical results agreed very well, as shown in Figs. 6.30, 6.31, and 6.34. The strain produced was almost uniform in the bottom slab, except at the erection of the first three segments. Figure 6.34 shows tensile strains developed in the bottom of the M1-S1 segments at the erection of the first two segments as predicted.

During the positive tendon stressing operations after casting the closure segment, Figs. 6.33 through 6.38 show that the values predicted by both SIMPLA2 and beam theory deviated from the experimental results in the top slab of the M1 and M9 segments. Although the experimental results were consistently greater than the theoretical calculations, no ready explanation for the difference is known. The small absolute values of the strain might be one of the factors for the discrepancy due to inherent difficulties in accurately measuring these very small strains.

Figure 6.33 shows that the maximum strains in the M1 and S1 segments occurred in the top slab at the erection of the 6th segments as predicted and at the completion of construction. Figure 6.34 shows the maximum strain in the bottom slab to occur at the erection of the M10 segment.

The magnitude of the maximum compressive strain in the M1 and S1 segments was approximately 330 $\mu\text{in./in.}$ in both the top and bottom slab. Therefore, the maximum compressive stress was about 1500 psi. This value was only 21 percent of the ultimate compressive strength of the concrete (7090 psi) and about half of the maximum allowable stress. The maximum strain in the bottom slab in the closure strip at the center of the main span was about 200 $\mu\text{in./in.}$ during construction of the bridge.

All readings were taken before and after the application of load and not cumulatively. Creep effects appeared very small, although the experimental strain values were generally larger than the values given by beam theory. Since the beam theory agreed fairly well with the experimental results, the BMCOL50 program can be modified for theoretical calculations for construction stages for this type of bridge with similar transverse and longitudinal stiffness.

In general, both theoretical solutions and the experimental results were in reasonable agreement when the change of strain in each stage was reasonably large, except for the local strains in the top slab during initial stages when the large local compressive forces from the tendons seemed to affect the strain distributions.

6.2.5 Reaction at Outer Supports during Positive Tendon Operations.

Prior to positive tendon prestressing operations in the main span, the end supports were adjusted to just bear on the underside of each web at the edge of the end pier segments. Reactions at the end supports were measured by sensitive load cells during each stage. Comparison between theoretical and experimental results is shown in Table 6.4.

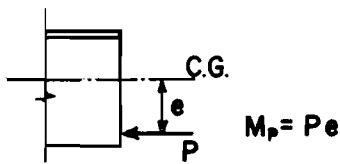
Figure 6.39 shows the simplified procedure used to calculate the reaction at the end. Prestressing forces were replaced by the vertical forces which produced the moment diagram due to prestressing. These reactions were calculated using the BMCOL50 program.²⁸

Experimental reactions agreed very well with the theoretical values for large values such as A1 and A2 tendons. As the reaction increment became smaller, the experimental readings became much smaller

TABLE 6.4. REACTION AT OUTER SUPPORT DURING PRESTRESSING IN MAIN SPAN

| Tendon | Experiment (kip) | BMCOL 50 (kip) |
|----------------------------------|------------------|----------------|
| A1 | 0.245 | 0.251 |
| A2 | 0.200 | 0.213 |
| A3 | 0.115 | 0.169 |
| A4 | 0.074 | 0.131 |
| A5 | 0.012 | 0.091 |
| A6 | 0.012 | 0.055 |
| Raise 0.26 in. at outer supports | 1.04 | 0.700 |
| Total | 1.698 | 1.610 |

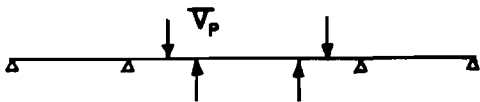
(A) PRESTRESSING FORCE AND ECCENTRICITY OF CABLE.



(B) MOMENT DUE TO PRESTRESSING.



(C) EQUIVALENT VERTICAL FORCE FOR M_p.



(D) POSITION OF LOAD FOR EACH CABLE.

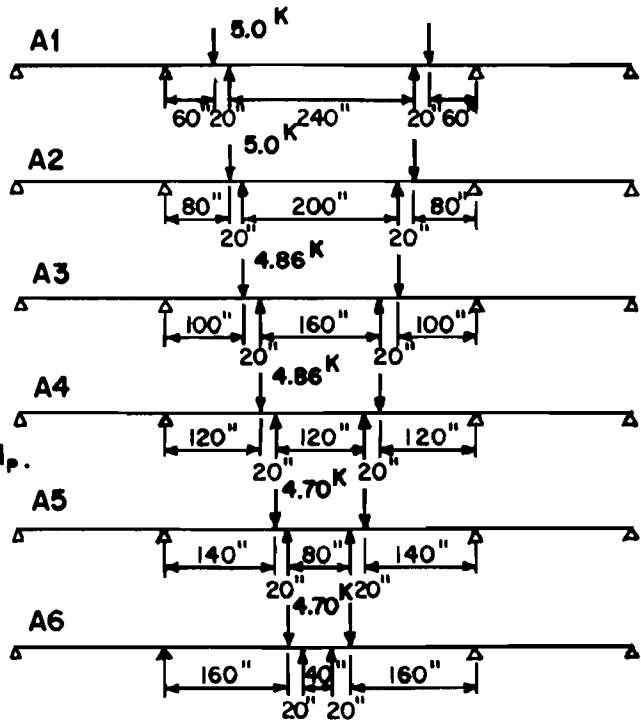


Fig. 6.39. Calculation of end reaction due to positive tendons

than the theoretical values. However, the total experimental reaction (1.698 kip) agreed very well with the total theoretical value (1.610 kip).

This page replaces an intentionally blank page in the original.

-- CTR Library Digitization Team

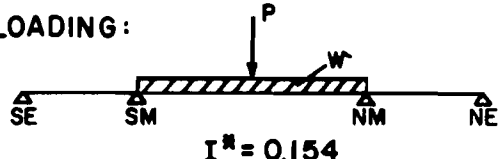
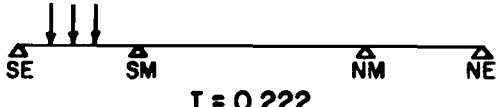
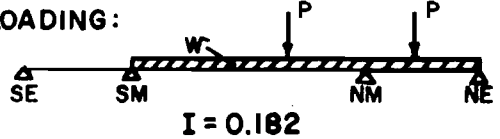
CHAPTER 7

DESIGN SERVICE AND ULTIMATE LOAD TESTS

7.1 General

The completed bridge was load tested for the governing AASHO design loading conditions²¹ shown in Table 7.1.

TABLE 7.1. CRITICAL LOADING CONDITIONS IN LONGITUDINAL DIRECTION

| CASE | CRITICAL CONDITION | LOADING CONDITION |
|------|---|---|
| (1) | MAXIMUM POSITIVE MOMENT AT THE CENTER OF THE MAIN SPAN. | LANE LOADING:  $I^* = 0.154$ |
| (2) | MAXIMUM POSITIVE MOMENT IN THE SIDE SPAN. | TRUCK LOADING:  $I = 0.222$ |
| (3) | MAXIMUM NEGATIVE MOMENT AT THE MAIN PIER. | LANE LOADING:  $I = 0.182$ |
| (4) | MAXIMUM SHEAR ADJACENT TO THE MAIN PIER. | LANE LOADING:  $I = 0.182$ |

* I = IMPACT FACTOR

The order of testing was as follows:

- (1) Service loading [1.0 DL + 1.0 (LL + IL)].
 - (a) Case (2)
 - (b) Case (1)
 - (c) Case (3)
 - (d) Case (4)

(2) Ultimate loading. The ultimate load criteria used in the actual design of the bridge was the Bureau of Public Roads 1969 Ultimate Design Criteria⁷ that $U = 1.35 \text{ DL} + 2.25 (\text{LL} + \text{IL})$. Prior to applying any of the ultimate design live loads, supplementary concrete blocks corresponding to 0.35 dead load were added to the structure. Then, design ultimate live load was applied in the following sequence:

- (a) Case (1)
- (b) Case (3)
- (c) Case (4)
- (d) Case (2)

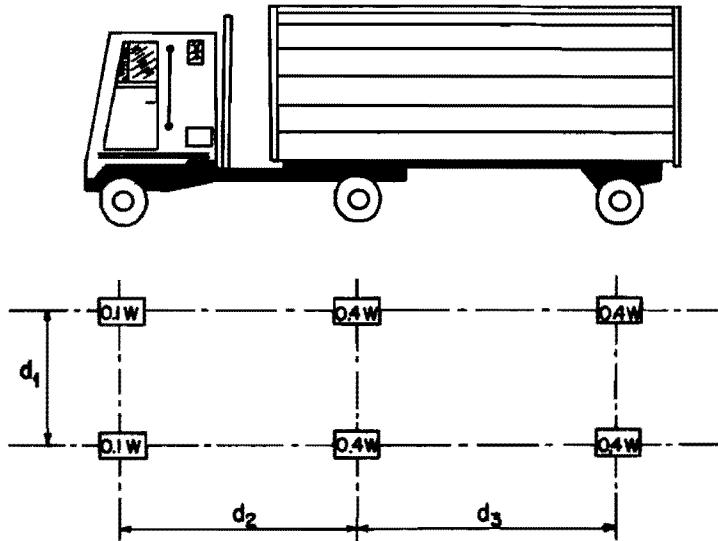
The AASHO reduction factors for load intensity were not used in any tests. These factors (reflecting improbable coincident maximum loading in all four lanes) would have allowed a 25 percent reduction in live load. Special loads were applied to study transverse moment distribution for the different types of truck loadings and lane loading (two lanes). The weight of the asphalt topping, which could be about 8 percent of the dead load, was not included in the model bridge test.

7.2 Test Procedures

7.2.1 Simulation of Loading

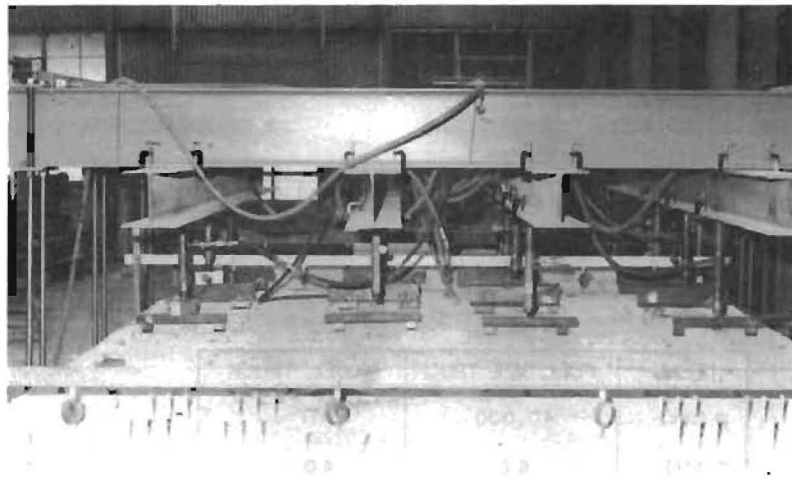
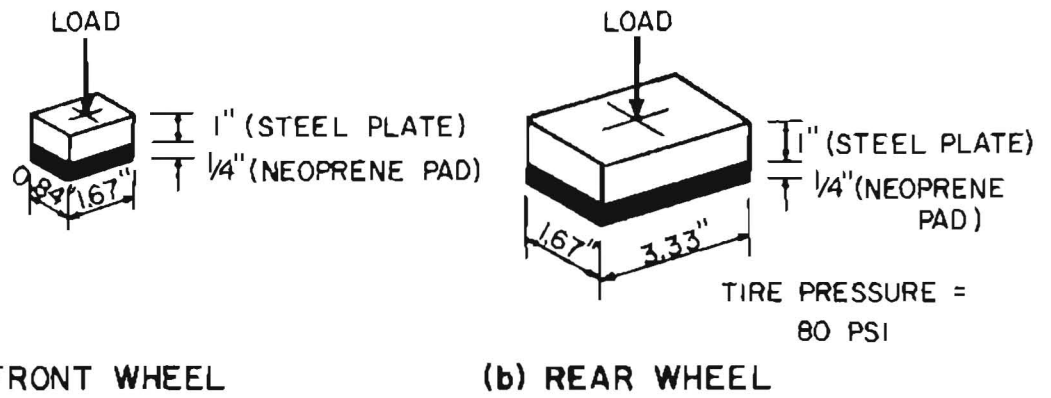
7.2.1.1 Truck Loading. AASHO⁶ HS20-S16-44 truck loadings were scaled as shown in Fig. 7.1. Tire pressure was assumed as 80 psi in sizing the loading pads, as shown in Fig. 7.2.

7.2.1.2 Lane Loading. Uniform lane loads were closely simulated by applying a series of concentrated loads at 4 ft. intervals. Since each lane is roughly centered over a web, as shown in Fig. 7.3, load was applied above each web in the main test series. Transverse distribution was checked in another series.



| ITEM | FULL SIZE TRUCK | MODEL TRUCK |
|-------------|-----------------|---------------------|
| W (lbs) | 40,000 | 1111 |
| d_1 (ft.) | 6.0 | 1.0 |
| d_2 (ft.) | 14.0 | $2\frac{1}{3}$ |
| d_3 (ft.) | 14.0~30.0 | $2\frac{1}{3}$ ~5.0 |

Fig. 7.1. Dimensions of full size and 1/6 scale model AASHO HS20-S16 truck



(c) 4 LANE AASHO HS20-16 TRUCK

Fig. 7.2. Scaled wheels and AASHO HS20-S16 truck

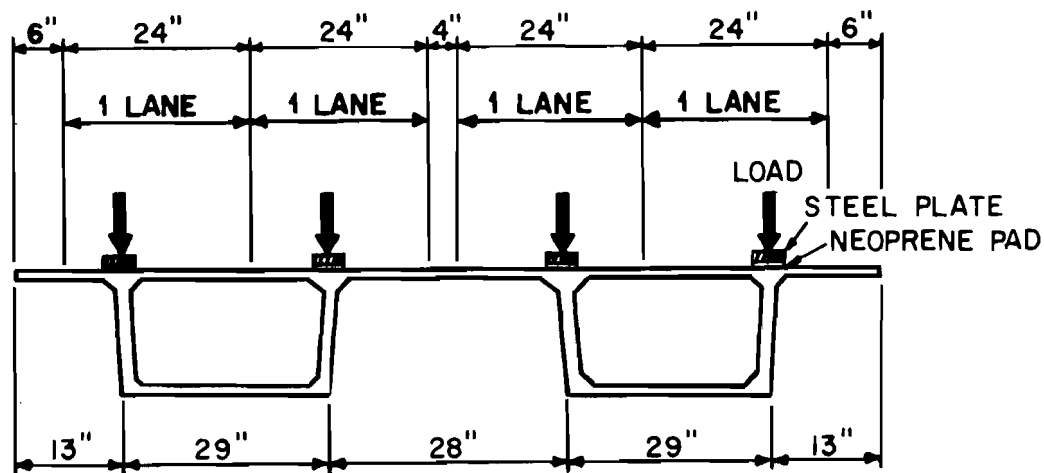


Fig. 7.3. Application of concentrated loads above the webs (in each lane)

Moments and shears for the uniform loads and the equivalent concentrated loads of Fig. 7.4 are compared in Table 7.2. Although extremely close agreement is shown for bending moment, there are some minor differences in shears. These are generally on the conservative side. The least conservative case represents a difference of only 4 percent.

7.2.2 Loading System and Instrumentation

7.2.2.1 Loading System. Loading reactions were furnished by steel beams attached to the structural test floor as shown in Fig. 7.5. Hydraulic rams were connected to pumps with hoses and the number of pumps was minimized by using many manifolds. Load was applied by electric or manual pumps. Two load cells were generally used in each loading system. One load cell was used to regulate pump pressure while the other load cell was used to check the load applied. In addition, hydraulic system pressure gage readings were also recorded for check purposes. Load control procedures worked well.

7.2.2.2 Instrumentation and Observation. Strain gage measurements were taken as shown in Fig. 4.14. Numerous dial gages measured deflections of the top slab, as shown in Fig. 7.6. Although nine gages were used at

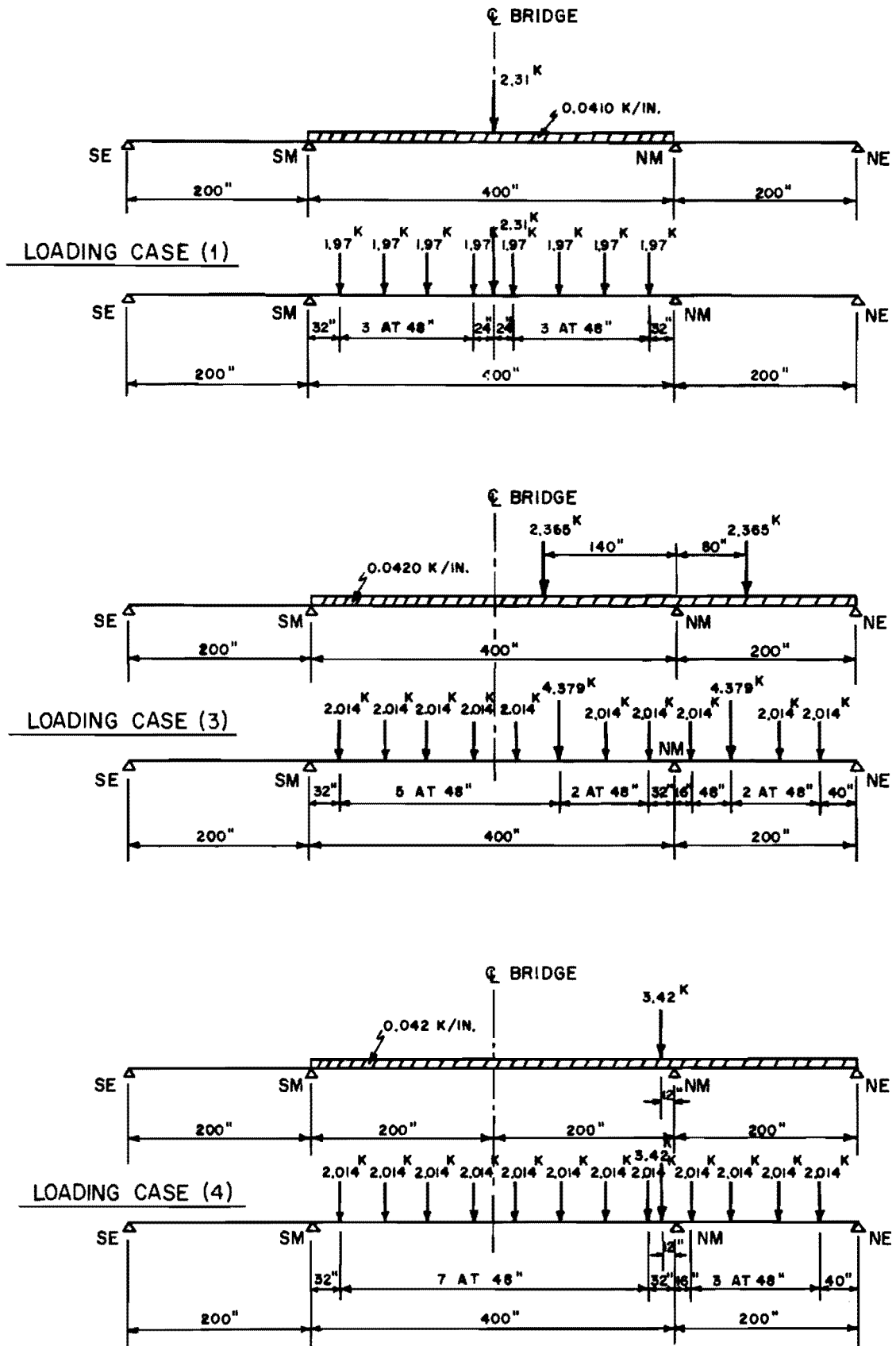
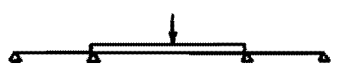
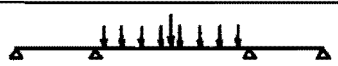
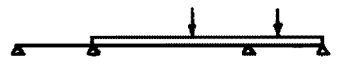
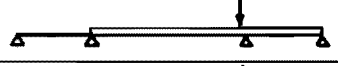
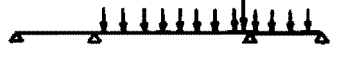
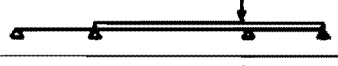
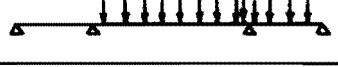
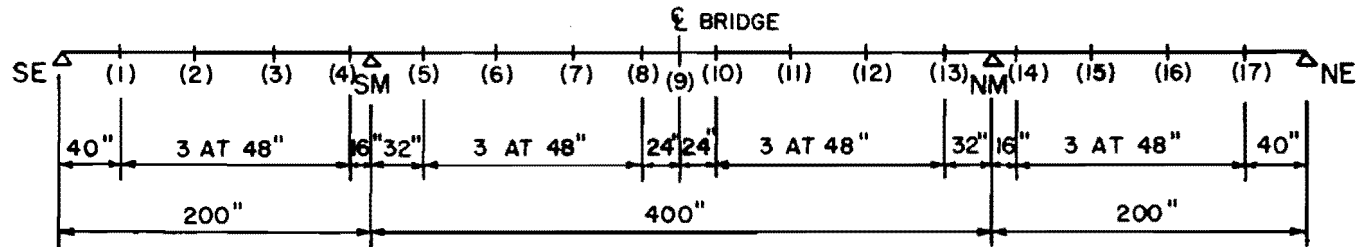
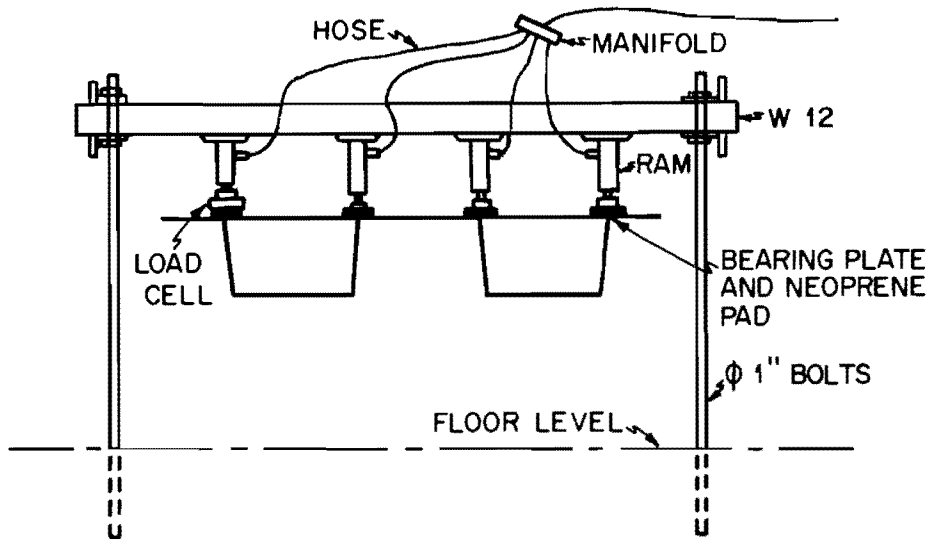


Fig. 7.4. Lane loads and equivalent concentrated loads for four lanes with impact allowances

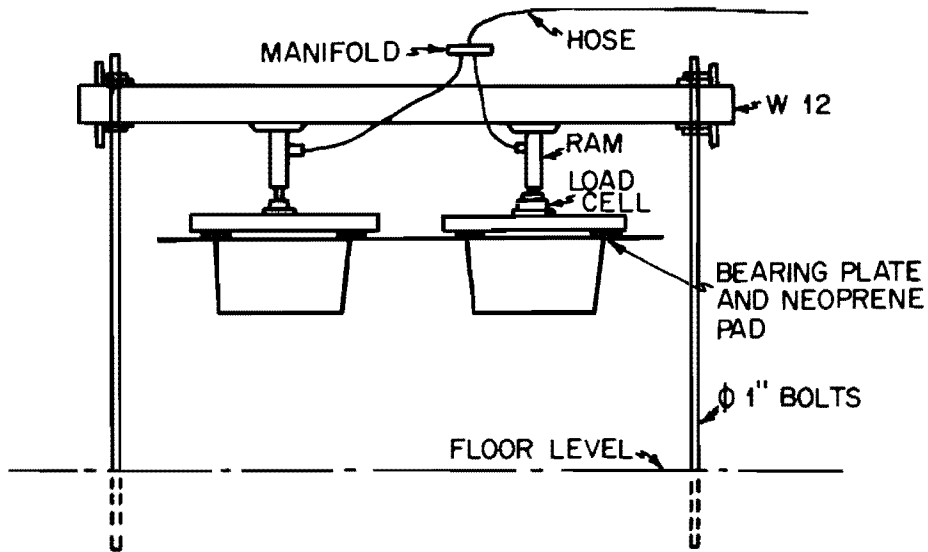
TABLE 7.2. MOMENT OR SHEAR FOR EACH LOADING CASE

| | | SE | (1) | (2) | (3) | (4) | SM | (5) | (6) | (7) | (8) | (9) | (10) | (11) | (12) | (13) | NM | (14) | (15) | (16) | (17) | NE | |
|-------------------|---|-------|-------|-------|-------|-------|-------|-------|-------|-------|-------|-------|-------|-------|-------|-------|-------|-------|-------|-------|-------|-------|-------|
| MOMENT FOR CASE 1 |  | 0 | -99 | -219 | -338 | -457 | -497 | -219 | +121 | +365 | +515 | +555 | +515 | +365 | +121 | -219 | -497 | -457 | -338 | -219 | -99 | 0 | |
| | (K-IN.)  | 0 | -100 | -220 | -340 | -460 | -500 | -221 | +129 | +373 | +524 | +552 | +524 | +373 | +129 | -221 | -500 | -460 | -340 | -220 | -100 | 0 | |
| MOMENT FOR CASE 3 |  | 0 | -89 | -197 | -297 | -412 | -447 | -188 | +120 | +332 | +447 | +467 | +464 | +356 | +68 | -319 | -630 | -494 | -154 | +13 | +46 | 0 | |
| | (K-IN.)  | 0 | -89 | -195 | -301 | -407 | -443 | -176 | +128 | +336 | +446 | +453 | +459 | +376 | +84 | -307 | -632 | -482 | -133 | +5 | +46 | 0 | |
| MOMENT FOR CASE 4 |  | 0 | -80 | -176 | -272 | -368 | -400 | -158 | +122 | +305 | +392 | +399 | +382 | +275 | +71 | -229 | -524 | -420 | -174 | -24 | +30 | 0 | |
| | (K-IN.)  | 0 | -80 | -176 | -272 | -368 | -400 | -150 | +130 | +314 | +401 | +396 | +390 | +289 | +81 | -221 | -526 | -412 | -166 | -16 | +36 | 0 | |
| SHEAR FOR CASE 4 |  | -2.00 | -2.00 | -2.00 | -2.00 | -2.00 | -2.00 | +8.19 | +6.85 | +4.83 | +2.81 | +0.80 | -0.21 | -1.21 | -3.24 | -5.26 | -7.29 | -12.0 | +6.15 | +4.13 | +2.11 | +0.10 | -1.58 |
| | (KIPS)  | -2.00 | -2.00 | -2.00 | -2.00 | -2.00 | -2.00 | +7.85 | +5.84 | +3.82 | +1.81 | -0.21 | -0.21 | -2.22 | -4.23 | -6.25 | -8.26 | +7.14 | +5.13 | +3.11 | +1.10 | -0.92 | -0.92 |

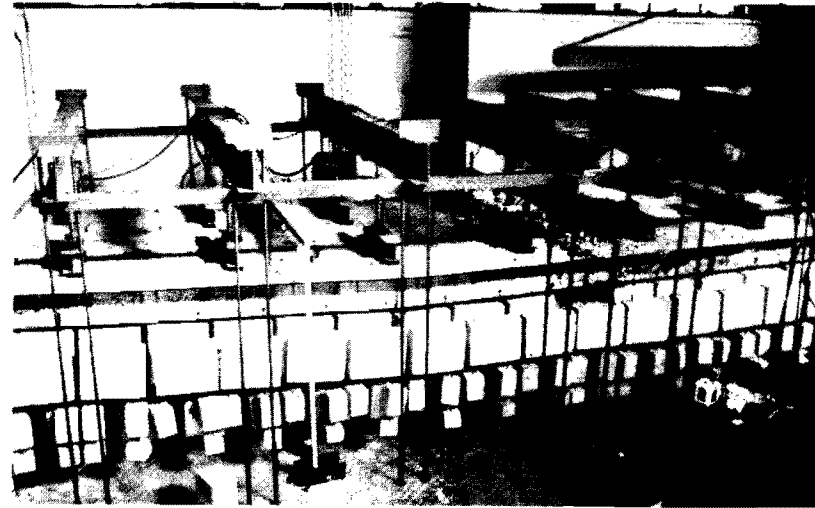




(a) LOADING SETUP 1

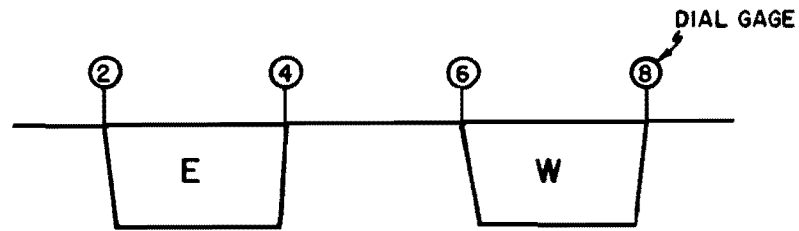


(b) LOADING SETUP 2

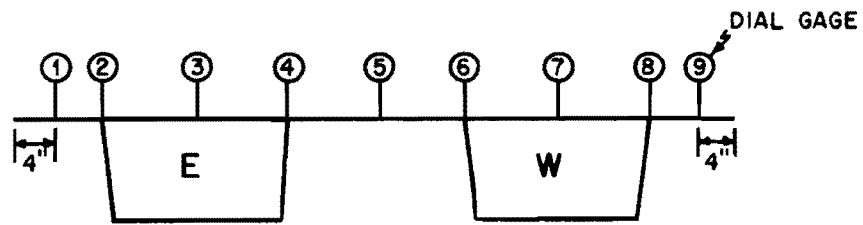


(c) ARRANGEMENT FOR LANE
LOADING

Fig. 7.5. Application of lane load



CASE (1) - 4 DIAL GAGES



CASE (2) - 9 DIAL GAGES

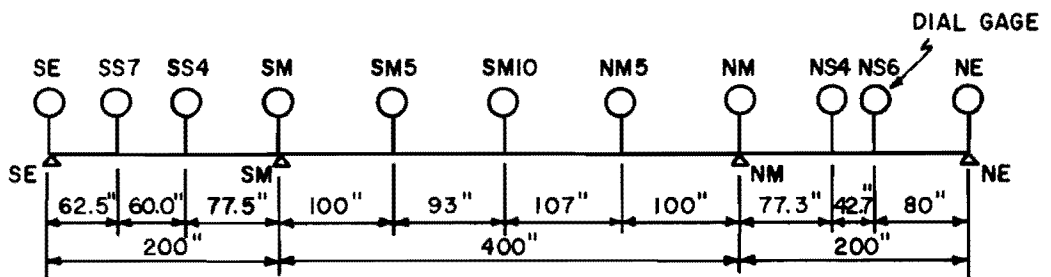


Fig. 7.6. Locations of dial gage readings

some stations, only the readings at the four webs were averaged for longitudinal deflections. Also, slip gages were provided to check relative movement across the critical joint in the maximum shear loading case.

Reactions were measured by load cells under two webs of one box at the outer piers. Load cells could not be used at the main piers because of the anchor bolts. Reaction readings from one box were generally sufficient because most of the loadings were applied uniformly (four lane loads). In the case of nonsymmetric (two lane) loadings, the loadings were repeated on the opposite side to allow reactions for four webs to be determined, taking advantage of symmetry.

Prior to any loading test, 1/4 of the service load was preloaded in order to get stable initial readings.

7.3 Test Results and Interpretations

7.3.1 General. The results of deflection, strain, and reaction measurements are compared with solutions of BMCOL50²⁸ and MUPDI³⁴ programs.

BMCOL50 is a beam-type analysis program which solves the linearly elastic beam or column by a discrete element analysis procedure. This program takes into account variable loads and nonlinear supports. Load-deflection relations for each neoprene pad were measured and these values were input to BMCOL50 as the spring constant at the supports.

MUPDI is a versatile generalized elastic analysis program which can analyze folded plate or box structures with interior rigid diaphragms or supports using folded plate theories which consider cross section warping.

Although BMCOL50 can treat variable sections, the section for MUPDI has to be uniform. This MUPDI limitation should not be serious in this case because of the small variations in the cross sections (thickened bottom slabs only at main pier and adjacent segments). BMCOL50 was used to analyze uniform transverse loadings (four lane loadings) while MUPDI was used primarily for nonuniform transverse loading as in the two-lane loading or in the transverse moment study. For a check and direct comparison of MUPDI and BMCOL50, both were run for one uniform loading case.

All external and thickness dimensions for each member of typical box sections were measured for several segments and averaged section properties were calculated by the BOX2 program.²¹ These "as built" section properties and the measured properties of the materials used in the theoretical calculations were listed in Table 4.2.

7.3.2 Service Loading

7.3.2.1 Four Lane Loadings. (a) Truck Loading. Four lanes of truck loadings were applied in the south span, as shown in Fig. 7.7, to produce the maximum positive moment. Theoretically, additional truck loads should also have been applied simultaneously in the north side span in order to get the maximum moment at the critical section. The calculated effect of loadings in the north span was so small that they were disregarded.

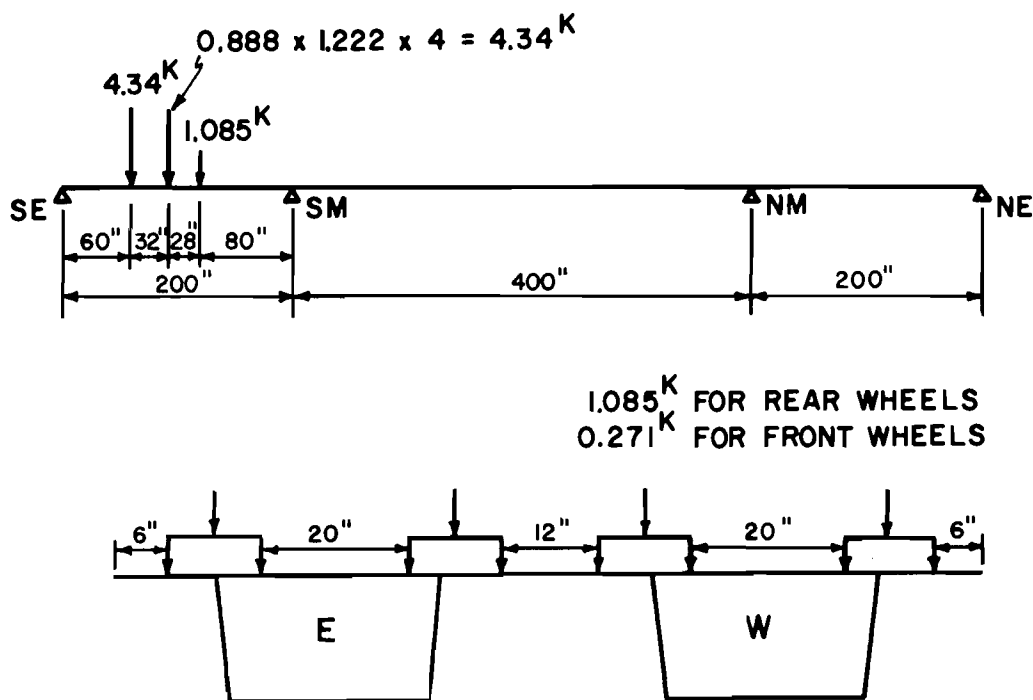


Fig. 7.7. Position of truck loading

As shown in Fig. 7.8(a), experimental and computed longitudinal vertical deflections agreed very well. However, transversely, Fig. 7.8(b) shows that the deflections of the cantilever slabs and the center of the midstrip closure at the SS7 segment were larger than predicted by BMCOL50, which does not consider transverse behavior. The deflection/span ratio under full design live load was approximately 1/7200 in the side span, which is much smaller than 1/300, which is generally considered as acceptable.

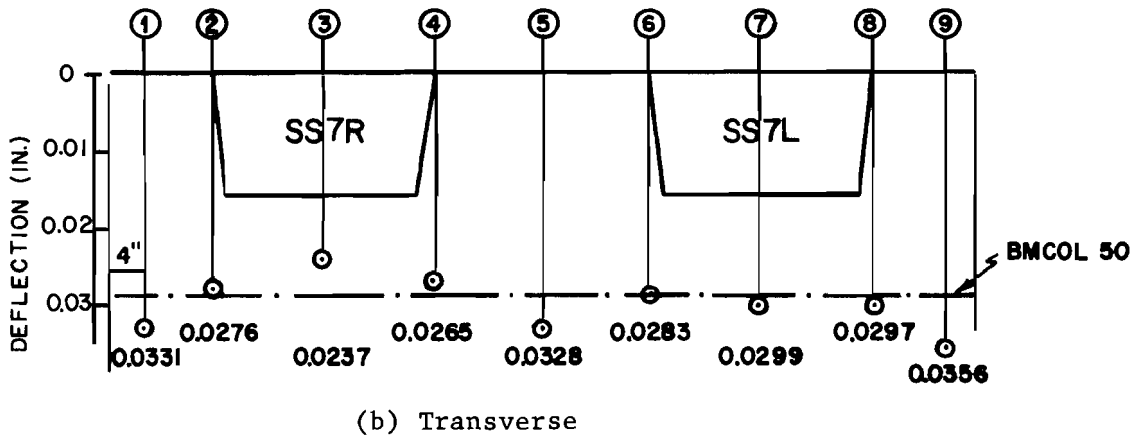
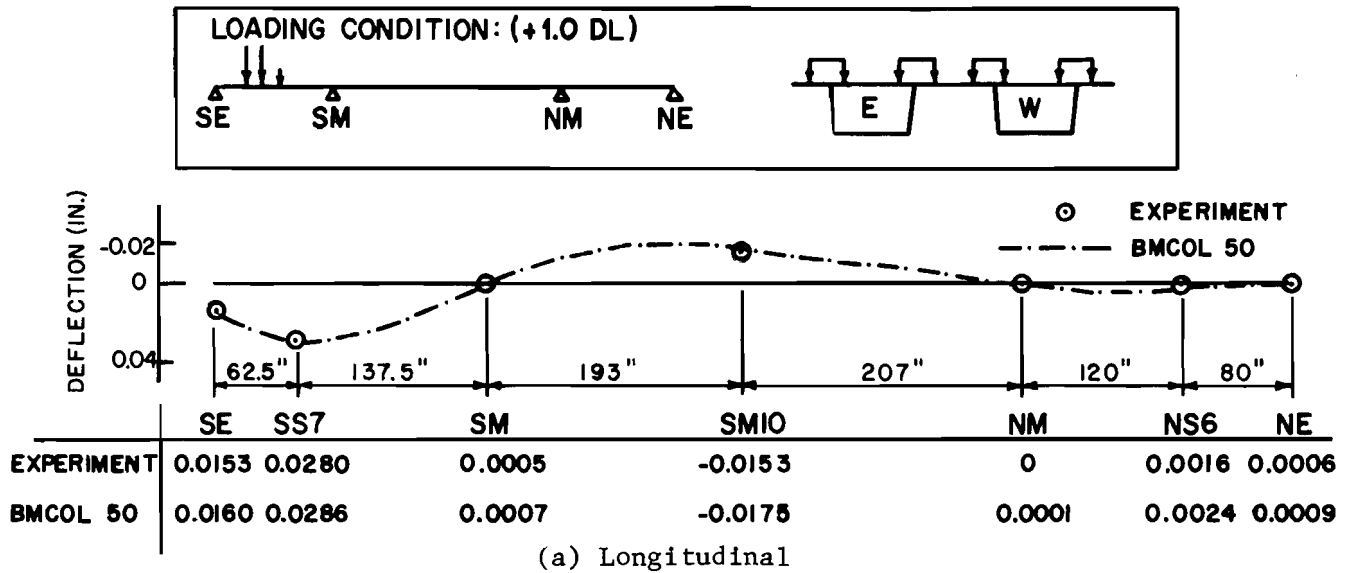
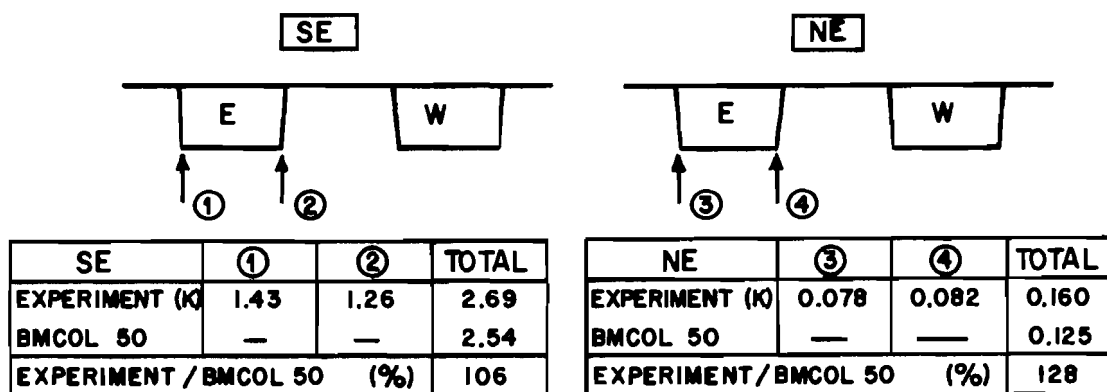


Fig. 7.8. Deflections for truck loadings (four lanes) in side span

Experimental and BMCOL50 reaction results, shown in Fig. 7.9, agreed fairly well at the outer support of the loaded span and showed reasonable agreement in the unloaded span considering the very small magnitude of that reaction.



(a) Loaded span

(b) Unloaded span

Fig. 7.9. Reactions at outer supports for truck loadings (four lanes) in side span

Strains shown in Fig. 7.10 showed larger values in the top slab above the webs than at midspan of the top slab. The bottom slab strains were almost uniform. The experimental and BMCOL50 results agreed very well except for the inability of BMCOL50 to treat section warping.

(b) Lane Loadings. Lane loadings were applied for maximum positive moment in the main span (see Figs. 7.11 to 7.13) and maximum negative moment at an interior pier (see Figs. 7.14 to 7.16).

Comparisons of experimental and theoretical data for service level four lane loadings show excellent agreement especially for longitudinal deflection.

Tensile strains due to the service level live loadings were smaller than the compressive strains induced by prestressing during construction so that the sections remained completely in compression.

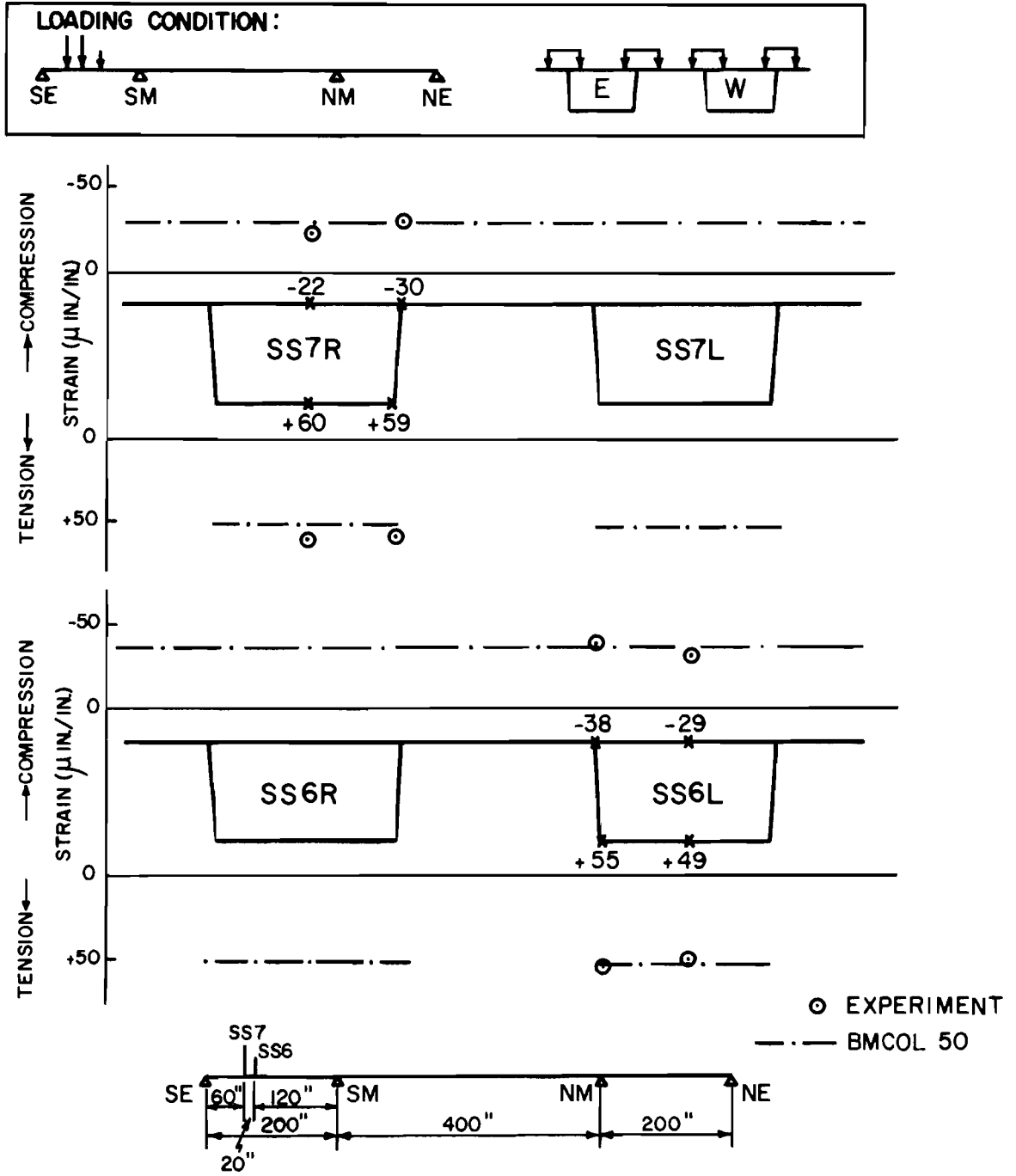


Fig. 7.10 . Longitudinal strains along SS7 and SS6 for truck loadings (four lanes) in side span

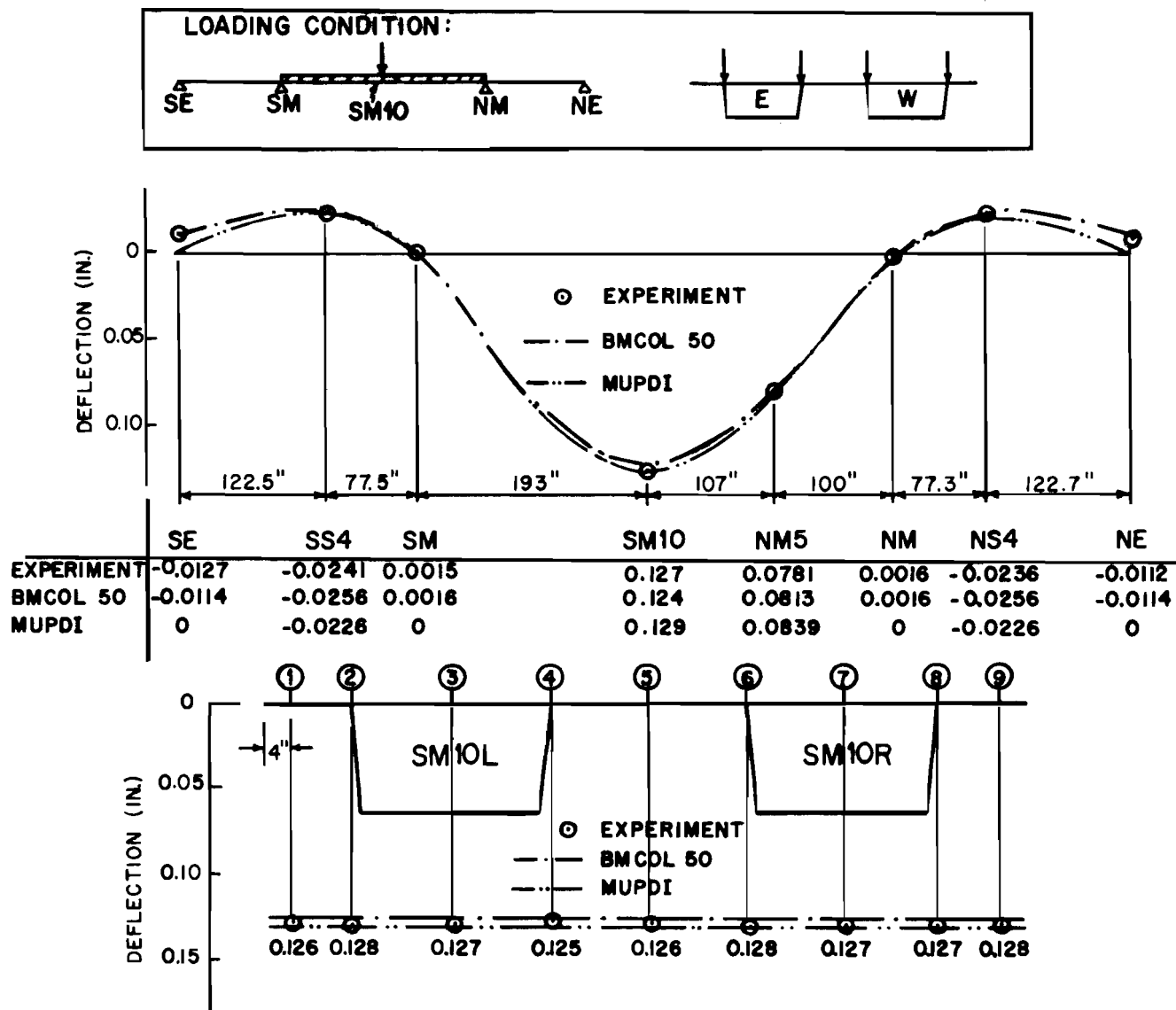


Fig. 7.11. Deflections for lane loadings (four lanes) in main span

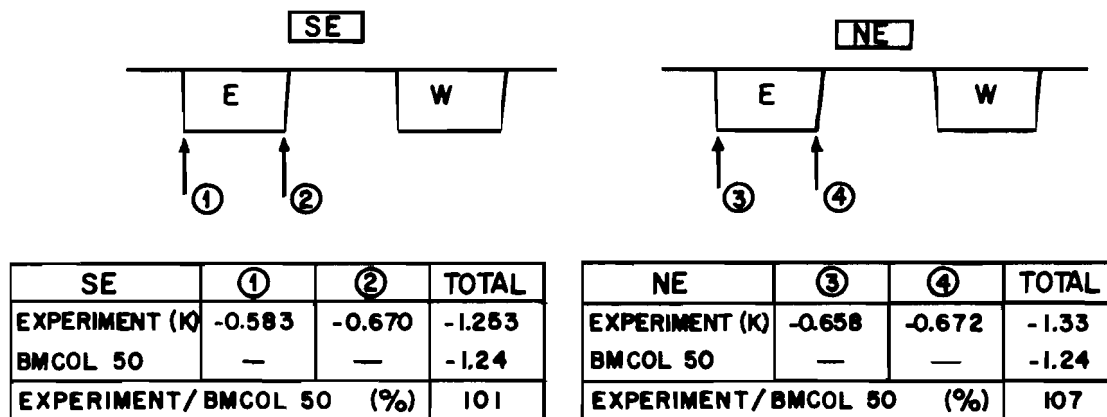


Fig. 7.12. Reactions at outer supports for lane loadings (four lanes) in main span

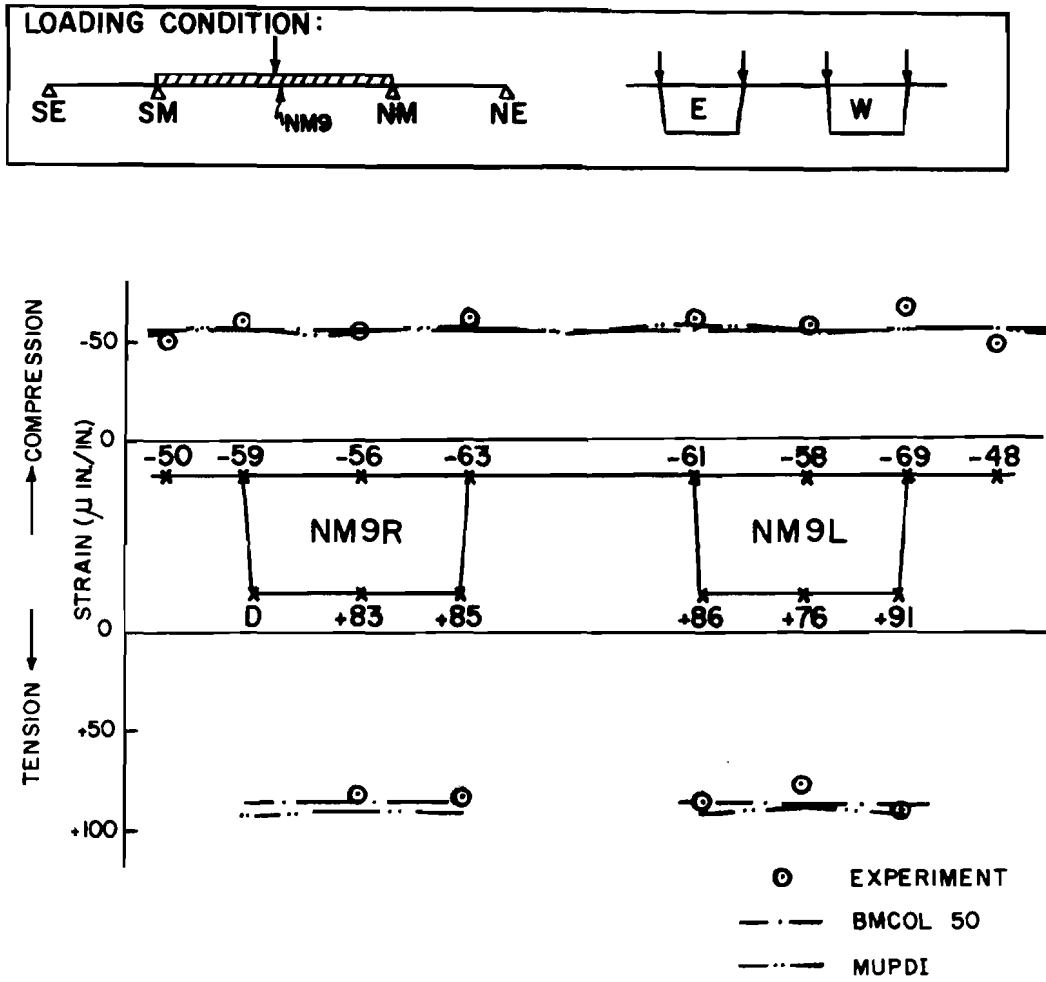


Fig. 7.13. Longitudinal strains along NM9 for lane loadings (four lanes) in main span

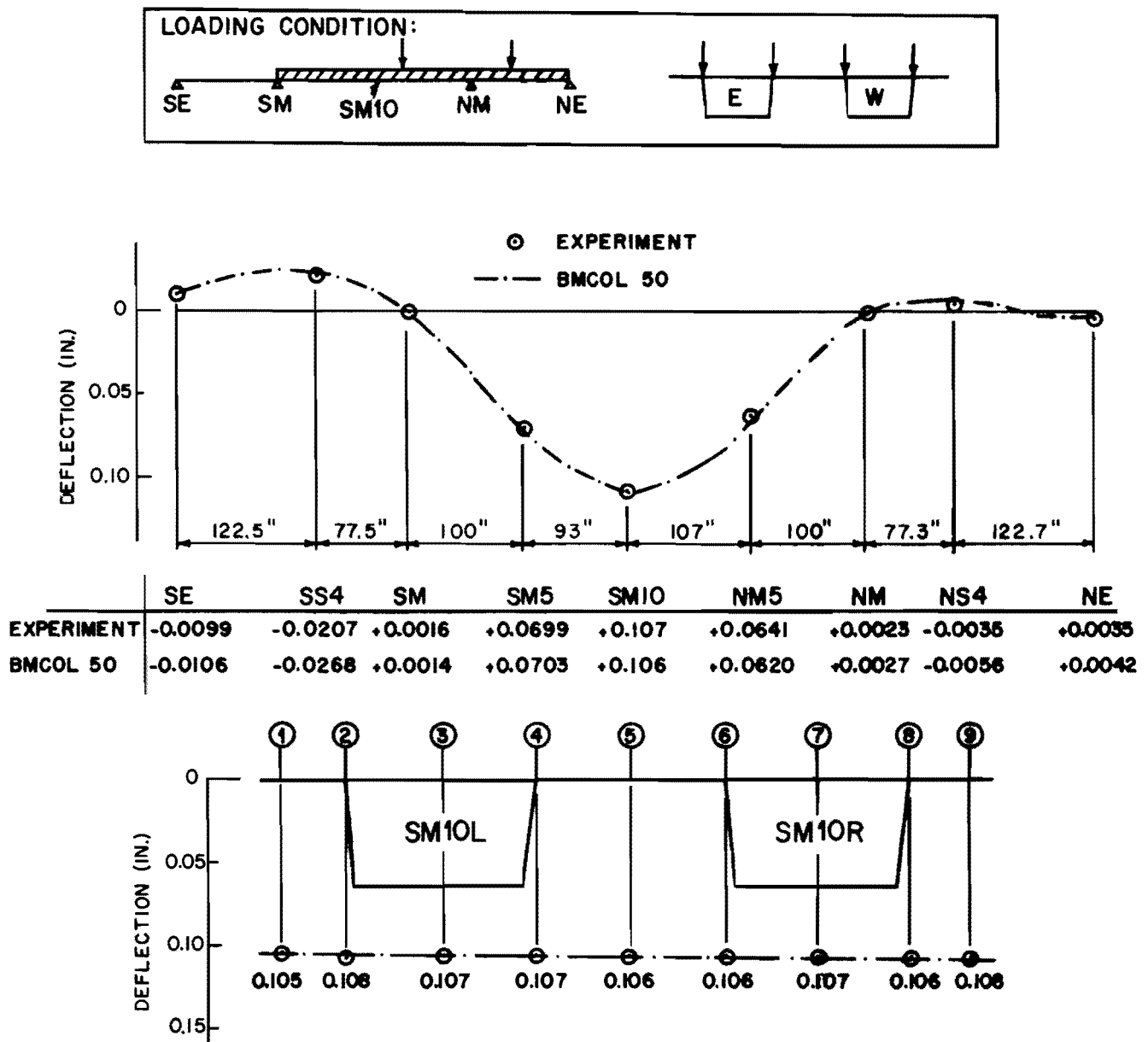


Fig. 7.14. Deflections for lane loadings (four lanes) in main and one side span

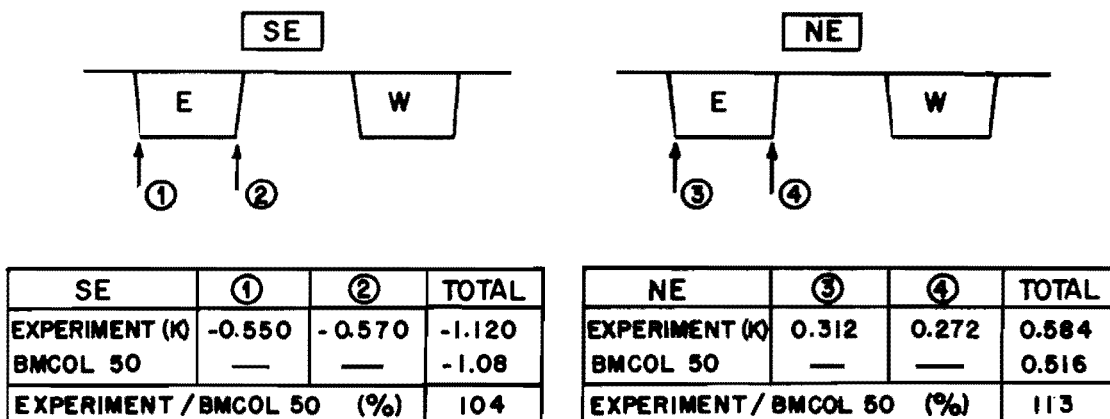


Fig. 7.15. Reactions at outer supports for lane loadings in main and one side span

The deflection/span ratio under full design live load was approximately $1/3200$ in the main span. This value is much smaller than $1/300$ which is generally considered as acceptable.

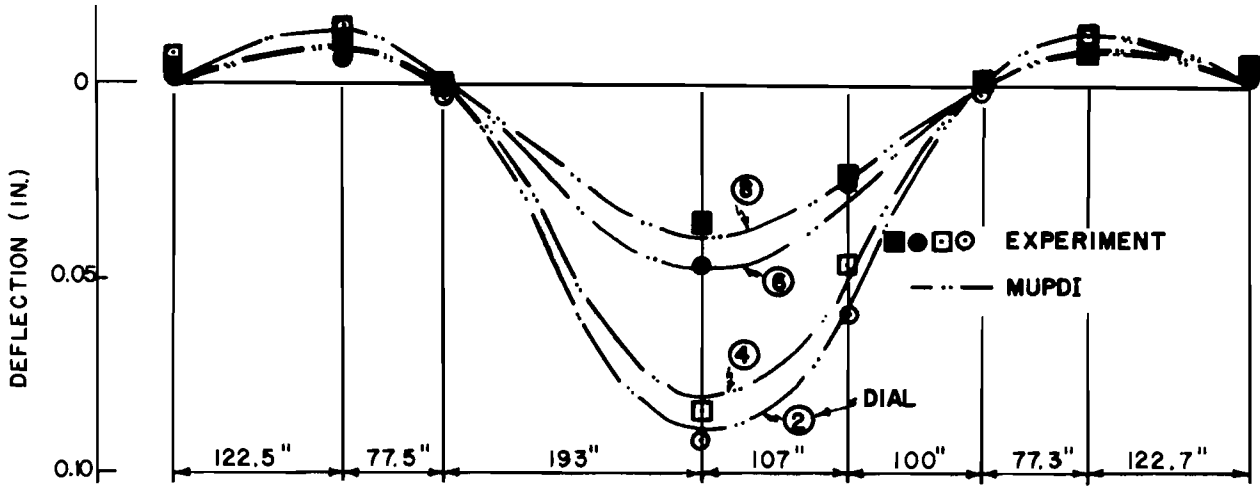
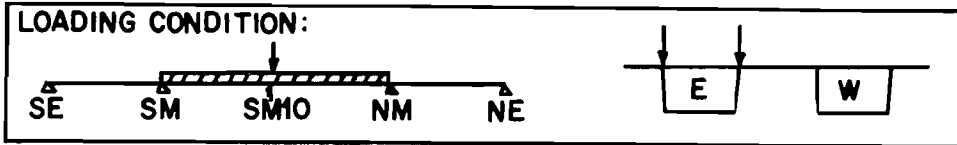
It is very difficult to determine possible warping or shear lag from the experimental data, because the low magnitude strain readings are very sensitive to the exact position of strain gages and dimensional placement tolerances. There was some indication of shear lag in the top slab, but it was negligible for design purposes. The twin box sections were generally acting as a beam and little warping occurred. Comparison of the predicted strain using BMCOL50 and MUPDI in Fig. 7.13 show this effect would be expected to be negligible.

Although no special instrumentation was included for the critical shear stress locations, the maximum shear loading case was also applied. There was no visible diagonal tension cracking around the NM pier and no slip at the joints.

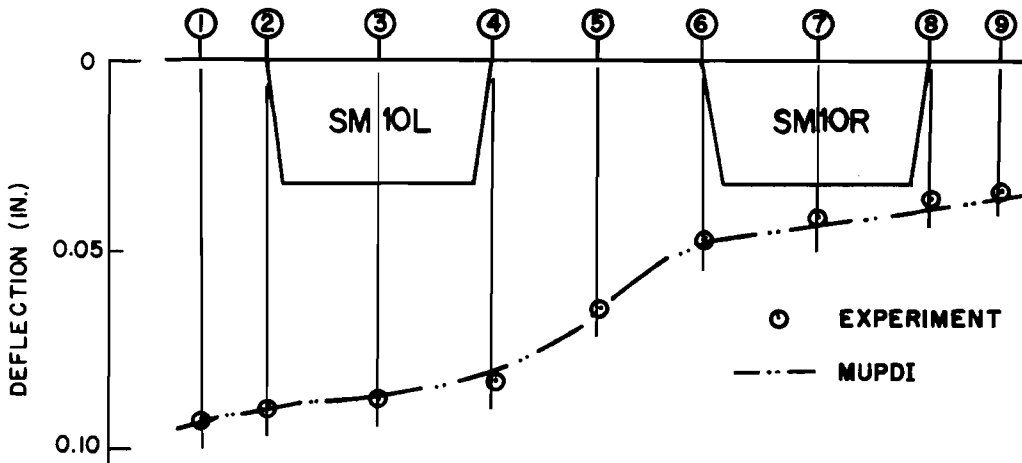
7.3.2.2 Two Lane Loadings (Loads on One Box). Two lanes on one side of the bridge were loaded with lane loadings to produce the critical moment at the midspan of the main span and then at the main pier. Test results for deflections and strains were compared with the results of MUPDI, since BMCOL50 cannot treat unsymmetrical loading across the section.

Comparison of the theoretical and experimental deflection and strain diagrams (Figs. 7.17, 7.18, 7.20, and 7.21) show that experimental results and the MUPDI analysis agreed extremely well in general. Approximately one-third of the load was distributed to the unloaded box section at midspan of the main span. Loading only in the main span was more critical transversely than was loading of both main and side spans. At the main supports the webs farthest from the loaded box deflected upward in both loading cases.

Strains across the bottom slab of each box were fairly uniform because of high torsional rigidity of the box section. However, strains across the top slab definitely decreased from one side to the other side. The reactions at the outer supports shown in Fig. 7.19 indicated that the



| | | SE | SS4 | SM | SM10 | NM5 | NM | NS4 | NE |
|------------|---|---------|---------|---------|---------|---------|---------|---------|---------|
| EXPERIMENT | ② | -0.0068 | -0.0140 | +0.0029 | +0.0913 | +0.0586 | +0.0019 | -0.0125 | -0.0057 |
| | ④ | -0.0072 | -0.0150 | +0.0007 | +0.0834 | +0.0465 | +0.0004 | -0.0118 | -0.0064 |
| | ⑥ | -0.0013 | -0.0067 | +0.0002 | +0.0463 | +0.0239 | +0.0013 | -0.0089 | -0.0033 |
| | ⑧ | -0.0039 | -0.0089 | -0.0006 | +0.0363 | +0.0227 | -0.0005 | -0.0091 | -0.0036 |
| MUPDI | ② | 0 | -0.0137 | 0 | +0.0895 | +0.0588 | 0 | -0.0137 | 0 |
| | ④ | 0 | -0.0143 | 0 | +0.0811 | +0.0524 | 0 | -0.0143 | 0 |
| | ⑥ | 0 | -0.0083 | 0 | +0.0479 | +0.0316 | 0 | -0.0083 | 0 |
| | ⑧ | 0 | -0.0090 | 0 | +0.0394 | +0.0251 | 0 | -0.0090 | 0 |



| | | | | | | | | | |
|------------|--------|--------|--------|--------|--------|--------|--------|--------|--------|
| EXPERIMENT | ① | ② | ③ | ④ | ⑤ | ⑥ | ⑦ | ⑧ | ⑨ |
| | 0.0931 | 0.0913 | 0.0875 | 0.0834 | 0.0653 | 0.0463 | 0.0408 | 0.0363 | 0.0339 |
| MUPDI | 0.0925 | 0.0895 | 0.0858 | 0.0811 | 0.0646 | 0.0473 | 0.0430 | 0.0389 | 0.0368 |

Fig. 7.17. Deflections for lane loadings (two lanes) in main span

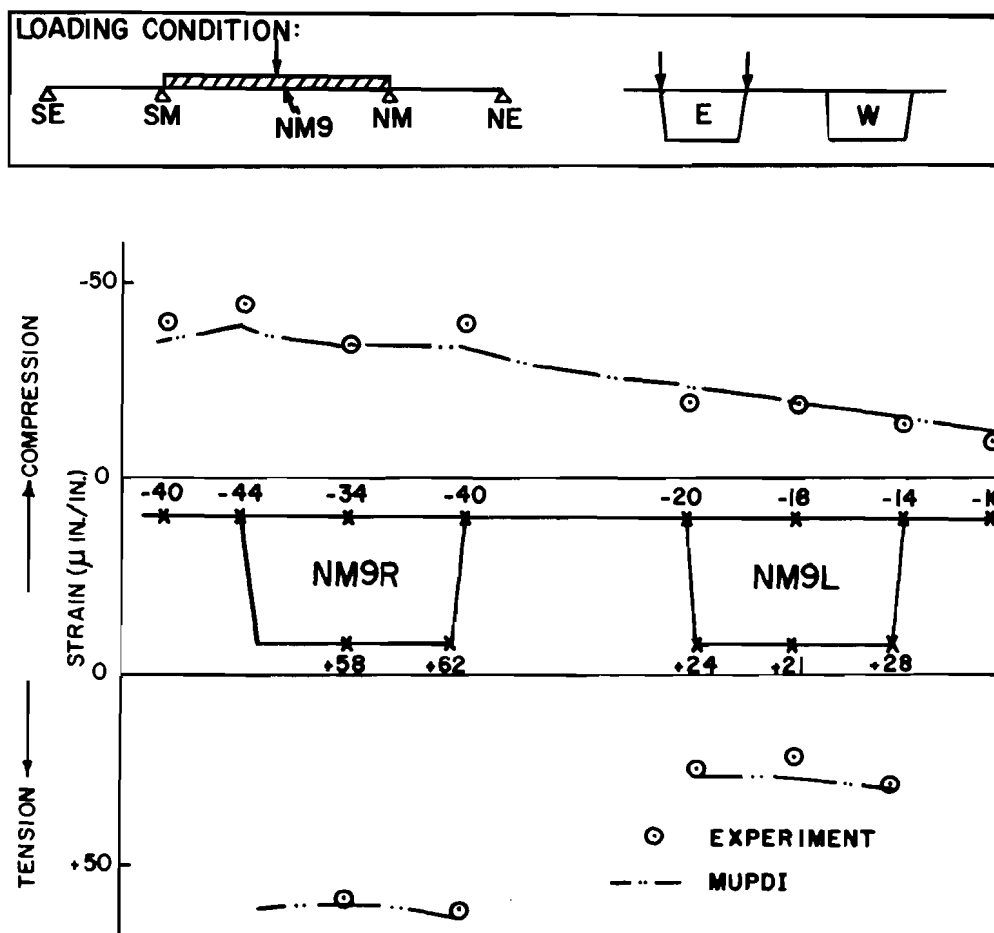


Fig. 7.18. Longitudinal strains along NM9 for lane loadings (two lanes) in main span

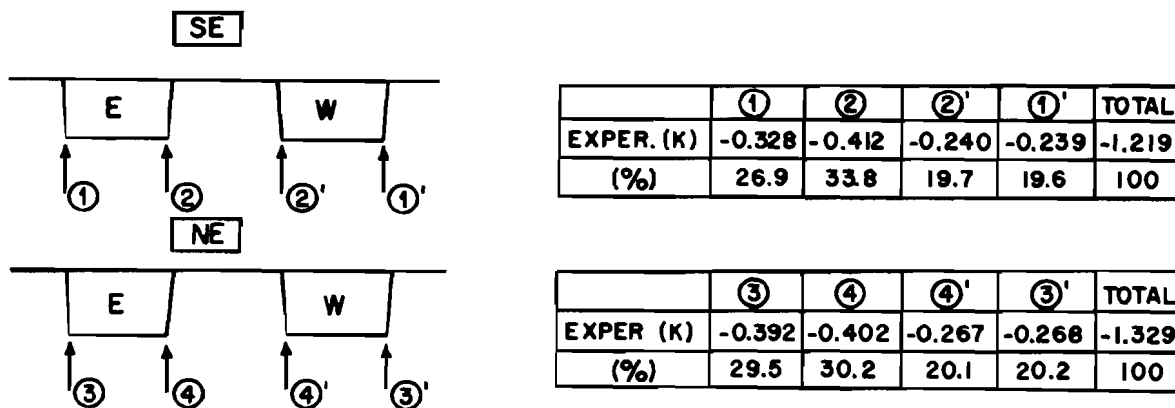
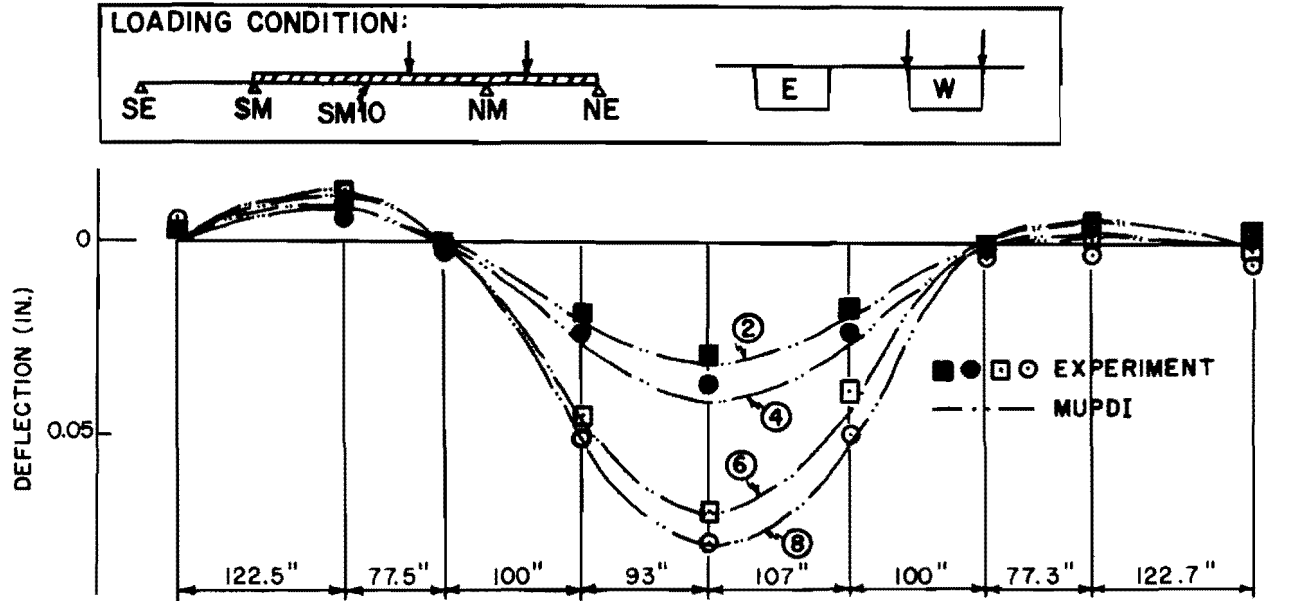
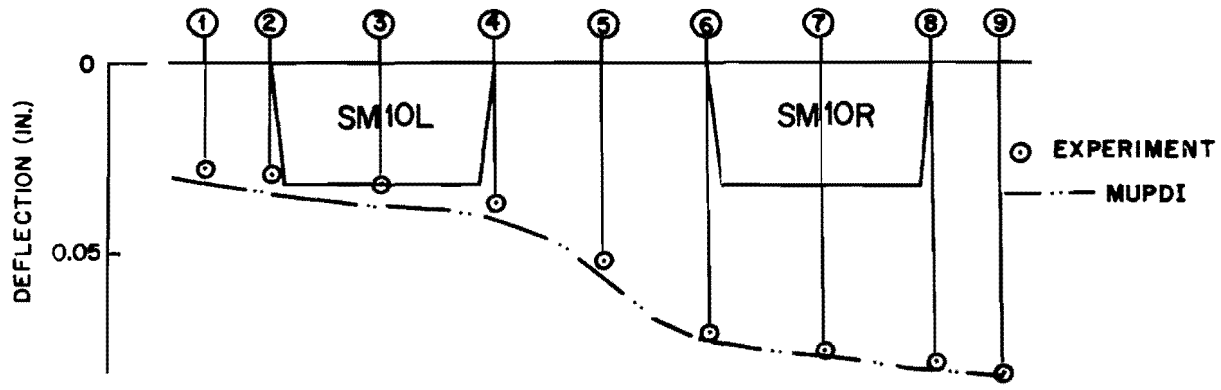


Fig. 7.19. Reactions at outer supports for lane loadings (two lanes) in main span



| | SE | SS4 | SM | SM5 | SM10 | NM5 | NM | NS4 | NE |
|-------------------|-----------|---------|---------|---------|---------|---------|---------|---------|---------|
| EXPERIMENT | ② -0.0033 | -0.0080 | -0.0005 | +0.0193 | +0.0296 | +0.0175 | -0.0010 | -0.0046 | -0.0029 |
| ④ -0.0025 | -0.0060 | +0.0016 | +0.0234 | +0.0368 | +0.0232 | +0.0010 | -0.0032 | -0.0007 | |
| ⑥ -0.0022 | -0.0138 | +0.0020 | +0.0455 | +0.0698 | +0.0386 | +0.0010 | -0.0005 | +0.0029 | |
| ⑧ -0.0050 | -0.0129 | +0.0018 | +0.0513 | +0.0775 | +0.0501 | +0.0038 | +0.0031 | +0.0061 | |

| | SE | SS4 | SM | SM5 | SM10 | NM5 | NM | NS4 | NE |
|--------------|---------|---------|---------|---------|---------|---------|---------|---------|----|
| MUPDI | ② 0 | -0.0080 | 0 | +0.0218 | +0.0339 | +0.0209 | 0 | -0.0063 | 0 |
| ④ 0 | -0.0073 | 0 | +0.0277 | +0.0417 | +0.0270 | 0 | -0.0048 | 0 | |
| ⑥ 0 | -0.0129 | 0 | +0.0467 | +0.0713 | +0.0461 | 0 | -0.0014 | 0 | |
| ⑧ 0 | -0.0123 | 0 | +0.0526 | +0.0791 | +0.0521 | 0 | 0 | 0 | |



| | ① | ② | ③ | ④ | ⑤ | ⑥ | ⑦ | ⑧ | ⑨ |
|-------------------|--------|--------|--------|--------|--------|--------|--------|--------|--------|
| EXPERIMENT | 0.0276 | 0.0296 | 0.0321 | 0.0368 | 0.0522 | 0.0698 | 0.0739 | 0.0775 | 0.0804 |
| MUPDI | 0.0315 | 0.0339 | 0.0372 | 0.0417 | 0.0566 | 0.0713 | 0.0756 | 0.0791 | 0.0819 |

Fig. 7.20. Deflections for lane loadings (two lanes) in main and one side span

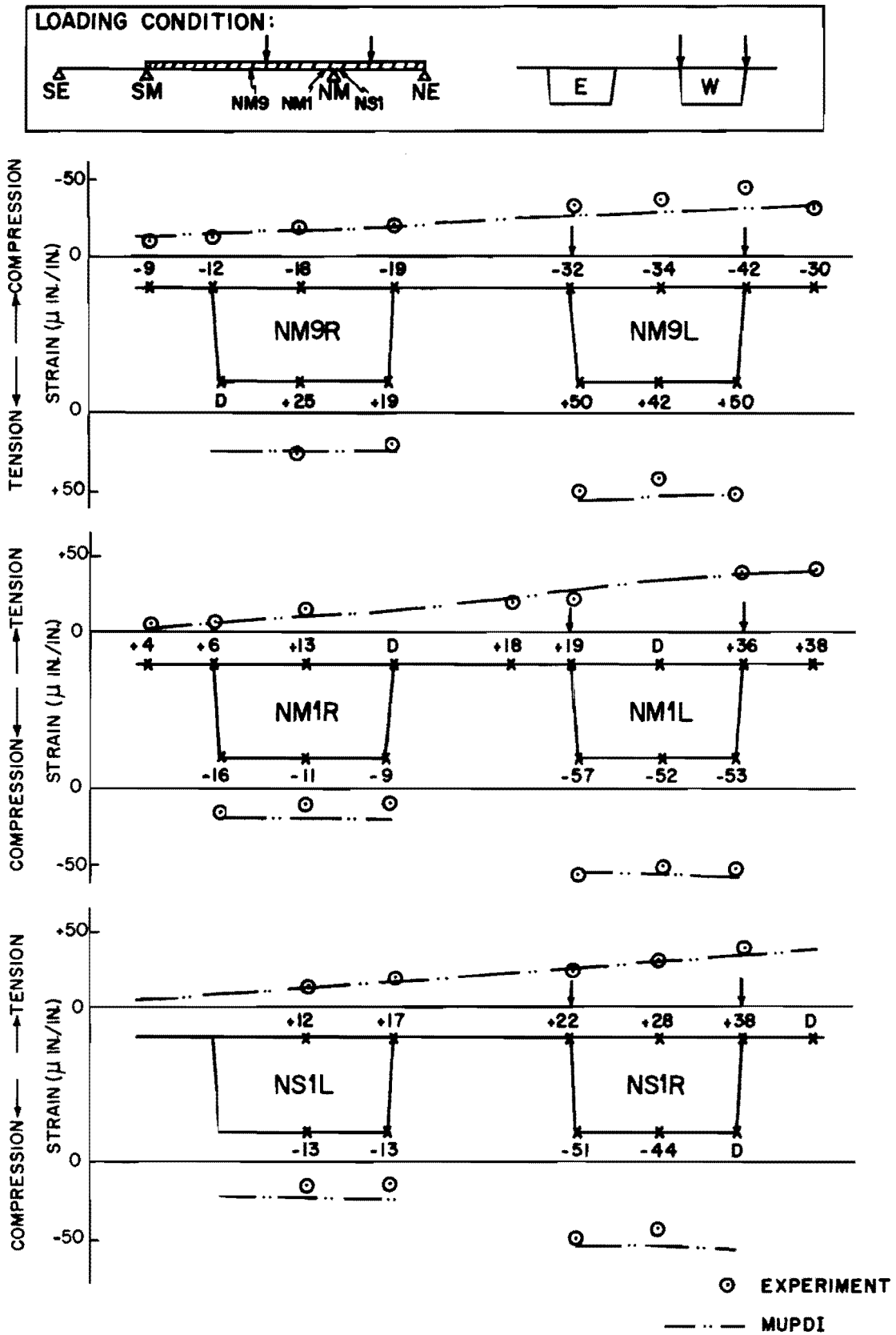
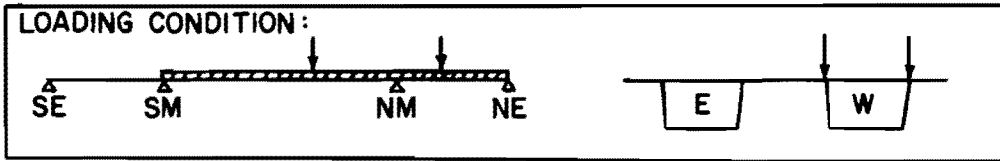
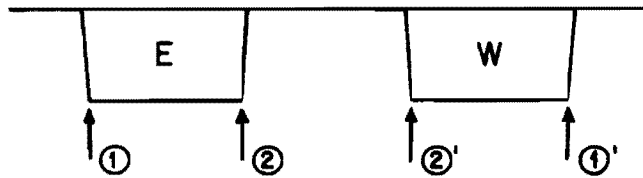


Fig. 7.21. Longitudinal strains for lane loadings (two lanes) in main and one side span

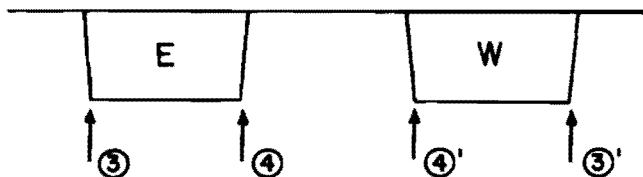


SE



| SE | ① | ② | ②' | ①' | TOTAL |
|----------------|--------|--------|--------|--------|--------|
| EXPERIMENT (K) | -0.239 | -0.197 | -0.347 | -0.314 | -1.097 |
| (%) | 21.8 | 18.0 | 31.6 | 28.6 | 100 |

NE



| NE | ③ | ④ | ④' | ③' | TOTAL |
|----------------|--------|--------|-------|-------|--------|
| EXPERIMENT (K) | -0.170 | -0.067 | 0.334 | 0.486 | +0.583 |
| (%) | -29.1 | -11.5 | 57.3 | 83.3 | 100 |

Fig. 7.22. Reactions at outer supports for lane loadings (two lanes) in main and one side span

loaded box is experiencing little twist because reactions under the two webs of the box section were almost equal when loading was only in the main span. When the loads were applied in both the main and side spans, Fig. 7.22 showed the end reactions were not uniform under each box of the loaded side span and showed substantial twist effects. However, the reaction under each box was reasonably uniform at the end support of the unloaded side span.

Although the support conditions and section properties input into MUPDI differed slightly from the actual model, the MUPDI results agreed very well with the experimental results. Therefore, MUPDI can be used in design to predict the longitudinal load distribution for nonuniform loading. Transverse moments from these loadings are discussed in Sec. 7.3.4 and are compared with MUPDI results.

7.3.3 Ultimate Design Loading Specified by BPR Criteria

7.3.3.1 Additional 0.35 DL. Ultimate design dead load is specified as 1.35 DL by the BPR criteria.⁷ The additional 0.35 DL was applied to the completed structure, as shown in Fig. 7.23, by using additional concrete blocks to supplement the previously adjusted 1.0 DL segment weight. These blocks were permanently added to the bridge, so 1.35 DL was the effective dead load in all later cases.

The experimental results are generally slightly larger than the theoretical values for both deflection and reactions, as shown in Figs. 7.24 and 7.25. Strain readings show considerable scatter and do not agree with the theoretical values, as shown in Fig. 7.26. The maximum moment due to this loading is less than that due to the service live load producing maximum positive moment at midspan of the main span. Thus, the bridge should still be in the elastic range. The large deviation of the experimental strain results from the theoretical values is probably due to temperature and time variations in the electrical data record instruments (it took about 10 hours to hang all concrete blocks).

7.3.3.2 Maximum Positive Moment, Main Span. Live loading, as shown in Fig. 7.27, was applied and incrementally increased to design

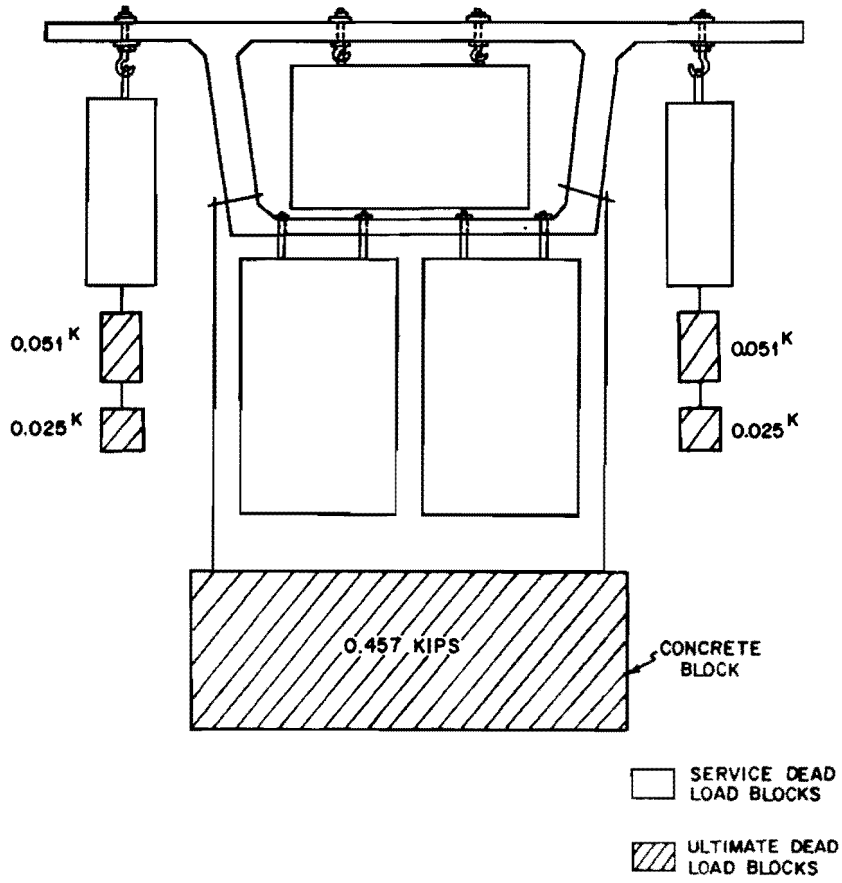


Fig. 7.23. Concrete blocks for 0.35 DL

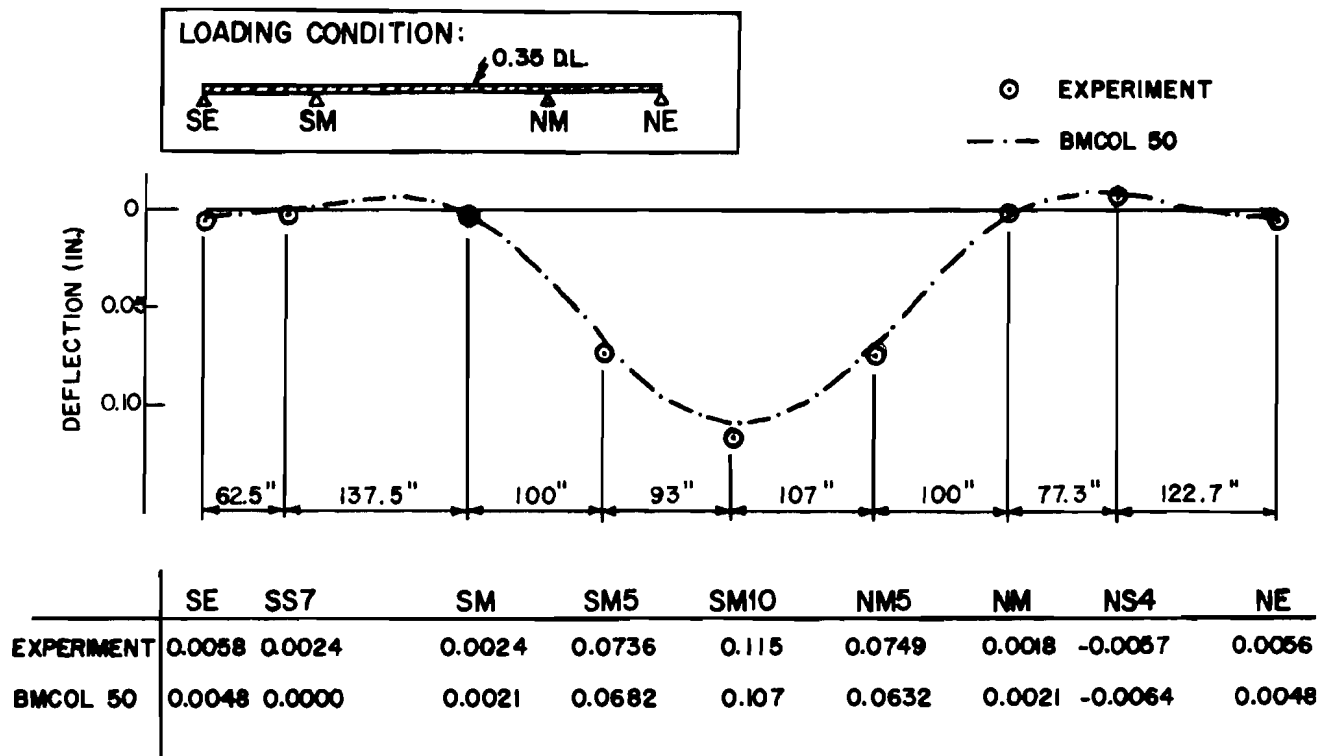


Fig. 7.24. Deflections for 0.35 DL

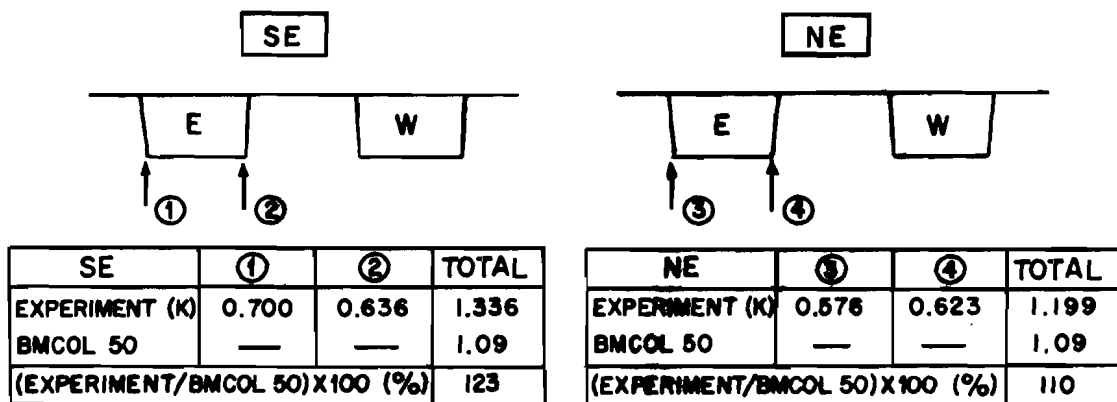


Fig. 7.25. Reactions at outer supports for 0.35 DL

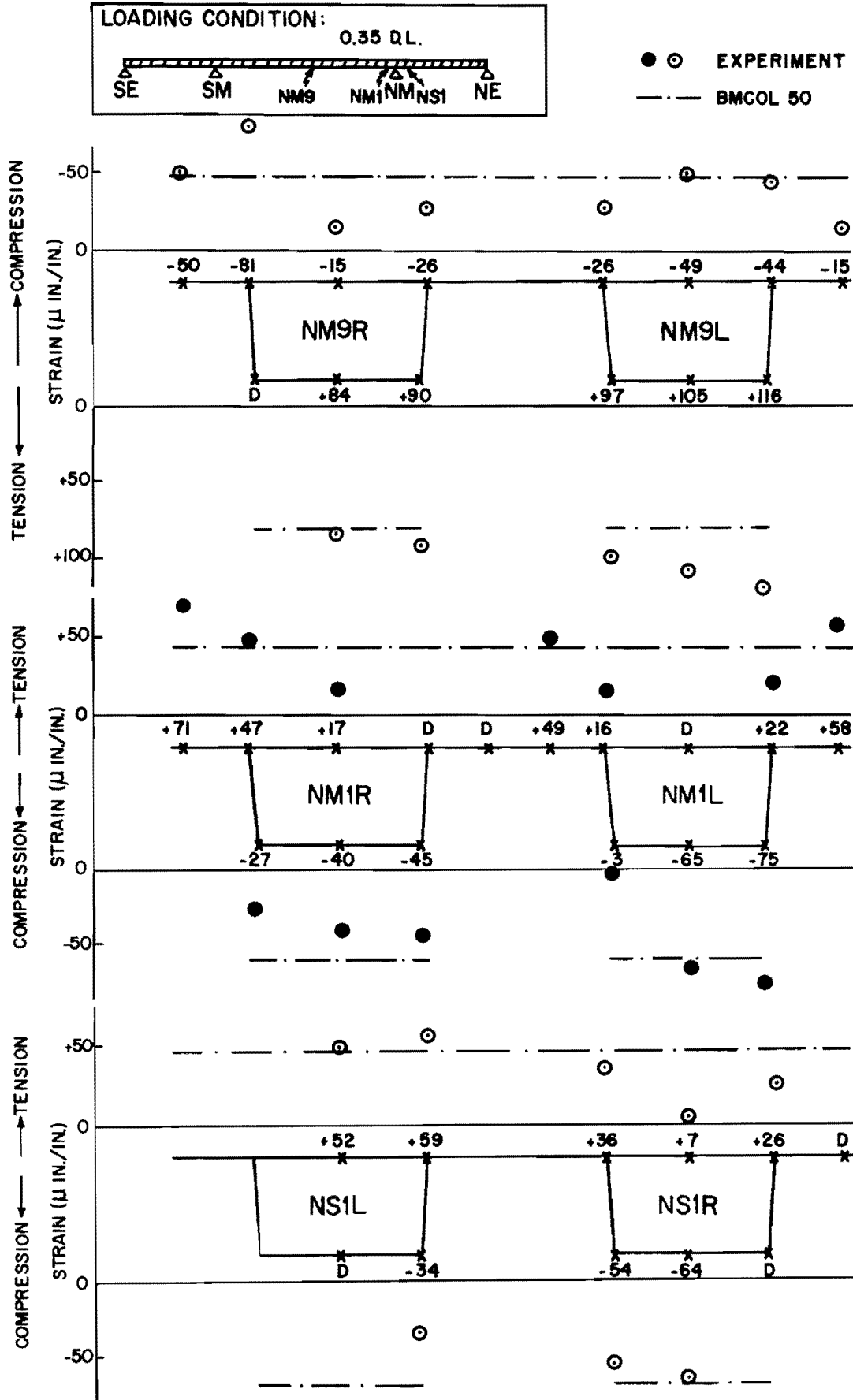


Fig. 7.26. Longitudinal strains along NM9, NM1 and NS1 for 0.35 DL

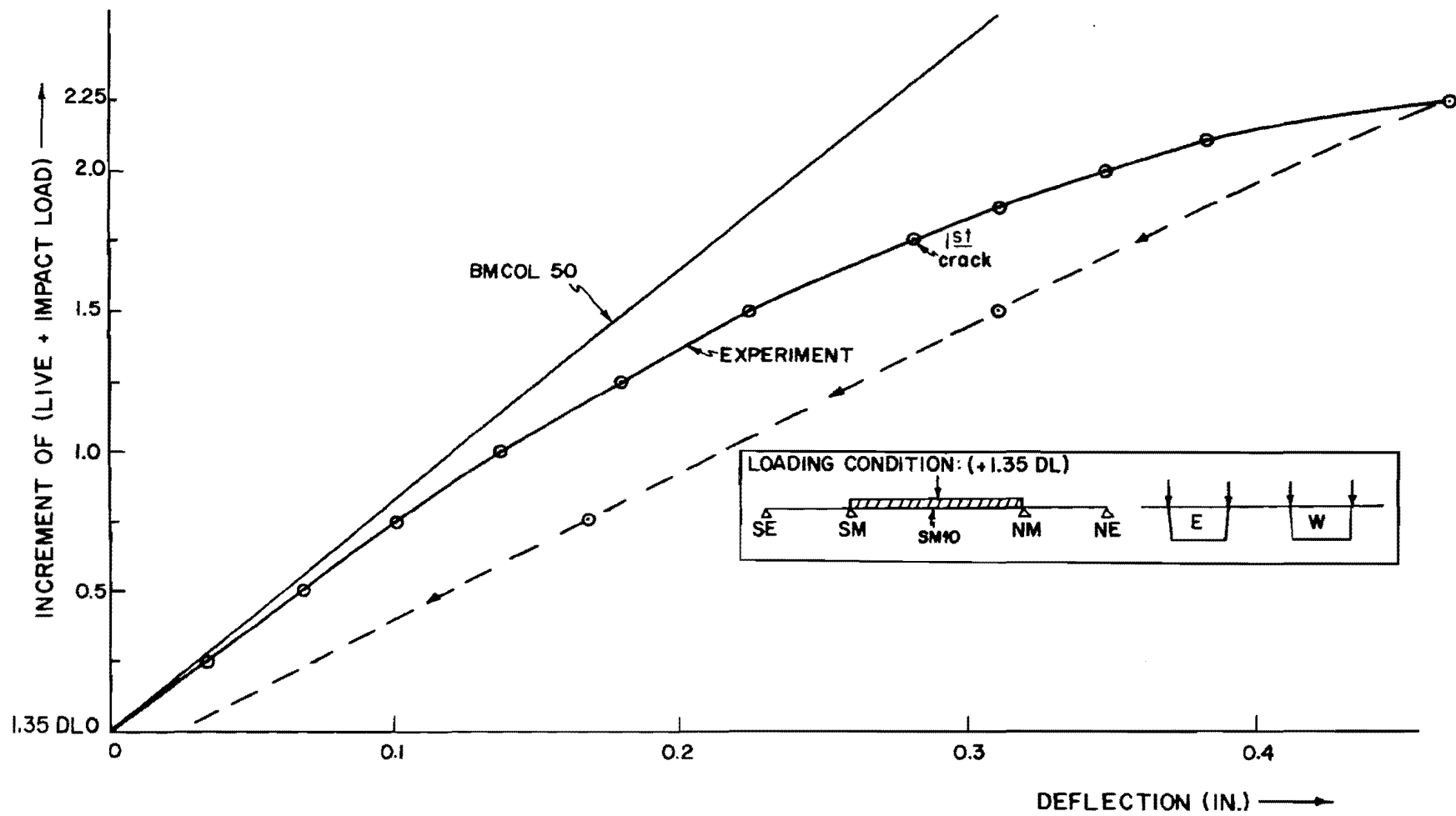


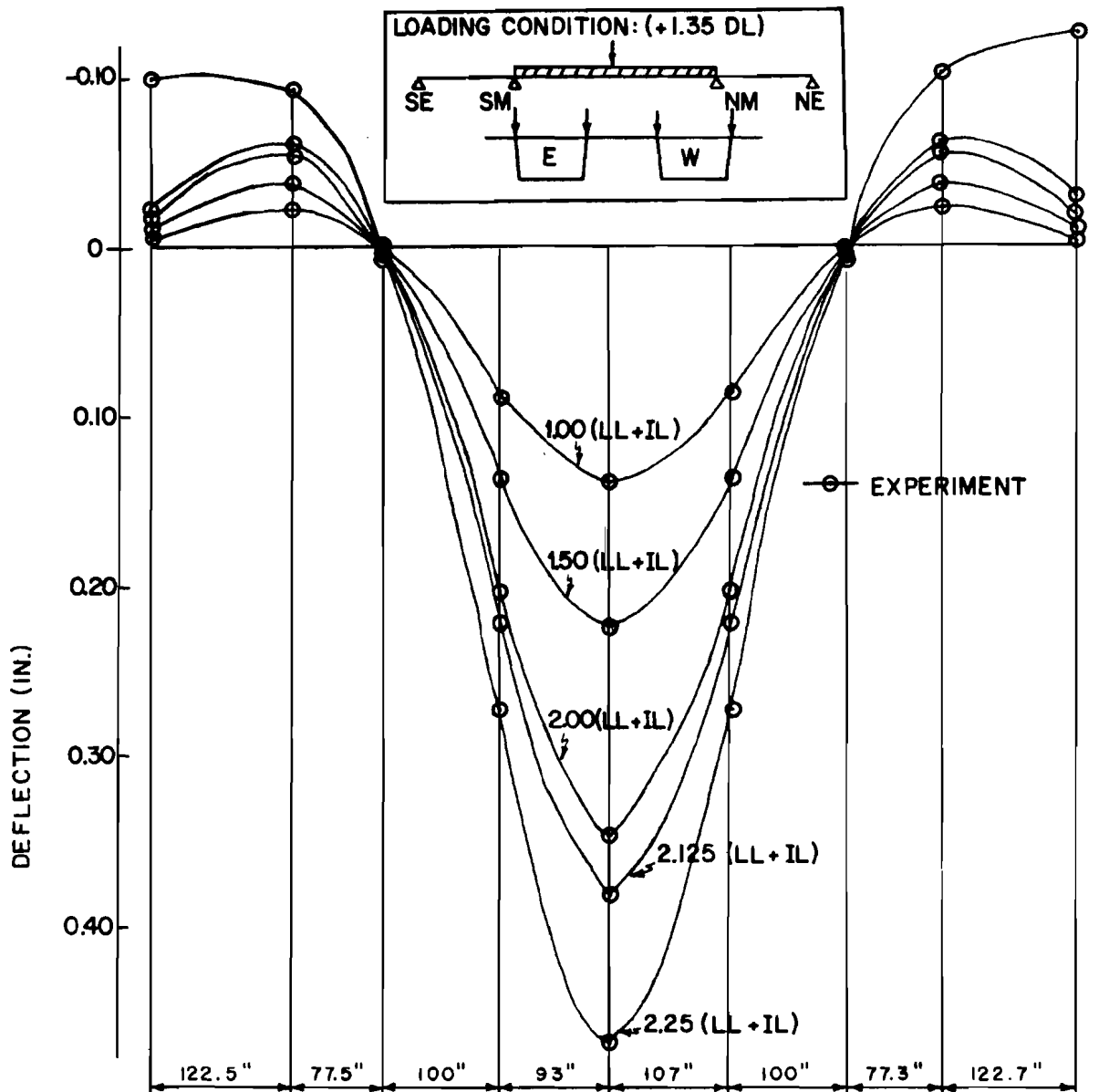
Fig. 7.27. Deflections at SM10 for lane loadings (four lanes) in main span (design ultimate)

ultimate load levels. As shown by the deflection diagram of Fig. 7.27, the measured deflections at midspan in the main span were larger than the theoretical values calculated by BMCOL50. The load-deflection relationship at midspan of the main span was linear up to the [1.35 DL + 0.75 (LL + IL)] increment and then started to change slope as the load increased. An appreciable change in slope was noted with formation of the first crack at [1.35 DL + 1.75(LL + IL)]. The increase of deflection at the increment of [1.35 DL + 2.25 (LL + IL)] was very large and the outer supports raised up suddenly, as shown in Fig. 7.28. The deflection at the midspan of the main span did not immediately come back to its original value after releasing the load. However, it recovered almost completely after several hours.

Figure 7.29 shows the increase of end reactions was linear up to the [1.35 DL + 1.25 (LL + IL)] increment and agreed with the theoretical values very well up to that point. The actual reactions become zero at about 2.13 (LL + IL), which is greater than the actual design ultimate if advantage is taken of the 25 percent design load reduction for a four lane bridge.

From the strain diagrams shown in Fig. 7.30, it can be seen that the rate of strain increase did not change very much up to the [1.35 DL + 1.5 (LL + IL)] level. Strain at the outer edges of the top slab was consistently less than the other positions. Strains along the bottom slab in the service loading test (Fig. 7.13) were almost uniform, but there was some deviation in this test even when the amount of live load was small. Strains in the bottom slab (tension side) started to deviate substantially at the [1.35 DL + 1.50 (LL + IL)] increment and varied widely at the [1.35 DL + 1.75 (LL + IL)] level.

As shown in Fig. 7.31, a crack appeared at the center of the closure segment (OE side) at the [1.35 DL + 1.75 (LL + IL)] increment and developed along the joint of the closure segment. On the OW side, the first crack appeared at the [1.35 DL + 1.88 (LL + IL)] increment. At the [1.35 DL + 2.25 (LL + IL)] increment, cracks extended to the midheight of the webs.



| (LL+IL) | SE | SS4 | SM | SM5 | SM10 | NM5 | NM | NS4 | NE |
|---------|---------|---------|---------|--------|--------|--------|---------|---------|---------|
| 1.00 | -0.0041 | -0.0229 | +0.0013 | +0.086 | +0.137 | +0.083 | +0.0014 | -0.0239 | -0.0049 |
| 1.50 | -0.0079 | -0.0367 | +0.0025 | +0.136 | +0.224 | +0.134 | +0.0020 | -0.0381 | -0.0090 |
| 2.00 | -0.0155 | -0.0553 | +0.0048 | +0.203 | +0.348 | +0.202 | +0.0032 | -0.0563 | -0.0175 |
| 2.125 | -0.0229 | -0.0617 | +0.0052 | +0.221 | +0.382 | +0.221 | +0.0038 | -0.0637 | -0.0321 |
| 2.25 | -0.101 | -0.0948 | +0.0059 | +0.271 | +0.469 | +0.272 | +0.0040 | -0.1038 | -0.128 |

Fig. 7.28. Deflections for lane loadings (four lanes) in main span (design ultimate)

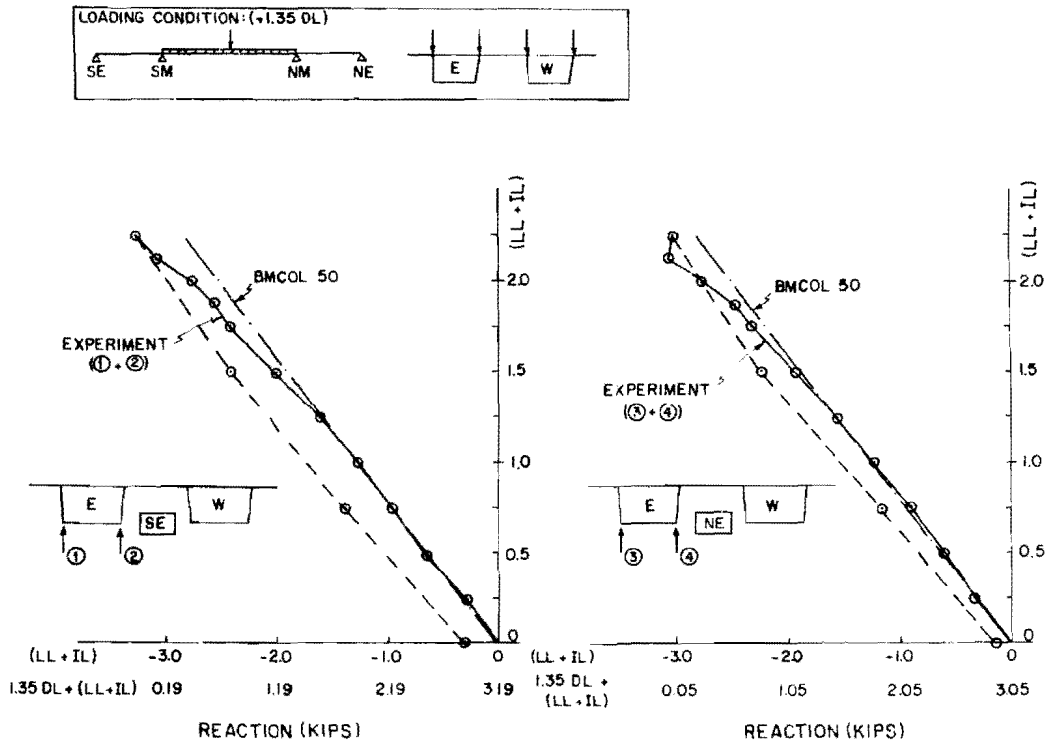


Fig. 7.29. Reactions at outer supports for lane loadings (four lanes) in main span (design ultimate)

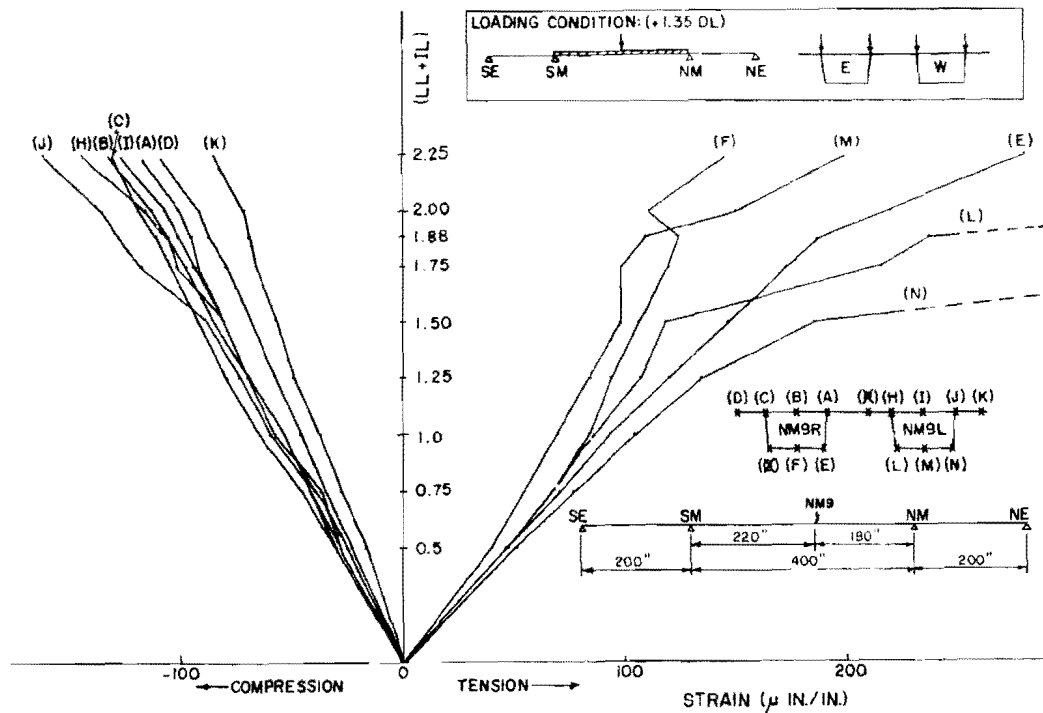
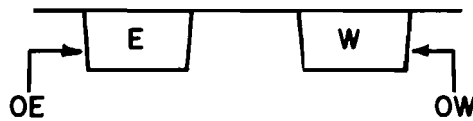
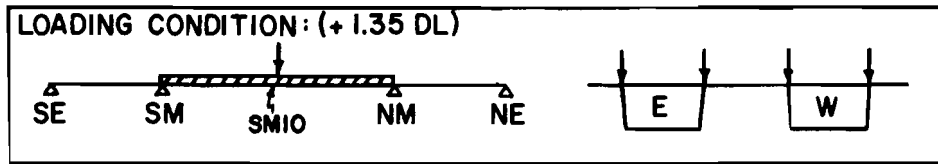
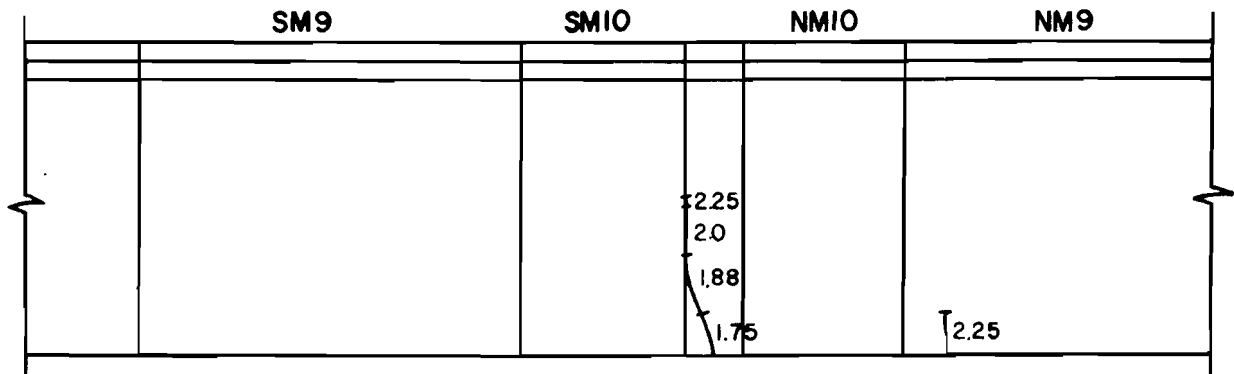


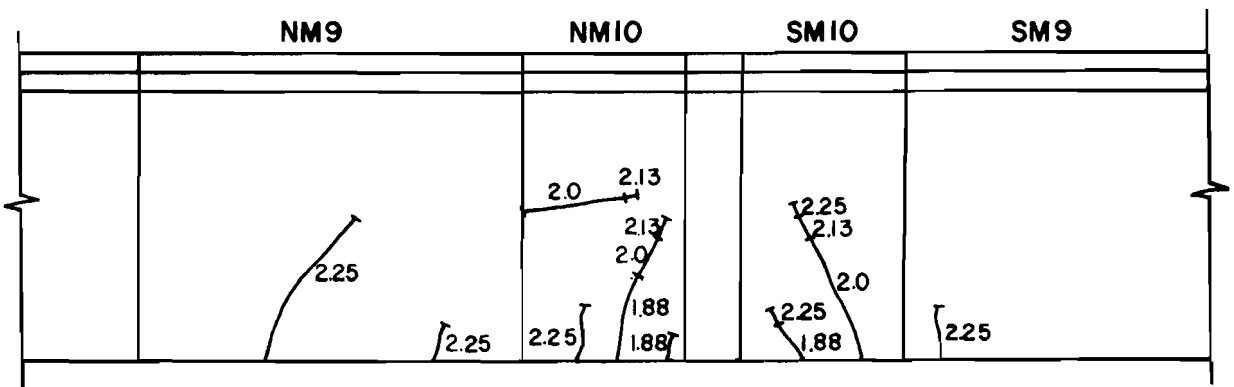
Fig. 7.30. Longitudinal strains along NM9 for lane loadings (four lanes) in main span (design ultimate)



* NUMBERS ALONG THE CRACK ARE MULTIPLES OF (LL + IL)



ON THE SURFACE OF OE



ON THE SURFACE OF OW

Fig. 7.31. Development of cracks for lane loadings (four lanes) in main span (design ultimate)

The theoretical cracking moment at the closure segment, as predicted by the 1963 ACI Building Code, is calculated as follows:²

$$\begin{aligned} M_{cr} &= W_b (f_{pe} + 6 \sqrt{f'_c}) - M_s \\ &= 1230 (1.34 + 0.505) - 740 \\ &= 1529 \text{ k-in.} \end{aligned}$$

where W_b = section modulus at bottom

f_{pe} = compressive stress of concrete due to prestressing only at bottom fiber

f'_c = compressive strength of concrete

M_s = moment due to end reaction caused by prestressing of the positive tendons in the main span and seating force at the outer supports

Therefore, the LF (load factor) of (LL + IL) for the load at which cracks might appear can be calculated as:

$$\begin{aligned} M_{cr} &= 1.35 M_{DL} + LF \times M_{(LL + IL)} \\ 1529 &= 481 + LF \times 552 \\ LF &= 1048/552 = 1.90 \end{aligned}$$

Since initial cracks appeared on one web at the LF = 1.75 level and on the other web at the 1.88 increment, the computed value [1.35 DL + 1.90(LL + IL)] was very accurate.

This method of calculation shows that the cracking moment is greatly affected by the adjusting force at the end supports. If the reaction force provided at the end supports is large, midspan cracks will appear at lower increments of (LL + IL). If the adjusting force provided at the end is small, the end segments will raise up from the neoprene pads under very small increments of (LL + IL). Therefore, where possible the end reactions for the prototype bridge should be selected at an optimum point which balances these two factors. Figure 7.32 shows the relation between the initial end reaction applied, the LF of (LL + IL) at which the end segments will raise up from the neoprene pads and the LF of (LL + IL) at which first cracks will appear. Therefore, 4.9 kips (176 kips in the

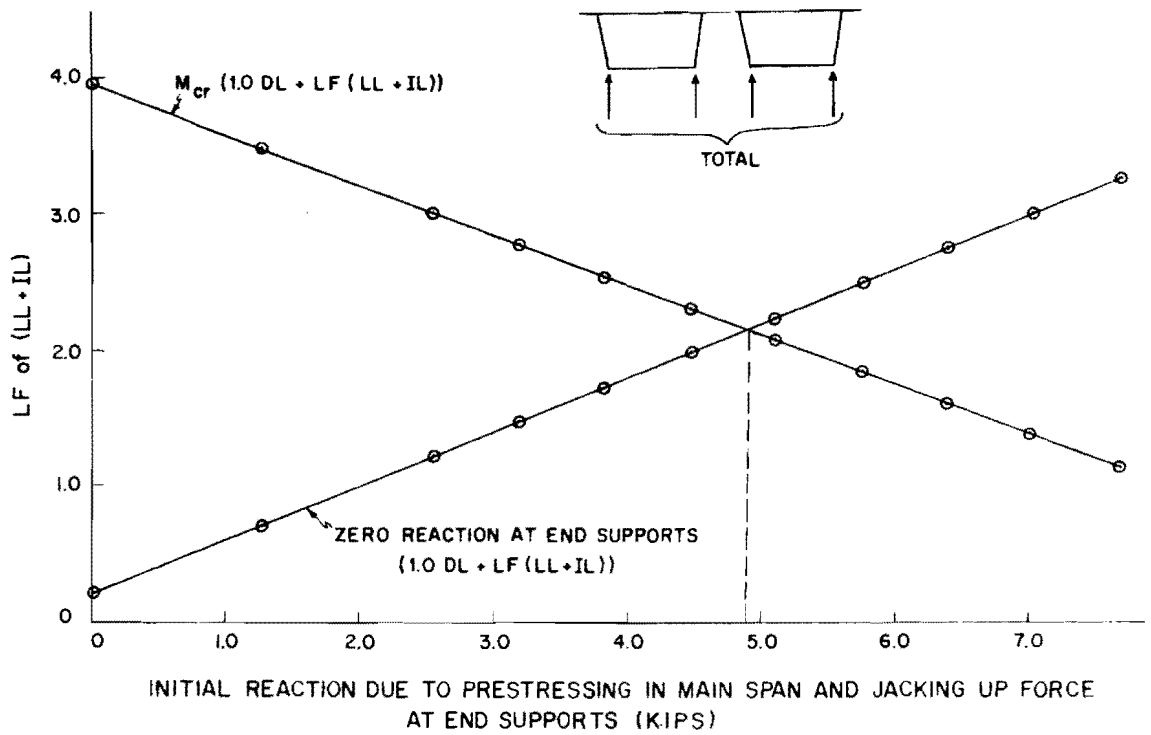


Fig. 7.32. Relation between the end reaction and cracking moment

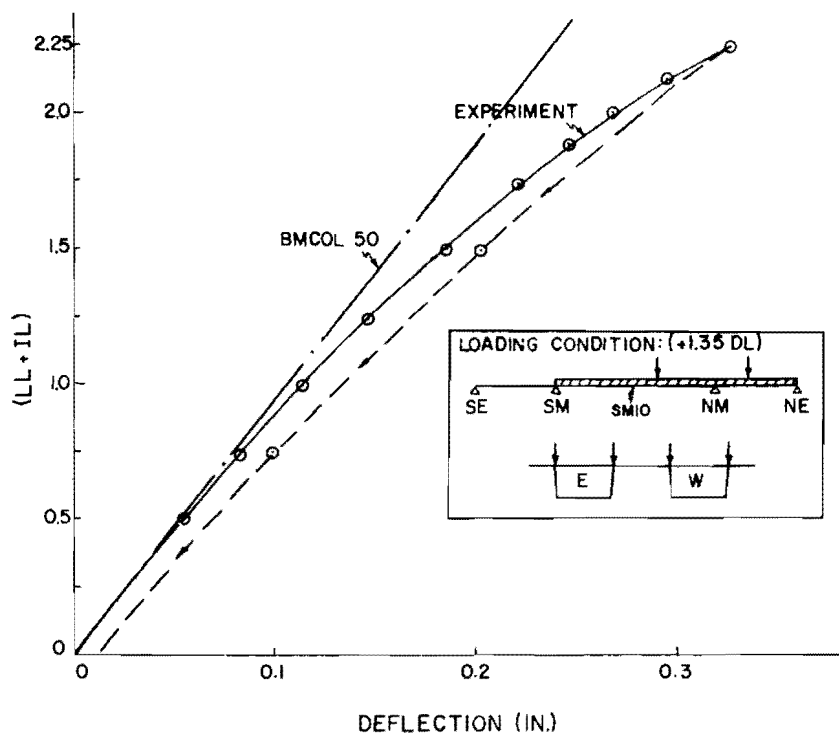


Fig. 7.33. Deflections at SM10 for lane loadings (four lanes) in the main and one side span (design ultimate)

prototype bridge) total for two boxes is the optimum initial reaction at each outer support. Although the weight of the asphalt topping, which is about 8 percent of the weight of the segment, was not included in the model bridge test, the effect of the asphalt is included in the dead load calculations on which Fig. 7.32 is based.

7.3.3.3 Maximum Negative Moment at the Main Pier. Under this loading condition the experimental deflection at midspan in the main span was slightly larger than the theoretical values (BMCOL50), as shown in Fig. 7.33. Increase in deflection was linear up to the $[1.35 \text{ DL} + 0.75 (\text{LL} + \text{IL})]$ increment. Increases of deflection at the unloaded span outer support (SE) became rapid at the $[1.35 \text{ DL} + 2.12 (\text{LL} + \text{IL})]$ increment, as shown in Fig. 7.34.

The trend of strains at the NM9 segment, as shown in Fig. 7.35, was the same as noted in Sec. 7.3.3.2. Strains in the top slab increased almost linearly up to the $[1.35 \text{ DL} + 2.25 (\text{LL} + \text{IL})]$ increment, but the strains in the bottom slab were linear only up to the $[1.35 \text{ DL} + 0.5(\text{LL} + \text{IL})]$ increment and started to deviate after that increment. The strains in the bottom slab showed considerable difference between the webs and the middle of the bottom slab. In the NM1 segment, strains in the top and bottom slabs increased linearly until $[1.35 \text{ DL} + 1.50(\text{LL} + \text{IL})]$ and $[1.35 \text{ DL} + 1.75(\text{LL} + \text{IL})]$ increments, respective, as shown in Fig. 7.36.

Reaction at the NE support increased linearly until the $[1.35 \text{ DL} + 1.00 (\text{LL} + \text{IL})]$ increment and that at the SE support decreased linearly up to the $[1.35 \text{ DL} + 1.50(\text{LL} + \text{IL})]$ increment, as shown in Fig. 7.37.

Besides reopening positive moment zone cracks developed in the earlier test (Sec. 7.3.3.2), cracks appeared along the trajectories of the negative moment prestressing cables in the 2nd and 3rd segments from the NM pier, as shown in Fig. 7.38. Appearance of these cracks along the tendons was probably due to a combination of high bending moments and shears around the NM pier and relatively thin covers in relation to the large diameter of the tendons (3/8 in. diameter) which were used to construct the 2nd and 3rd segments. It is believed that NM1 and NS1, which

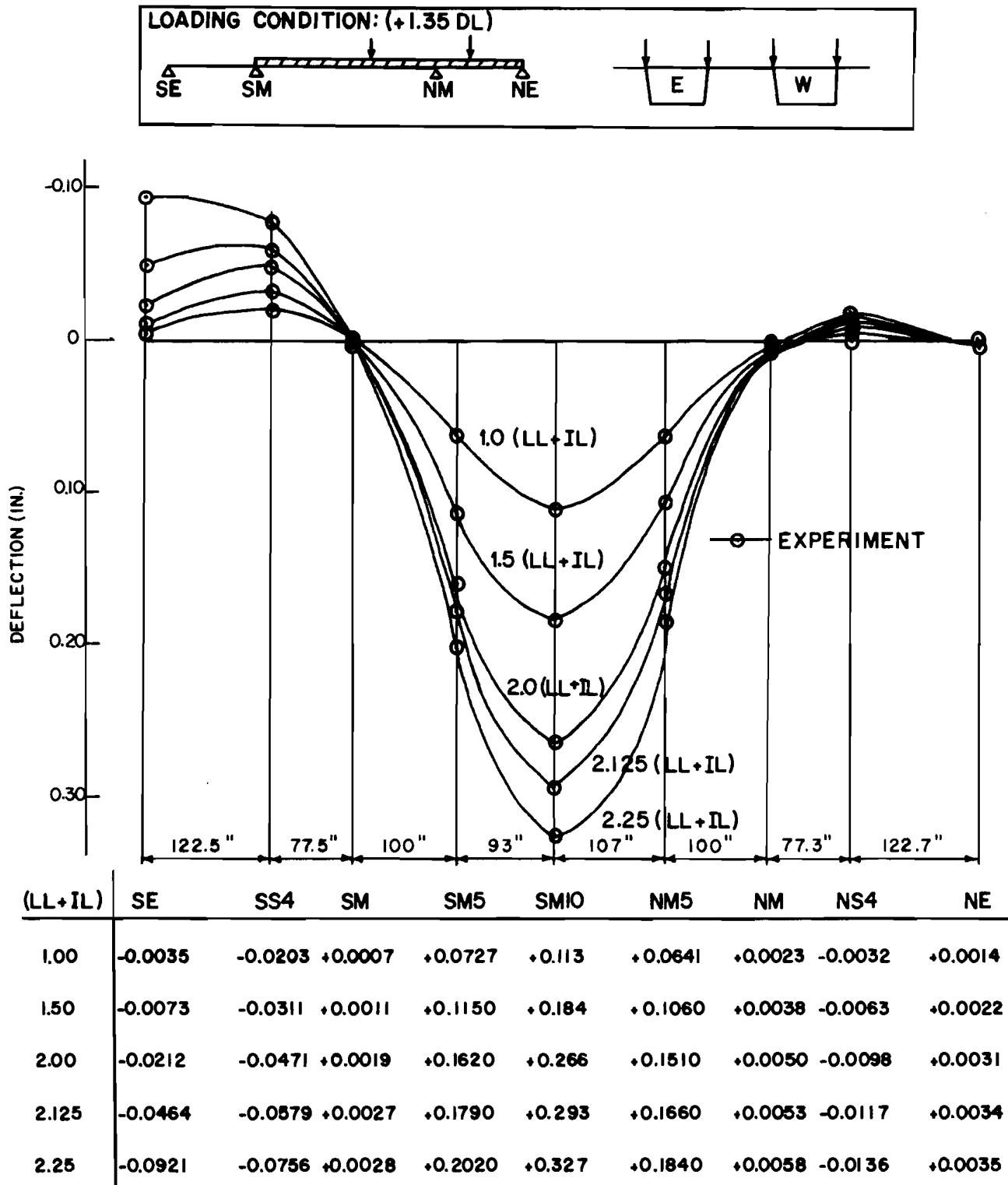


Fig. 7. 34. Deflections for lane loadings (four lanes) in the main and one side span (design ultimate)

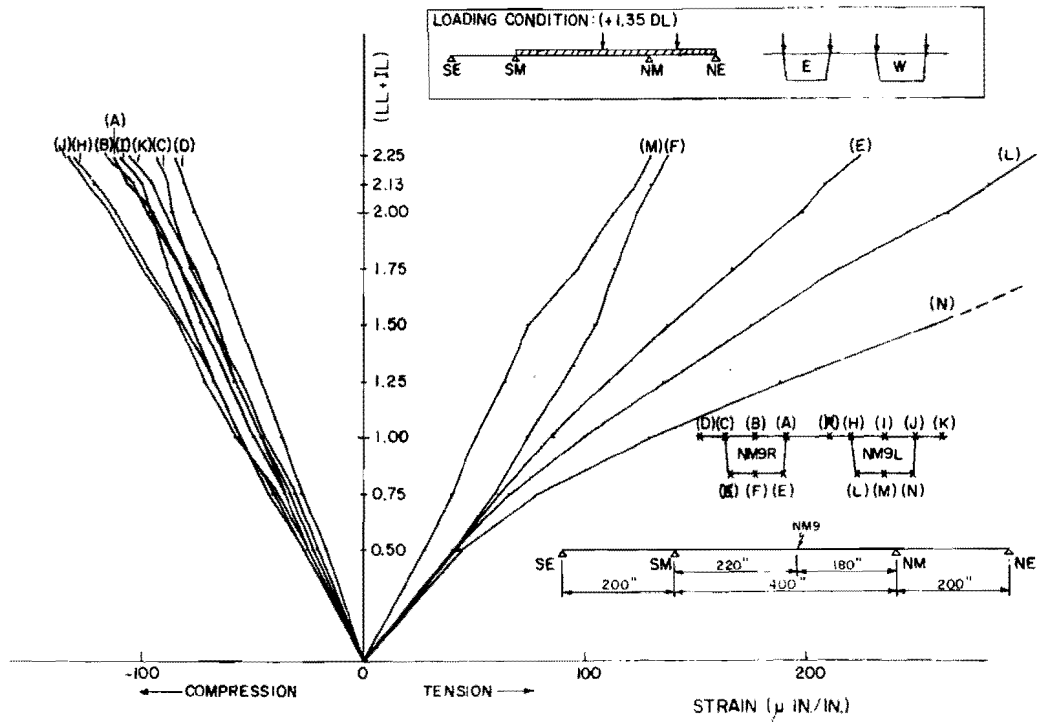


Fig. 7.35. Longitudinal strains at NM9 for lane loadings (four lanes) in the main and one side span (design ultimate)

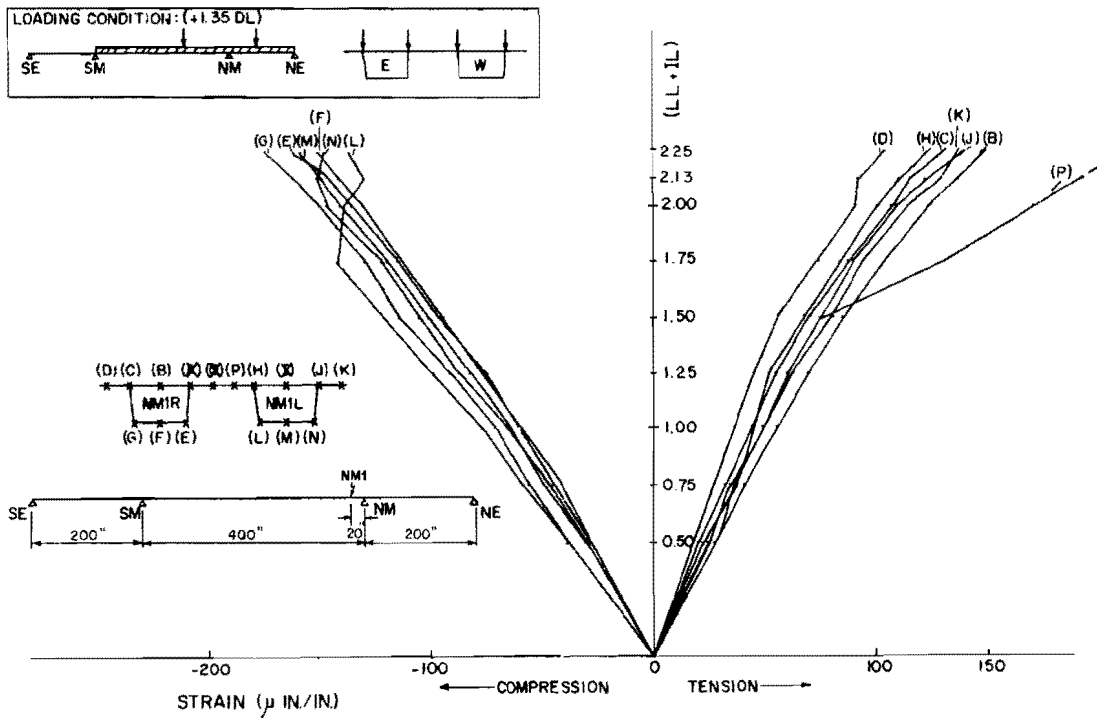


Fig. 7.36. Longitudinal strains at NMI for lane loadings (four lanes) in the main and one side span (design ultimate)

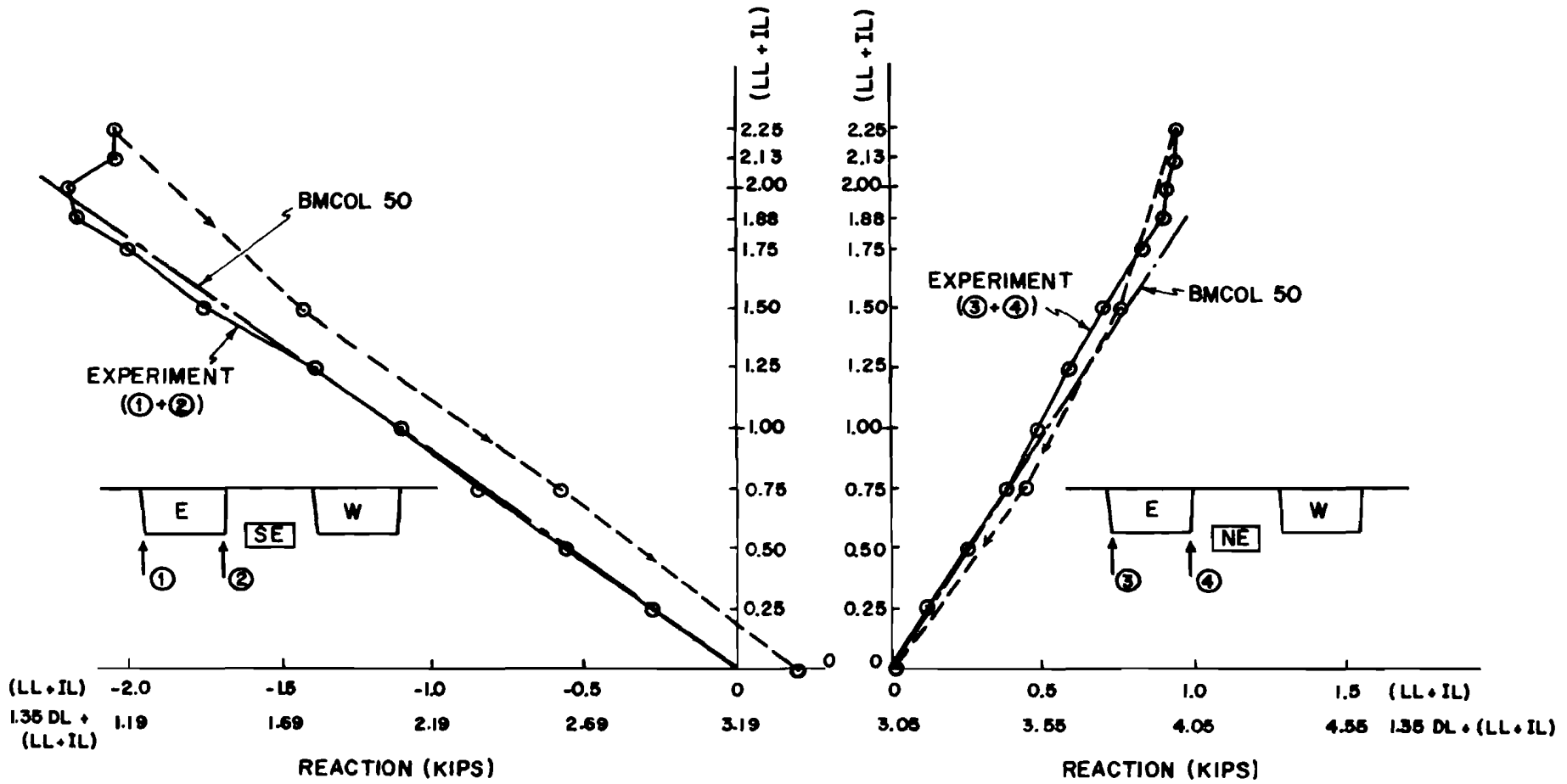
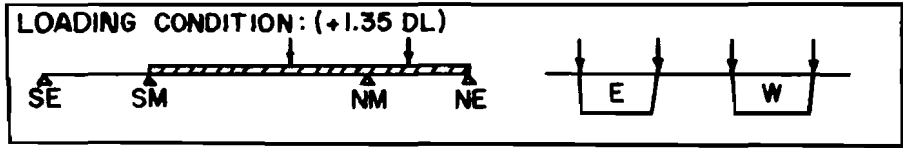


Fig. 7.37. Reactions at outer supports for lane loadings (four lanes) in the main and one side span (design ultimate)

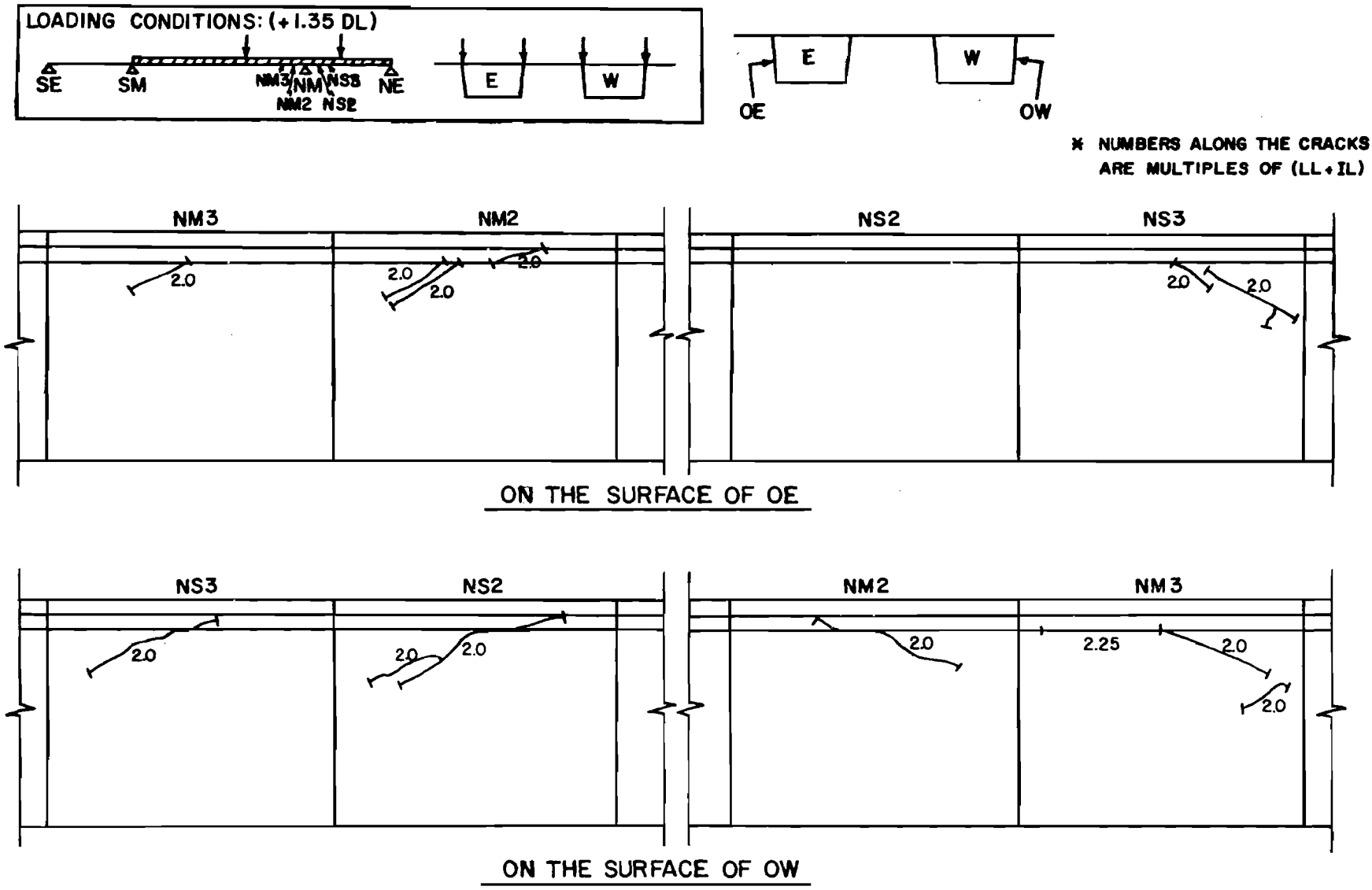


Fig. 7.38. Development of cracks for lane loadings (four lanes) in the main and one side span (design ultimate)

were subjected to higher moments and shears, did not have such cracks because of double tendons and the smaller size of tendon ducts. Because of high compressive stress due to negative tendons in the top slab around the main pier, no flexural cracks appeared around the main pier. Therefore, this loading condition was not critical.

7.3.3.4 Maximum Shear Loading Adjacent to the Main Pier. No special strain instrumentation was provided for shear loadings. Design loadings for maximum shear were applied until the $[1.35 \text{ DL} + 2.25 \text{ LL}(\text{LL} + \text{IL})]$ ultimate design increment.

The moment diagram for this loading is very similar to the maximum negative moment loading case in Sec. 7.3.3.3 and the magnitudes of the maximum positive and negative moments for this loading are only about 17 percent less than this previous loading case. Therefore, the experimental results were very similar to those of Sec. 7.3.3.3, except slightly reduced at each level of load. Because one of the major questions was the dependability of the joints under high shear, this type of loading was applied to the bridge in a later test to failure.

No additional flexural or diagonal tension cracks were observed in this test. Slip gages set across the critical first joint in the main span (as shown in Fig. 7.39) showed zero movement during the loading test.

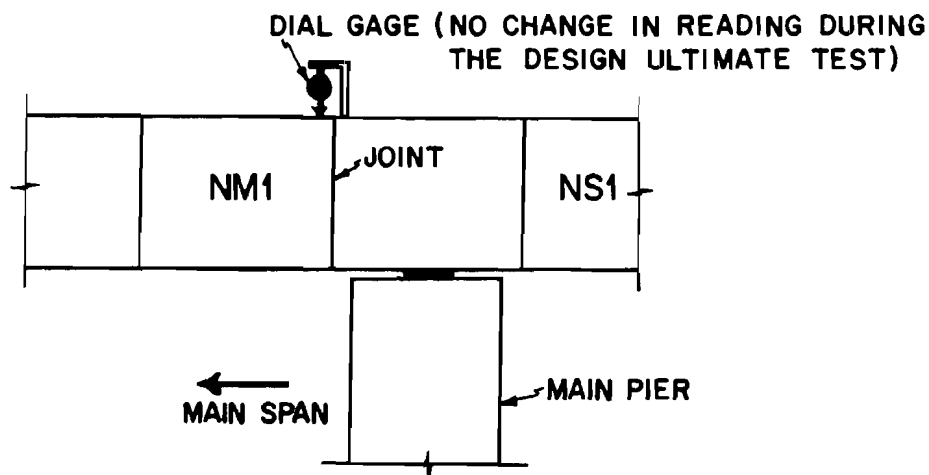


Fig. 7.39. Arrangement of slip gage at the first joint

7.3.3.5 Maximum Positive Moment in Side Span. Truck loads (four lanes) were applied at the same longitudinal position as shown in Fig. 7.7, but the transverse positions were changed to those shown in Fig. 7.40.

Deflection at the center of the SS7 segment, as shown by Fig. 7.41, was exactly the same as the theoretical values at the $[1.35 \text{ DL} + 0.5(\text{LL} + \text{IL})]$ increment. The experimental deflections became larger than the theoretical values after this point. The experimental deflection was about 14 percent larger than the theoretical deflection at the $[1.35 \text{ DL} + 2.25(\text{LL} + \text{IL})]$ increment. Also, the transverse deflection at the center of the box section (3), in Fig. 7.42, was increasing as the load increased. Details of transverse moment distribution are discussed in Sec. 7.3.4. Observed strains and reactions, as shown in Figs. 7.43 to 7.45, were generally linear. No cracking was observed during this loading test.

Transverse strain was measured at the center of the top slab of SS7R and compared very favorably with MUPDI results, as shown in Fig. 7.46. Transverse strain increased almost linearly up to the $2.25(\text{LL} + \text{IL})$ increment and agreed with MUPDI.

7.3.4 Study of Transverse Moment. It is very hard to accurately simulate the behavior of the prototype bridge transversely because of the increased difficulty in reducing the scale correctly for the very shallow slab sections used.

Transverse strain gages were put on the surface of the segments at some points and these strain readings were compared with MUPDI analysis results.

The loading cases considered in this section are shown in Fig. 7.47. Since the transverse effect of dead load is small,²¹ $(\text{LL} + \text{IL})$ only was considered at the service load level. Experimental transverse deflections agreed very well with MUPDI for case (3), as shown in Fig. 7.17. Transverse gage locations on the SS7 segment are shown in Fig. 7.47. Experimental strain readings agreed very well with MUPDI results, as shown in Table 7.3.

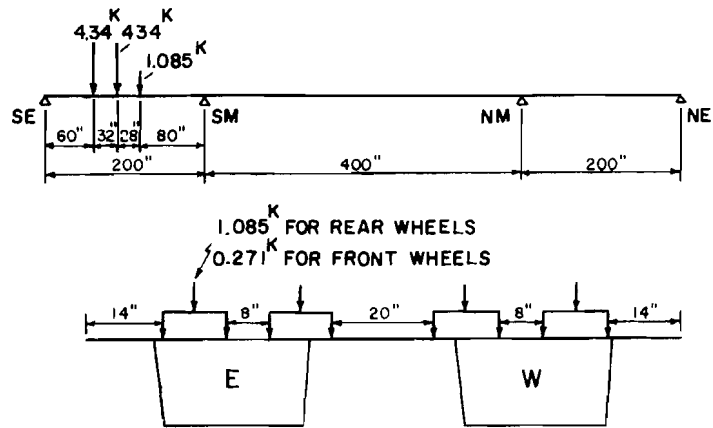


Fig. 7.40. Position of truck loadings (design ultimate)

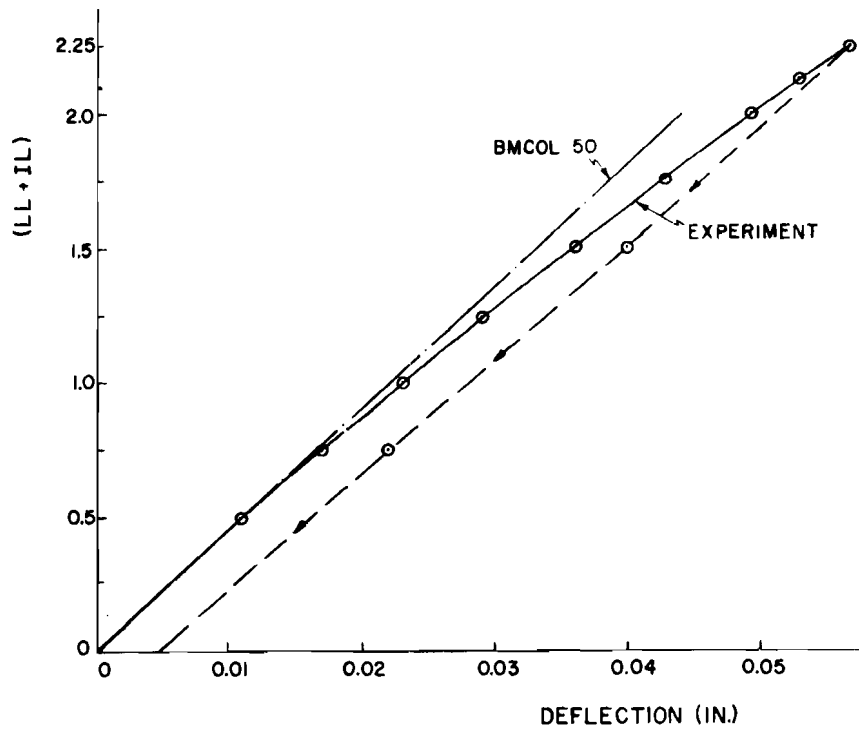
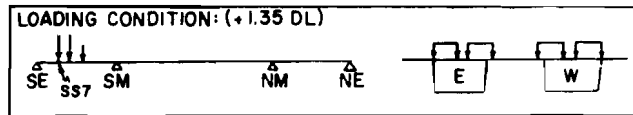


Fig. 7.41. Deflections at SS7 for truck loadings (four lanes) in side span (design ultimate)

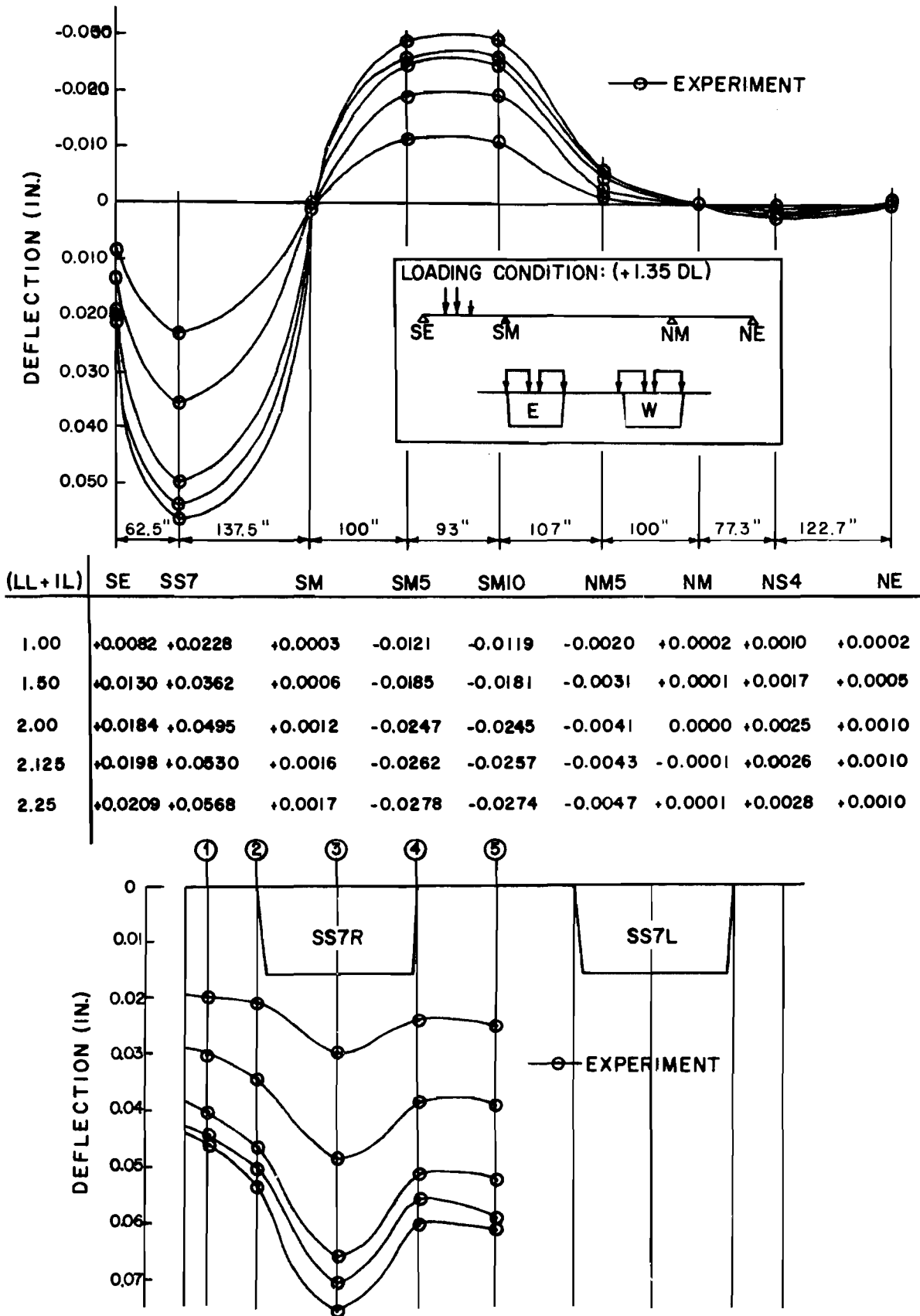


Fig. 7.42. Deflections for truck loadings (four lanes) in side span (design ultimate)

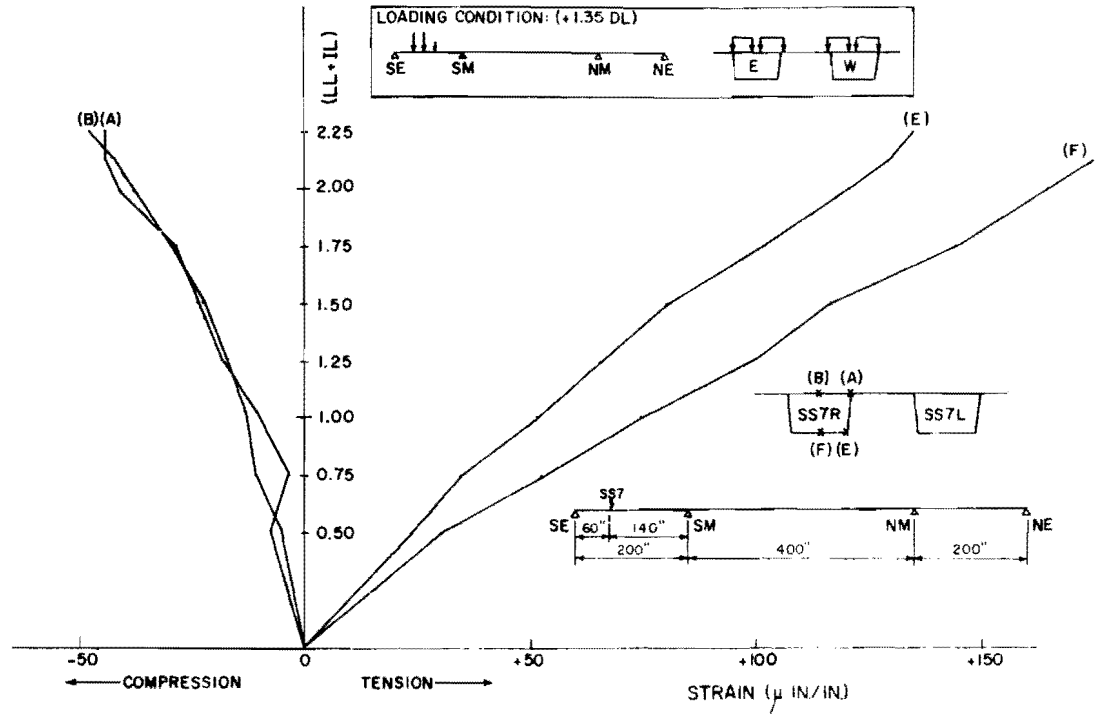


Fig. 7.43. Longitudinal strains at SS7 for truck loadings (four lanes) in side span (design ultimate)

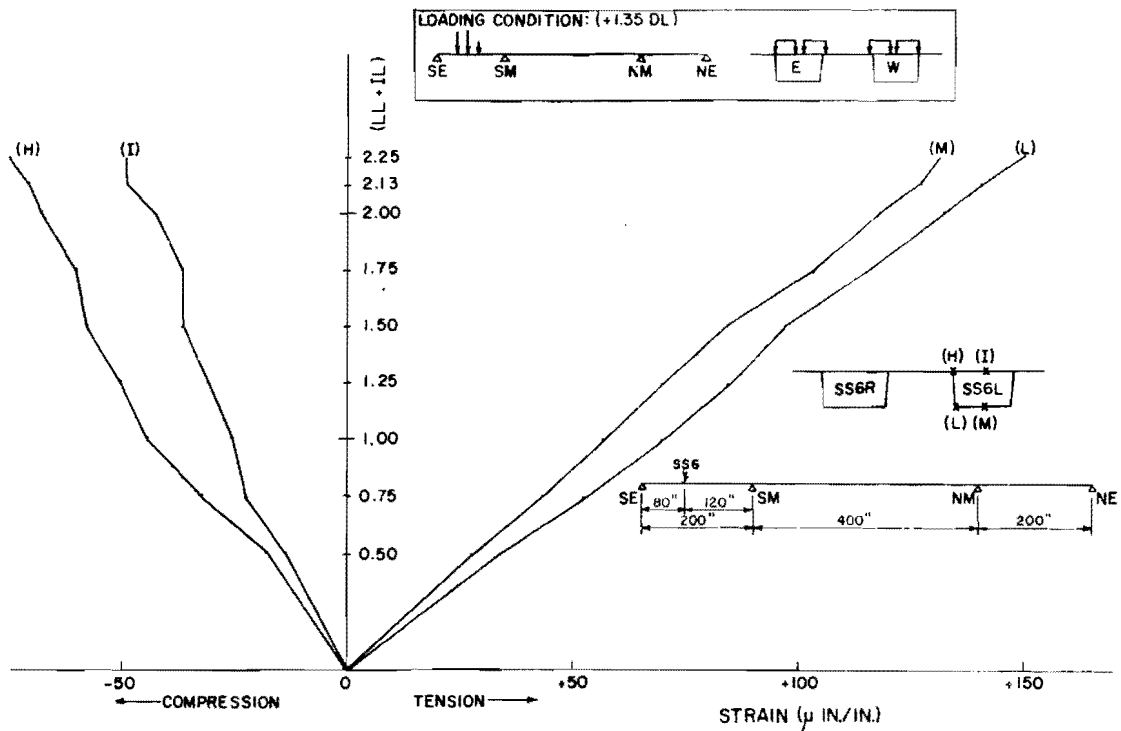


Fig. 7.44. Longitudinal strains at SS6 for truck loadings (four lanes) in side span (design ultimate)

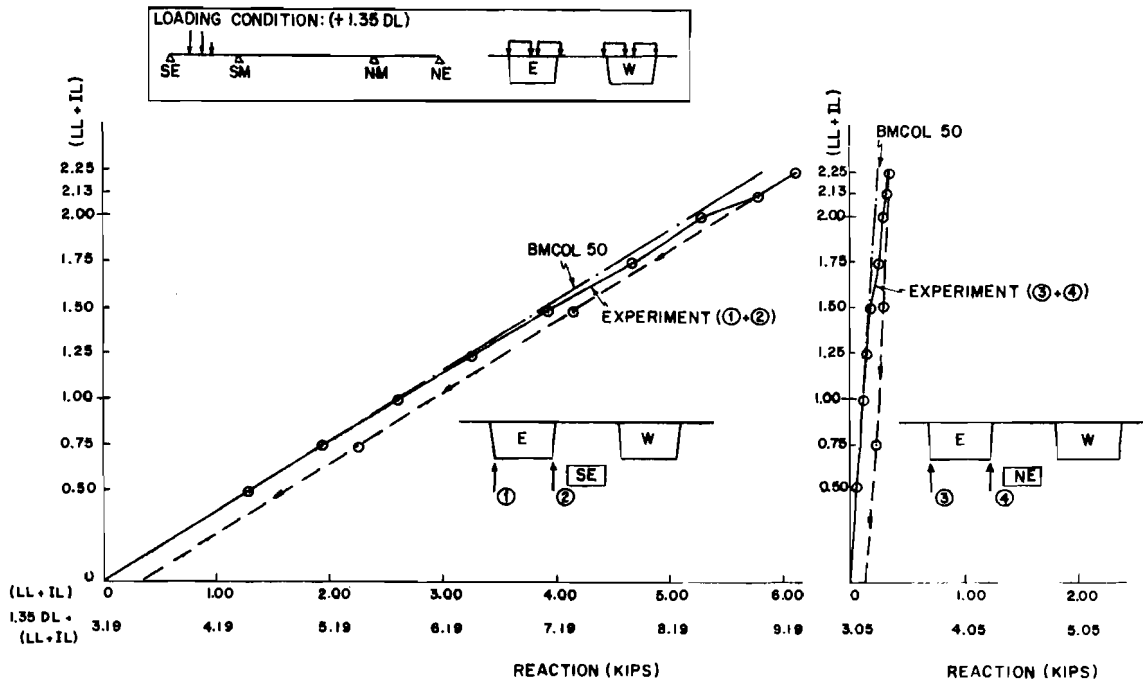


Fig. 7.45. Reactions at outer supports for truck loadings (four lanes) in side span (design ultimate)

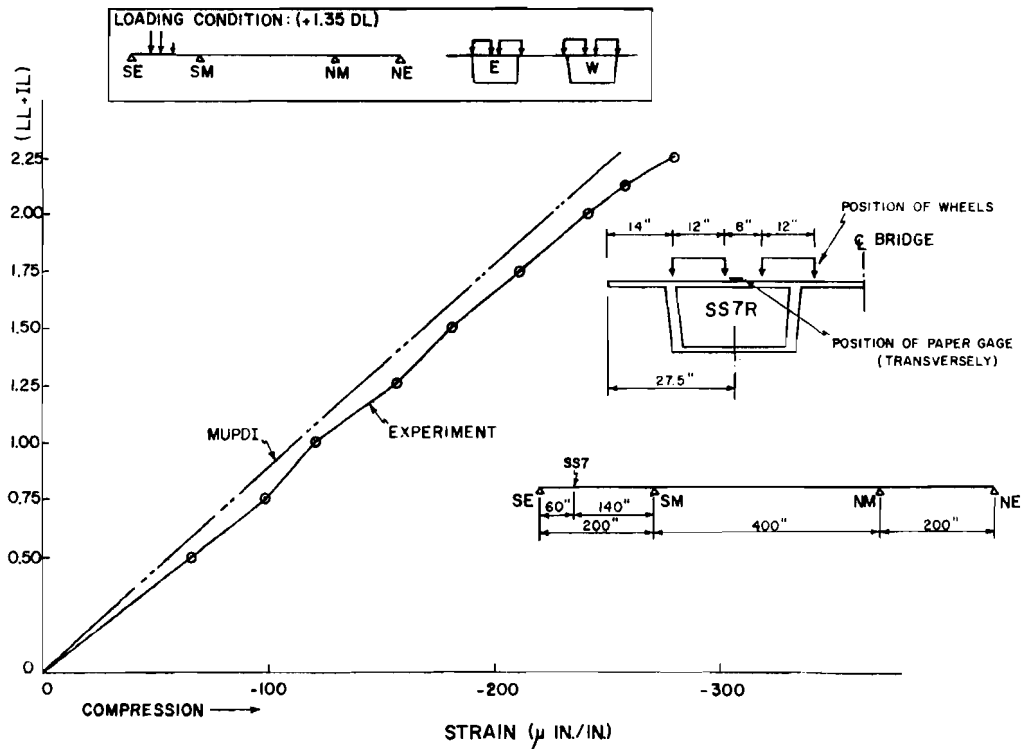
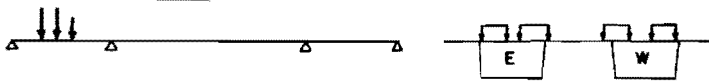


Fig. 7.46. Transverse strain at SS7 R for truck loadings (four lanes) in side span (design ultimate)

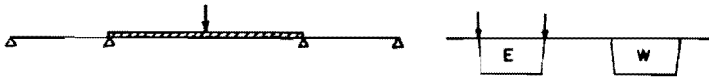
CASE (1) - DETAILS OF LOADING ARE IN SEC. 7.3.2.1.



CASE (2) - DETAILS OF LOADING ARE IN SEC. 7.3.3.5.



CASE (3) - DETAILS OF LOADING ARE IN SEC. 7.3.2.2.



CASE (4) - NOT TESTED.

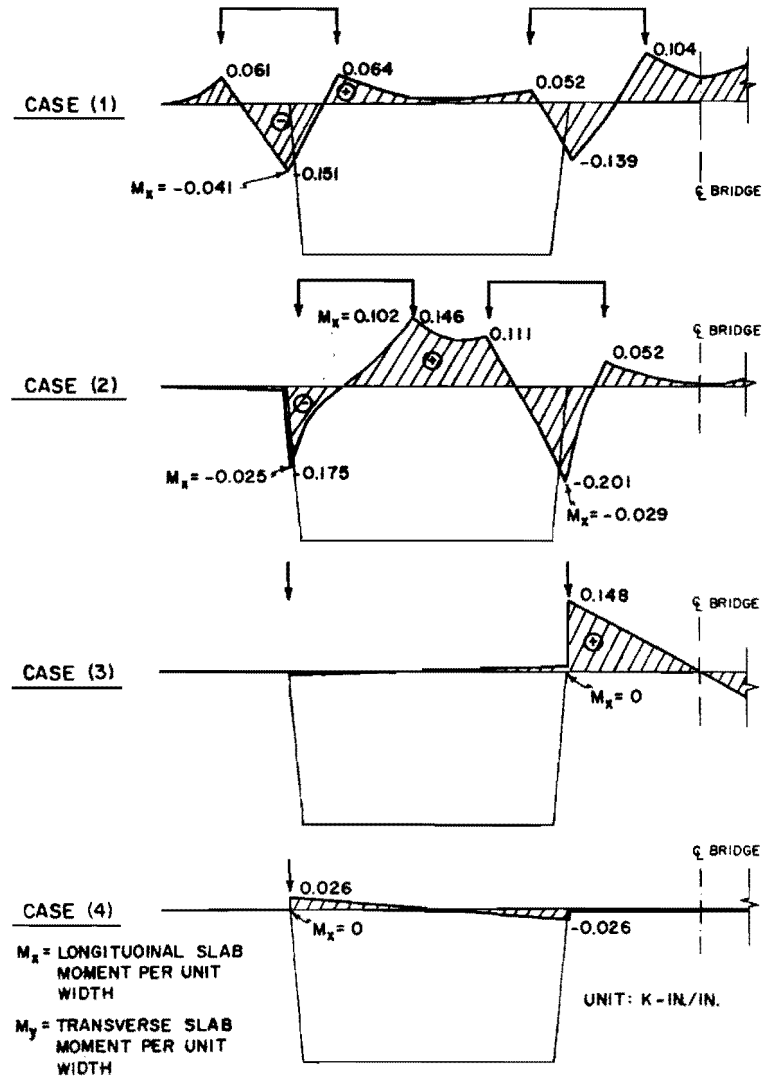
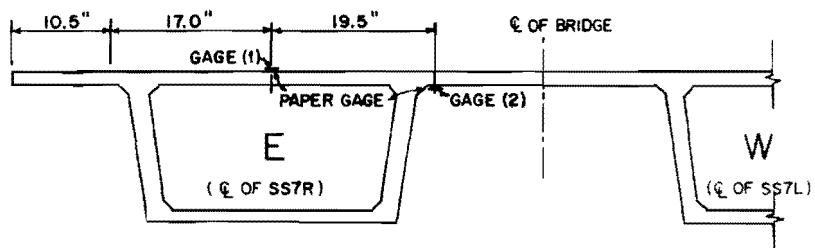
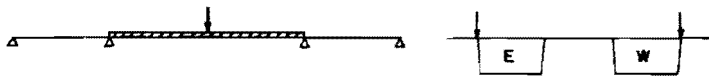


Fig. 7.47. Transverse slab moment (M_x) diagram for different loading cases as computed by MUPDI

TABLE 7.3. COMPARISON OF EXPERIMENTAL AND THEORETICAL TRANSVERSE STRAINS

| Loading Case | Gage No. | Strain (μ in./in.) | | Experiment/MUPDI |
|--------------|----------|-------------------------|-------|------------------|
| | | Experiment | MUPDI | |
| (1) | (2) | 64 | 63 | 1.02 |
| (2) | (1) | 122 | 107 | 1.14 |

Because MUPDI showed good agreement with the experimental results, transverse moment diagrams for each case were drawn (Fig. 7.47) using the MUPDI results. The computed longitudinal slab moment (M_x) at the location of the maximum transverse moment is also shown in Fig. 7.47. Among these four cases, case (2) gave the largest values in transverse positive and negative moments. In order to judge the transverse strength of the section, several strain gages were put at these critical positions in later punching shear tests (punching shear test results are given in Sec. 8.4) and strain readings were taken almost to failure. Transverse and longitudinal slab moments at the service load level were calculated from the experimental results for the loading cases shown in Fig. 7.48. These moments are much larger than the values calculated for the above four cases and strains increased linearly almost to the punching shear failure loads which were about 18 and 7 times (LL + IL) at the middle of the twin boxes and the edge cantilever, respectively. Also, loading case (1) in Fig. 7.47 was applied at the 5.25(LL + IL) increment in the failure test of Sec. 8.2 and no visible crack was observed in the top slab. Although it is not possible to relate these results directly to the prototype because of casting tolerances at this section being exceeded in the model (the thickness of the top slab was about 15 percent thicker than thickness specified), the above results indicate that there is ample safety in transverse bending for the top slab.

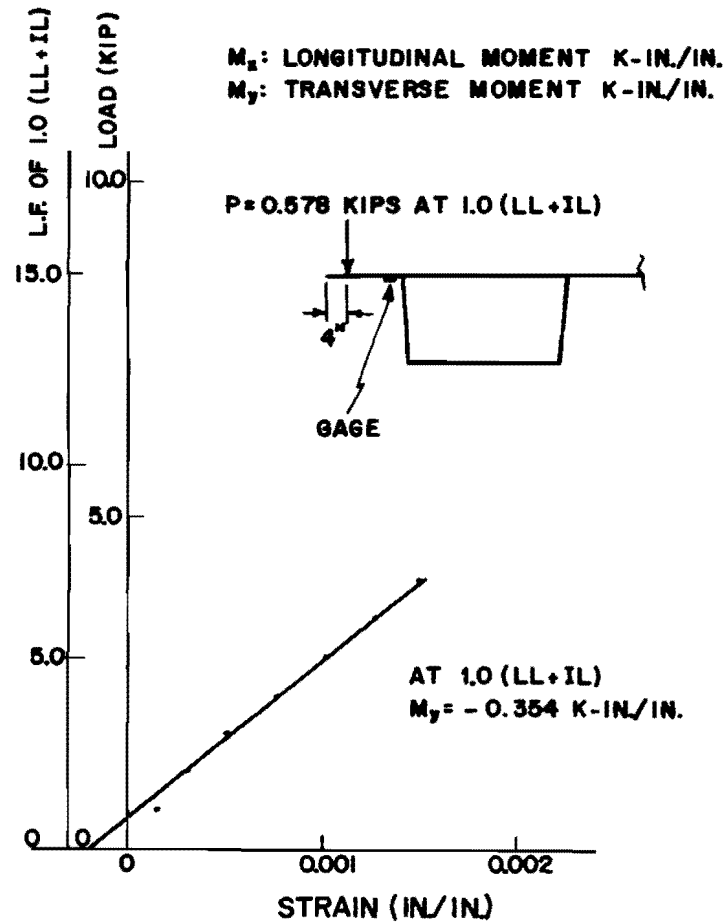
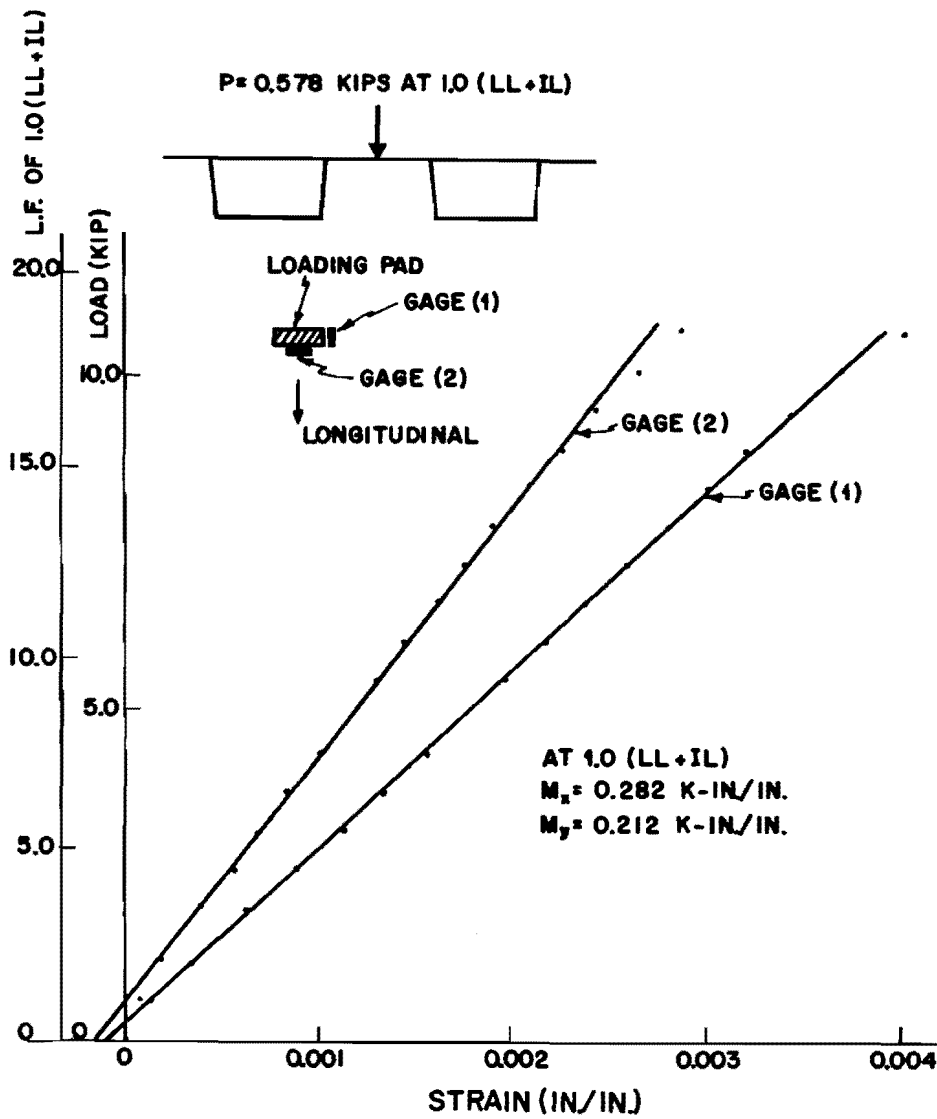


Fig. 7.48. Typical strain readings in punching shear tests

7.4 Summary

The excellent agreement obtained between analytical and experimental results at the service live load level indicates that this structure can be analyzed very accurately for transversely uniform loading by an elastic beam-type analysis, such as BMCOL50. When loaded nonuniformly in the transverse direction, the beam-type analysis is not applicable. For this case, the elastic folded plate type analysis such as MUPDI showed excellent agreement. The effect of shear lag in this section was small.

The structure behaved in a most acceptable manner under design ultimate load conditions $[1.35 \text{ DL} + 2.25(\text{LL} + \text{IL})]$. If advantage is taken of the 25 percent load reduction in a four lane bridge, this load corresponds to $[1.35 \text{ DL} + 3.0(\text{LL} + \text{IL})]$. Only minor cracking occurred at midspan under positive moment loading and near the piers along the tendon paths in several segments under negative moment loading. No sign of joint slip or diagonal tension cracking was noted under design ultimate shear loading.

CHAPTER 8

FAILURE LOAD TESTS

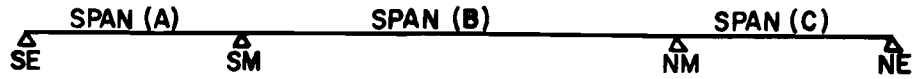
8.1 General

The bridge model readily carried the BPR design ultimate load for all critical flexural and shear loading conditions, as shown in the previous chapter. To obtain maximum return from the model, several failure load tests were planned to determine ultimate capacity. In the first test to failure, factored AASHO truck loads were applied in one side span to produce a bending failure, as shown in Fig. 8.1(b). This loading was selected even though the calculated failure live load factor for this case was larger than that which was calculated for maximum moment loading in the main span. Since both of these type failures would be flexural, it was felt that a failure test in the side span could verify flexural ultimate calculations. Such a test would leave the structure with two relatively undamaged spans so that a shear test to failure could also be run by applying lane loadings to the main and opposite side span. This loading, as shown in Fig. 8.1(c), would produce maximum shear at the main pier and be an effective test of epoxy joint performance. Truck loading on the side span [Fig. 8.1(b)] was stopped after distinct yielding had occurred in the side span and at support SM, as judged by the deflection and strain readings, but before complete collapse of the side span. Although loads were applied in this test after formation of a plastic hinge, the effect of this loading on the ultimate bending and shear strength of spans (B) and (C) during the second failure loading test shown in Fig. 8.1(c) was judged negligible. No live load would be applied on span (A) and the end segment at SE would deflect upward.

8.2 Side Span Failure Load Test

8.2.1 General. The scaled AASHO HS20-S16 truck loads shown in Fig. 8.2 were applied to all four lanes of the side span to produce

(A) SPAN AND SUPPORT NOTATION



(B) ULTIMATE LOADING CONFIGURATION FOR MAXIMUM MOMENT IN SIDE SPAN.



(C) ULTIMATE LOADING CONFIGURATION FOR MAXIMUM SHEAR ADJACENT TO NM IN THE MAIN SPAN.

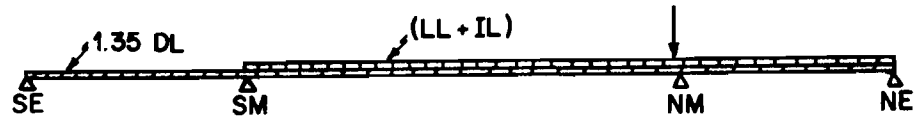


Fig. 8.1. Bridge failure loading

1.0 (LL + IL) = 1.222 LL FOR 4 LANES

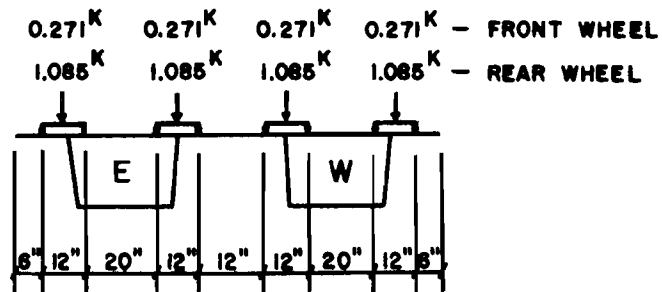
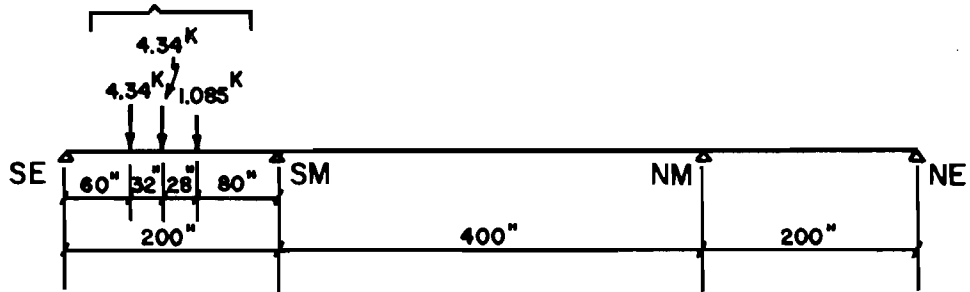


Fig. 8.2. Truck loadings at 1.0 (LL + IL) for maximum positive moment in the side span

maximum moment. The allowable load reduction for a four lane bridge was ignored. The live loads applied were in addition to the already applied 1.35 dead load. Live and impact loads were increased to the 5.25(LL + IL) level. Load increments of 0.25(LL + IL) or 0.125(LL + IL) were used after the 0.75(LL + IL) level was reached.

8.2.2 Test Results. At the 2.88(LL + IL) increment, appreciable deviations from the generally linear load vs. deflection diagram (Fig. 8.3) were noted. Strains in the bottom slab of the SS6L segment changed rapidly at the 2.75(LL + IL) increment, as shown in Fig. 8.4. It appears as though cracking may have started to develop in the inner webs, although no cracking was visible in the outer webs. At the 3.25(LL + IL) increment, a flexural crack on the outer web around the center of the SS7R segment was visible almost up to midheight and the strain gages in the bottom slab showed a large increase in strain, as shown in Fig. 8.5.

At the 4.25(LL + IL) increment, a wide crack (more than 1/8 in. visually) developed suddenly at the SS6-7 joint in the outer web of the west side (OW), as shown in Fig. 8.6. At the 4.38(LL + IL) increment a major crack formed near the SS6-7 joint in the outer web of the east side (OE), as shown in Fig. 8.6. After these cracks developed, Figs. 8.3 to 8.5 indicate changes in strain at the center of the SS7R and SS6L segments stopped, and deformations were concentrated in the vicinity of these large cracks. From the strain diagram for the SS1 segment shown in Fig. 8.7, the strains are seen to increase rapidly at the 4.38(LL + IL) increment and to increase less rapidly after that increment. The rapid increase of the strain at the SS1 segment, and in the reaction at the NE support (as shown in Fig. 8.8) around the 4.25 or 4.38(LL + IL) increment means that a plastic hinge was formed at the SS6-7 joint. After forming the plastic hinge the loads were redistributed and more load was carried at the SM pier region. Since the bridge is a three-span continuous beam, plastic hinges have to be formed at (A) and (B) in Fig. 8.9 to have a complete failure mechanism for loading in the side span. The average reaction at the SE support increased fairly linearly, as shown in Fig. 8.8. Changes in the individual web reactions at the SE support can be seen at the 2.88 and 4.38(LL + IL) increments.

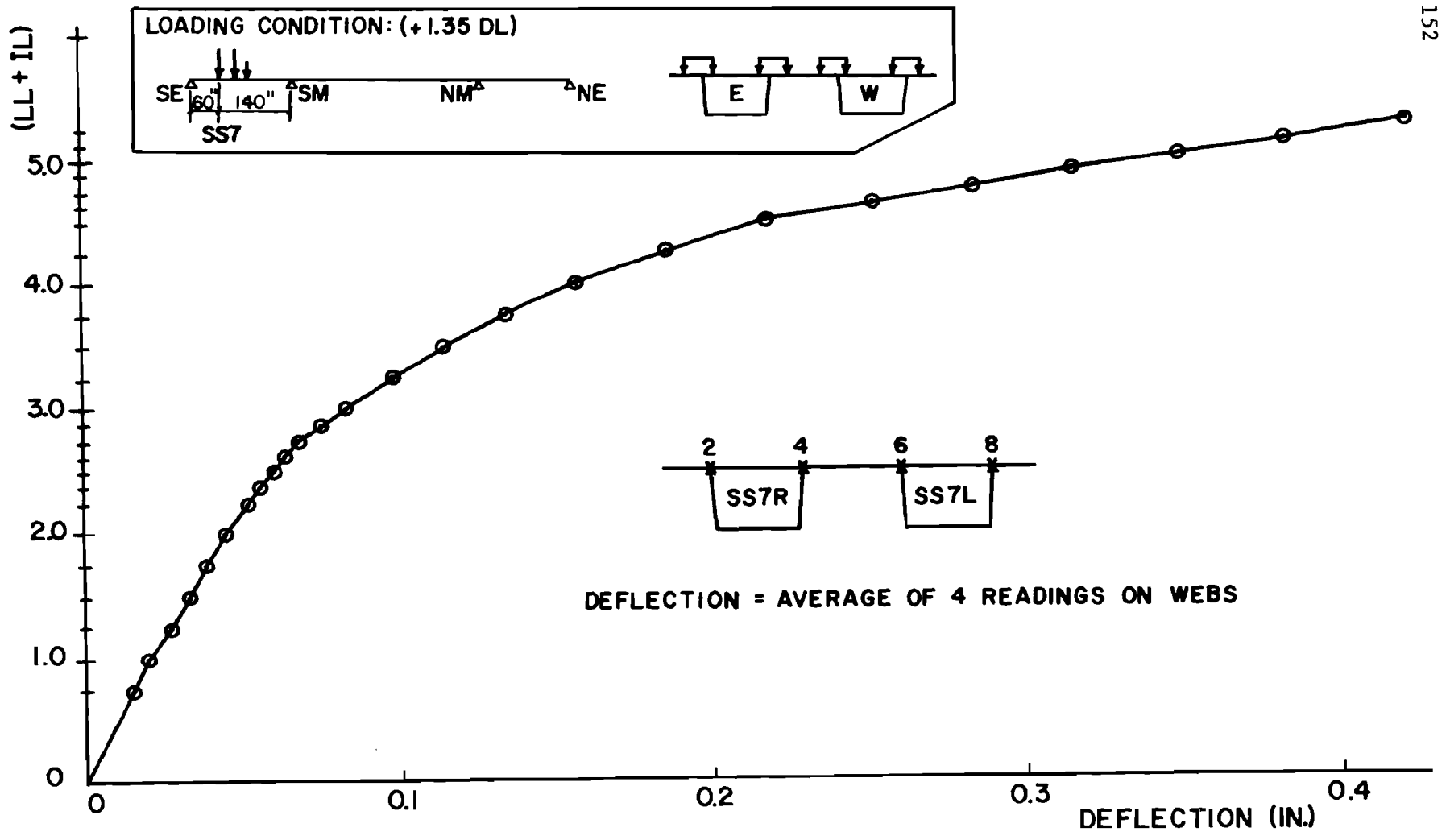


Fig. 8.3. Deflections at the center of the SS7 segment in side span

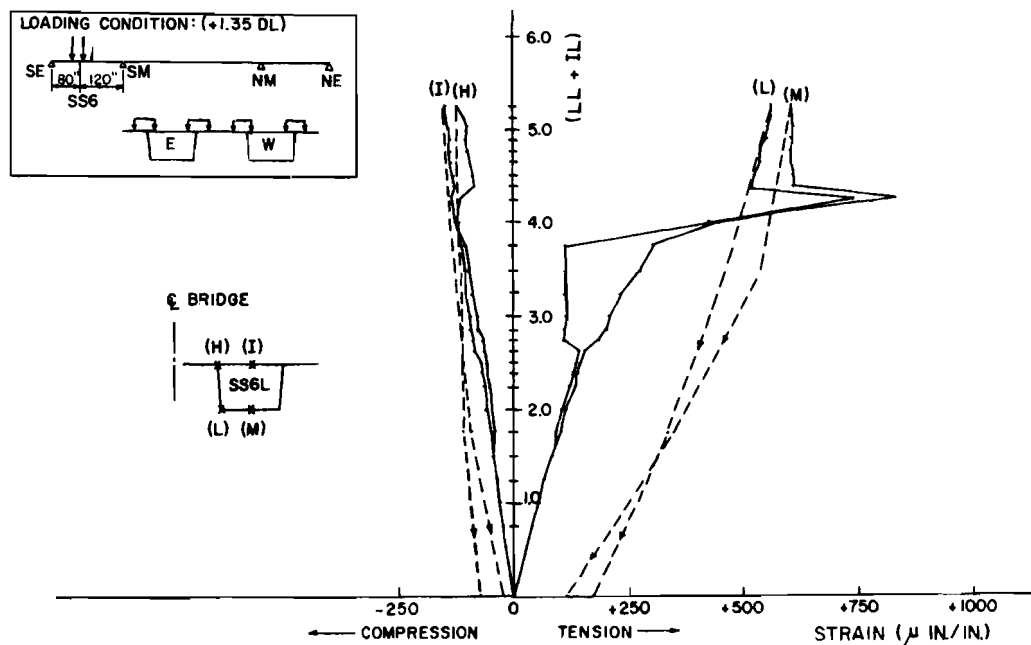


Fig. 8.4. Longitudinal strains at the center of the SS6L segment

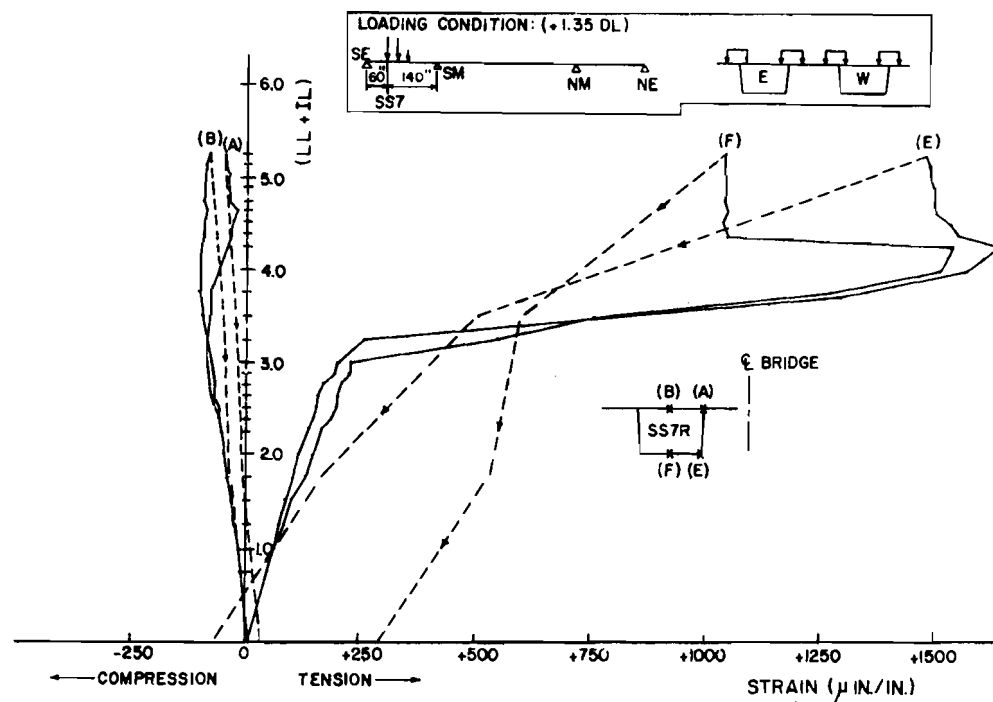


Fig. 8.5. Longitudinal strains at the center of the SS7R segment

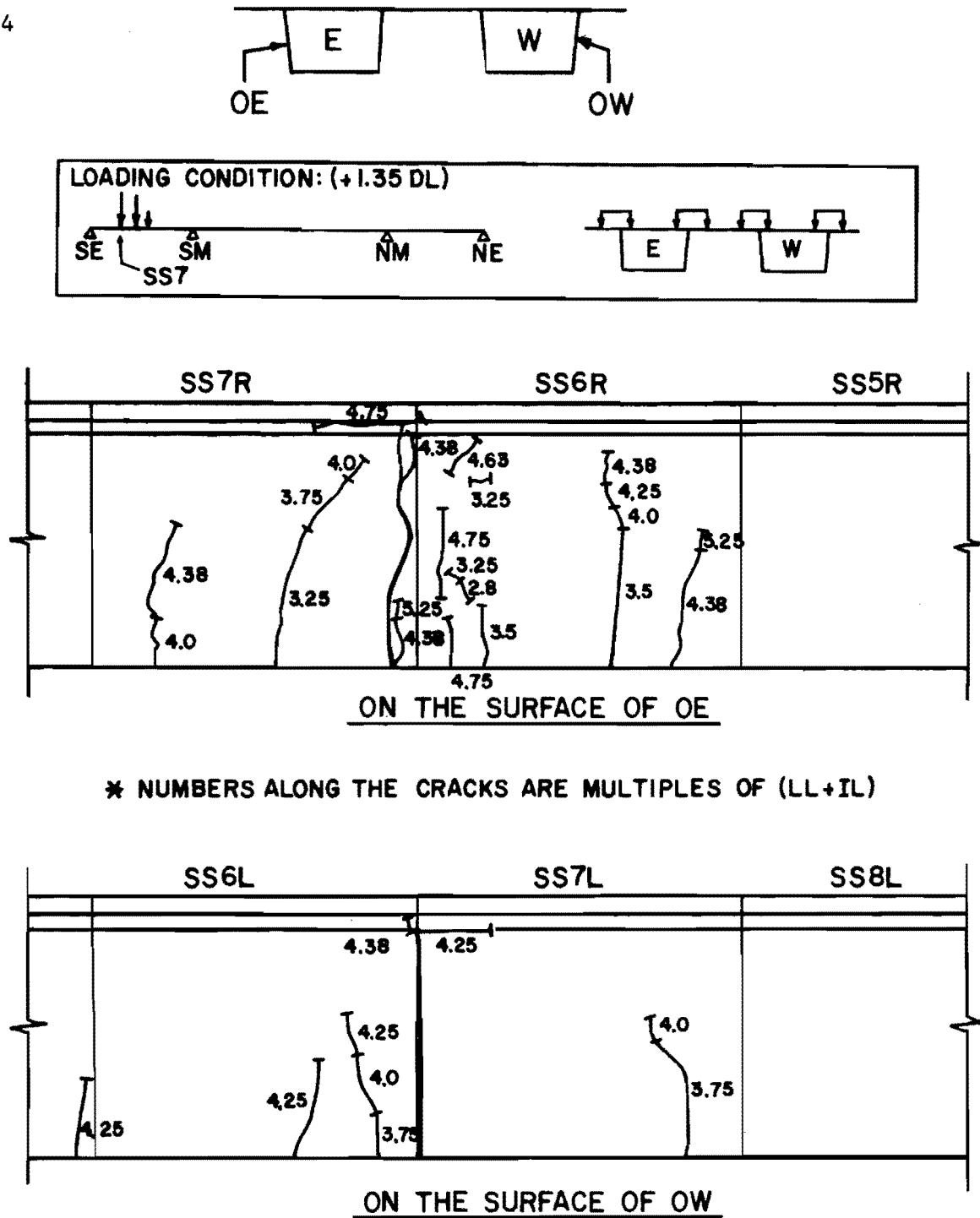


Fig. 8.6. Development of cracks during loading

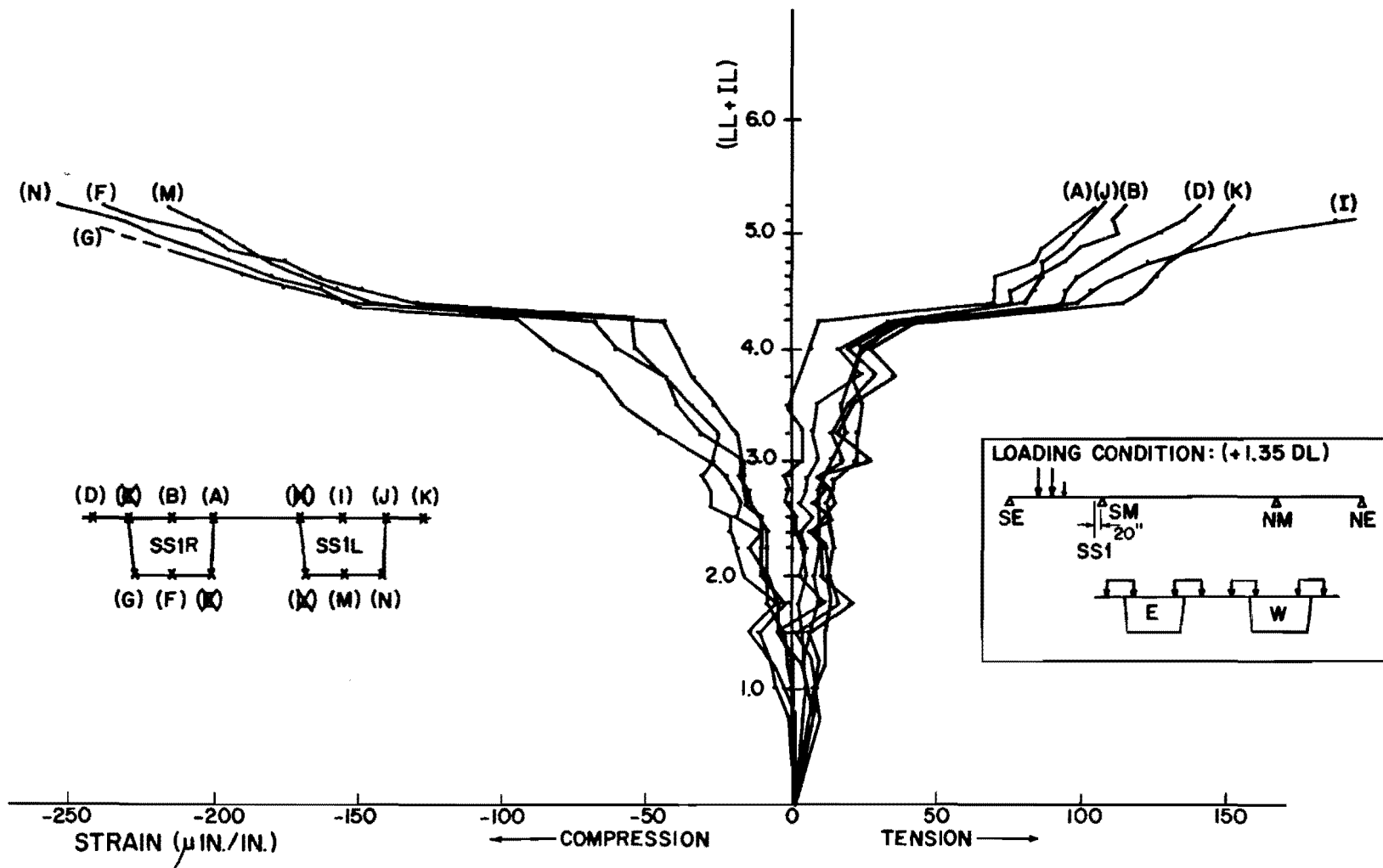


Fig. 8.7. Longitudinal strains at the center of the SS1 segment

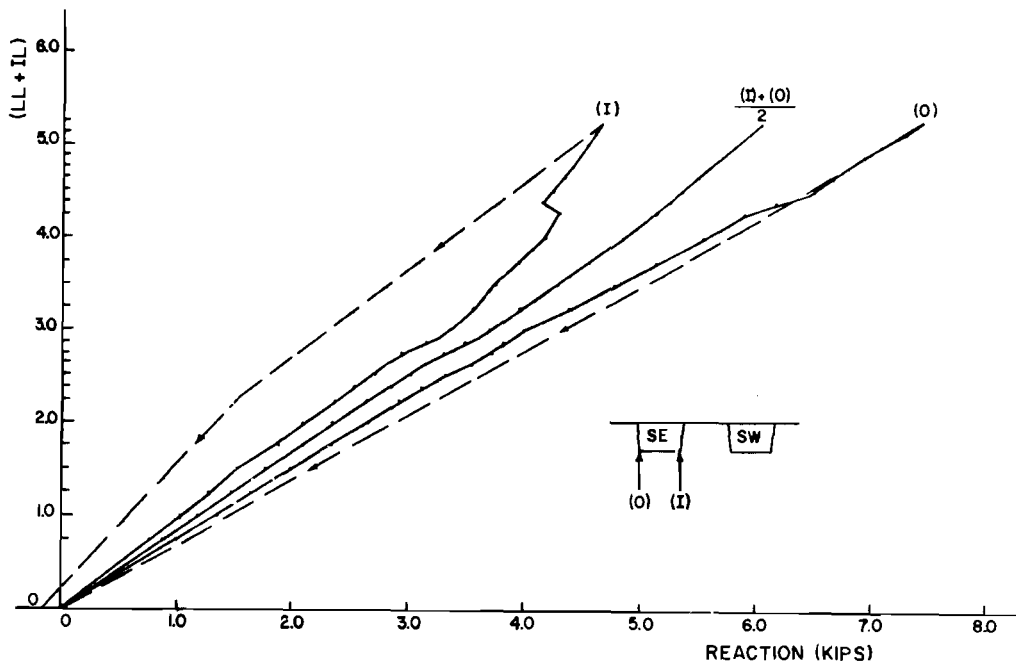
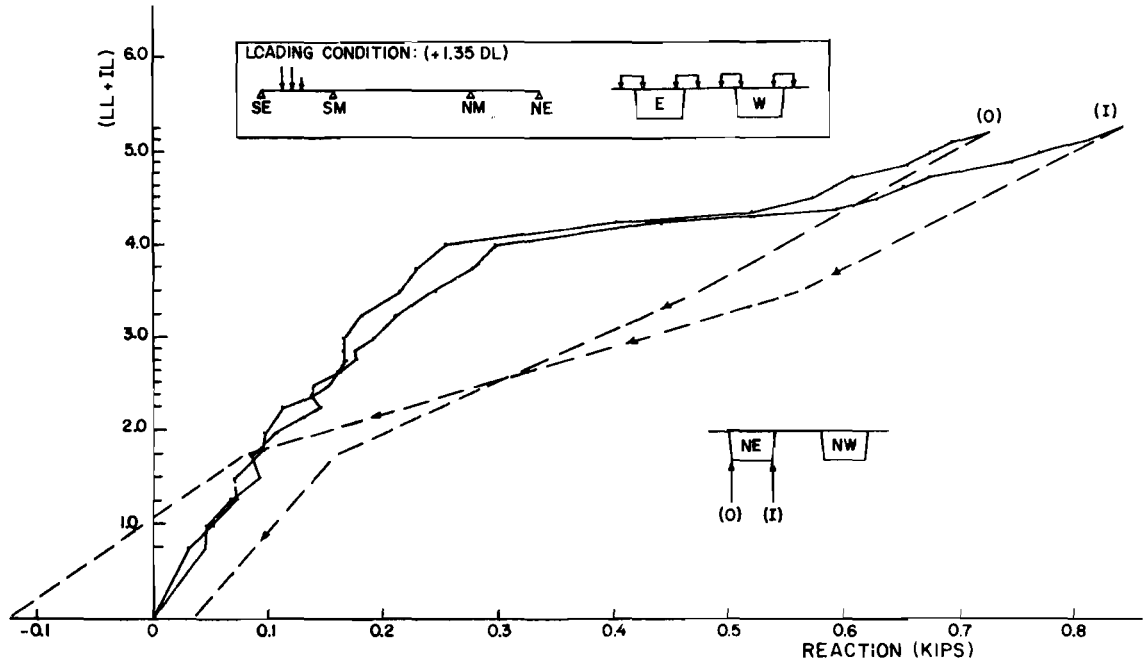
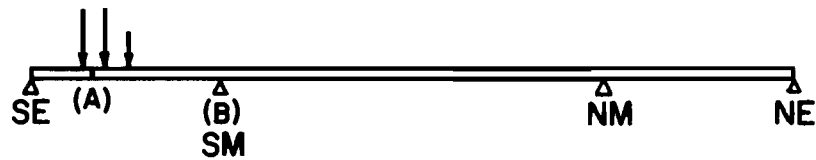
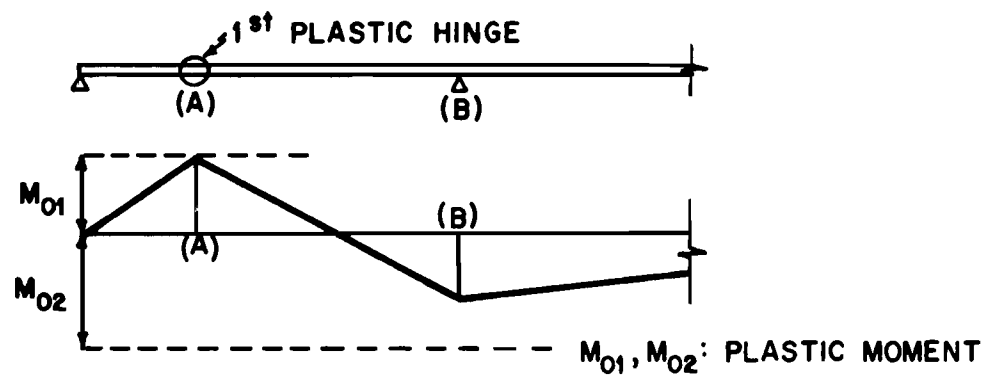


Fig. 8.8. Reactions at the outer supports

(A) LOADING CONDITION: (+1.35 DL)



(B) FIRST PLASTIC HINGE AND MOMENT DIAGRAM.



(C) SECOND PLASTIC HINGE AND MOMENT DIAGRAM AT COLLAPSE.

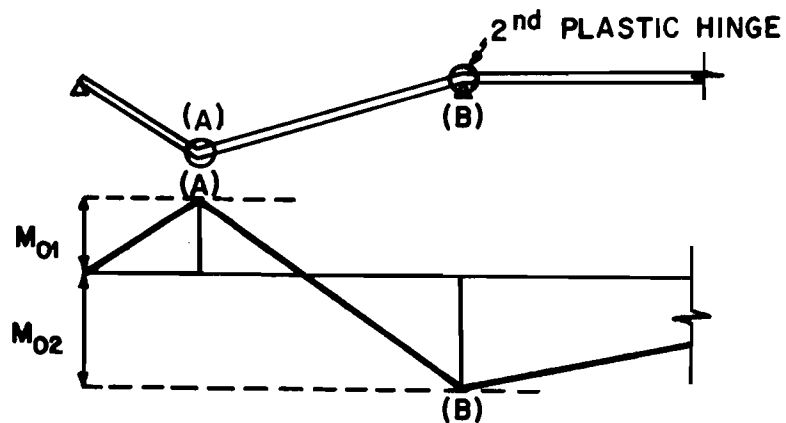


Fig. 8.9. Failure mechanism for truck loadings in the side span

Due to the extreme widening of the crack at the SS6-7 joint, an unexpected horizontal force occurred on the top of the SE pier. It could be visually observed at high load levels that the SE pier was tilting and inclining after the large cracks opened around the SS6-7 joint. Apparently a significant horizontal force due to the deformation of the bridge was induced at the top of the SE pier, as shown in Fig. 8.10. The moment connection between the end pier and the test floor was not strong enough to keep the pier from tilting under this force.

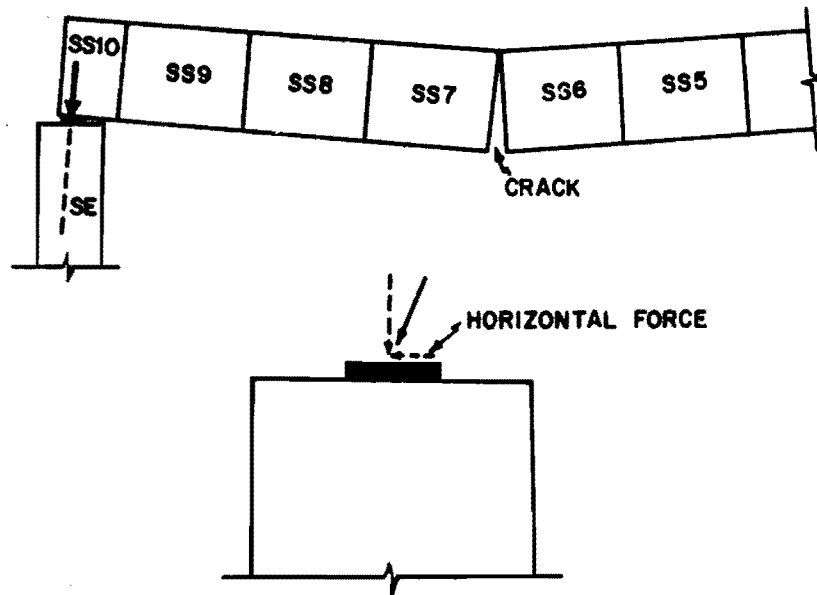


Fig. 8.10. Horizontal force on the top of the outer pier

Because it was obvious that a plastic hinge had formed near the 4.38(LL + IL) increment and because of the inclination of the end pier, it was decided to stop loading and release all live load at the 5.25(LL + IL) increment. This represented practical failure of the side span, although total collapse did not occur. In this way further load testing could be completed in the other two spans.

The maximum width of the crack at the SS6-7 joint was 1/4 in. on the outer west web (OW) and about 1/8 in. on the outer east web (OE) under the maximum load increment. Cracks were distributed more in the outer

east web than in the outer west web. This might be due to a somewhat weaker joint in the west side of the box because there was not much apparent difference in the grouting effectiveness.

In the transverse direction, as seen in Fig. 8.11, deflections were reasonably uniform across the SS7 segment at small loading increments. Relative deflections increased in the cantilever slabs and at the middle of the midstrip closure as loading increased. Transverse strains on the bottom face of the top slab were measured by paper gages, as shown in Fig. 8.12. Transverse strains also increased rapidly at the 4.38(LL + IL) increment.

8.2.3 Calculation of Side Span Live Load Capacity. In order to find the actual live load capacity factor (LF) for the truck loading in the side span, it is necessary to consider all forces and moments acting on the bridge.

Each time precast segments were erected and joined in symmetrical cantilever construction, negative tendons were prestressed in order to hold the precast segments in the proper balanced position, as shown in Fig. 8.13(a). For a typical construction stage, if a section is cut at A-A, the prestressing force ΣP is acting as shown in Fig. 8.13(b) and produces a moment $M_p = [(\Sigma P) \times e]$. These forces and moments can be calculated at each section and a force diagram for ΣP and a moment diagram for M_p can be drawn as in Fig. 8.13(c) and (d), respectively. The opposing dead load moment due to the weight of the segments is shown in Fig. 8.13(e). Although vertical forces are acting along the curved portions of the tendon ducts, no vertical forces are included, since all negative tendons are horizontal at the joint. At the completion of the balanced cantilever construction scheme, the diagrams of the total force and the total moment due to prestressing cables (negative tendons) and the total moment due to dead load (weight of segments) are shown in Fig. 8.14. The moment due to the external load (weight) and prestressing cables were designated as the external moment (M_{E1}) and the internal moment (M_{I1}), respectively. The force due to the prestressing cables was designated as the internal force (F_{I1}).

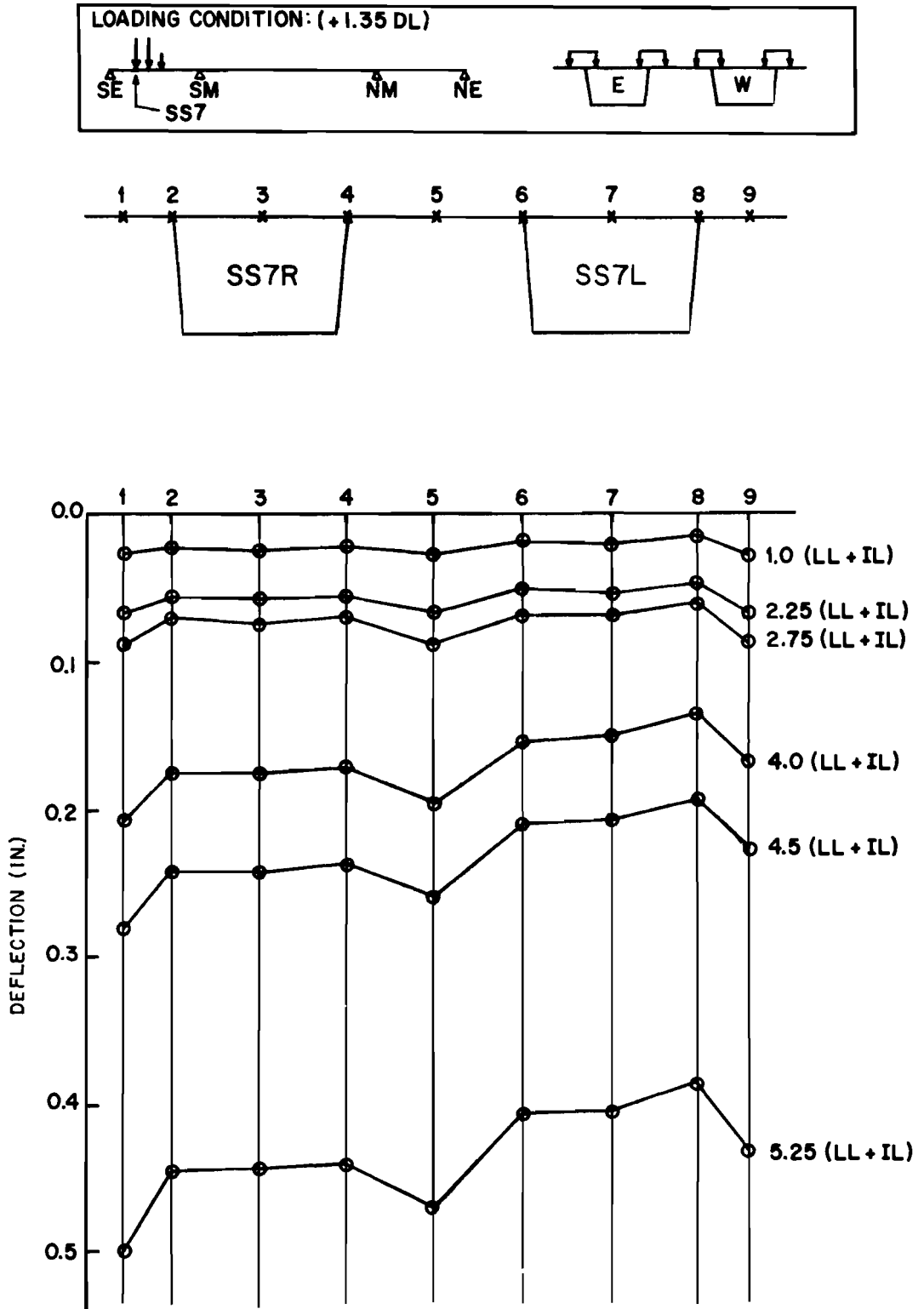


Fig. 8.11. Deflections along the center of the SS7 segment in side span

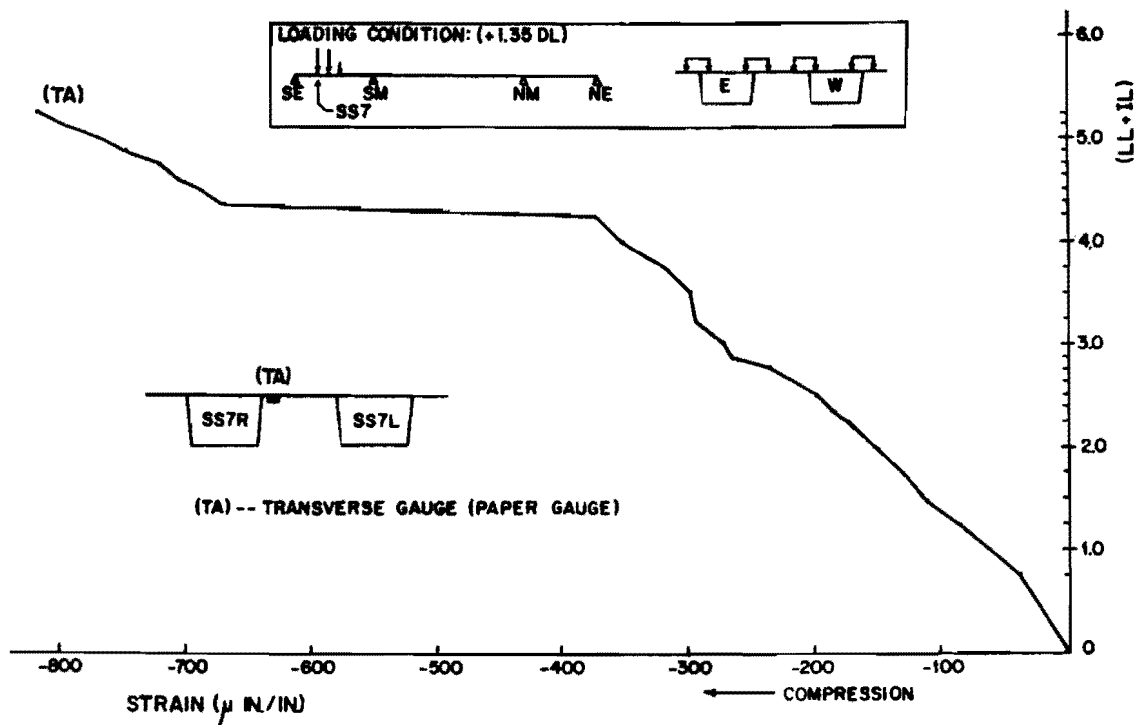
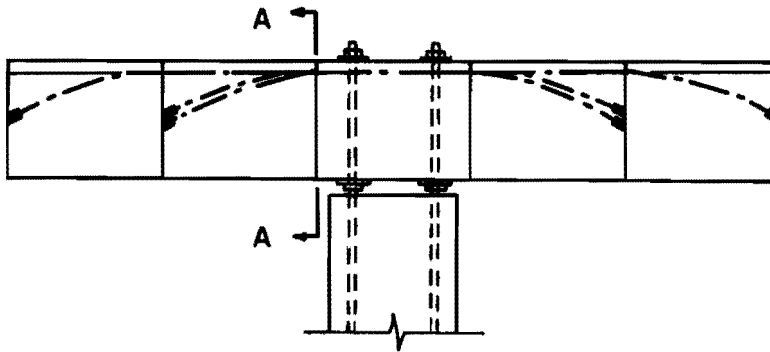
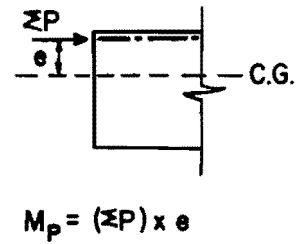


Fig. 8.12. Transverse strains at the center of the SS7 segment

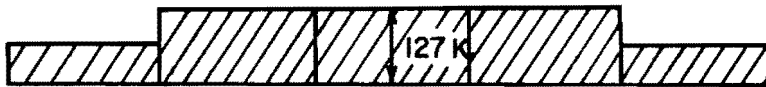
(A) CANTILEVER CONSTRUCTION



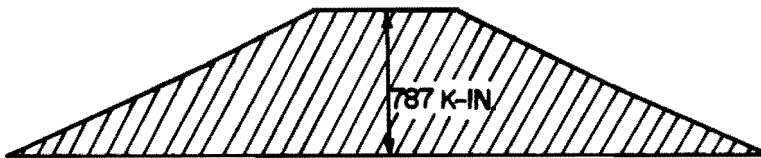
(B) PRESTRESSING FORCES AND MOMENTS AT A-A



(C) PRESTRESSING FORCES ALONG SEGMENTS



(D) MOMENTS DUE TO PRESTRESSING FORCES



(E) MOMENTS DUE TO WEIGHT OF SEGMENTS

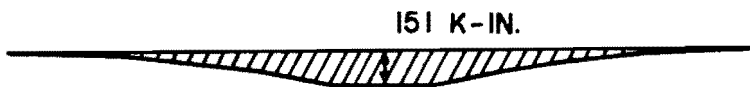


Fig. 8.13. Forces and moments acting on the bridge for a typical cantilever stage

(A) COMPLETION OF CANTILEVER CONSTRUCTION

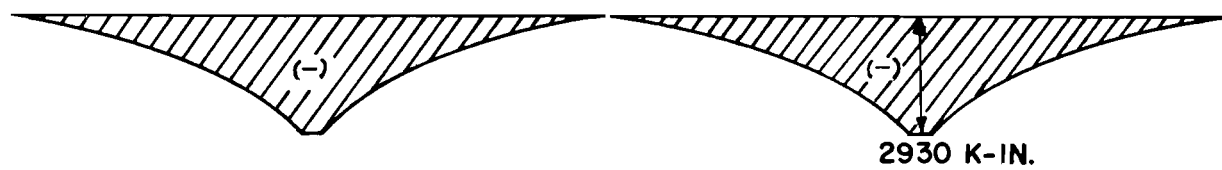
(B) HORIZONTAL FORCES DUE TO PRESTRESSING (F_{H1})(C) MOMENTS DUE TO PRESTRESSING (M_{P1})(D) MOMENTS DUE TO WEIGHT OF SEGMENTS (M_{E1})(E) $M_{I1} + M_{E1}$ 

Fig. 8.14. Horizontal forces and moments at completion of cantilever erection

Positive tendons in the side spans were inserted and prestressed after completing the cantilever construction. Prestressing of positive tendons in the side spans cause an internal force (F_{I2}) and moment (M_{I2}), as shown in Fig. 8.15.

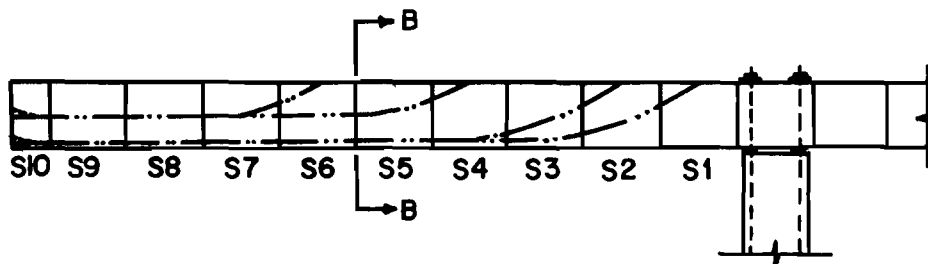
The closure segment at the center of the main span was then cast. At this stage there were external moments due to 1.0 DL, (M_{E1}), and internal force (F_{I1}) and moment due to negative tendons (M_{I1}) in the main span. However, the moment at the closure segment was zero. The positive moment cables at midspan essentially need to resist only live loads. Thus, the amount of center span positive prestressing cables should be less in a bridge constructed by cantilever construction than in a bridge constructed on falsework. Details of these differences are referred to in Muller's paper.³⁰

After the required strength of concrete in the closure was developed, the positive tendons in the main span were prestressed. Outer supports were set in position touching the girder ends prior to prestressing the positive tendons in the main span. Thus, resultant forces were produced at the outer supports when the positive tendons were prestressed, since the side span outer ends tried to deflect downward. In addition, to ensure that no uplift at the outer supports occurs at service level loading, specified additive vertical reactions were jacked into the outer supports at completion of the stressing (see Sec. 7.3.3.2). Internal forces (F_{I3}) and moments (M_{I3}) due to positive tendons in the main span are shown in Fig. 8.16(b) and (c). The moment (M_{E2}) caused by the resultant forces due to prestressing and the applied forces used to adjust the reactions and elevations at the outer supports are shown in Fig. 8.16(d).

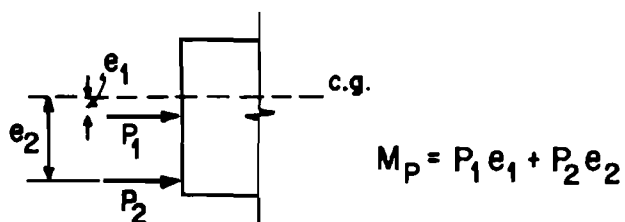
F_{I1} , F_{I2} , F_{I3} , and M_{I1} , M_{I2} , M_{I3} , M_{E1} , and M_{E2} are the forces and moments acting on the bridge at the time of completion of construction. Figure 8.17 shows the total or net horizontal forces and moments at each joint at the completion of all prestressing operations.

In order to compute the ultimate capacity of the bridge under factored dead and live load, the construction history must be considered.

(A) PRESTRESSING OF POSITIVE TENDONS IN SIDE SPAN



(B) PRESTRESSING FORCE AND MOMENT AT B-B



(C) HORIZONTAL FORCES DUE TO PRESTRESSING IN SIDE SPAN (F_{12})



(D) MOMENTS DUE TO PRESTRESSING IN SIDE SPAN (M_{12})

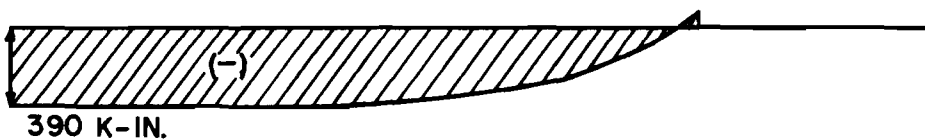


Fig. 8.15. Horizontal forces and moments due to prestressing in side span

(A) PRESTRESSING OF POSITIVE TENDONS IN MAIN SPAN

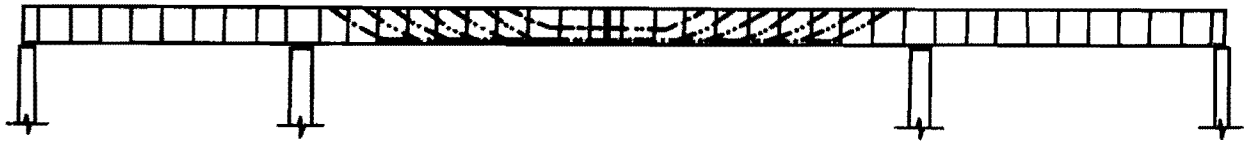
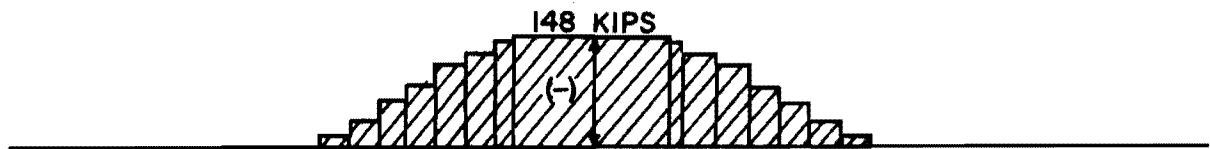
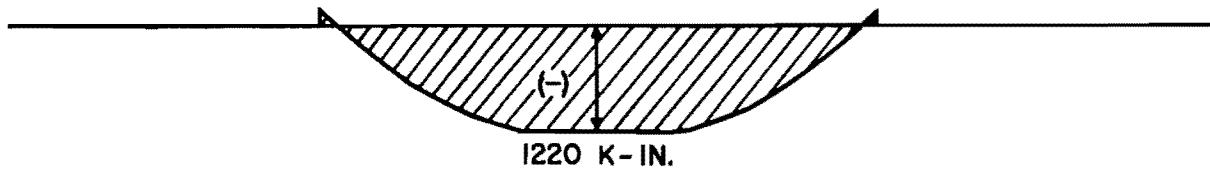
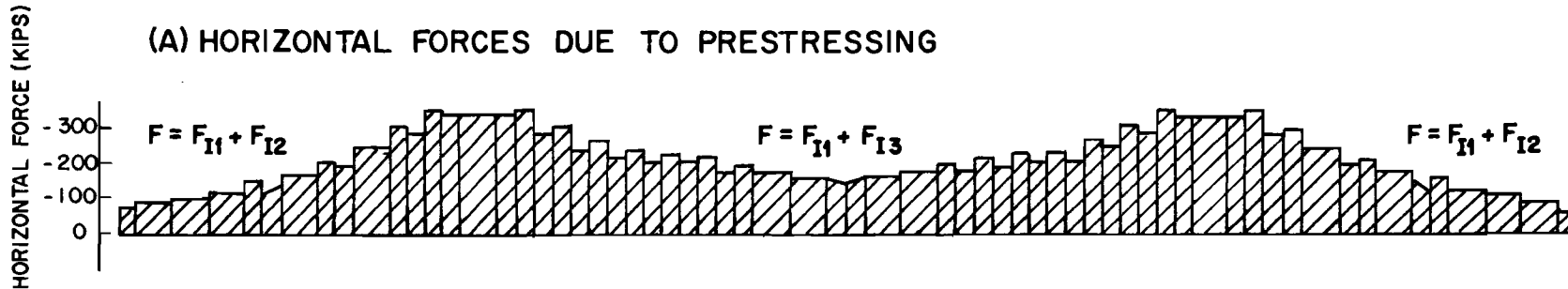
(B) HORIZONTAL FORCES DUE TO PRESTRESSING IN MAIN SPAN (F_{I3})(C) MOMENTS DUE TO PRESTRESSING IN MAIN SPAN (M_{I3})(D) MOMENTS DUE TO RESULTANT FORCE OF PRESTRESSING IN MAIN SPAN AND JACKING FORCES AT OUTER SUPPORTS (M_{E2})

Fig. 8.16. Horizontal forces and moments due to prestressing in main span



(A) HORIZONTAL FORCES DUE TO PRESTRESSING



(B) MOMENTS DUE TO PRESTRESSING AND WEIGHT OF SEGMENTS

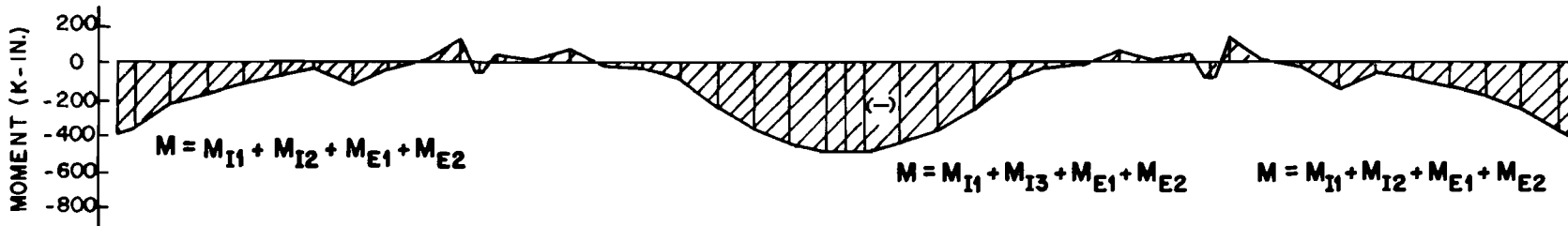


Fig. 8.17. Horizontal forces and moments at completion of all prestressing operations

The basic ultimate design guide used, the 1969 BPR "Strength and Serviceability Criteria, Reinforced Concrete Bridge Members, Ultimate Design,"⁷ specifies $1.35 M_{DL}$ as the ultimate dead load moment. This value ($1.35 M_{DL}$) was used in the design of the bridge by Lacey²¹ assuming that the basic structural configuration would be the same for both the 1.0 DL and 0.35 DL. Actually the 1.0 DL was applied in the cantilevering stage and the 0.35 DL was applied to the three span continuous structure in the model test. In designing the positive tendons of the prototype, the external design ultimate moment was calculated for an ideal three span continuous beam, as follows:

$$M_u = 1.35 M_{DL} + 2.25 M_{(LL + IL)} + M_{s1} + M_{s2} + M_{s3}$$

where M_{DL} = moment due to dead load
 $M_{(LL + IL)}$ = moment due to (live + impact) load
 M_{s1} = secondary moment due to prestressing of negative tendons
 M_{s2} = secondary moment due to prestressing of positive tendons in the main span
 M_{s3} = secondary moment due to prestressing of positive tendons in the side span

Secondary moments induced by the prestressing of all negative and positive tendons were considered in the calculation of the design ultimate moment, as shown in the above equation.²¹ The additional factored 0.35 DL may represent additional weight due to heavier sections which would be caused by casting errors, or allow for later dead load changes in the bridge such as resurfacing, or simply be a safety margin. Since these types of segments are precast under close control, there seems to be a low probability of section overweight occurrence. It would seem logical to apply some of the 0.35 DL on the balanced cantilever and the remainder of the 0.35 DL on the completed continuous structure. However, such a division of the factored load was not simulated in the model test. The additional 0.35 DL was applied as if a live load on the three span structure after completion of construction. Thus, it is necessary to calculate the moment due to 1.0 DL and 0.35 DL separately. The moment for 1.0 DL should be calculated for the determinate structure (balanced cantilever) and that for the

0.35 DL (which was applied to the completed structure after service load testing) should be calculated for the indeterminate three span continuous beam structure. The moment due to 0.35 DL (M_{E3}) is shown in Fig. 8.18. Figure 8.19 shows the critical design truck loading in the side span and the corresponding moment diagram at service load of 1.0 (LL + IL). When the service (live + impact) load is increased to ultimate, a flexural failure of the bridge will occur by either rupture of the concrete or of the prestressing cables. The positive tendons in the positive moment region and the negative tendons in the negative moment region as well as the concrete compression zones present primary flexural resistance to live load.

The following equations for the ultimate external moment were used to calculate the LF of (LL + IL) in the model tests.

$$\begin{aligned}
 M_u &= M_{u1} + M_{u2} \\
 M_{u1} &= 1.0 M_{DL} \text{ to be computed as a balanced cantilever } (= M_{E1}) \\
 M_{u2} &= 0.35 M_{DL} + LF \times M_{(LL + IL)} + M_s \text{ to be computed as an} \\
 &\quad \text{ideal three span continuous beam}
 \end{aligned}$$

where $0.35 M_{DL} = M_{E3}$

$$M_{(LL + IL)} = M_{E4}$$

$$M_s = M_{E2}$$

In very underreinforced sections with bonded tendons, as in the positive moment region, the ultimate compressive force (C) and the tensile force ($\sum T_i$) may be calculated by assuming the bottom layer of prestressing cables as its ultimate strain (ϵ'_s). If joint 6-7 in the side span is taken for the free body, prestressing forces (P) due to negative tendons remain relatively constant and add to C and T, as shown in Fig. 8.20. These P forces have to be taken into account in computing the ultimate moment capacity, except at the closure segment where $P = 0$.

Since the positive tendons were placed in multiple layers in some sections, it is necessary to use the stress-strain curve for each tendon in order to find T. Although several specimens were tested in an attempt

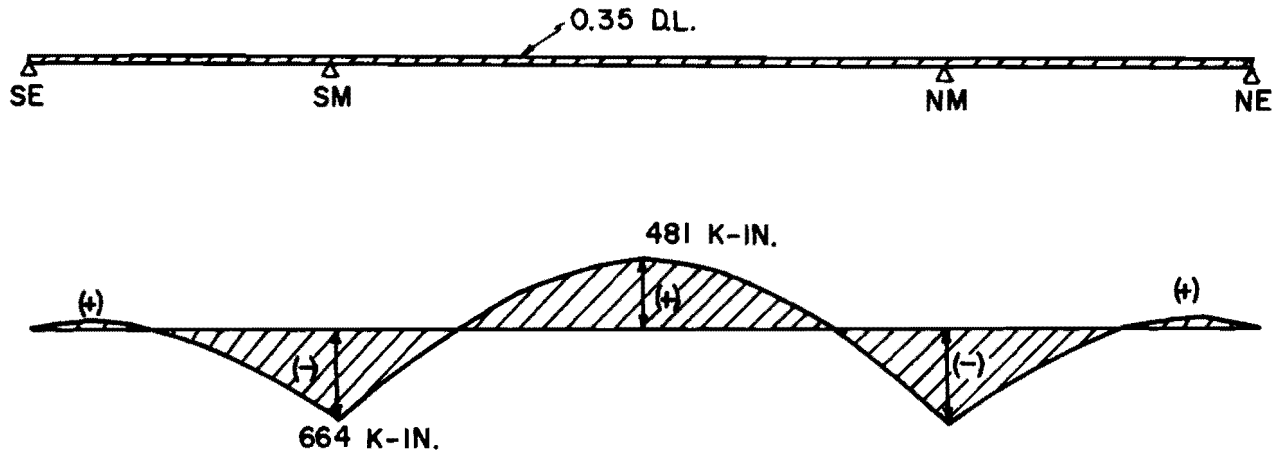


Fig. 8.18. Moment diagram for 0.35 DL (M_{E3})

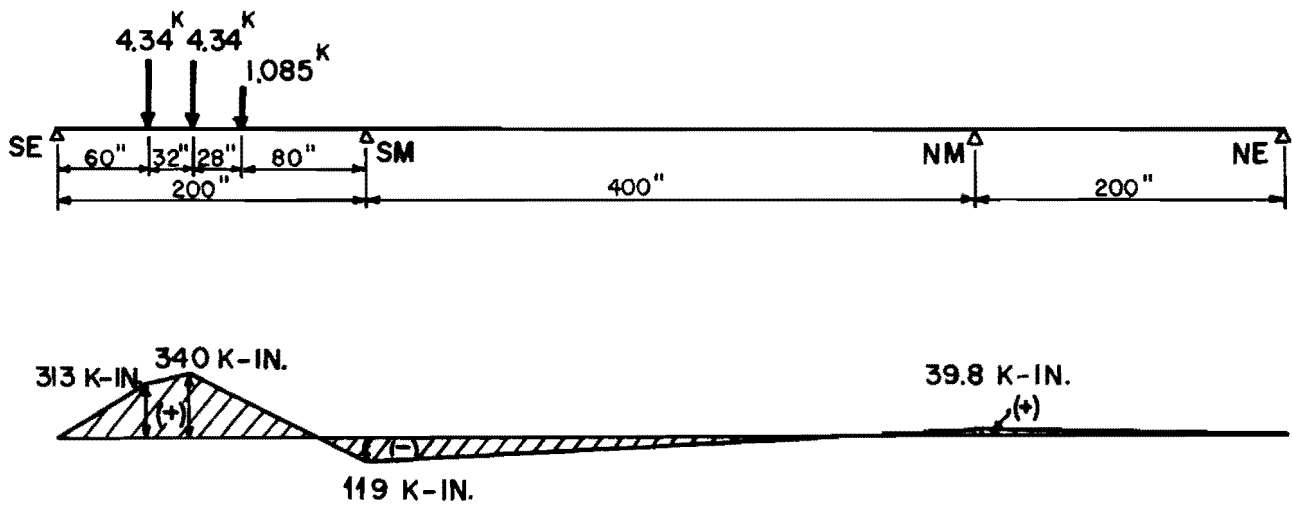


Fig. 8.19. Moment diagram for truck loads in side span (M_{E4})

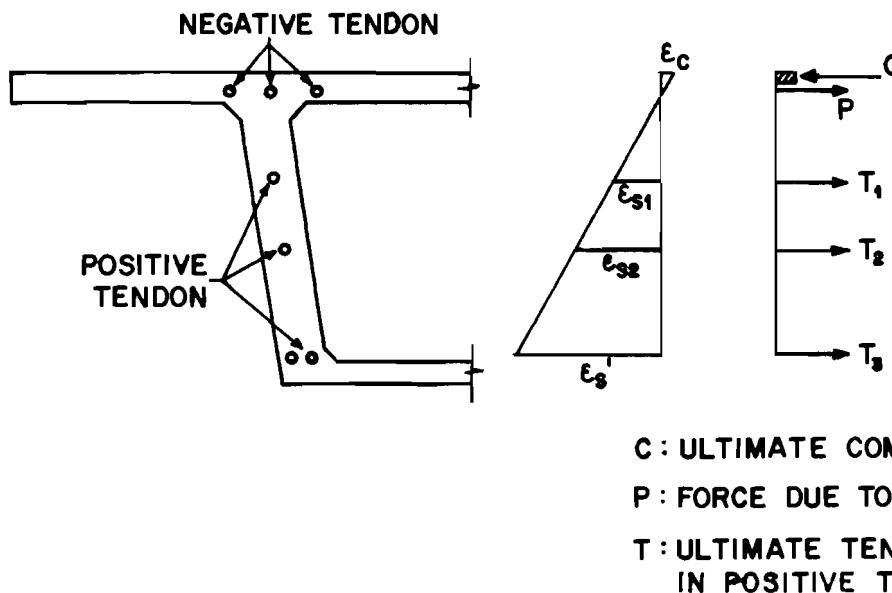


Fig. 8.20. Ultimate force at a certain section

to obtain actual stress-strain curves for samples of the wires and strands, a complete stress-strain curve up to failure was not obtained. The specimens usually failed at the grips in the testing machine outside the strain-gaged length. Based on stress-strain curves for a 270k grade 7-wire strand furnished by a manufacturer, typical stress-strain curves were developed, as shown in Fig. 8.21. These curves were based on known ultimate strengths for all of the prestressing tendons and measured E_s and strains from the incomplete material tests. The ultimate strain of the prestressing cables was assumed as 0.06 in./in.²⁶

In order to find the ultimate forces at joint 6-7 in the side span, T_i values were found from strain compatibility by using the stress-strain curves of Fig. 8.21. Compressive strains for the concrete in the top fiber were assumed for three different cases ($\epsilon_c = 0.003, 0.002, \text{ and } 0.0015$ in./in.) and then $\sum T_i$ were found, as shown in Fig. 8.22. There was no difference in $\sum T_i$ computed whether ϵ_c at the compression fiber was assumed as 0.003, 0.002, or 0.0015 in./in., so that it was not necessary to make further iterations for T_i in order to find the internal ultimate moment capacity. By assuming $\epsilon_c = 0.003$ in./in. at the extreme compression fiber and a rectangular stress block, as shown in Fig. 8.23(a), C and P were calculated as follows:

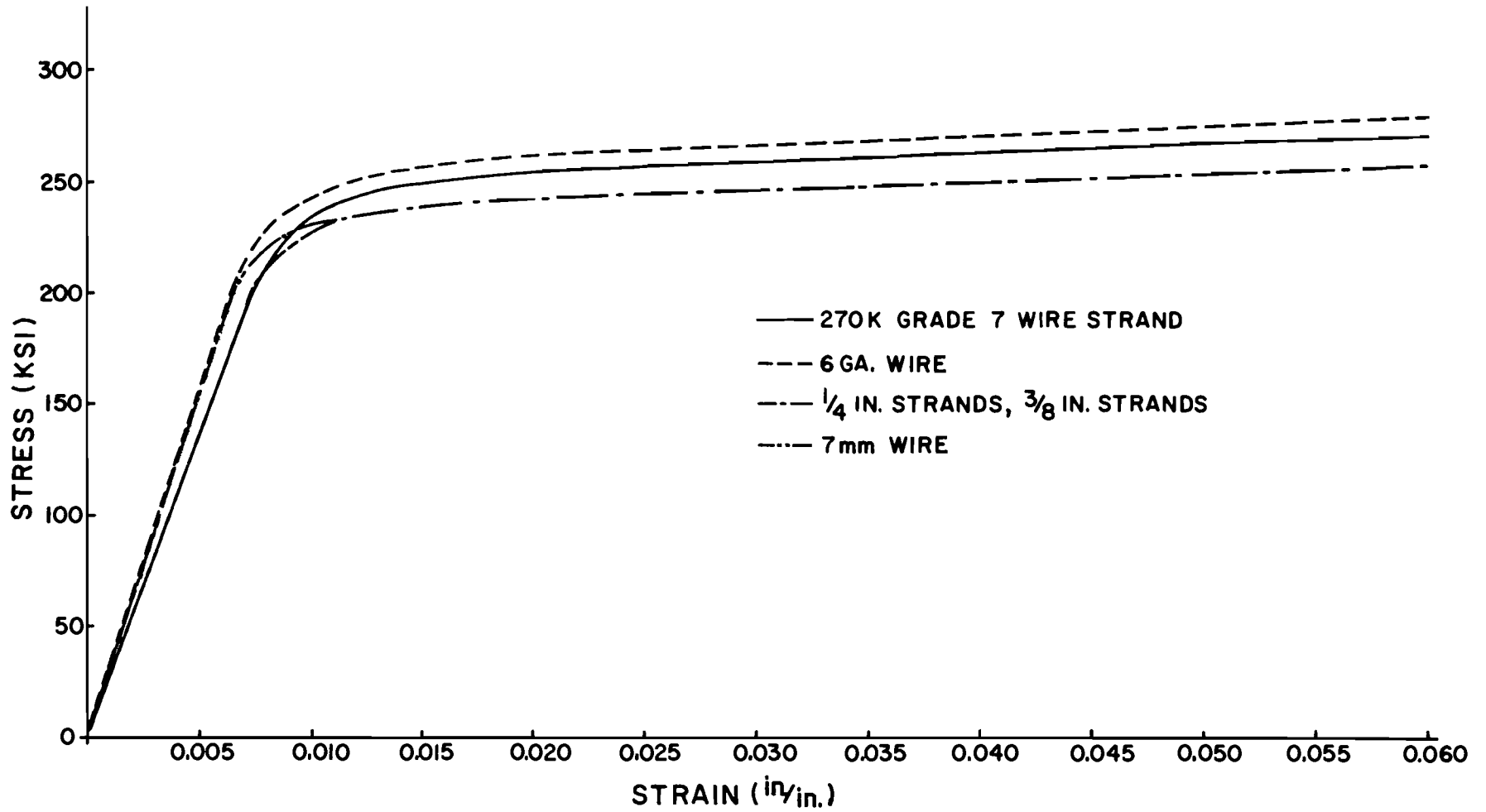
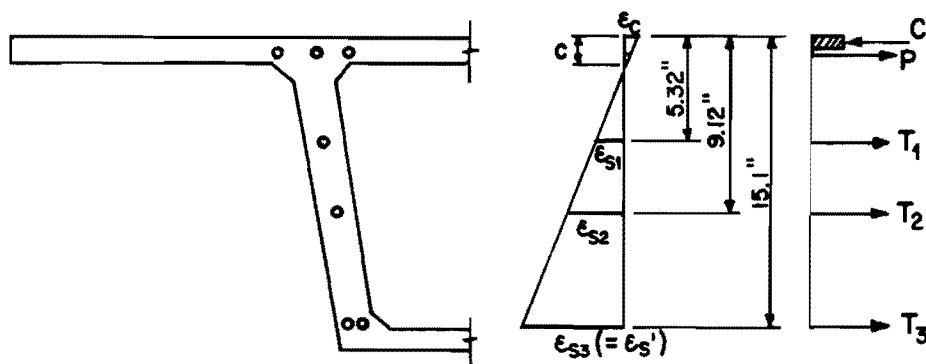


Fig. 8.21. Stress-strain curves of prestressing cables



CASE (1) - $\epsilon_{s3} = 0.06$ IN./IN., $\epsilon_c = 0.003$ IN./IN., $c = 0.72$ IN.

| ϵ_s (IN./IN.) | σ_s (KSI) | T_i (KIPS) | T_i for 2 boxes (KIPS) | ΣT_i (KIPS) |
|-------------------------|------------------|--------------|--------------------------|---------------------|
| $\epsilon_{s1} = 0.019$ | 261 | 7.57 | 30.3 (T_1) | 127 |
| $\epsilon_{s2} = 0.035$ | 269 | 7.80 | 31.2 (T_2) | |
| $\epsilon_{s3} = 0.06$ | 280 | 8.11 | 65.0 (T_3) | |

CASE (2) - $\epsilon_{s3} = 0.06$ IN./IN., $\epsilon_c = 0.002$ IN./IN., $c = 0.49$ IN.

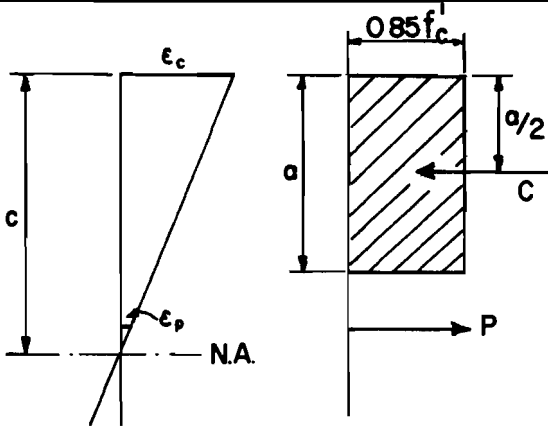
| ϵ_s (IN./IN.) | σ_s (KSI) | T_i (KIPS) | T_i for 2 boxes (KIPS) | ΣT_i (KIPS) |
|-------------------------|------------------|--------------|--------------------------|---------------------|
| $\epsilon_{s1} = 0.020$ | 262 | 7.60 | 30.4 (T_1) | 127 |
| $\epsilon_{s2} = 0.035$ | 269 | 7.80 | 31.2 (T_2) | |
| $\epsilon_{s3} = 0.06$ | 280 | 8.11 | 65.0 (T_3) | |

CASE (3) - $\epsilon_{s3} = 0.06$ IN./IN., $\epsilon_c = 0.0015$ IN./IN., $c = 0.37$ IN.

| ϵ_s (IN./IN.) | σ_s (KSI) | T_i (KIPS) | T_i for 2 boxes (KIPS) | ΣT_i (KIPS) |
|-------------------------|------------------|--------------|--------------------------|---------------------|
| $\epsilon_{s1} = 0.020$ | 262 | 7.60 | 30.4 (T_1) | 127 |
| $\epsilon_{s2} = 0.036$ | 269 | 7.80 | 31.2 (T_2) | |
| $\epsilon_{s3} = 0.06$ | 280 | 8.11 | 65.0 (T_3) | |

Fig. 8.22. Calculation of T_i for different strain profiles

(A) RECTANGULAR STRESS BLOCK



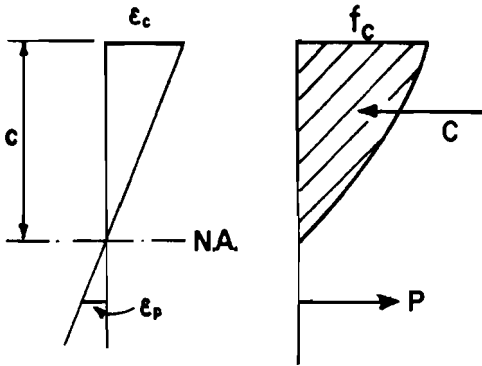
ϵ_c = CONCRETE STRAIN

c = DISTANCE FROM EXTREME COMPRESSION FIBER TO NEUTRAL AXIS AT ULTIMATE STRENGTH

a = DEPTH OF EQUIVALENT RECTANGULAR STRESS BLOCK = $k_1 C$

f'_c = COMPRESSIVE STRENGTH OF CONCRETE

(B) PARABOLIC STRESS BLOCK



b = WIDTH OF COMPRESSION FACE OF FLEXURAL MEMBER

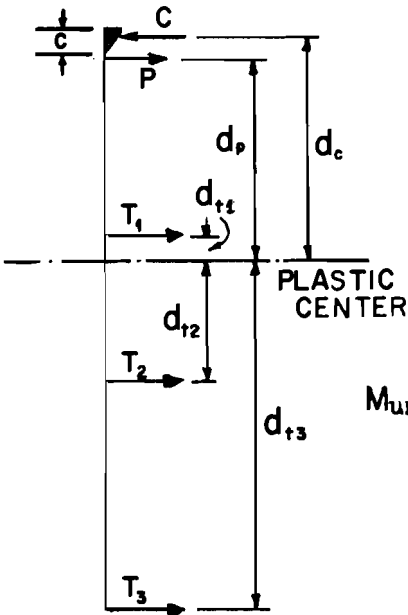
ϵ_p = STRAIN AT LEVEL OF PRESTRESSING CABLES (NEGATIVE TENDONS)

A_p = AREA OF PRESTRESSING CABLES

C = ULTIMATE COMPRESSIVE FORCE

P = FORCE DUE TO NEGATIVE TENDON

(C) CALCULATION OF ULTIMATE INTERNAL MOMENT



T = ULTIMATE TENSILE FORCE

d_c, d_p, d_{t_i} = DISTANCE FROM PLASTIC CENTER TO EACH FORCE

$$M_{ult} = C \times d_c - P \times d_p - T_1 \times d_{t1} + T_2 \times d_{t2} + T_3 \times d_{t3}$$

Fig. 8.23. Calculation of ultimate internal moment

$$\epsilon'_s = 0.06 \text{ in./in.}$$

$$\epsilon_c = 0.003 \text{ in./in.}$$

$$c = 0.72 \text{ in.}$$

$$a = 0.70 \times 0.72 = 0.504 \text{ in.}$$

$$C = 0.85f'_c \times a \times b = 0.85 \times 7.09 \times 0.504 \times 112 = 340 \text{ kips}$$

$$P = 49.6 - A_p \times E_s \times \epsilon_p = 49.6 - 0.348 \times 30 \times 10^3 \times 0.00025 \\ = 49.6 - 2.7 = 46.9 \text{ kips}$$

$$C = 340 \gg P + T_i = 46.9 + 127 = 174 \text{ kips}$$

This indicated that the compressive strain at the top fiber had not reached 0.003 in./in. Then, by assuming the strain at the bottom of steel as 0.06 in./in. and the parabolic stress block shown in Fig. 8.23(b), C and P were found after several iterations in which various neutral axes were assumed until $C = \sum T_i + P$. The internal ultimate moment was then calculated as follows [see Fig. 8.23(c)]:

$$\epsilon'_c = 0.0015 \text{ in./in.}$$

$$c = 0.37 \text{ in.}$$

$$f_c = 0.95 \times f'_c = 0.95 \times 7.09 = 6.74 \text{ ksi}$$

$$\epsilon_p = 0.0012 \text{ in./in.}$$

$$P = 49.6 + 0.348 \times 30.9 \times 10^3 \times 0.0012 = 62.5 \text{ kips}$$

$$C = 187 \text{ kips}$$

$$C = 187 = \sum T_i + P = 62.5 + 127 = 189.5 \text{ kips}$$

$$M_{UI} = C \times d_c - P \times d_p - T_1 \times d_{t1} + T_2 \times d_{t2} + T_3 \times d_{t3} \\ = 187 \times 5.90 - 62.5 \times 5.46 - 30.4 \times 0.8 + 31.2 \times 3.0 + 65 \times 8.98 \\ = 1103 - 341 - 24.3 + 93.6 + 584 = 1415 \text{ k-in.}$$

At the peak compressive strength of concrete, experiments²⁵ indicate that strains reach about 0.002 in./in. for various strengths of concrete. If the strain at the peak stress is assumed as 0.002 in./in., about 95 percent of f'_c will develop at the extreme fiber for 0.0015 in./in. strain.²⁷ Therefore, f_c was assumed as $0.95 \times f'_c$ in the above calculation.

In all calculations of the ultimate moment and shear capacity, $\phi = 1.0$ was used, since all as built dimensions and material strengths were known for the model.

In overreinforced sections with bonded tendons (around the main pier), the concrete strain at failure at the bottom fiber was assumed as 0.003 in./in. according to the ACI Code² and strains were calculated at the level of the prestressing cables. The compressive stress block was assumed as rectangular. Several trials were made until C equalled T by varying assumed values of c in Fig. 8.24(c). T was determined from the stress-strain curves of Fig. 8.21 for $\epsilon_s = \epsilon_{sp} + \epsilon_{sl}$. Although some compressive strain existed at the bottom fiber before applying any live load, the magnitude (about 0.00015 in./in.) was very small compared to $\epsilon_c = 0.003$. Therefore, this effect was neglected and the strain was simply assumed as 0.003 in./in. at the bottom fiber in order to calculate the ultimate moment at the pier. After determining the proper c , the internal ultimate moment was calculated as follows:

$$c = 2.46 \text{ in.}$$

$$\epsilon_c = 0.003 \text{ in./in.}$$

$$a = 0.7c = 1.72 \text{ in.}$$

$$b = 52 \text{ in.}$$

$$C = 0.85f'_c \times a \times b = 0.85 \times 7.09 \times 1.72 \times 52 = 539 \text{ kips}$$

| | Area (in. ²) | ϵ_{sp} (in./in.) | ϵ_{sl} (in./in.) | $\epsilon_s = \epsilon_{sp} + \epsilon_{sl}$ (in./in.) | σ_s (ksi) | T (kip) | T for 2 boxes (k) |
|--------------------|-----------------------------|------------------------------|------------------------------|---|---------------------|----------------|-------------------------|
| 3/8 in. strands | 0.085 | 0.00600 | 0.0159 | 0.0219 | 243 | 20.7 | 166 |
| 7mm wire | 0.0593 | 0.00495 | 0.0159 | 0.0199 | 242 | 14.4 | 288 |
| 6ga. wire | 0.029 | 0.00462 | 0.0159 | 0.0205 | 242 | 7.0 | 84 |
| | | | | | | Total T | = 538 |

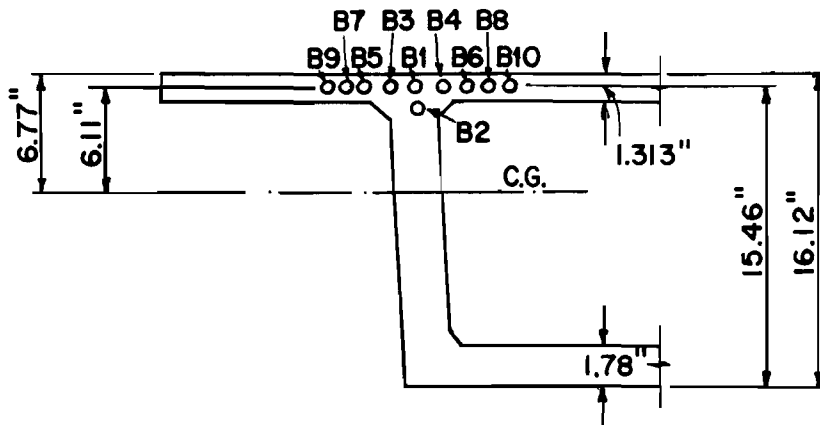
$$jd = 15.46 - a/2 = 15.46 - 0.86 = 14.6 \text{ in.}$$

Ultimate Internal Moment:

$$M_{UI} = 538 \times 14.6 = 7855 \text{ k-in.}$$

Since the completed bridge is a three span continuous beam, it has to form two plastic hinges for complete failure in the side span,

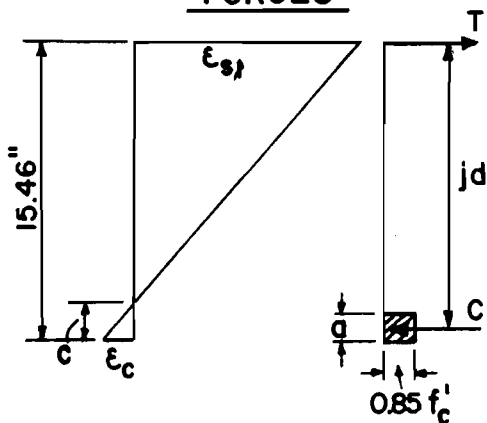
(A) POSITION OF TENDONS AT MAIN PIER



(B) PROPERTIES OF EACH TENDON

| TENDONS | | AREA (IN. ²) | EXPERIMENTAL VALUE | | | APPLIED VALUE | | |
|--------------|--------------------|-----------------------------|----------------------------|---------------------------|-------------------------|--------------------------------|-------------------------------|--|
| | | | F _s ' (KIPS) | f _s ' (KSI) | E _s (KSI) | 0.6 F _s ' (KIPS) | 0.6 f _s ' (KSI) | ε _{sp} AT 0.6 f _s ' (IN./IN.) |
| 7 MM. WIRE | B1, B2, B5, B6, B7 | 0.0594 | 15.31 | 258 | 30.5x10 ³ | 8.94 | 151 | 0.00495 |
| 3/8" STRANDS | B3, B4 | 0.085 | 22.05 | 259 | 27.0x10 ³ | 13.75 | 162 | 0.00600 |
| 6 GA. WIRE | B8, B9, B10 | 0.029 | 8.13 | 280 | 30.9x10 ³ | 4.14 | 143 | 0.00462 |

(C) ULTIMATE INTERNAL FORCES

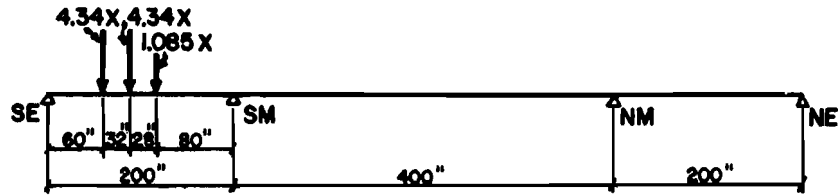


- ε_{sp} = STRAIN DUE TO PRESTRESSING (IN./IN.)
- ε_{sj} = STRAIN DUE TO EXTERNAL LOAD (IN./IN.)
- ε_s = ULTIMATE STRAIN OF PRESTRESSING CABLE
= ε_{sp} + ε_{sj} (IN./IN.)
- ε_c = 0.003 IN./IN.
- f_c = COMPRESSIVE STRENGTH OF CONCRETE
- T = TENSILE FORCE AT ULTIMATE (KIPS)
- C = ULTIMATE COMPRESSIVE FORCE
- c = DISTANCE FROM EXTREME COMPRES. FIBER TO NEUTRAL AXIS AT ULT. STRENGTH (IN.)
- jd = DISTANCE BETWEEN T & C (IN.)
- a = DEPTH OF EQUIV. RECT. STRESS BLOCK (IN.)
- b = WIDTH OF COMPRESSION FACE OF FLEXURAL MEMBER (IN.)

Fig. 8.24. Calculation of ultimate internal moment at pier section

as shown in Fig. 8.25(b). The LF for (LL + IL) to produce the first plastic hinge was calculated as follows.

(A) LOADING CONDITION



(B) FORMATION OF PLASTIC HINGE



(C) PLASTIC MOMENT

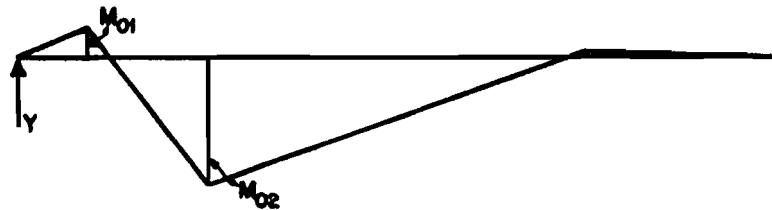


Fig. 8.25. Plastic hinges and moment diagram

Internal moment and external moment at the ultimate capacity are equated.

$$\begin{aligned}
 M_{UI} &= M_{E1} + M_{E2} + M_{E3} + LF \times M_{E4} \\
 LF \text{ for (LL + IL)} &= \frac{M_{UI} - M_{E1} - M_{E2} - M_{E3}}{M_{E4}} \\
 &= \frac{1415 + 319 - 259 - 34}{322} \\
 &= 1441/322 = 4.48
 \end{aligned}$$

Therefore, a first plastic hinge should form at the 1.35 DL + 4.48 (LL + IL) increment at the SS6-7 joint. Since the plastic hinge at the SS6-7 joint was observed to form between 4.25 to 4.38 (LL + IL) in the experiment, the calculated value (4.48) is very accurate.

Tensile strength of the only available 6 gage wire, which was used for the positive tendons in the side span was about 18 percent higher than the specified minimum, although all other prestress wires or strands had tensile strengths very close to the minimum values specified. It would therefore be expected that the first plastic hinge in a prototype with strands having exactly the specified minimum tensile strength would form at a loading somewhat less than the test 4.48(LL + IL) increment [at about 3.8(LL + IL)]. However, if the 25 percent live load reduction is used for the four lane bridge, a LF of 5.1 would be calculated which is ample.

If a second plastic hinge is assumed to form at the SM pier segment as shown in Fig. 8.25(b), the LF of (LL + IL) for complete failure can be calculated as follows:

Assume

Y = reaction at the SE support.

M_{01} = plastic moment at the SS6-7 joint (M_{UI} at the SS6-7 joint).

M_{02} = plastic moment at the SM pier segment (M_{UI} at the SM pier segment).

X = LF of (LL + IL).

From equilibrium, at the SS6-7 joint

$$M_{01} = - 4.34 \times 10X + 70Y \quad (1)$$

and at the center of the SM pier segment

$$\begin{aligned} -M_{02} = & - (4.34 \times 140 + 4.34 \times 108 + 1.085 \times 80)X \\ & + 200 Y \end{aligned} \quad (2)$$

From Eq. (1)

$$1415 = - 43.4 X + 70 Y \quad (1)'$$

From Eq. (2)

$$- 7855 = -1164 X + 200 Y \dots (2)'$$

$$[(2)' \times 0.35] - 2750 = -408 X + 70 Y \dots (3)$$

$$[(1)' - (3)] \quad 4165 = 364 X \therefore X = 11.4$$

Therefore, the second plastic hinge would form around the [1.35 DL + 11.4(LL + IL)] increment and the SM pier segment would fail in compression, if the initial plastic hinge had sufficient ductility. It is thus conservative to assume that the side span is fully capable of carrying [1.35 DL + 4.48(LL + IL)] considering four lanes fully loaded. Using AASHO load reduction factors for a four lane bridge, this would become [1.35 DL + 6.0(LL + IL)].

8.3 Failure in the Main Span

8.3.1 General. Four AASHO lane loads were applied to the main span and one adjacent side span to produce the critical shear condition at the first joint in the main span. It was anticipated from computations that with full development of shear strength the bridge would fail in flexure even though under a maximum shear loading. However, it was decided to check the shear capacity since basic information about flexural capacity was obtained by applying the truck loads to the side span. Lack of published information made it very desirable to check the performance of the epoxy joints under realistic high shear loadings.

In addition to the 1.35 dead load, live and impact loadings, shown in Fig. 8.26 were applied by rams and increased until failure. The position of the heavy concentrated load could greatly affect the shear strength of the bridge. It was considered that a direct shear failure might occur as the effective depth decreased due to flexural cracks, so concentrated loads were applied outside but adjacent to the first joint in the main span. Loading increments of 0.5(LL + IL) were used up to a loading of 2.0(LL + IL), after which the increments were reduced to 0.25(LL + IL) up to failure.

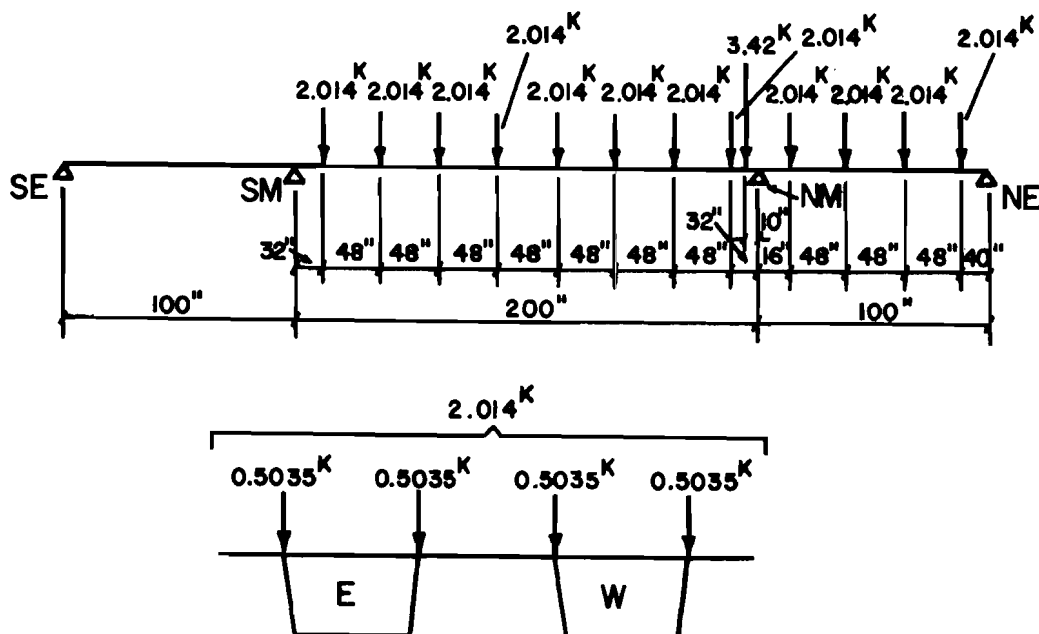


Fig. 8.26. $1.0(LL + IL)$ loading for maximum shear at the NM pier

8.3.2 Test Results. After the load reached $2.25(LL + IL)$, the reaction at the north end (NE) started to decrease and at higher loads the north reaction was unloading the dead load effects, as shown in Fig. 8.27. At the $2.63(LL + IL)$ increment, the south end segment (SE) raised completely from the neoprene pad support. At this load level the crack which had previously developed at the joint of the main span closure segment during the positive moment ultimate design load test (see Sec. 7.3.3.2) started to reopen. Figures 8.28 to 8.30 show that strains in segments SS7, SS6, SS1, and SM1 increased almost linearly up to $2.63(LL + IL)$, but remained constant after that increment because the south end reaction became zero and no load was applied to the unloaded side span. Strains at NS6 were very low until the $2.5(LL + IL)$ increment, then increased steadily until failure, as shown in Fig. 8.31. This change was caused by the alteration in structural configuration when the south side span became a free cantilever.

At the $3.25(LL + IL)$ increment, the strain increases at the NM6 segment stopped, as shown in Fig. 8.32. This was due to the concentration

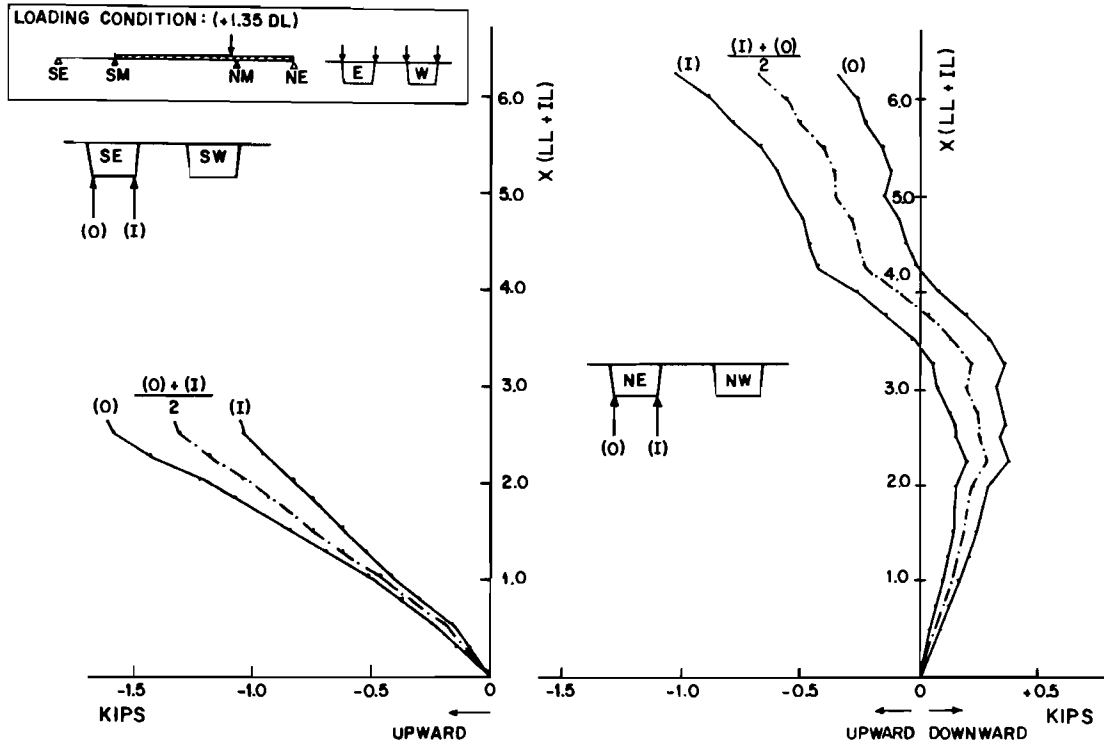


Fig. 8.27. Reaction at outer supports during loading to failure

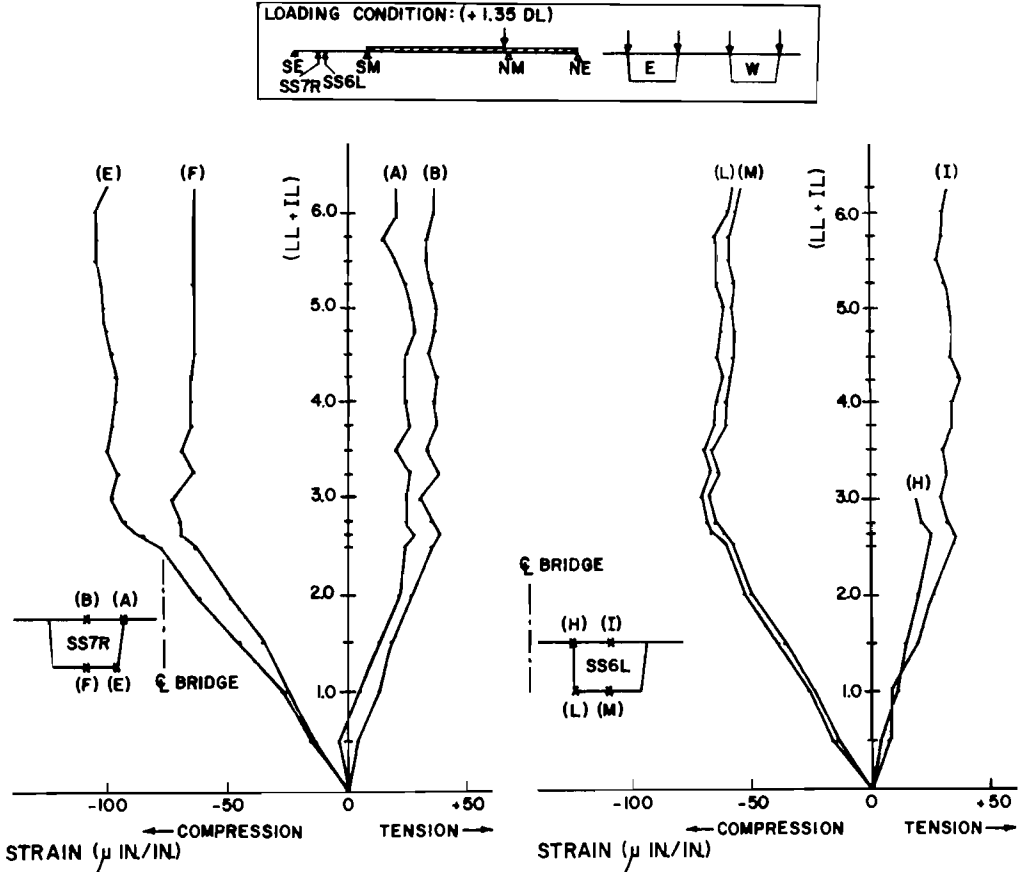


Fig. 8.28. Longitudinal strains at SS7R and SS6L during loading to failure

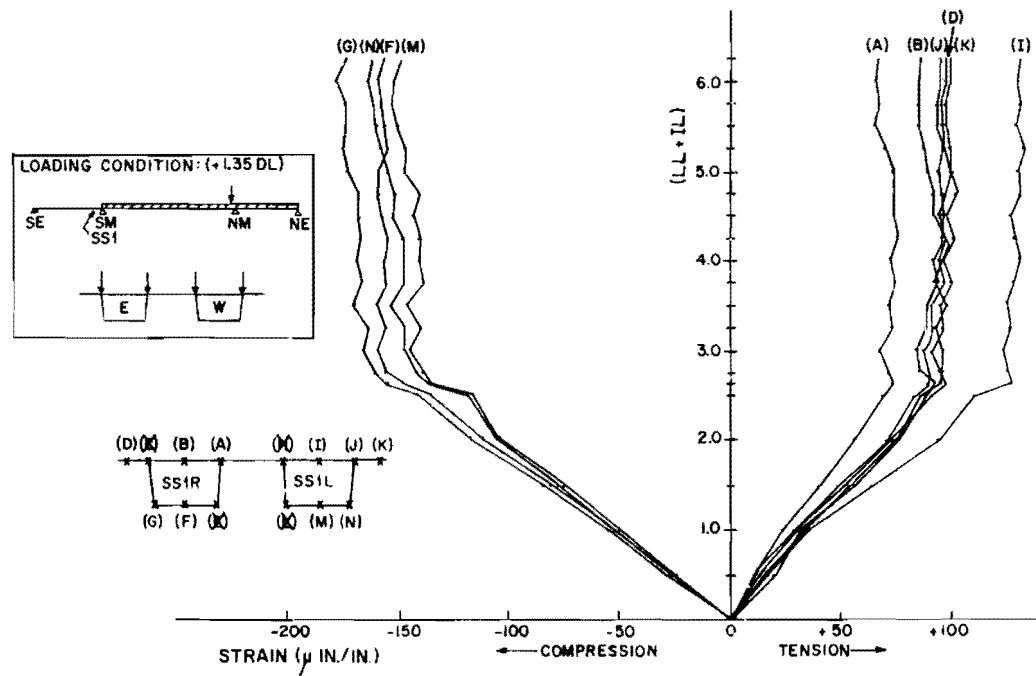


Fig. 8.29. Longitudinal strains at SS1 during loading to failure

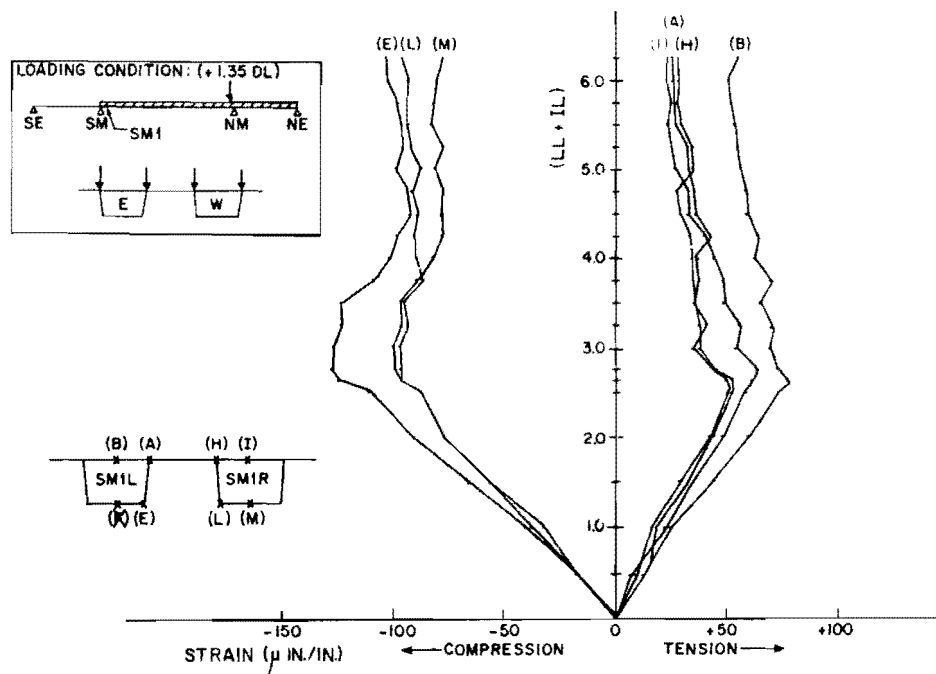


Fig. 8.30. Longitudinal strains at SM1 during loading to failure

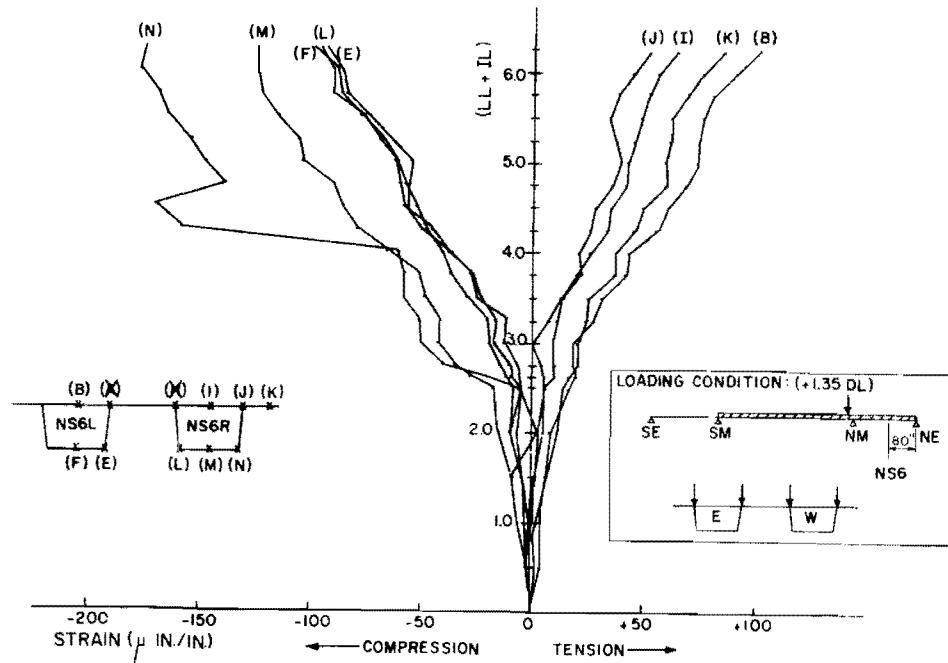


Fig. 8.31. Longitudinal strains at NS6 during loading to failure

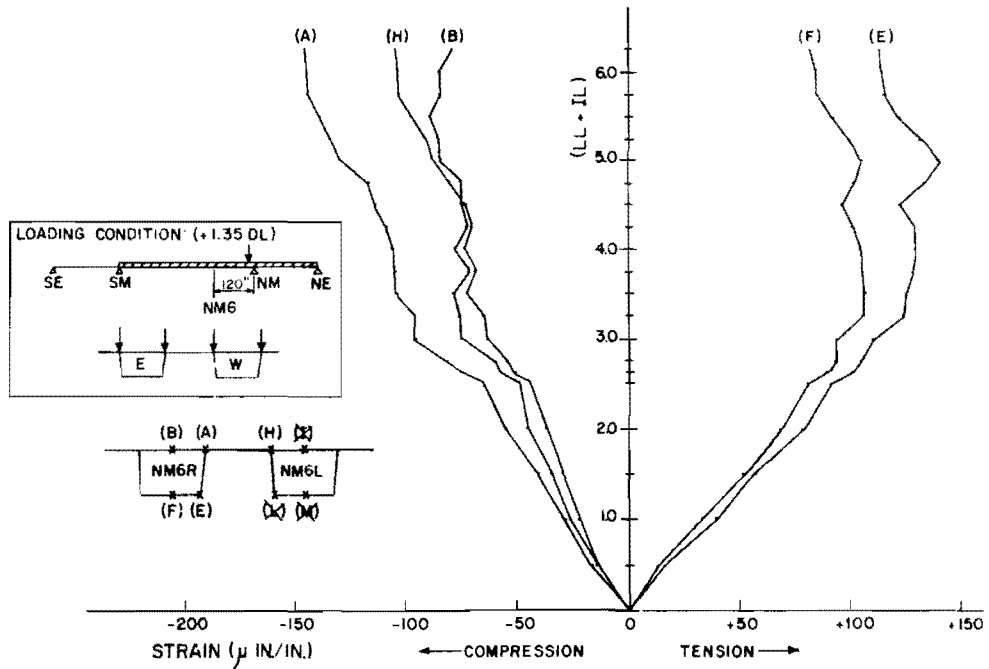


Fig. 8.32. Longitudinal strains at NM6 during loading to failure

of deformation in the crack around the center of the main span. By observing the deflection diagram for the SM10 segment in Fig. 8.33, it is seen that the rate of deflection increase changed substantially at 3.25(LL + IL). Also, a diagonal tension crack started to develop at the first segment in the main span (outer web on the west side) as shown in Fig. 8.34.

At the 3.75(LL + IL) increment, a flexural crack at the joint of the closure segment extended to near the top of the web and many cracks started to develop in the region of segments SM6 to SM9, as shown in Fig. 8.35.

At the 4.25(LL + IL) increment, the diagonal tension crack and the flexural crack around the NM pier joined (see Fig. 8.34) and a wide flexural crack developed about 1 in. away from the first joint in the main span. At this stage, the flexural crack on the top slab was only in the outer cantilever portion. At this loading the south end segment raised up about 1 in. from the surface of the neoprene pad support.

At the 4.25(LL + IL) increment in the east side and the 4.75(LL + IL) increment in the west side, very wide flexural cracks developed at the SM6-7, SM7-8, and SM8-9 joints, as shown in Fig. 8.35. These cracks developed near the epoxy joints in the web portion (in the flexural tension zone) and about 1 in. away from the joint in the bottom slab (in the pure tension zone), as shown in Fig. 8.36. The cracks at these joints went nearly to the top of the web with an increase of one increment of loading. The increase of strain around the 4.00 to 4.75(LL + IL) increment range at NM9, NM1, and NS1 stopped because of concentration of deformations at these joints and at the first joints from the main pier. Figures 8.37 to 8.39 show the effect of the concentration of deformation on strain at higher load.

At the 5.0(LL + IL) increment, the crack on the top slab of segment NS1 and the NM pier segment extended the full width of the slab (on the east side of the box).

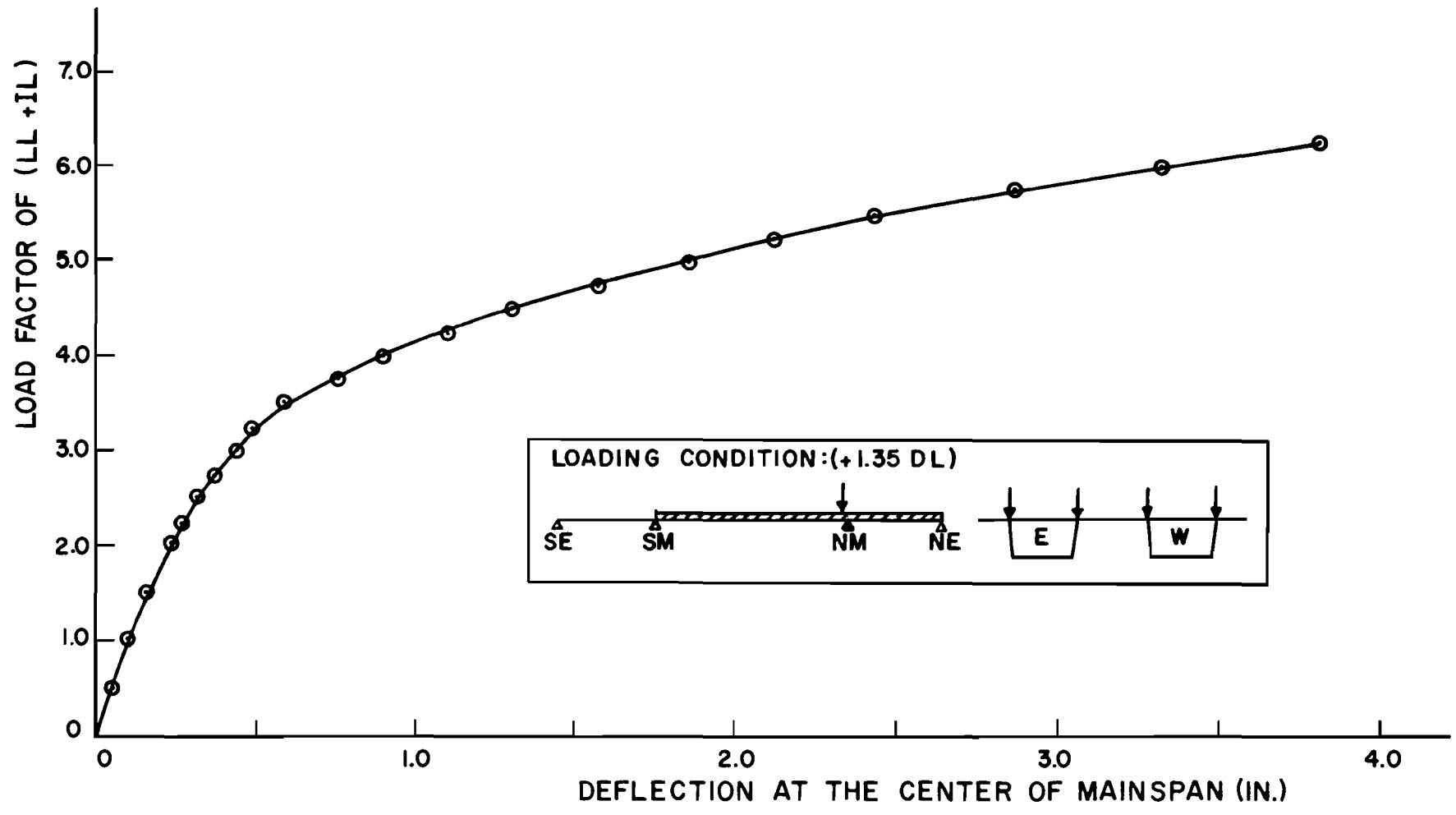
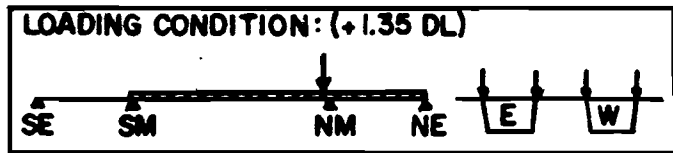


Fig. 8.33. Deflections at SM10 during loading to failure



* NUMBERS ALONG THE CRACKS ARE MULTIPLES OF (LL+IL)

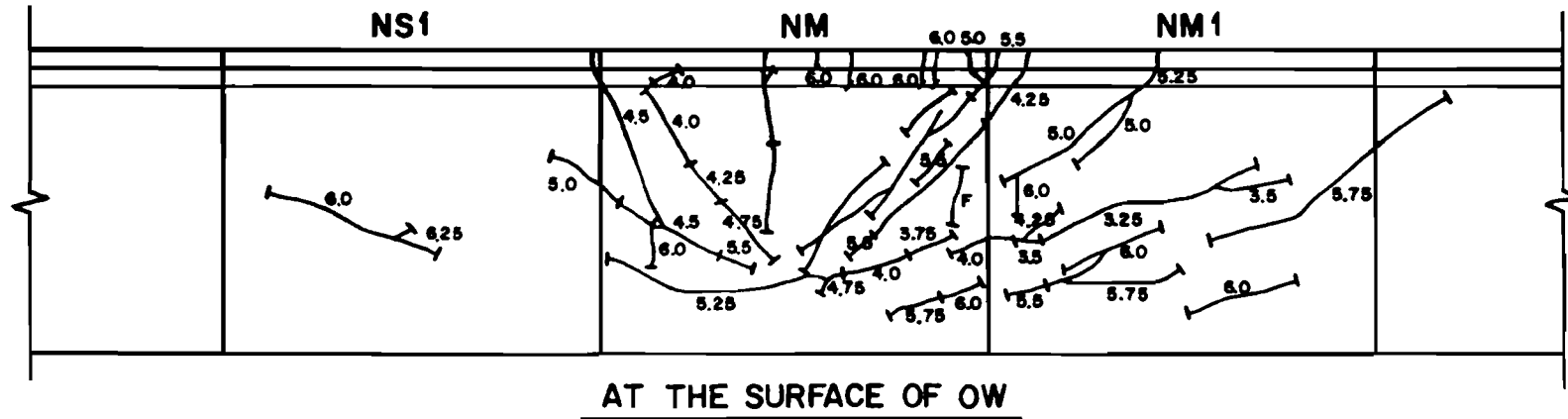
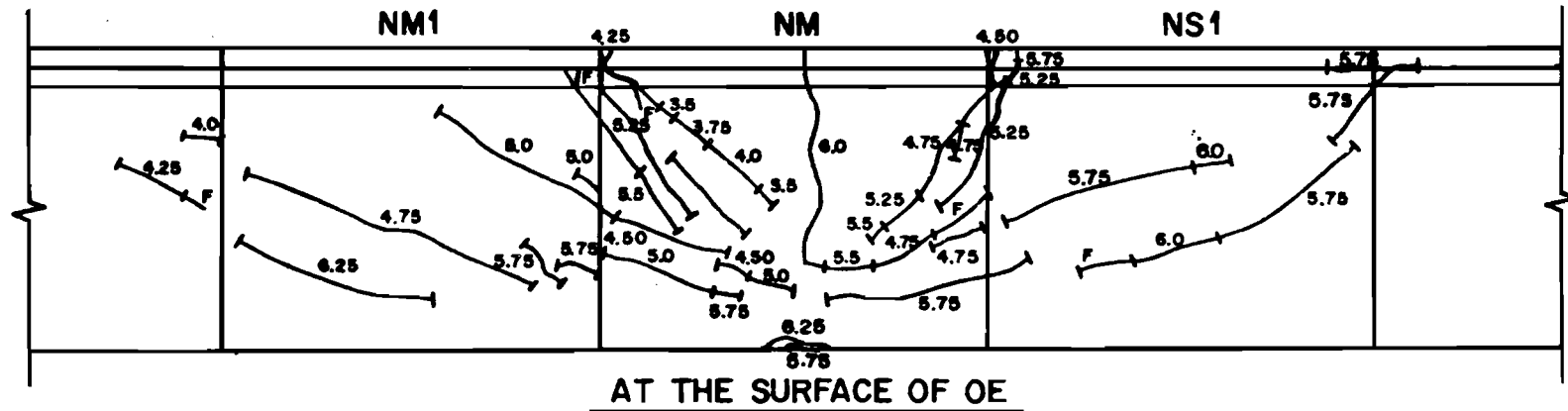


Fig. 8.34. Development of cracks around NM pier during loading to failure

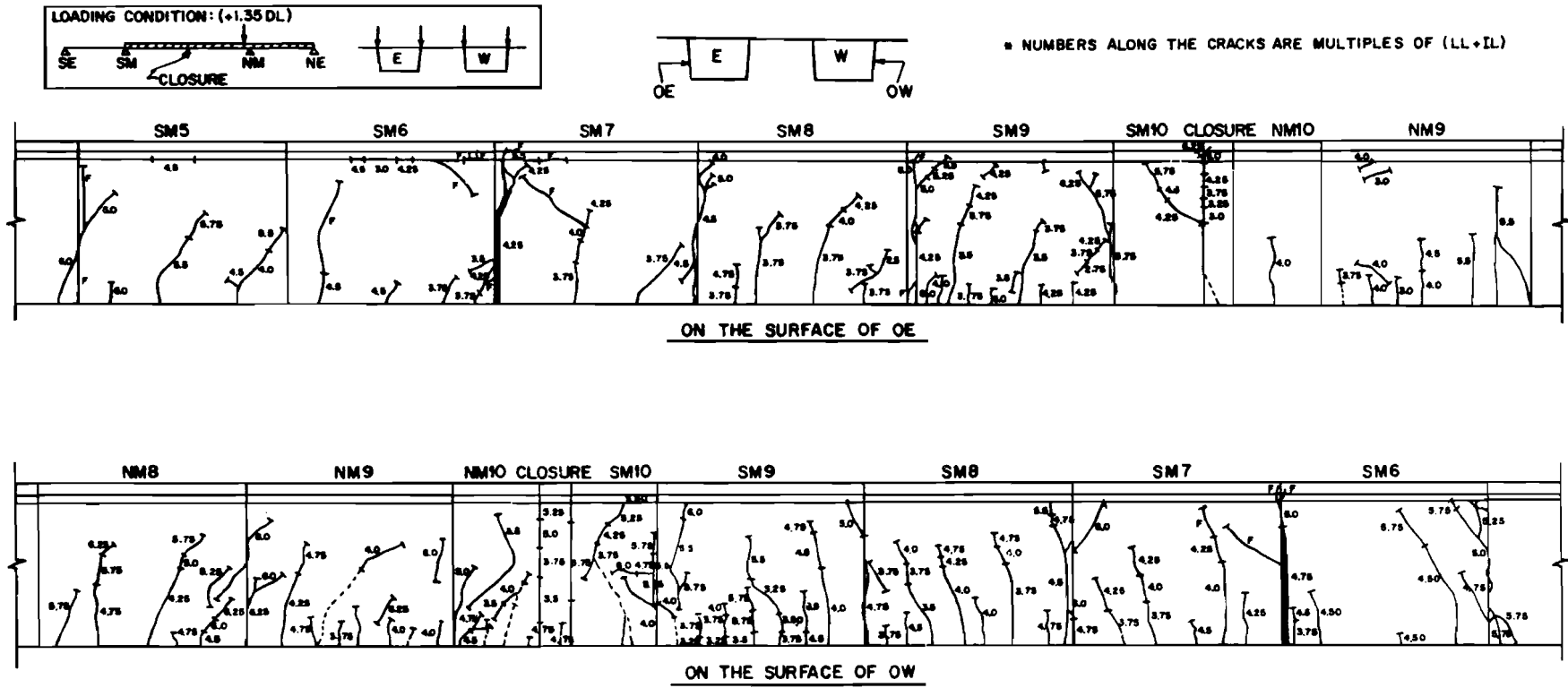


Fig. 8.35. Development of cracks around the center of main span during loading to failure

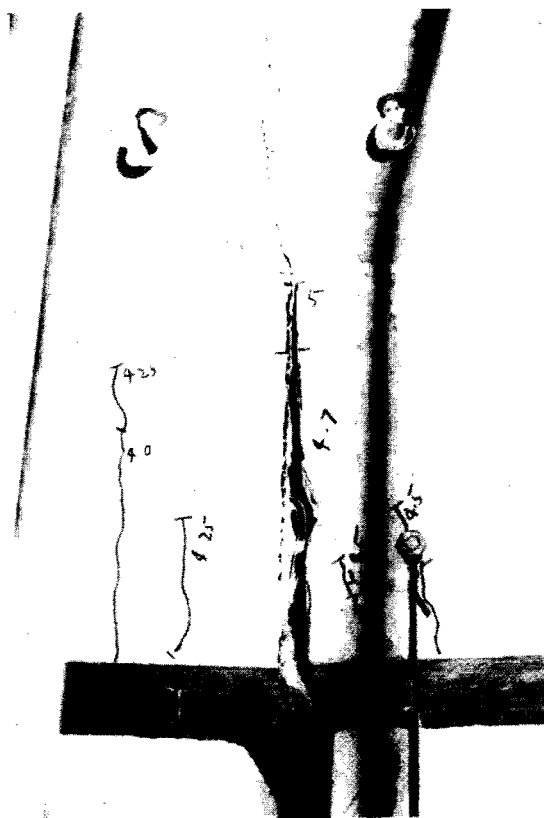


Fig. 8.36. Typical crack around the joint (after failure)

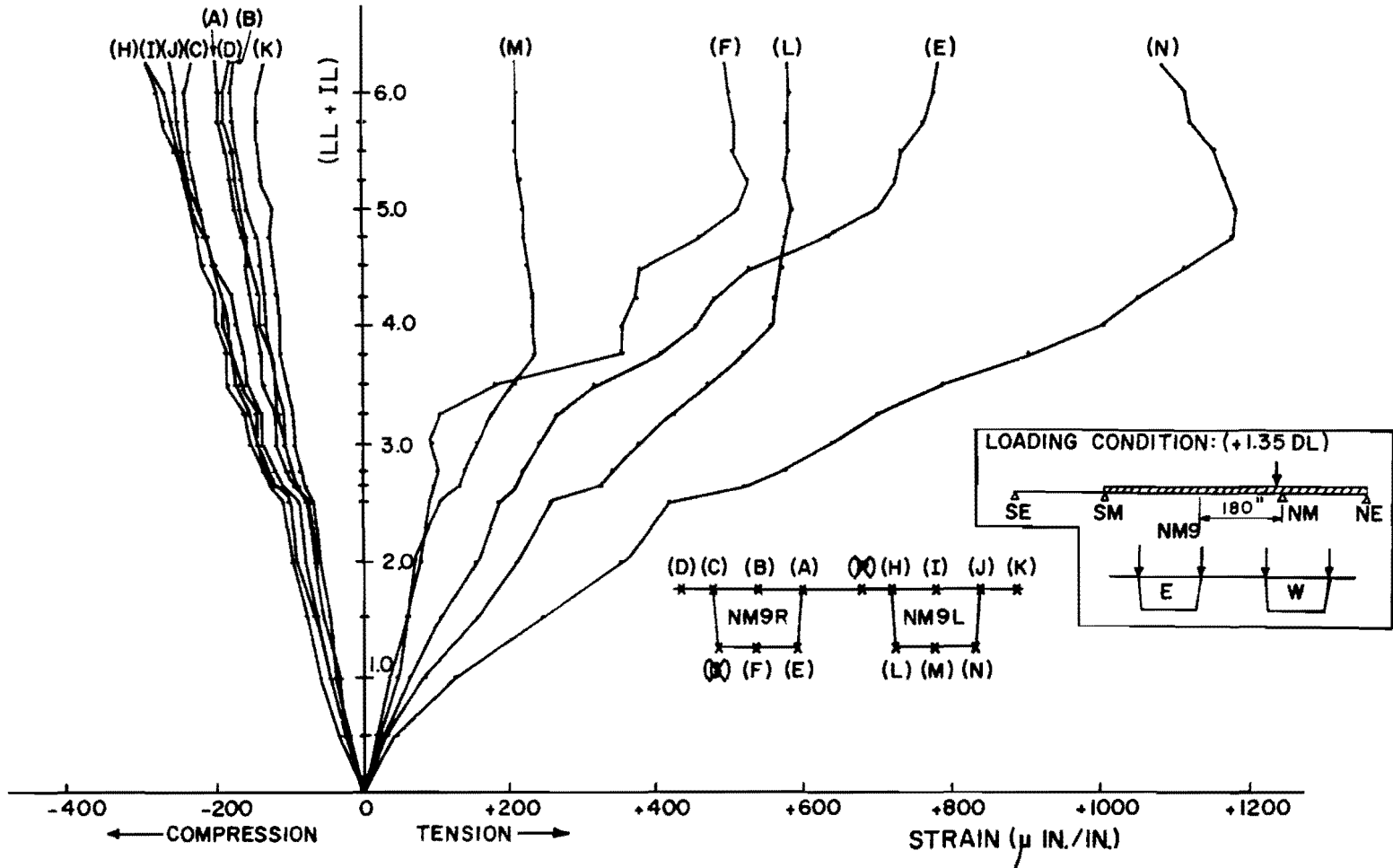


Fig. 8.37. Longitudinal strains at NM9 during loading to failure

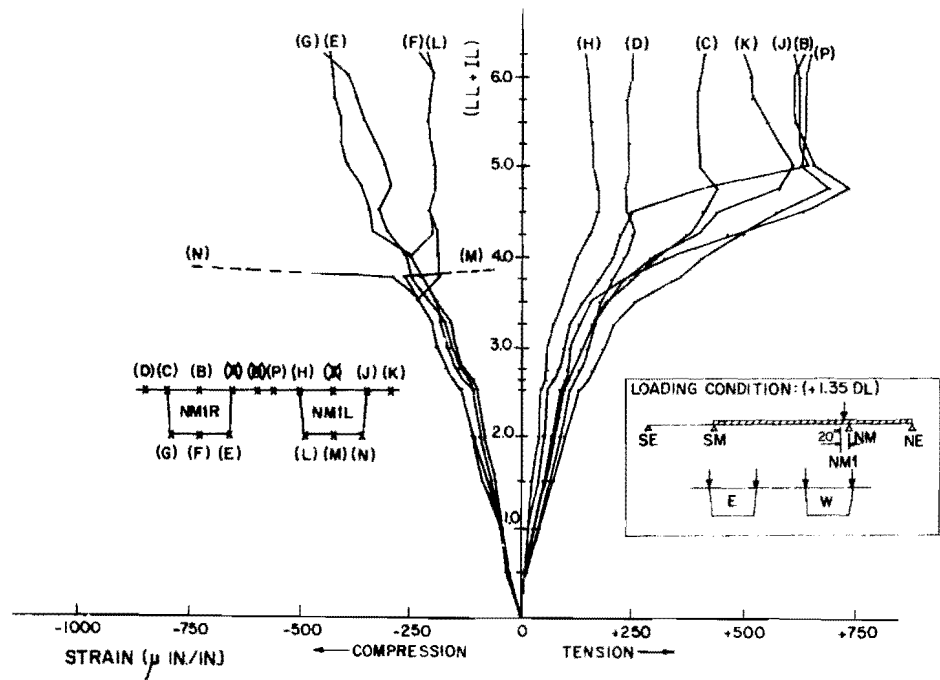


Fig. 8.38. Longitudinal strains at NMI during loading to failure

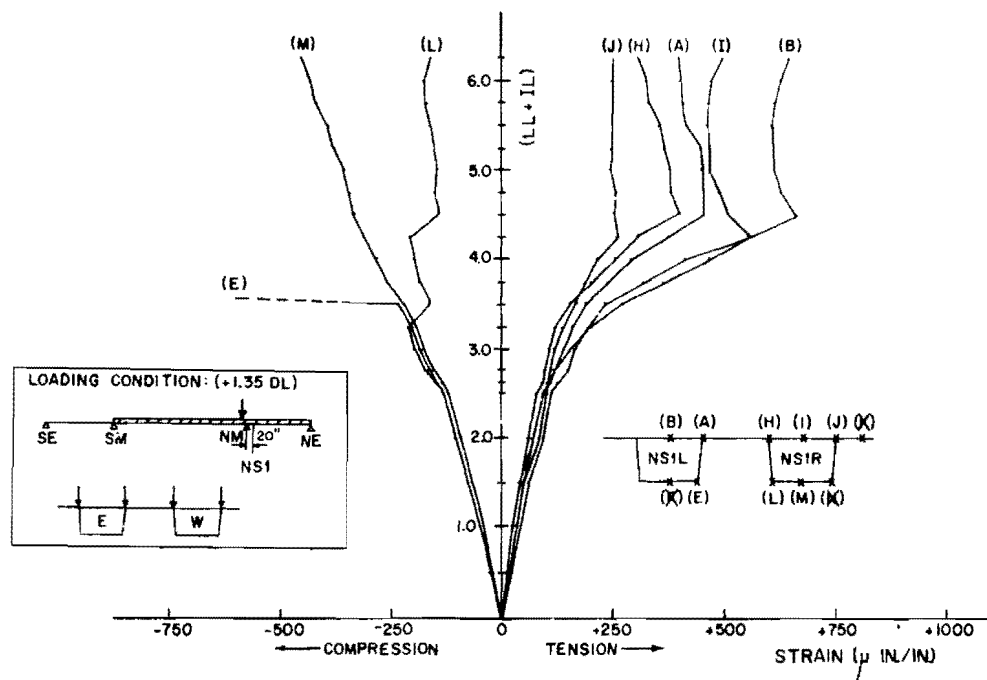


Fig. 8.39. Longitudinal strains at NS1 during loading to failure

At the 5.75(LL + IL) increment, the flexural cracks at the top slab near the NM pier extended the full width of the slab (two boxes). The flexural cracks at the SM6-7 and SM7-8 joints were getting wider, but the width of cracks in some other portions were small. At this stage, the bridge looked straight from the SE pier to the SM6-7 joint and all major deformation was concentrated at the SM6-7 joint. The NM pier segment on the neoprene pad support started to crush on the east side, due to the high compression force.

At the 6.0(LL + IL) increment, the width of the flexural crack at the SM6-7 joint was about 1/8 in. and the SE segment raised up about 4.5 in.

After taking the instrument readings at the 6.25(LL + IL) increment, the loads were being increased to the 6.50(LL + IL) increment when a sudden rupture of the positive moment prestressing cables occurred at joint SM6-7 on the west side. This failure occurred before applying less than half of the planned increment and the load dropped immediately after the failure. The load was then brought back to the 6.25(LL + IL) increment and rupture of the positive moment prestressing cables in the east side box occurred after a small increase in load. Figure 8.40 shows the general view of the failed bridge. Even after rupture of the positive moment cables, the bridge exhibited great toughness and continued to carry 1.35 DL as balanced cantilevers.

The strain at the various positions in the same cross section varied as the load increased, although the tendency of strain change was similar at each position. However, the increase of deflection at the same station in each cross section was uniform as the load increased. Figure 8.41 shows the deflection along the bridge during the failure loading test.

8.3.3 Determination of the Main Span Live Load Capacity

8.3.3.1 Flexure. One major difference between this bridge and the generally assumed three-span continuous bridge is the lack of upward vertical restraint as usually assumed for pin supports. The completed bridge rested on neoprene pads at all four piers with no hold-down

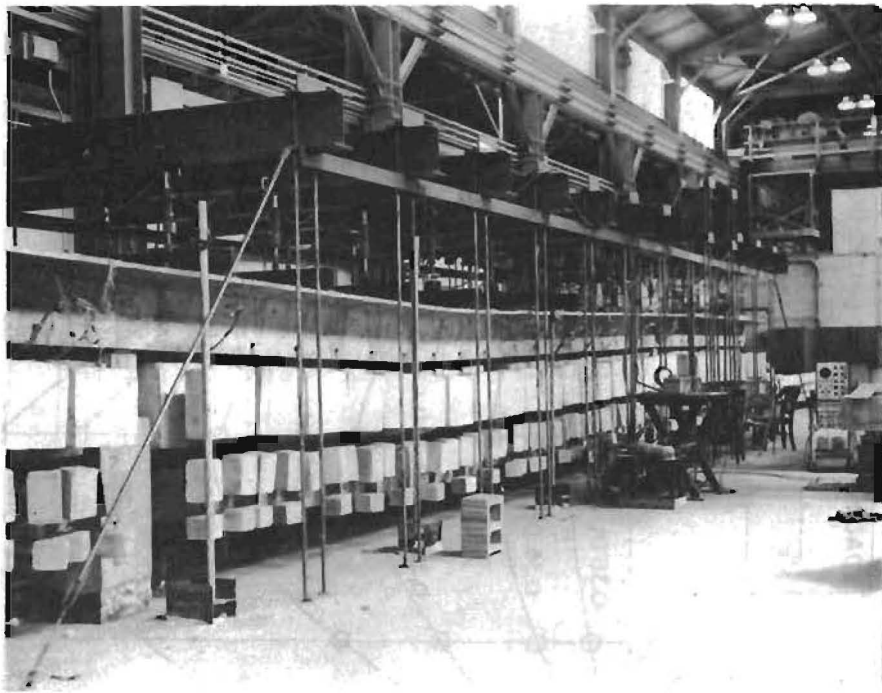


Fig. 8.40. General view of the bridge after failure

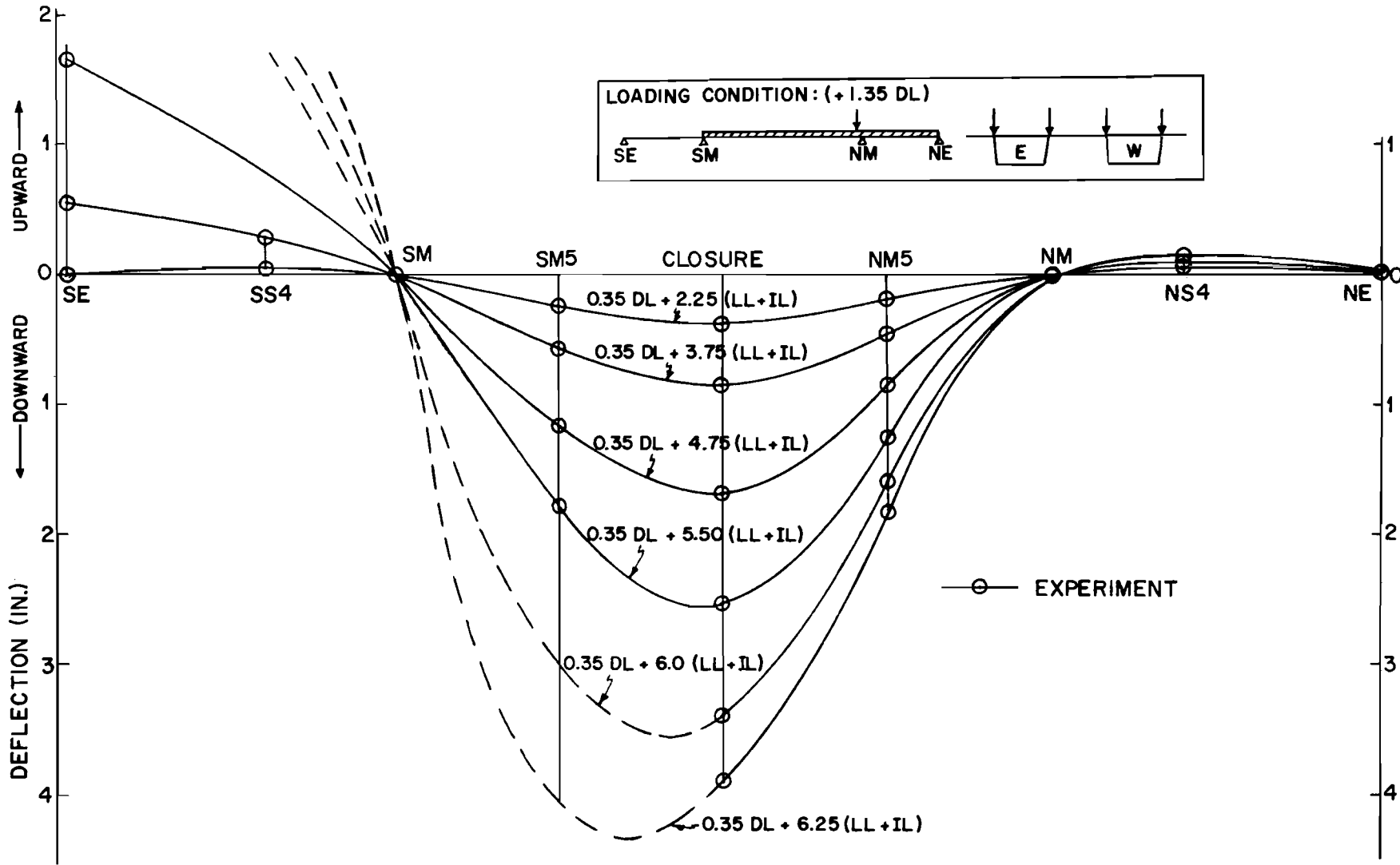


Fig. 8.41. Deflections along the bridge during loading to failure

devices. The bridge behavior would be that of a three-span continuous beam only if the tendency for uplift at the outer supports was restricted at higher loads. However, to match the prototype support conditions, no upward motion restrictions at the outer supports were added. Therefore, under high levels of loading in the center span, the bridge started to act as a two-span continuous beam with an overhang or a simple beam with two overhangs.

It is, therefore, necessary to calculate M_{UI} , M_{E1} , M_{E2} , M_{E3} , and M_{E4} for three different support conditions (M_{UI} and M_{E1} are the same for the three cases). The latter are calculated using the same procedure as explained in Sec. 8.2.3. Moment diagrams for M_{E2} , M_{E3} , and M_{E4} for the three different support conditions are shown in Figs. 8.42, 8.43, and 8.44.

By examining Fig. 8.44, it can be seen that the value of positive moment for 1.0(LL + IL) in the main span increased substantially in the critical region due to the change of structural configuration. Also, the shift in position of the maximum moment is clearly shown in Fig. 8.44. There is not much difference in moment between the two-span continuous beam with an overhang and the simple span beam with two overhangs for this loading case (Fig. 8.44).

In contrast, Fig. 8.43 indicates that the positive moment caused by the additional 0.35 DL is erased by the change of structural configuration from three continuous spans or two continuous spans with an overhang to a simple beam with overhangs. However, the negative moment around the NM pier increased.

The LF or level of (LL + IL) which would form the first plastic hinge for this loading was calculated for each type structure (Table 8.1). The first plastic hinge would form at the joint of the closure segment at an increment of [1.35 DL + 5.21(LL + IL)] if the structure was ideally supported by pins and there was no uplift possible at the end supports. However, it is not proper to calculate the LF for a three-span continuous beam since the SE support raised off its support pad at the

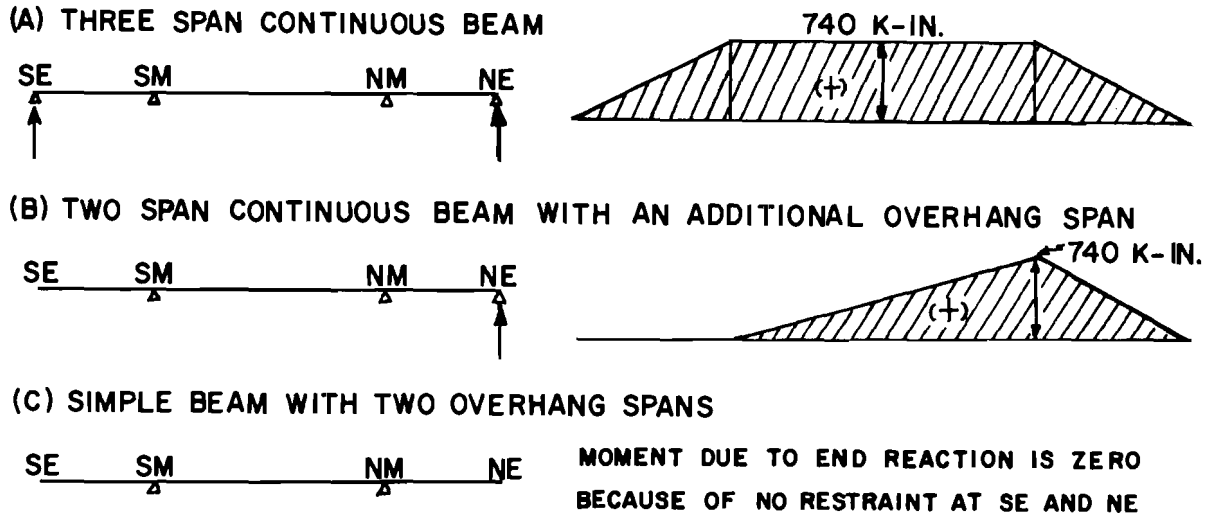


Fig. 8.42. Moment diagram due to resultant force of prestressing and jacking force at end supports (M_{E2})

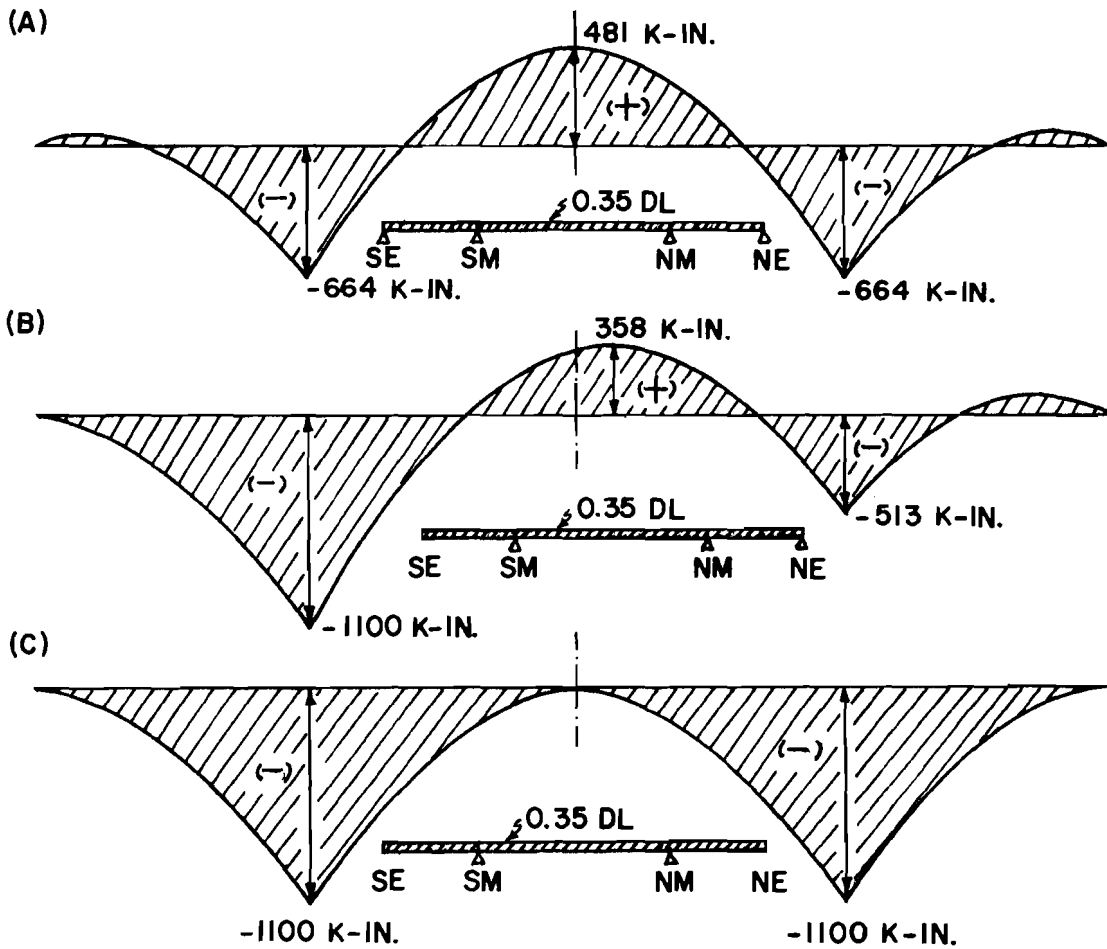


Fig. 8.43. Moment diagram for 0.35 DL for three different conditions (M_{E3})

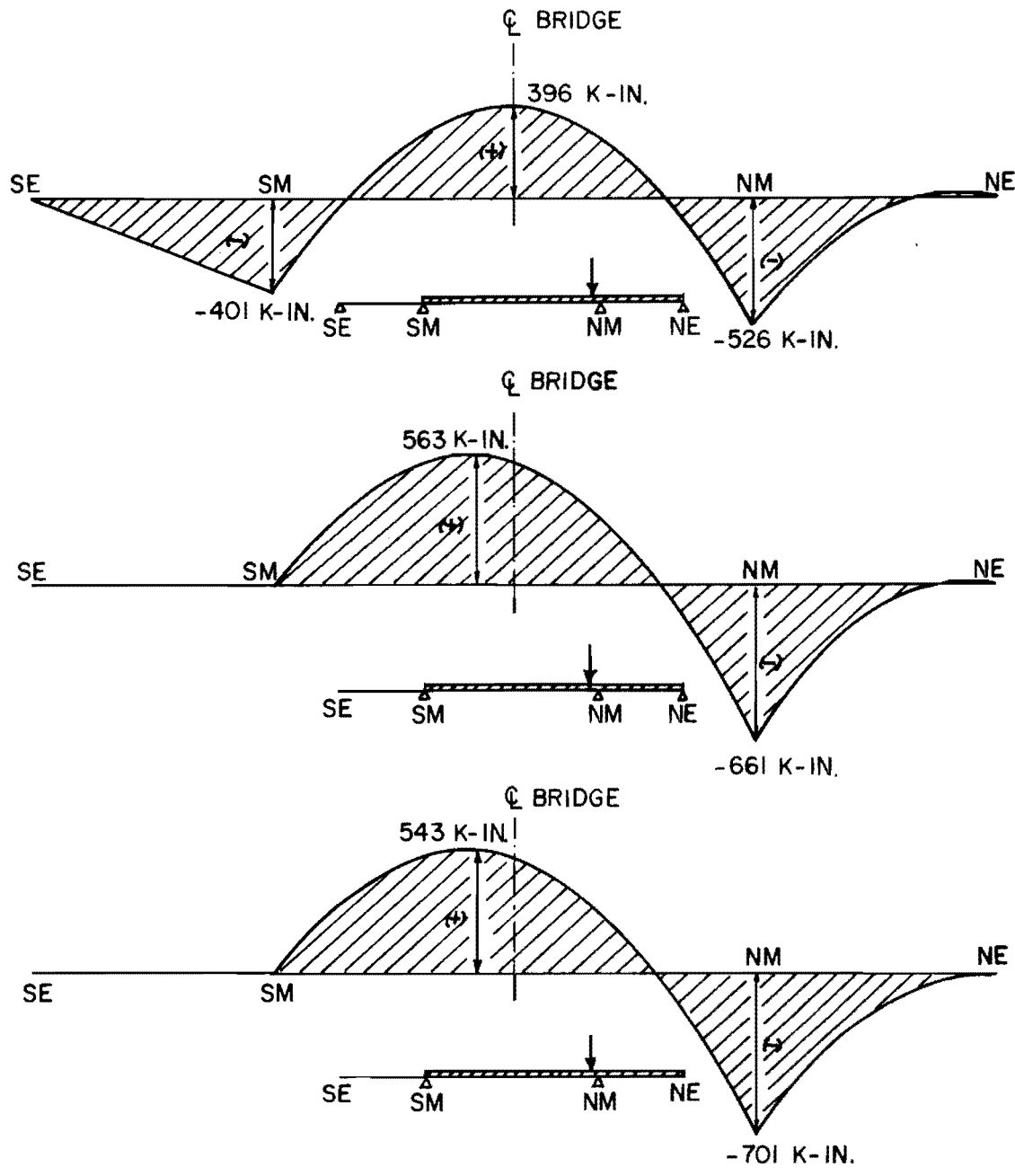
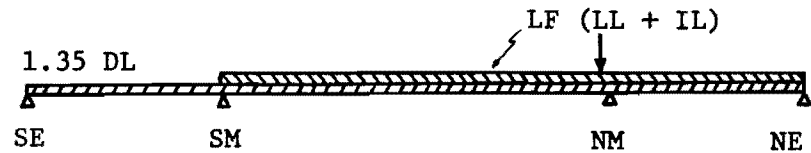


Fig. 8.44. Moment diagram for 1.0 (LL + IL) for three different conditions (M_{E4})

TABLE 8.1. LF OF (LL + IL) FOR THE FIRST PLASTIC HINGE AT EACH JOINT

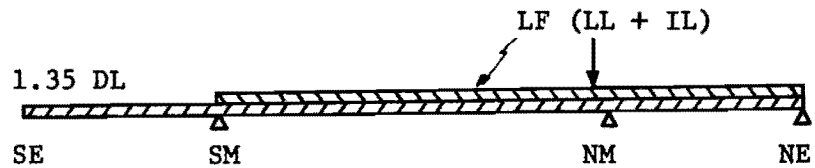
Case (1) 3 span continuous beam



| Joint | Ultimate Internal Moment M_{UI} (k-in.) | Moment due to 1.0 DL M_{E1} (k-in.) | Moment due to end support forces M_{E2} (k-in.) | Moment due to 0.35 DL M_{E3} | $\Sigma M = M_{UI} - M_{E1}$ $-M_{E2} - M_{E3}$ (k-in.) | Moment due to 1.0 (LL + IL) M_{E4} (k-in.) | LF of (LL + IL) $\frac{\Sigma M}{M_{E4}}$ |
|-----------|---|---|---|--------------------------------------|---|---|---|
| SM 5 - 6 | 2342 | -603 | 740 | 255 | 1950 | 245 | 7.96 |
| 6 - 7 | 2873 | -361 | 740 | 346 | 2148 | 318 | 6.75 |
| 7 - 8 | 3395 | -181 | 740 | 415 | 2421 | 354 | 6.84 |
| 8 - 9 | 3558 | - 62 | 740 | 458 | 2422 | 390 | 6.21 |
| 9 - 10 | 3558 | - 6 | 740 | 479 | 2345 | 398 | 5.89 |
| closure | 3285 | 0 | 740 | 481 | 2064 | 396 | 5.21 |
| NM 10 - 9 | 3558 | - 6 | 740 | 479 | 2345 | 394 | 5.95 |
| 9 - 8 | 3558 | - 62 | 740 | 458 | 2422 | 378 | 6.41 |
| 8 - 7 | 3395 | -181 | 740 | 415 | 2421 | 333 | 7.27 |
| 7 - 6 | 2873 | -361 | 740 | 346 | 2148 | 289 | 7.43 |
| 6 - 5 | 2342 | -603 | 740 | 255 | 1950 | 208 | 9.38 |

TABLE 8.1 (Continued)

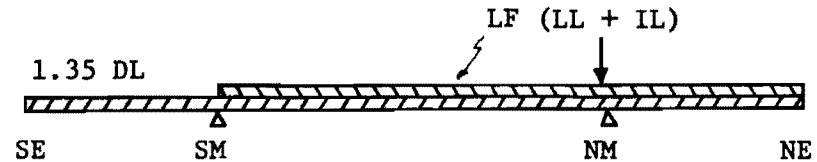
Case (2) 2 span continuous beam with an overhang



| Joint | Ultimate Internal Moment M_{UI} (k-in.) | Moment due to 1.0 DL M_{E1} (k-in.) | Moment due to end support forces M_{E2} (k-in.) | Moment due to 0.35 DL M_{E3} | $\Sigma M = M_{UI} - M_{E1} - M_{E2} - M_{E3}$ (k-in.) | Moment due to 1.0 (LL + IL) M_{E4} (k-in.) | LF of (LL+IL) $\frac{\Sigma M}{M_{E4}}$ |
|-----------|---|---------------------------------------|---|--------------------------------|--|--|---|
| SM 5 - 6 | 2342 | -603 | 204 | - 22 | 2763 | 498 | 5.55 |
| 6 - 7 | 2873 | -361 | 241 | 99 | 2894 | 544 | 5.32 |
| 7 - 8 | 3395 | -181 | 278 | 196 | 3102 | 554 | 5.60 |
| 8 - 9 | 3558 | - 62 | 315 | 270 | 3035 | 563 | 5.39 |
| 9 - 10 | 3558 | - 6 | 352 | 320 | 2892 | 544 | 5.32 |
| closure | 3285 | 0 | 370 | 337 | 2578 | 529 | 4.87 |
| NM 10 - 9 | 3558 | - 6 | 389 | 350 | 2825 | 513 | 5.51 |
| 9 - 8 | 3558 | - 62 | 426 | 358 | 2836 | 470 | 6.03 |
| 8 - 7 | 3395 | -181 | 463 | 344 | 2769 | 399 | 6.94 |
| 7 - 6 | 2873 | -361 | 500 | 307 | 2427 | 328 | 7.40 |
| 6 - 5 | 2342 | -603 | 537 | 245 | 2163 | 220 | 9.83 |

TABLE 8.1 (Continued)

Case (3) Simple beam with overhangs



| Joint | Ultimate Internal Moment M_{UI} (k-in.) | Moment due to 1.0 DL M_{E1} (k-in.) | Moment due to end support forces M_{E2} (k-in.) | Moment due to 0.35 DL M_{E3} | $\Sigma M = M_{UI} - M_{E1} - M_{E2} - M_{E3}$ (k-in.) | Moment due to 1.0 (LL + IL) M_{E4} (k-in.) | LF of (LL + IL) $\frac{\Sigma M}{M_{E4}}$ |
|-----------|---|---------------------------------------|---|--------------------------------|--|--|---|
| SM 5 - 6 | 2342 | -603 | 0 | -207 | 3152 | 485 | 6.50 |
| 6 - 7 | 2873 | -361 | 0 | -120 | 3354 | 530 | 6.33 |
| 7 - 8 | 3395 | -181 | 0 | - 57 | 3633 | 536 | 6.78 |
| 8 - 9 | 3558 | - 62 | 0 | - 16 | 3636 | 543 | 6.70 |
| 9 - 10 | 3558 | - 6 | 0 | 0 | 3564 | 523 | 6.81 |
| closure | 3285 | 0 | 0 | 0 | 3285 | 507 | 6.48 |
| NM 10 - 9 | 3558 | - 6 | 0 | 0 | 3564 | 487 | 7.32 |
| 9 - 8 | 3558 | - 62 | 0 | - 16 | 3636 | 445 | 8.17 |
| 8 - 7 | 3395 | -181 | 0 | - 57 | 3633 | 372 | 9.77 |
| 7 - 6 | 2873 | -361 | 0 | -120 | 3354 | 295 | 11.4 |
| 6 - 5 | 2342 | -603 | 0 | -207 | 3152 | 188 | 16.8 |

[1.35 DL + 2.63(LL + IL)] increment. Since the south end support raised completely from the neoprene pad supports, all forces applied at the time of construction (such as end reaction due to positive tendon prestressing in the main span or the jacking force at the end supports to adjust the reaction) were erased and the structure became a two-span continuous beam with an overhang. If the structure were an ideal two-span continuous beam with an overhang, the reaction at the NE support would have to increase as the load increased. But the reaction at the NE support decreased after the [1.35 DL + 2.25(LL + IL)] increment due to the appearance of cracks and concentration of deformation around the center of the main span. Observations indicated that a plastic hinge was not formed at the closure segment at [1.35 DL + 2.25(LL + IL)] as would be indicated by Table 8.1(2) for a two-span continuous beam with an overhang. Since the calculation for case (3) in Table 8.1 indicated that the minimum LF of 6.33(LL + IL) for the first plastic hinge was at the SM6-7 joint for a simple beam with overhangs, it will be proper to calculate the LF of (LL + IL) for that case and then take into account the reaction left at the NE support. If the structure is an ideal simple beam with overhangs, the first plastic hinge would form at the 6.33(LL + IL) increment. The effect of the reaction left at the NE support was small and 5.88(LL + IL) is the calculated increment to form the first plastic hinge when taking into account the end reaction at the NE support. This value agreed well with the 6.25(LL + IL) experimental value. If the AASHTO allowance for load reduction on a four lane bridge was considered, the bridge would withstand [1.35 DL + 8.33(LL + IL)] in this load configuration.

All section properties used to calculate LF of (LL + IL) in Table 8.1 were based on the measured values.

After demolishing the bridge, the joints where failure occurred were carefully examined and it was found that the five positive tendons in each web were completely broken through.

Although the side span positive tendons were adequately proportioned by the design procedure which assumed ideal three-span continuous beam action. The positive moment reserve was reduced in the main span because the design did not consider the upward unrestrained end support

condition. Therefore, it is also necessary to check the LF for the loading condition which would produce maximum moment at the center of the main span, as shown in Fig. 8.45. In the loading case of Fig. 8.45 it is certain that the end supports (SE and NE) would raise up at failure (because the supports raised up in the previous test in Sec. 7.3.3.2). The structure at failure will be a simply supported beam with overhangs and the calculated LF is $[1.35 \text{ DL} + 3.13(\text{LL} + \text{IL})]$, as shown in the following calculation:

$$M_{E4} \text{ at } 1.0(\text{LL} + \text{IL}) = 1051 \text{ k-in.}$$

$$\Sigma M = M_{UI} - (M_{E1} + M_{E2} + M_{E3}) = 3285 \text{ [case (3) in Table 8.1]}$$

$$\text{LF of } (\text{LL} + \text{IL}) = 3285/1051 = 3.13$$

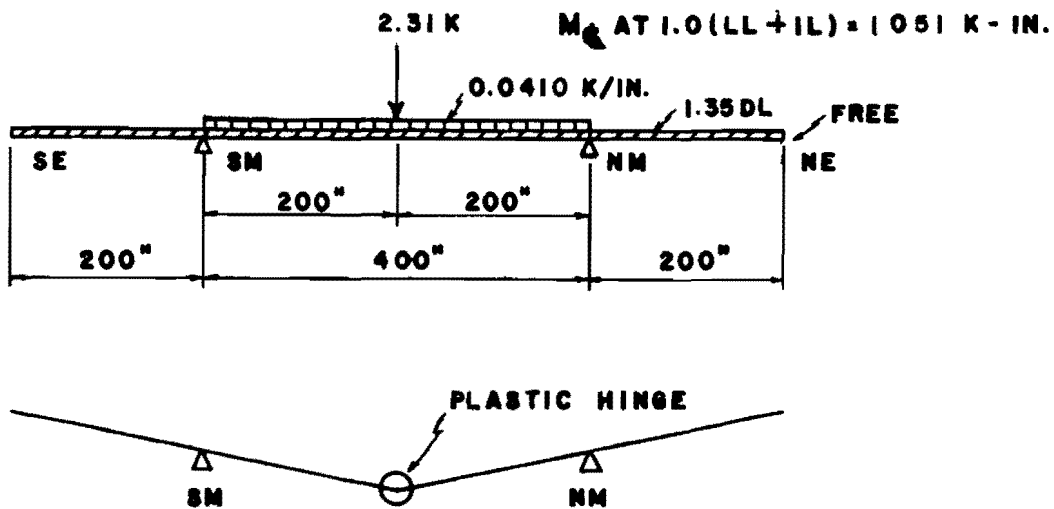


Fig. 8.45. Failure loading at the center of the main span

Therefore, the support condition does not unduly affect the safety of the bridge, although the main span maximum positive moment flexural capacity is reduced to $[1.35 \text{ DL} + 3.13(\text{LL} + \text{IL})]$ if the AASHTO load reduction for multiple lanes is ignored. This would be $[1.35 \text{ DL} + 4.17(\text{LL} + \text{IL})]$ if the normal design specifications are used for a four lane bridge. While

this load case was not tested to failure, the good agreement of other flexural test results and calculations indicated that this value would undoubtedly have been attained.

In order to match the test loading conditions, the model's external dead load moment was computed with 1.0 DL acting on a balanced cantilever and 0.35 DL acting on the completed continuous structure. It has been shown that because of the construction sequence it is not logical to base the analysis of the completed structure on fully continuous beam dead load moments for 1.35 DL. A more rational load factor procedure for computation of the ultimate design moments in the completed structure should consider possible uncertainty in the dead load at various stages of construction. Based on experience in this program, the following factors are suggested for analysis of the completed structure to check the negative moment and shear capacity:

Load factors are chosen to conform to the BPR general load factor philosophy

$$U = 1.35 DL + 2.25(LL + IL)$$

For a segmental bridge erected in cantilever, during the construction phase $M_u \geq M_{u1}$ based on

$$U_1 = 1.35 DL_1 + 2.25(LL_1 + IL_1) \text{ to be computed for a balanced cantilever}$$

Also, upon completion $M_u \geq M_{u2} + M_{u3}$, where

$$U_2 = 1.35 DL_1 \text{ to be computed for a balanced cantilever}$$

$$U_3 = 1.35 DL_3 + 2.25(LL_3 + IL_3) + SL \text{ to be computed for the completed continuous structure}$$

where DL_1 = dead load during cantilevering

DL_3 = dead load applied after completion of closure (topping, railing, etc.)

LL_1 = live load due to construction operations

LL_3 = design live load

IL_1 = impact load of construction operations

IL_3 = design impact load

SL = resultant reactions due to prestressing of tendons and seating forces at outer supports

Negative tendons can be designed by WSD or USD to balance the dead load of segments and the weight of construction equipment on the segments during the balanced cantilever stages. However, the ultimate negative moment capacity of the cantilever structure should be checked for U_1 . The ultimate negative moment capacity of the completed structure should be checked for $U = U_2 + U_3$.

In determining positive moment tendons it will be unconservative to use $U_2 = 1.35 DL_1$. A highly conservative approach would be to use $U_2 = 0.90 DL_1$ computed for the balanced cantilever and the preceding equations.

8.3.3.2 Shear. Initial formation of shear cracking is practically independent of the amount of web reinforcement,²⁶ so this design appears to have an adequate safety factor for shear without undue reliance on shear reinforcement, since the initial diagonal tension crack appeared at the $[1.35 DL + 3.25(LL + IL)]$ increment. This exceeds the specified design ultimate load.

Observation of cracks around the main pier showed there was no shear weakness due to the epoxy joint. The flexural cracks which formed on the top slab at the first joint in the main span did not extend straight along the joint and these flexural cracks connected to the diagonal tension cracks in the web. Cracking was frequent along the webs and the extremely well-distributed crack patterns of Figs. 8.34 and 8.35 indicate that both the epoxy joints and the grouting worked well.

The truss analogy is widely accepted as a simple and safe design procedure for shear. Shear reinforcement at ultimate strength can be checked by ignoring the effect of the concrete, but a portion of the shear is carried by concrete at the ultimate.²⁶ The ACI Code² specifies that shear reinforcement should be not less than $A_v = (V_u - \phi V_c) / (\phi f_y)$. The ACI Code also specifies another equation for shear reinforcement (not less than $A_v = (A_p/80) \times (f'_s/f_y) \times (s/d) \times \sqrt{d/b'}$).

It is suggested by Lin²⁶ that the critical section for shear computation be taken at a distance d ($= 15.4$ in.) away from the theoretical point of maximum shear. However, the critical section for shear was considered to be at the first joint from the pier in this bridge because the flexural cracks occurred at the top slab of the first joint and

extended into the diagonal tension cracks. Many of the diagonal tension cracks appeared around the first joint in the main span. The LF of (LL + IL) for shear capacity was calculated by using the prestressed concrete equations in the 1963 ACI Code.² Since the bridge at failure was a simply supported beam with overhangs, shear and moment due to dead and live load were calculated for a simple beam with overhangs, as follows:

(a) Shear capacity carried by concrete and web shear reinforcement
Shear carried by concrete:

$$\begin{aligned} V_{ci} &= 0.6b'd\sqrt{f'_c} + \frac{M_{cr}}{M/V - d/2} + V_d \\ &= 0.6 \times 8.81 \times 15.4 \times 0.0842 + 1490/36.0 + (10.9 + 28.6) \\ &= 6.85 + 41.4 + 39.5 = 87.75 \text{ kips} \end{aligned}$$

where $b' = 8.81$

$$d = 15.4$$

$$\sqrt{f'_c} = \sqrt{7090}/1000 = 84.2/1000 = 0.0842 \text{ ksi}$$

$$\begin{aligned} f_{pe} &= -P/A - M/W_T = -338/(2 \times 179) - \frac{338 \times 6.20}{2 \times 1020} \\ &= -0.944 - 1.027 = -1.971 \text{ ksi} \end{aligned}$$

$$\begin{aligned} f_d \text{ (= due to 1.35 DL)} &= M/W_T \\ &= 2630/2040 + 990/2090 \\ &= 1.29 + 0.474 = 1.764 \text{ ksi} \end{aligned}$$

$$\begin{aligned} M_{cr} &= \frac{I}{y} (6\sqrt{f'_c} + f_{pe} - f_d) \\ &= 2090(6 \times 0.0842 + 1.97 - 1.76) \\ &= 1494 \text{ k-in.} \end{aligned}$$

$$\begin{aligned} M/V - \frac{d}{2} &= 572/13.1 - 15.4/2 \\ &= 43.7 - 7.7 = 36.0 \end{aligned}$$

$$\begin{aligned} V_d \text{ (due to 1.35 DL)} &= 10.9 + 28.6 \\ &= 39.5 \text{ kips} \end{aligned}$$

$$\begin{aligned} V_{cw} &= b'd(3.5\sqrt{f'_c} + 0.3f_{pc}) + V_p \\ &= 8.81 \times 15.4(3.5 \times 0.0842 + 0.3 \times 0.944) + 0 \\ &= 78.5 \text{ kips} \end{aligned}$$

where $b' = 8.81 \text{ in.}$

$$d = 15.4$$

$$\sqrt{f'_c} = 0.0842 \text{ ksi}$$

$$f_{pc} = 0.944 \text{ ksi}$$

$$V_p = 0 \text{ kip}$$

Therefore,

$$V = 78.5 \text{ kips (= } V \text{)}$$

Shear carried by the shear reinforcement:

$$V_s = A_v d f_y / s$$

$$= 0.165 \times 15.4 \times 70 / 2.5 = 71.1 \text{ kips}$$

where $A_v = 0.0206 \times 8 = 0.1648 \text{ in.}^2$

$$f_y = 70 \text{ ksi}$$

$$d = 15.4 \text{ in.}$$

$$s = 2.5 \text{ in.}$$

Total shear carried by concrete and shear reinforcement:

$$V_u = \phi(V_c + V_s) = 1.0(78.5 + 71.1) = 149.6 \text{ kips}$$

(b) Shear due to dead and live load

$$V_u = 1.35(\text{DL shear}) + \text{LF}(\text{LL} + \text{IL shear})$$

$$= 39.5 + \text{LF} \times 13.1$$

(c) LF of (LL + IL) for shear capacity at the first joint in the main span

$$\text{LF of (LL + IL)} = (150 - 39.5) / 13.1 = 8.44$$

(d) Shear developed in test at flexural failure

$$V_u = 1.35(\text{DL shear}) + 6.25(\text{LL} + \text{IL shear}) = 121.4 \text{ kips}$$

Therefore, the shear capacity was not critical at the time of flexural failure. The test developed 81 percent of the calculated shear capacity prior to the flexural failure, and indicates successful jointing.

As explained in Sec. 7.2.1.2, simulation for shear was not as accurate as that for bending moment. The LF of (LL + IL) for the ideal loading condition would be slightly higher than the value obtained in the model test.

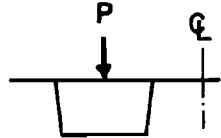
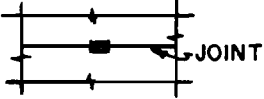
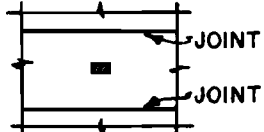
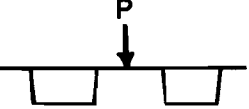
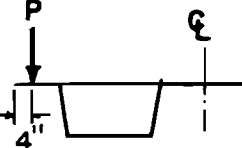
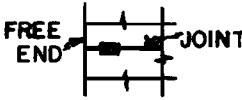
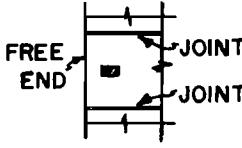
8.4 Punching Shear Tests

After failure of the bridge in the longitudinal tests, a series of punching shear tests were performed by using a rear wheel (HS20) loading pad in the north side span which did not get any appreciable damage. Since the positive tendons in the main span were broken and wide flexural cracks appeared around the main pier segments in the overall failure test, no estimate of the amount of residual compressive stress in

the top slab is possible. Compressive stress of 150 to 250 psi would exist in the longitudinal direction in the top slab where punching shear tests were performed, if the grouting were still effective. Ultimate two-way shear stress V_{u2} was assumed as $4\sqrt{f'_c}$ for the calculations, as used in reinforced concrete. If longitudinal compressive stress in the top slab is taken into account, the principal stresses will increase 25 to 45 percent.

Most of the experimental values of punching shear were approximately twice the ACI value in the normal punching shear test [case (A) in Table 8.2]. Even if the increase in shear stress due to the longitudinal compressive stress is considered it appears that the value of the ultimate shear stress as specified by the 1963 ACI Code is extremely conservative. Punching shear tests on the cantilever overhangs of case (B) in Table 8.2 were an abnormal condition, since wheel loads would not be able to be applied this close to the edge in the prototype. Several flexural cracks appeared at 60 to 70 percent of the punching shear load and ringed the loading pad. Shear failure still occurred in a small area around the loading pad. Even under this abnormal condition, failure loads were more than eight times that of a service load level rear wheel (HS20), and 20 to 30 percent more conservative than the Code values. Thus, the bridge should have no problem with punching shear. Punching tests across the joints show there was no weakness of the epoxy joints under punching shear in the top slab.

TABLE 8.2. PUNCHING SHEAR TEST RESULTS

| CASE | TRANSVERSE POSITION OF LOADING | LONGITUDINAL POSITION OF LOADING | ULTIMATE LOAD (KIPS) | AVERAGE ULT. LOAD AND $\bar{\xi}$ (KIPS) | L.F. OF (LL+IL) = L.F. OF 1.3 LL | CALCULA. BY EQUA. IN ACI (KIPS) |
|------|---|---|----------------------|--|----------------------------------|------------------------------------|
| A |  |  | 9.81 | 10.3 ($\bar{\xi} = 0.9$) | 17.8 | 5.09 |
| | | | 11.8 | | | |
| | |  | 9.30 | | | |
| |  | 10.3 | | | | |
| |  |  | 10.9 | | | |
| B |  |  | 5.63 | 5.12 ($\bar{\xi} = 0.37$) | 8.85 | 4.11* * ASSUME ONE FACE IS OPEN |
| | | | 4.76 | | | |
| | |  | 4.97 | | | |

CHAPTER 9

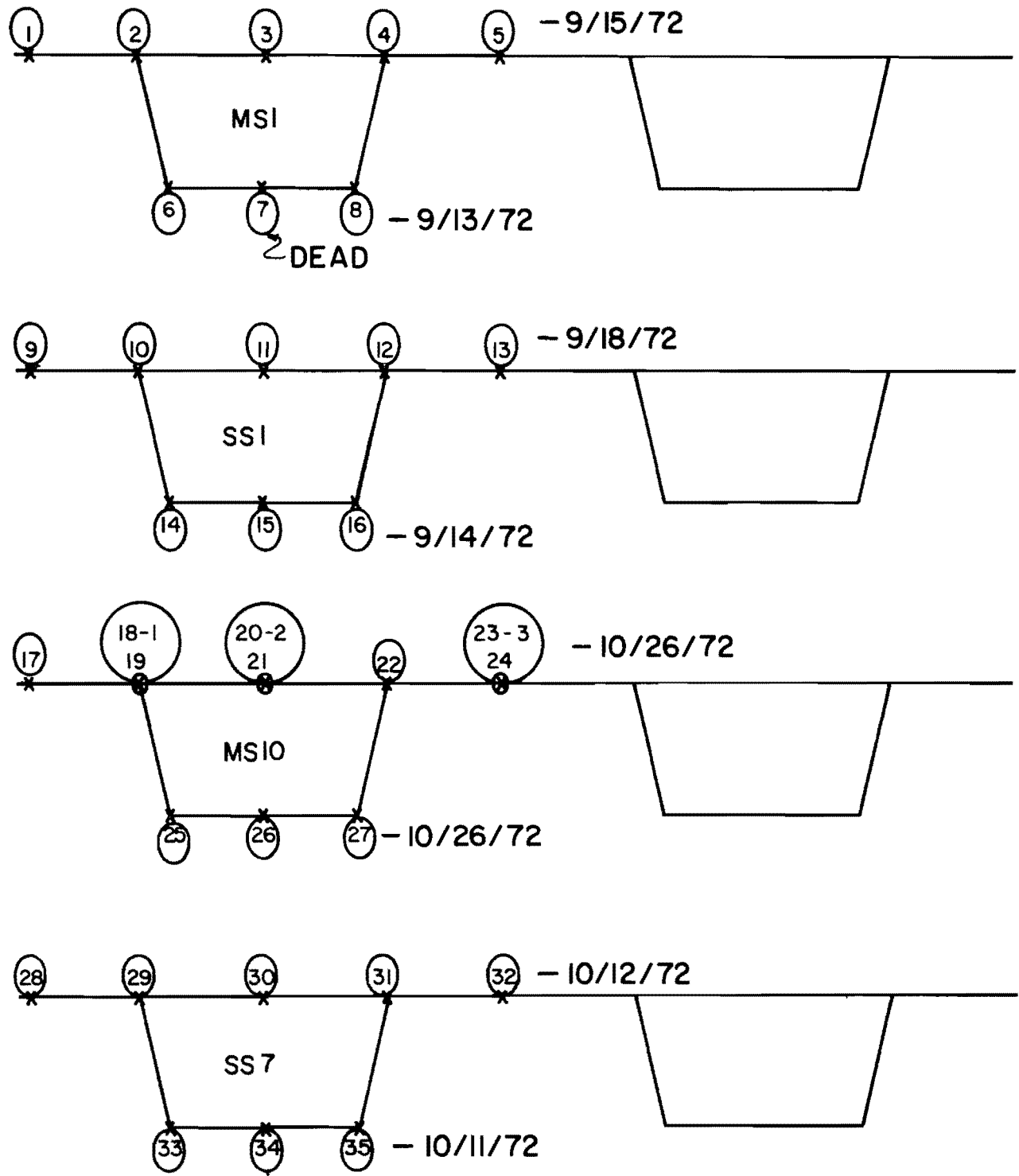
SPECIAL MEASUREMENTS

9.1 General

The unique nature of this type of construction and the extreme efforts to maintain close similitude between the model construction and loadings and that to be expected in the prototype structure at Corpus Christi presented an opportunity for comparison between laboratory and field measurements. A modest program of field measurements was undertaken on the prototype structure to obtain information similar to that found in the model. Measurements were limited to strains in a few segments at the time of construction operations and during a load test using maximum weight limit truck vehicles upon completion of the bridge. A brief summary of the results of these tests is included in this chapter, along with the report of a special model test undertaken to verify the shear capacity of the segments as part of a study of the effect of minor anchorage cracking in the webs. This latter study was undertaken as a result of minor cracking which occurred in the prototype structure during stressing and was not related to the main model tests described in the earlier chapters.

9.2 Prototype Instrumentation

Four segments were chosen for a limited field instrumentation program. Figure 9.1 indicates the location of strain gage stations. Two of the segments chosen were immediately adjacent to a main pier unit, one segment was at the third point of a side span, and the other segment was near the midpoint of the main span. Sixteen inch lengths of #3 deformed reinforcing bars were instrumented with strain gages at the Balcones Research Center Laboratories. These bars were used as a form of extensometer and were buried in the flanges of the segments, being wired to



x -- LONGITUDINAL STRAIN GAGE
 O -- TRANSVERSE STRAIN GAGE

Fig. 9.1. Location of strain gages in prototype bridge

reinforcing bars in the assembled cages in the forms in the precast yard. Lead wires were run to junction boxes, which were cast into the curb units of the segments. All cages were thoroughly waterproofed and protected from concrete placement and vibration hazards. The gaging followed the same general pattern as described for the model tests.

At the time of erection of a segment, the gages were connected to a strain indicator and measurements were made of the strains during placement. Results on similar gages were averaged, as in the data reduction in the model tests. The general strain instrumentation program was successful, with over thirty of the gages giving readings during various construction stages.

9.3 Measurements during Construction

9.3.1 Strains during Balanced Cantilever Construction. Figure 9.2 shows the strains measured in the M1 and S1 segments immediately adjacent to the main pier segment during two stages of the balanced cantilever construction. For comparison the values of strains measured in the model at the same stages of construction are shown, as well as the strains predicted for the model by beam theory. These predicted strains should be of the same general magnitude for the prototype construction, since the only difference in the method of calculation would be a slight variation in modulus of elasticity between the model and the prototype concrete. The prototype concrete would have a 5 to 10 percent higher value of modulus of elasticity, which would result in a reduction of 5 to 10 percent in the magnitude of the calculated strains using beam theory for a given loading condition.

Values of measured strain are shown both at the time of erection of the M1 and S1 segments and at the time of erection of the M7 and S7 segments. Strains measured in the prototype at time of erection of M1 and S1 show significantly less scatter in the top flange. This is undoubtedly due to the much greater distance of the strain gage from the anchorage. The compressive stresses noted are only approximately half the magnitude of those found in the model, while slightly higher tension was noted in the prototype lower flange than in the model. The existence of this tension confirmed the

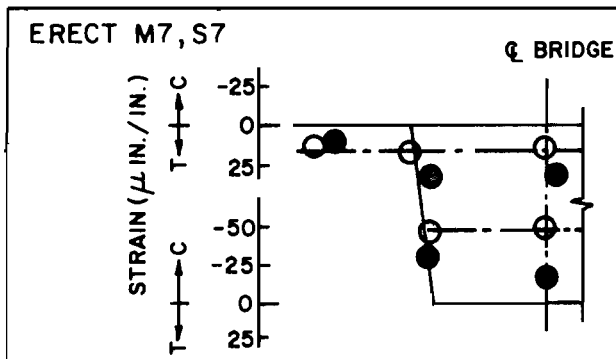
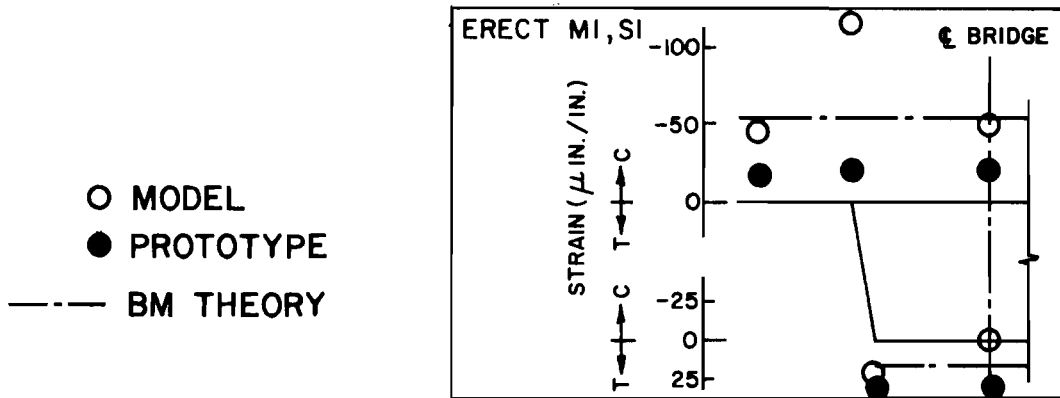
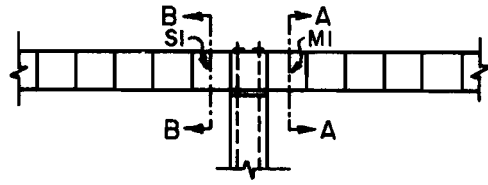


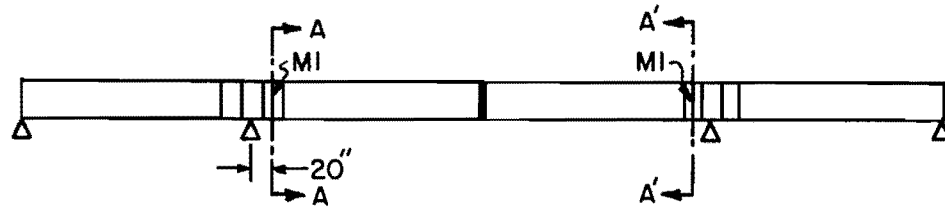
Fig. 9.2. Measured strain in M1 and S1 segments during several stages of balanced cantilever construction

tendency of the lower flange to open under initial erection stresses. The inability of the fresh epoxy joint to resist such tensile stresses was compensated for by provision of temporary stress across the joints.

Strains measured in the prototype adjacent to the piers at time of erection of the 7th segments indicate substantially less compressive stress at the piers and suggest substantial friction losses in the prototype construction. On numerous occasions, difficulty was encountered in stressing cables in the prototype because of suspected strictures in the tendon conduit and apparently high friction.

Because of the low magnitude of strains in these units and the sensitivity of the field equipment, the data measurement cannot be considered highly accurate. Substantial scatter was noted between individual data points in several cases. The authors feel that the field measurements during erection can only be regarded as a general indication of the actual strains experienced in the prototype structure and do not necessarily contradict the results of the model tests. Unfortunately, they do not necessarily confirm the results either.

9.3.2 Closure Operations. A greatly improved opportunity for making a number of strain measurements in the prototype was presented by the closure operations. In contrast to the balanced cantilever erection techniques which were scattered throughout several months, final closure stressing was accomplished in one day. After all of the main span positive tendon cables were inserted, tendons A1 through A4 were sequentially tensioned, the end reactions were jacked to attain proper elevations, and tendons A5 and A6 were prestressed. This was a slightly different sequence than that used in the model, wherein tendons A1 through A6 were stressed and then the end supports were raised. During the tensioning of all of these cables, strain readings were taken in segmental units M1, S1, S7, and M10. Typical comparison of data from the model and the prototype construction during closure are shown in Figs. 9.3 and 9.4. The slight difference in sequence involved in jacking the end supports to the final elevation is ignored in these comparisons. Figure 9.3 shows that the values measured in the main span segment immediately adjacent to the pier



○ MODEL

● PROTOTYPE

----- BM THEORY

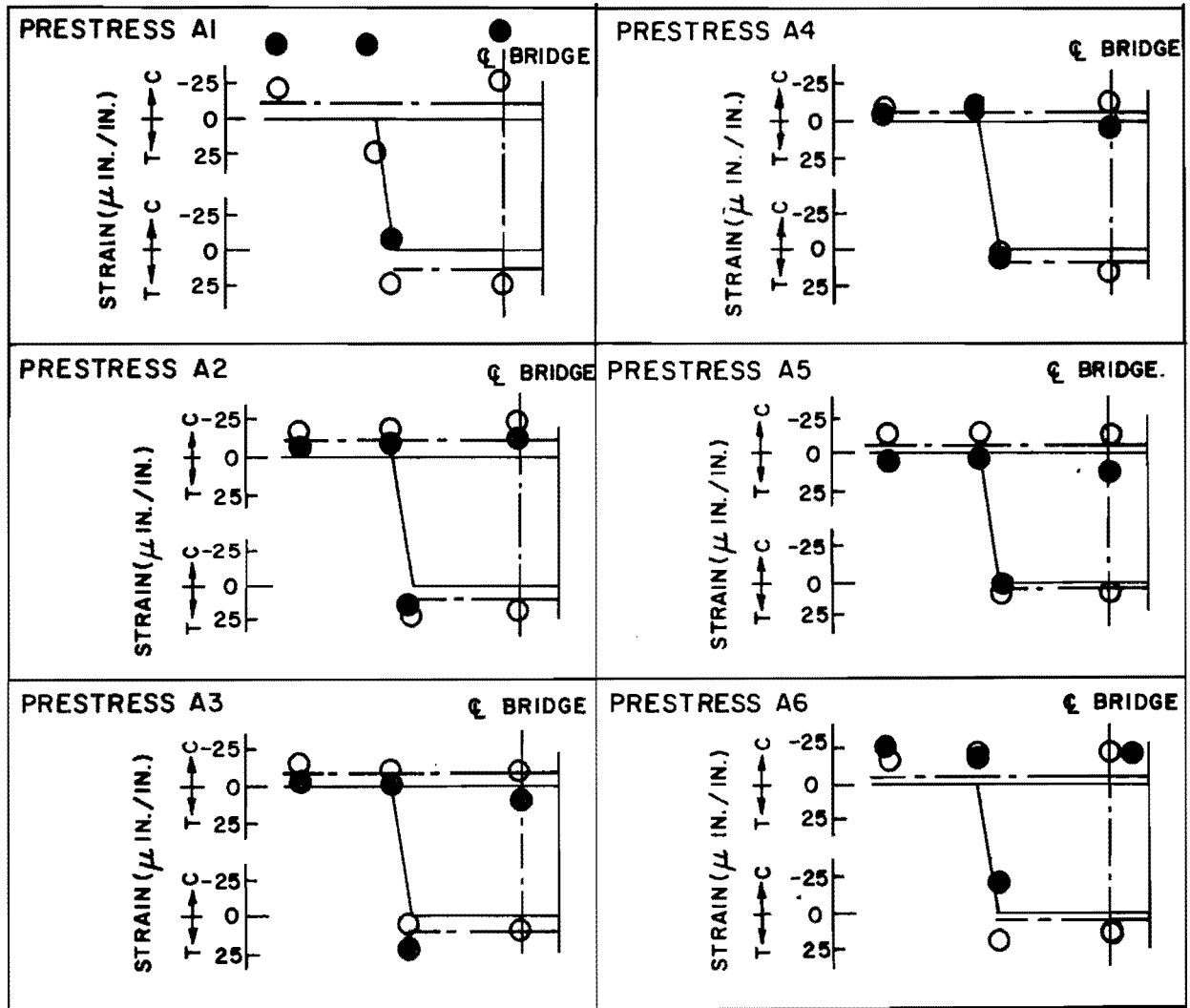
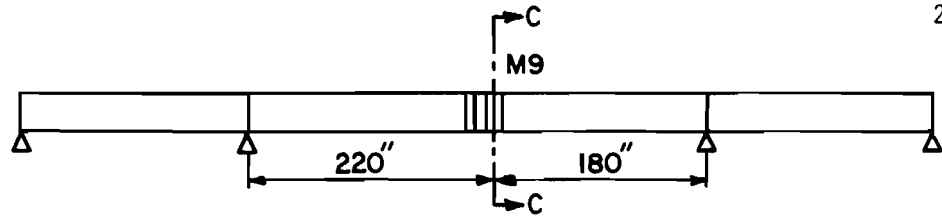


Fig. 9.3. Measured strains in M1 segments during closure operation



○ MODEL
 ● PROTOTYPE
 - - - - BM THEORY

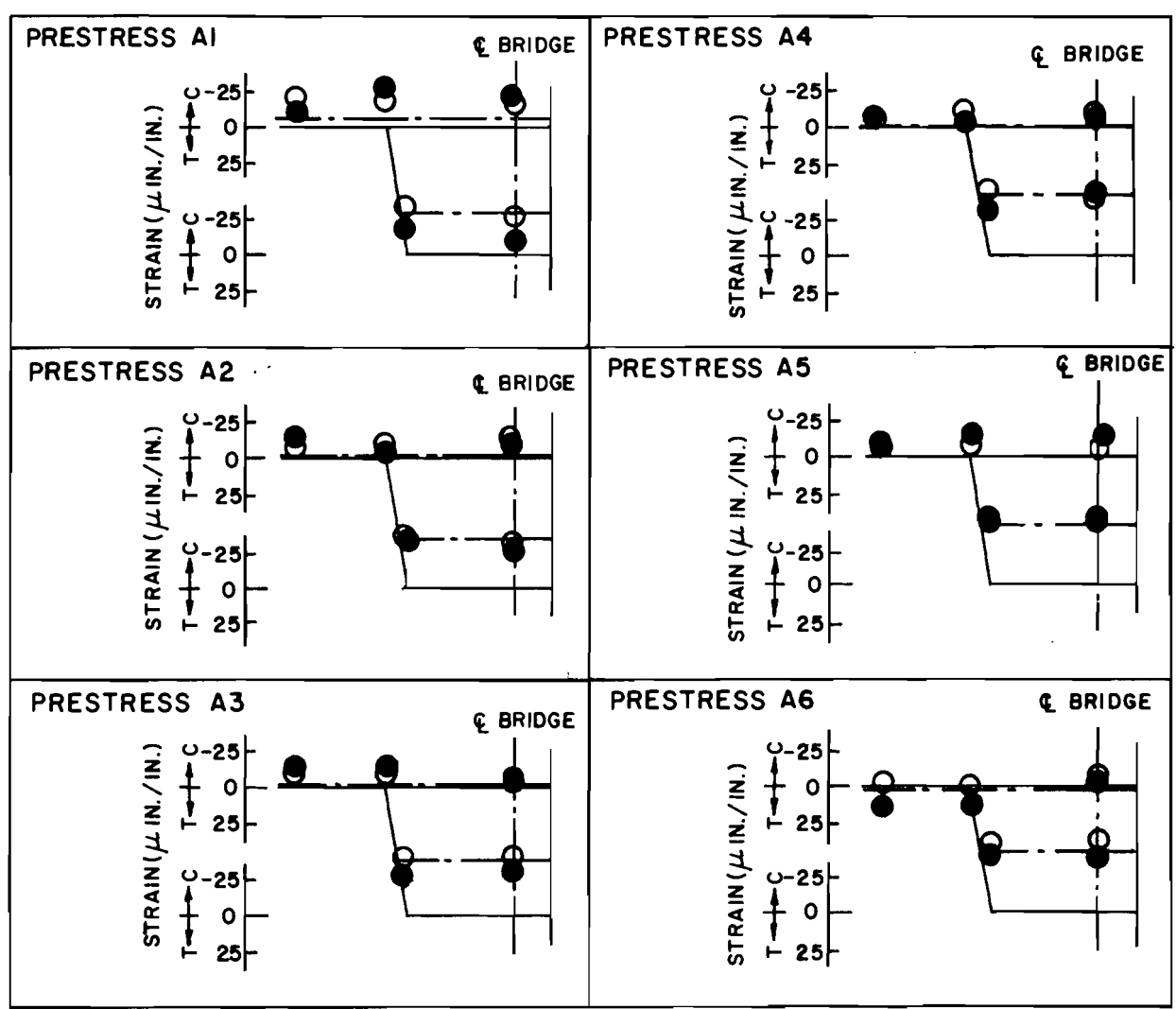


Fig. 9.4. Measured strains in the model M9 segment and prototype M10 during closure operations

are in very good agreement in the model and the prototype tests, except for the stressing of the initial cable. In this case the prototype compressive stresses substantially exceed the model and the theoretical stresses. Substantial difficulty was reported in the prototype stressing in obtaining the required elongations. During stressing of tendons A1, the rams were bled off, then brought back to required pressure several times before the proper elongation was obtained. Greatly improved agreement was noted in the strains near midspan. The comparison shown in Fig. 9.4 is not completely valid, since the model was instrumented in segment M9 while the prototype was instrumented in the adjacent segment M10. However, these two units are close enough together to give a good general indication of the nature of strains. The beam theory line shown corresponds to the model M9 segment. It is almost exactly the same as the values that would be calculated for the M10 segment.

The generally good agreement shown during the complex closure stage indicates the applicability of the elastic calculations for this type of structure.

9.4 Prototype Load Testing

Upon completion of all construction and immediately prior to opening the structure to traffic, a modest load test was performed to check on design and calculation procedures. Since it was impractical to impose the design lane loadings used in service load level tests of the model structure and in the actual design of the bridge, two heavily loaded trucks were used to obtain "influence lines" for bending strains at the various locations in the structure where strain gages had been implanted in segments. The time available for load testing was very limited and an extremely modest program was undertaken. However, it is felt that the results are significant and further indicate the validity of general calculation procedures and the completely continuous nature of the actual structure. Two trucks approximating HS20 loading were used as shown in Fig. 9.5. Because the single axle allowable load limitation in Texas does not allow the HS20 vehicle to be operated on the highways, the trucks had tandem rear axles. They were loaded with sand and carefully



Fig. 9.5. (a) Truck loading tests

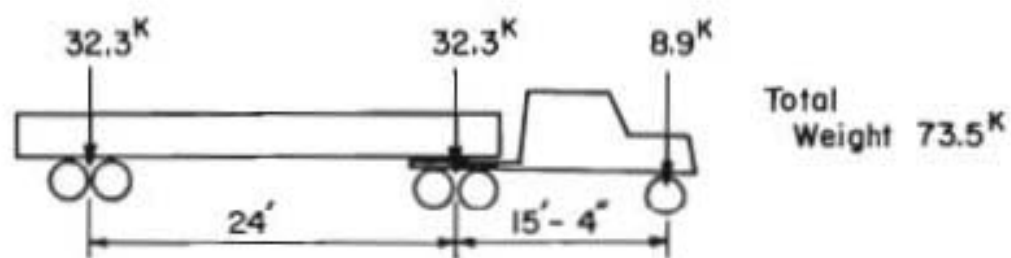


Fig. 9.5. (b) Average truck properties

weighed. The final weight of the two trucks was approximately 2 percent higher than that of an HS20 truck. Actual axle weights are shown in Fig. 9.5(b) as averages for the two trucks. No axle value varied more than 5 percent between the two vehicles.

During the load testing an individual truck was first positioned in various locations on the bridge. In general, the measured strain values were so low as to be unmeaningful within the general accuracy of the equipment. In order to obtain relatively measurable strains, the two trucks were placed side by side on one-half of the bridge with the centers of the trucks being essentially above the box girder webs. The trucks were moved to an initial position with the centroid of the load at Station 0 plus 25 ft. from the side pier. A complete set of readings was taken of all gages in each of the four segments which were instrumented. The pair of trucks were then advanced 25 ft., stopped, and a new set of readings was taken. This sequence was continued for the length of the bridge.

Results of typical strain measurements are shown in Figs. 9.6 through 9.9. The measured strains at a given station as the truck advanced along the structure represent a strain influence line. On each figure, the measured strain values are compared to a theoretical strain influence line. This influence line was calculated in the following manner. Using elastic theory and assuming no variation in EI along the member, influence lines were obtained for bending moment at stations corresponding to the middle of the segments indicated. These values were obtained in terms of nondimensional ordinates for a nondimensional load and length. Multiplying by the combined weight of the trucks and the length of the span, influence lines were obtained for a bending moment at the indicated measurement stations. The values of bending moment are then divided by the average section modulus for the structure and by an assumed modulus of elasticity of 4.62×10^6 psi for $f'_c = 6000$ psi concrete. In this way the influence line ordinates were reduced to equivalent total strain values for the whole bridge. However, since the loading was applied only above one box of the section, and since the loading was resisted by

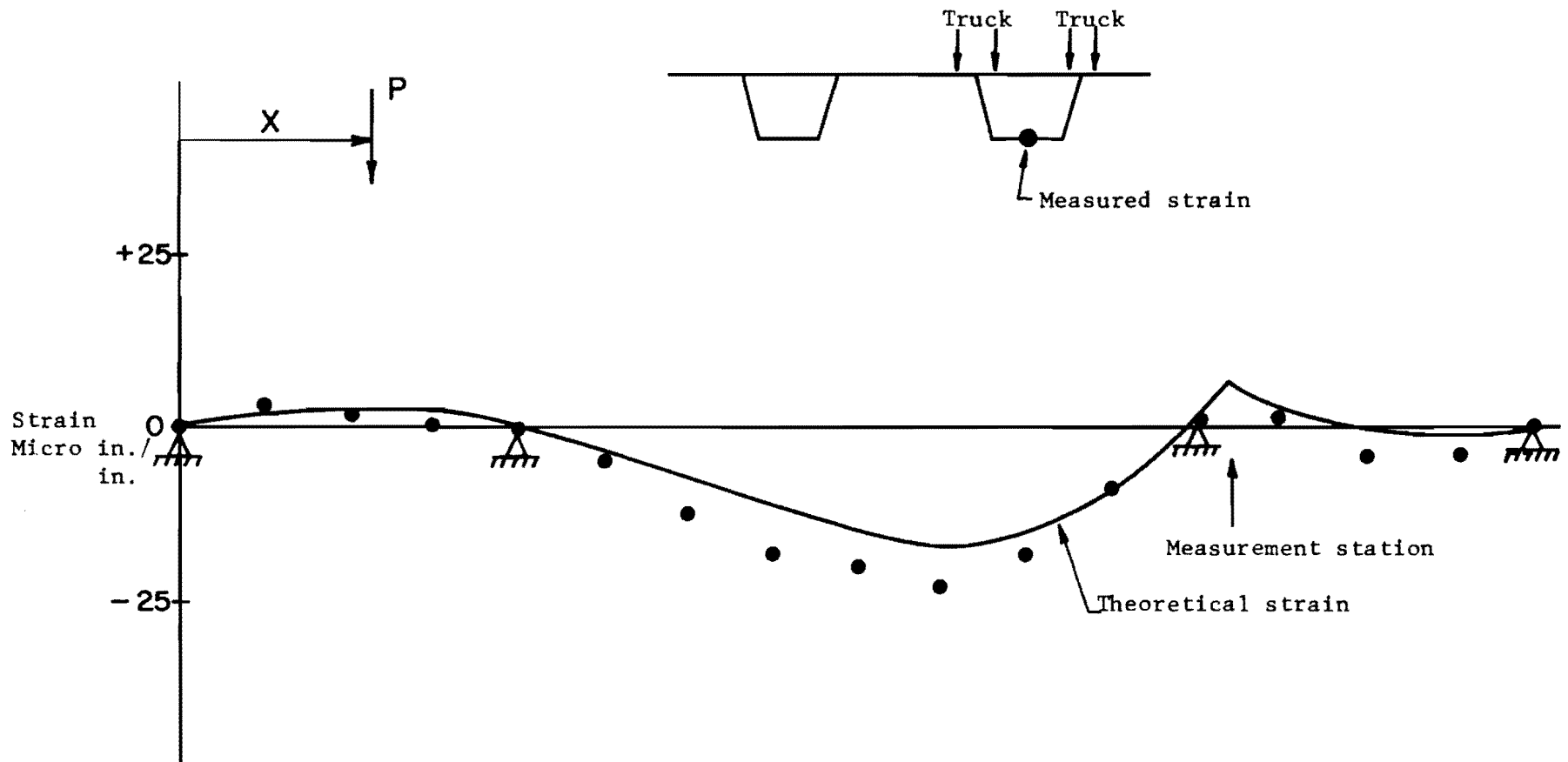


Fig. 9.6. Influence line for bottom flange strain, Station SS1

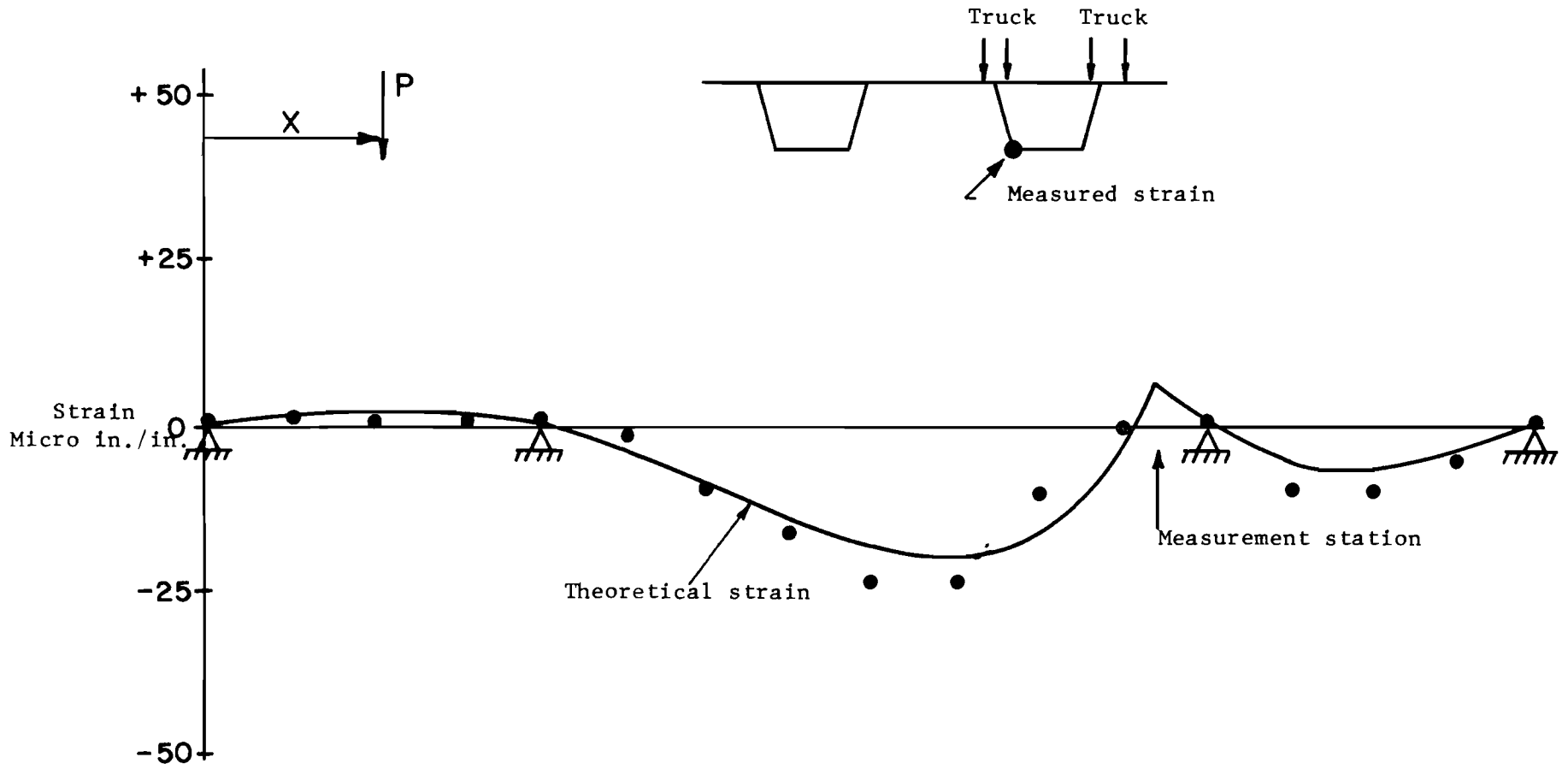


Fig. 9.7. Influence line for bottom flange strain, Station MS1

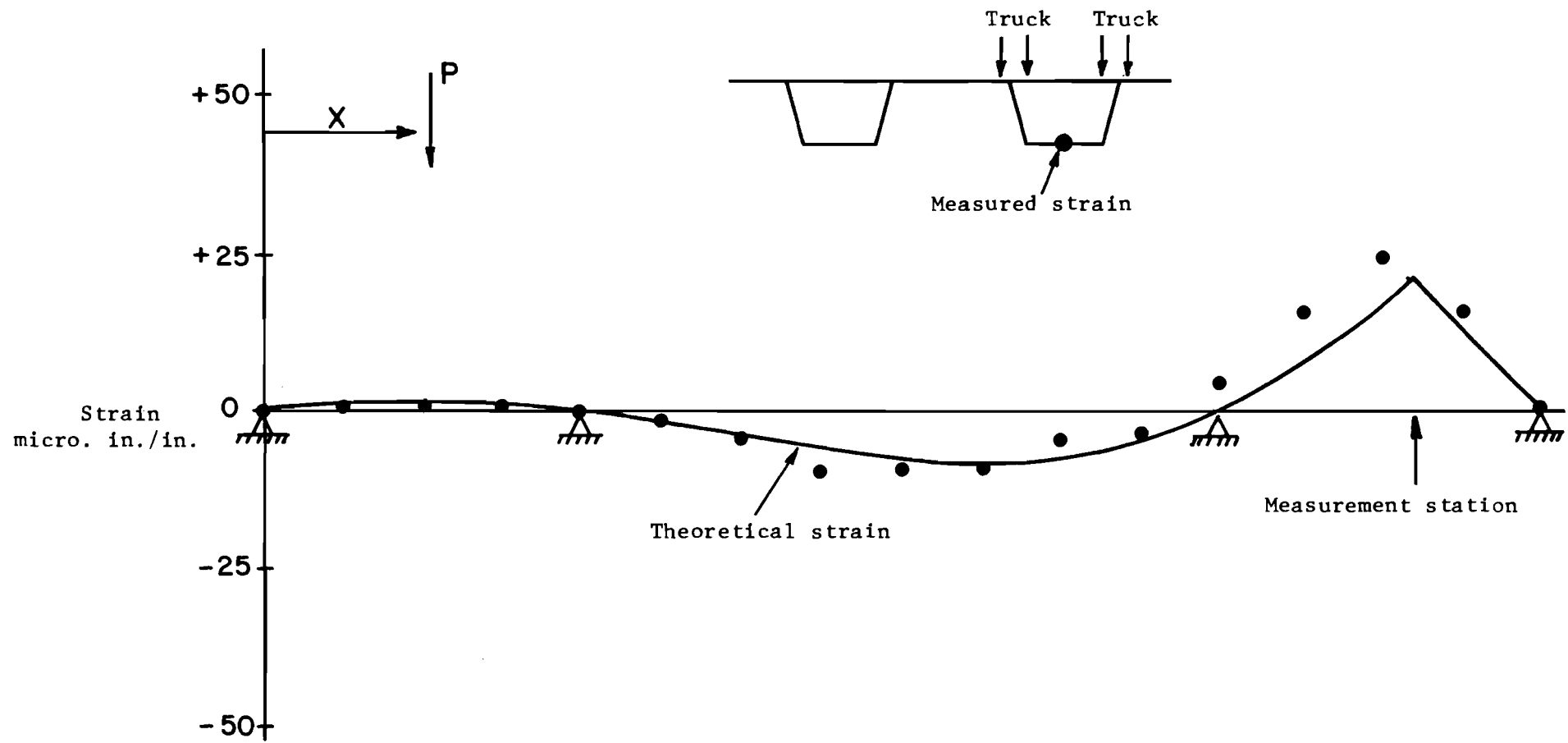


Fig. 9.8. Influence line for bottom flange strain, Station SS7

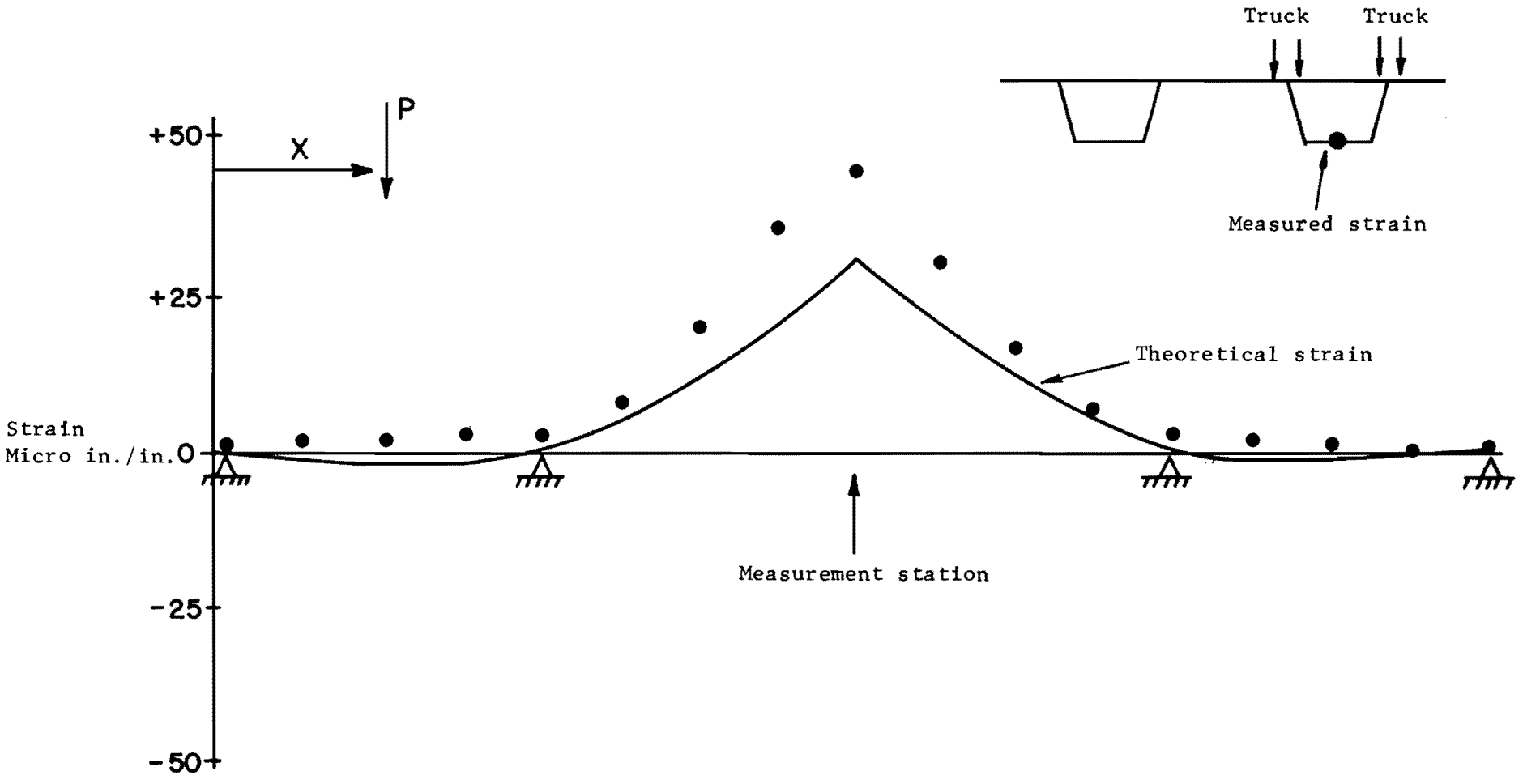


Fig. 9.9. Influence line for bottom flange strain, Station MS10

two boxes in an unsymmetrical fashion, this value of strain would be unrealistically high. Using the results reported in Sec. 7.3.2.2 for loads on one box only, the measured value of strains on the loaded box as a function of total strain was computed. It was found that for almost all load cases, this ratio was 70 percent. Accordingly, Figs. 9.6 through 9.9 were plotted assuming that the same proportion (70 percent) would hold in the prototype.

Comparison of the measured strain values with the theoretical influence lines in Figs. 9.6 through 9.9 indicates generally good agreement. In all cases, the general shape of the influence line is very near that of the distribution of the measured points. At the maximum value the measured strains run 10 to 30 percent higher than the theoretical strains. This could be due to calculation inaccuracies, since the calculation procedures assumed a uniform cross section and station MS10 in particular is somewhat less rigid than the pier sections, or to errors in the assumption that the strain in the loaded boxes would be approximately 70 percent of the total strain. It is particularly interesting that the strains noted in segment MS10 seem to be most in error. Since this unit is farthest away from the rigid pier section with its diaphragms, the load distribution between the two boxes is probably the least effective.

In general, the agreement between measured and computed points is well within the state of the art at this low level of load. It is particularly reassuring that even under these heavily loaded trucks the maximum change in stress noted would correspond to less than 1500 psi steel stress, or 250 psi concrete stress. These tests confirm the adequacy of the design procedure.

9.5 Ultimate Shear Test

During the actual construction of the prototype structure in Corpus Christi, a series of inclined cracks appeared in the webs of units being stressed. These fine cracks generally became visible immediately ahead of the anchorage assembly and propagated along the inclined tendon path into the flange. No similar cracking had ever been noted in the model

construction. Careful examination of details indicated that the manufacturer of the post-tensioning system and the contractor had not utilized the spiral confinement along the tendon path, as shown in Fig. 4.6. In order to investigate various factors which may have caused or contributed to this cracking and to determine if the inclined cracking reduced the anchorage or shear strength of the units, a special test was programmed using three model segments. These segments were constructed to model the "worst probable construction conditions" in the prototype. Any error or omission which could be attributed to prototype construction was modeled in the units. Several segments had transverse bars cut or relatively small portions of the web reinforcement omitted. In general, the units had a much reduced spiral reinforcement along the tendon path to model the exact anchoring used in the prototype.

Three segments were erected using the epoxy used in the prototype. The level of prestressing used corresponded to the values for segments M1, M2, and M3. The units were not erected in a balanced cantilever fashion, but rather cantilevering off of a pier and steel frame, as shown in Fig. 9.10.

During the stressing of each segment, careful observation was made of the webs and very definite cracking similar to that in the prototype was noted in the webs of segment 1. Later visual examination of the interior of the webs indicated the same type of cracking inside the webs of segment 2, but no visible cracking was noted in segment 3. A positive moment tendon similar to tendon A1 was then inserted in segment 1 (near the pier) and the tendon was taken up to the design value and then a 50 percent overload with no apparent damage in the positive moment anchorage vicinity. All indications were that the inclined cracks were slightly controlled by the stressing of the positive moment tendon.

In order to determine the behavior of the cracked units under heavy shear loads, hydraulic rams were then used to apply shear loads to the outer or third segment. Initially the rams were brought up to the level corresponding to the dead load shear for the structure. Loading was then increased to 1.35 dead load with nothing dramatic happening. Load was then increased in increments of one-half the design live plus impact loading,

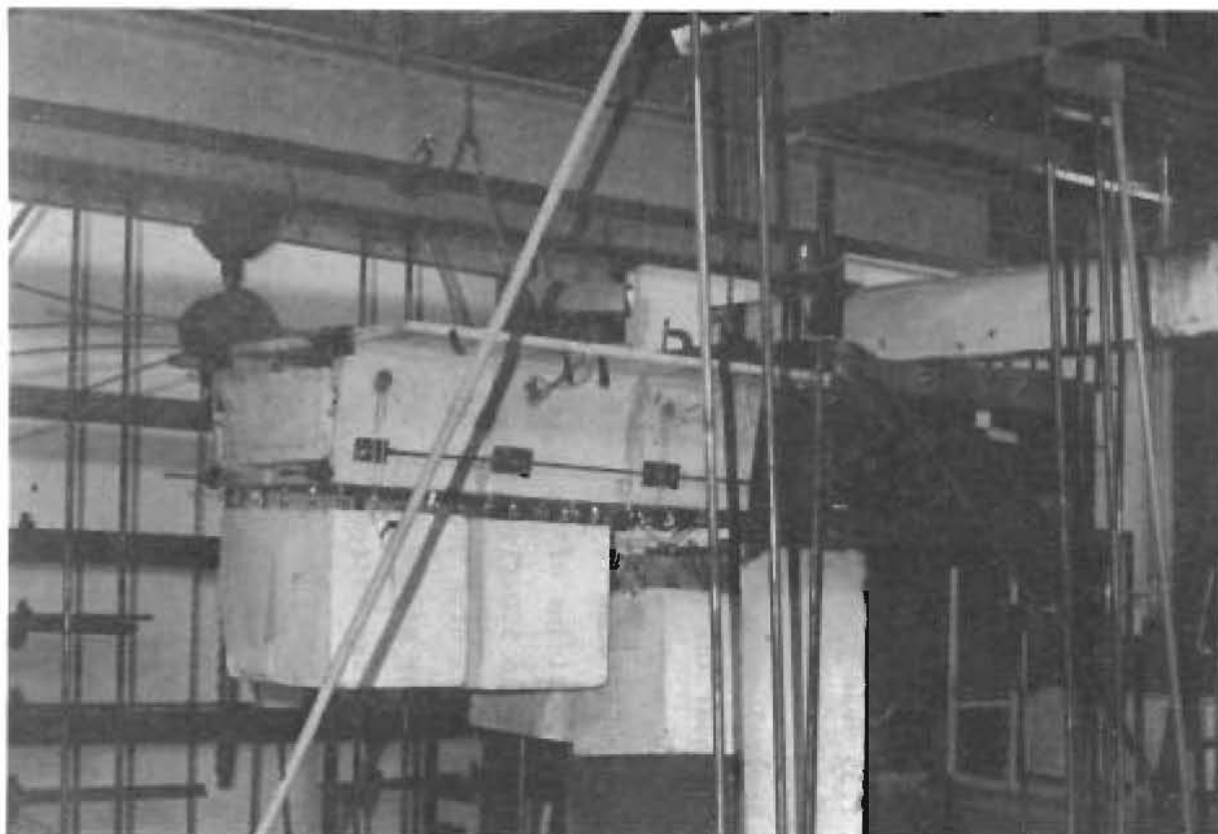


Fig. 9.10. Test arrangement--ultimate shear test

based on the maximum shear loading and the heavy concentrated load which accompanies shear at the support. Initial inclined shear cracks occurred at a level of 1.35 dead plus 2.25 (live plus impact). These cracks were generally in the direction opposite to those formed along the tendon paths. Due to flexural capacity difficulties, additional rams were inserted at the midpoint of the second segment and the loading was increased by 0.25 (live plus impact) values.

Loading was increased to 1.35 dead plus 3.0 (live plus impact) and a very large, flat inclined crack appeared extending almost the full length along segment 1. The crack started about 2 in. from the support and extended to within about 2-1/2 in. of the joint. It was a very low crack going only up about to the height of the specimen. Live load was increased in increments to 1.35 dead plus 5.0 (live plus impact). The inclined shear crack was quite wide and extended through the epoxy joint up towards the load point. Several substantial inclined cracks passed right through the tendon anchorage near the top of the shear key and extended into the web of the adjacent segment. Because of the high moment, the jacks on the outer segment were dropped down to 1.35 dead load and they were maintained at that level for the remainder of the test. The jacks on the second segment were incremented up to 5.0 (live plus impact) and then increased in small increments at a level of 6.0 (live plus impact). The shear crack, which extended from the top of the shear key in the first segment down through the lower flange, was extremely wide. Additional shear cracks began to appear below the shear key toward the bottom of the web. In the bottom flange it was obvious that the web reinforcement began to yield in the shear key area. Some evidence of cracking on the bottom flange was visible. Loading was advanced but at 1.35 dead plus 6.1 (live plus impact) a massive shear crack opened below the shear key and a compression crack extended well back along the web. The entire joint ripped apart at the top flange level and final failure occurred.

Using the calculation procedure for ultimate shear strength outlined in Sec. 8.3.3.2, the theoretical shear strength can be compared to the actual shear applied to the model. The actual applied shear at ultimate during

the test on the joint between the first and second segments where principal failure occurred was 61.4 kips. Using the calculation procedure of Sec. 8.3.3.2, based on a $f'_c = 5400$ psi for these segments, 120 kip prestressing force, and 60 ksi web reinforcement, the calculated ultimate shear strength would be 63.9 kips. Thus, the test specimen developed 96 percent of the theoretical shear strength. Considering the large variations inherent in shear tests, this must be considered as an extremely satisfactory test. This is especially so since the units were made to represent the worst possible construction and deliberately had some reinforcement misplaced, altered, or omitted. The results of this test can be taken as a conclusive indication of the efficiency of properly applied epoxy joints in segmental construction. Provision of these joints did not significantly lower the shear strength of the unit.

This page replaces an intentionally blank page in the original.

-- CTR Library Digitization Team

C H A P T E R 1 0

CONCLUSIONS AND RECOMMENDATIONS

10.1 Conclusions

10.1.1 Primary Conclusions. (1) The segmental bridge model safely carried the ultimate design loads for all critical moment and shear loading configurations on which its design had been based, as specified by the 1969 Bureau of Public Roads Ultimate Strength Design Criteria. Detail results were shown in Sec. 7.3.3.

(2) The deflection under design live load in four lanes (only three lanes required by live load reduction factors) was approximately $L/3200$ in the main span. This is much smaller than $L/300$ which is generally considered as acceptable.

(3) Positive tendons in the main span were designed as if an ideal three-span continuous beam. Since the completed bridge was supported on neoprene pads which have no vertical restraint against uplift, the outer ends were able to rise off their supports so that the structure did not act continuously at ultimate conditions under main span positive moment loading. Even so, there was sufficient reserve strength in the main span to carry design ultimate load as shown in Sec. 8.3.

(4) Under very high combined moment and shear loading (see Sec. 8.3), flexural cracks appeared near the epoxy joints in the top slab near the main pier. However, they joined the diagonal tension cracks and did not extend along the joints. There was no sign of any direct shear failure at the joints. In tests of the full bridge model, approximately 75 percent of the theoretical ultimate shear load was applied in the maximum shear loading test prior to failure of the bridge during that test by flexure. No sign of shear distress was evident. Subsequent tests of a three-segment model under severe shear loading as a cantilever section indicated that full

shear strength of the unit was developed. Hence, the epoxy joint technique used did not reduce the design shear strength.

(5) During erection of the first few segments, tensile stress occurred in the bottom slab as predicted in the design (Sec. 6.1.5(b) and Sec. 6.2.3). Temporary prestress devices successfully controlled the effects of these stresses.

(6) Theoretical calculation of the load factor for live and impact loads required to form the first plastic hinge agreed very well with the experimental results, as shown in Sec. 8.2 and 8.3. These tests proved the accuracy and applicability of the ultimate load calculation procedure of Sec. 8.2.3.

10.1.2 Secondary Conclusions. (1) Near failure, major cracks concentrated near the epoxy joints which had no continuous conventional reinforcement (Secs. 8.2 and 8.3). However, throughout the loading sequence cracks were generally well-distributed because of the effective grouting and the strength of the epoxy joints (Secs. 7.3.3, 8.2, and 8.3).

(2) While behavior of the epoxy joints was quite satisfactory, it should be considered that the model segments were joined in a dry condition. Ref. 19 indicates that while most of the epoxy resins performed adequately for joining dry specimens, the strengths developed by most of the epoxy joints were very weak when joined with concrete segments in a saturated condition.

(3) Transverse moment capacity of the bridge cross section was very adequate, as shown by the punching shear load test results of Secs. 7.3.4 and 8.4.

(4) There was no adverse effect of the epoxy joints on the slab punching shear strengths, as shown in Sec. 8.4.

(5) Bolts used for the temporary connection of the pier segments to the main piers yielded locally under the most critical unbalanced loading, although the calculated direct compressive stress was less than the actual yield strength. The bolts used in the model were also below the yield strength specified for the bolts in the prototype. Yielding was apparently

caused by the large gap between the pier segments and the pier, with consequent local bending, and was accentuated by the stress concentrations in the threads (Chapter 6).

(6) Most of the theoretical calculations were in good agreement with the experimental results, although there were some appreciable deviations between the experimental and theoretical values of strain in the top slab in some stages of cantilever construction (Chapters 6 and 7).

The BMCOL50 program was very useful in predicting the behavior of the bridge during construction and for uniform loading tests. The BMCOL50 results agreed very well with the experimental results for longitudinal strains and deflections. The relatively simple data input for BMCOL50 is another advantage when compared to the folded plate theory programs.

The SIMPLA2 program reasonably predicted the variation of the longitudinal strain under very high stress levels across the top slabs of the newly erected segments.

The MUPDI program, which can be used only for a constant cross section, agreed very well with the experimental results at the service load level. The variation of cross section along this bridge was very small. MUPDI can be used to determine the transverse moments and shears under unsymmetrical loading and can be used effectively in designing the transverse reinforcement.

(7) The initial overstressing to $0.8f'_s$ with release to $0.65f'_s$ before seating, suggested by Brown,¹⁰ worked well. The friction factor and wobble coefficient used with SIMPLA2 were reasonable, as confirmed by the tests (Sec. 6.2.2).

(8) Separation of the match cast segments was smoothly carried out without any damage to the segments, by careful application of uniform force using hydraulic rams (Sec. 4.4).

10.2 Recommendations

10.2.1 Design Recommendations. (1) Since the structural configuration changes from a statically determinate cantilever structure to a multispan continuous structure during construction of this type of bridge, the ultimate design load for effects (moment, shears, etc.) for this bridge should be specified as two values which must each be satisfied, as follows:

$$U = U_1$$

and

$$U = U_2 + U_3$$

where $U_1 = 1.35 DL_1 + 2.25 (LL_1 + IL_1)$ to be computed for a balanced cantilever

$U_2 = 1.35 DL_1$ for negative moments and $0.9 DL_1$ for positive moments to be computed for a balanced cantilever

$U_3 = 1.35 DL_3 + 2.25 (LL_3 + IL_3) + SL$ to be computed for the completed continuous structure

DL_1 = dead load during cantilevering

DL_3 = dead load applied after completion of closure (topping, railing, etc.)

LL_1 = live load due to construction operations

LL_3 = design live load

IL_1 = impact load of construction operations

IL_3 = design impact load

SL = resultant reaction due to prestressing of the tendons* and seating force at outer supports

(2) Negative tendons should be designed so that no tensile stress is developed across any joint during erection. Otherwise some temporary erection procedure must be required to keep the joint in compression until erection stresses change from tension to compression.

(3) In calculating the internal ultimate moment in the positive moment region, possible contributions of the negative tendons present at that section should be considered.

*Resultant reaction is zero for the tendons stressed while a determinate structure.

(4) Negative moment and shear capacity must be checked for both cantilever erection stages and for the completed structure under design and ultimate loads, as shown in the design of this bridge.²¹

(5) If the outer support details provide no restraint to upward vertical movement, this should be considered in designing positive moment tendons. Alternate solutions should be examined to decide whether the positive moment prestress should be increased, vertical restraints provided at outer supports, or outer spans lengthened. The designer must be aware of the effects of change of structure configuration if the side spans rise up from their supports under ultimate loading in the central span, as shown in Sec. 8.3.3.1.

(6) The jacking forces required to adjust the end reaction or elevation of the bridge should be carefully calculated to prevent premature cracks at service load levels, as shown in Sec. 7.3.3.2.

(7) The sequence of positive moment tendon stressing operations should be specified to minimize or preferably eliminate tension in the top slab, especially at the closure segment.

(8) Although the model bridge was safely supported by the bolt details used during cantilever erection, Sec. 6.2.1 and Fig. 6.25 suggest an improved temporary support system to reduce the high compressive stresses on the bolts in the unbalanced loading condition and stiffen the connection and thus reduce unbalanced deflections.

(9) Although the effects of creep and shrinkage were minimal in this study, Muller³⁰ points out for this class of structure:

The effect of steel and concrete creep must be considered with regard to moment distribution, together with the possible effect of moment reversal. Final adjustment and compensation for shrinkage and concrete creep may help the structure to reach the optimum equilibrium.

10.2.2 Construction Recommendations. (1) The pier segments should be carefully placed on the piers to close vertical and horizontal alignments, in order to minimize the final closure adjustments.

(2) If practical, positive tendons in the main span should be inserted before casting the closure segment, in order to make sure that ducts are clear, since concrete may penetrate into the tendon duct near the joint during casting of the closure joint.

(3) If there is any small damage on the surface of the segment, it will be better to fill it with the epoxy material at the time of jointing than to patch it earlier and risk the danger of the units not mating due to an excess of patching material.

REFERENCES

1. Aldridge, W. W., and Breen, J. E., "Useful Techniques in Direct Modeling of Reinforced Concrete Structures," Models for Concrete Structures, ACI Publication SP24, 1970, pp. 125-140.
2. American Concrete Institute, Building Code Requirements for Reinforced Concrete (ACI 318-63), Detroit, June 1963.
3. American Concrete Institute, Building Code Requirements for Reinforced Concrete (ACI 318-71), Detroit, 1971.
4. American Concrete Institute, "Guide for Use of Epoxy Compound with Concrete (ACI 403)," Journal of the American Concrete Institute, August 1962.
5. American Society for Testing and Materials, "Standard Method of Test for Working Life of Liquid or Paste by Consistency and Bond Strength (ASTM D 1338-56)," ASTM Standard, Part 16, June 1969, pp. 498-500.
6. American Association of State Highway Officials, Standard Specifications for Highway Bridges, Tenth Edition, American Association of State Highway Officials, Washington, D.C., 1969.
7. Bureau of Public Roads, Strength and Serviceability Criteria, Reinforced Concrete Bridge Members, Ultimate Design, Second Edition, Bureau of Public Roads, U. S. Department of Transportation, Washington, D.C., 1969.
8. Breen, J. E., and Orr, D. M. F., "A Rapid Data Acquisition and Process System for Structural Model Usage," Proceedings of Structural Model Symposium, Sydney, Australia, 1972.
9. Breen, J. E., and Burns, N. H., "Design Procedures for Long-Span Prestressed Concrete Bridges of Segmental Construction," Research Study Proposal, Center for Highway Research, The University of Texas at Austin, 1968.
10. Brown, R. C., "Computer Analysis of Segmentally Constructed Prestressed Box Girders," unpublished Ph.D. dissertation, The University of Texas at Austin, 1972.
11. Brown, R. C., Burns, N. H., and Breen, J. E., "Computer Analysis of Segmentally Erected Precast Prestressed Box Girder Bridges," Research Report No. 121-4, Center for Highway Research, The University of Texas at Austin, November 1974.

12. Corley, W. G., Carpenter, J. E., Russell, H. G., Hanson, N. W., Cardenas, A. E., Helgaston, T., Hanson, J. M., and Hognestad, E., "Design Ultimate Load Test of 1/10-Scale Micro-Concrete Model of New Potomac River Crossing, I-266," Journal of the Prestressed Concrete Institute, Vol. 16, No. 6, pp. 70-84.
13. Ferguson, P. M., Reinforced Concrete Fundamentals, Second Edition, John Wiley & Sons, Inc., New York, 1965.
14. Gallaway, T. M., "Industrialization and Modeling of Segmentally Precast Box Girder Bridges," unpublished Master's thesis, The University of Texas at Austin, 1971.
15. Henneberger, Wayne, and Breen, John E., "First Segmental Bridge in the U.S.," Civil Engineering, Vol. 44, No. 6 (June 1974), pp. 54-57.
16. Ikeda, T., Precast Segmental Construction Method, Nikkan Kōgyō News Paper Inc. (JAPAN), 1969.
17. Kashima, S., "Experimental Study of Epoxy Resins as a Jointing Material for Precast Concrete Segments," unpublished Master's thesis, The University of Texas at Austin, 1971.
18. Kashima, S., "Construction and Load Tests of a Segmental Precast Box Girder Bridge Model," unpublished Ph.D. dissertation, The University of Texas at Austin, January 1974.
19. Kashima S., and Breen, J. E., "Epoxy Resins for Jointing Segmentally Constructed Prestressed Concrete Bridges, Center for Highway Research, Research Report No. 121-2, Center for Highway Research, The University of Texas at Austin, August 1974.
20. Lacey, G. C., and Breen, J. E., "State-of-the-Art--Long Span Prestressed Concrete Bridges of Segmental Construction," Research Report 121-1, Center for Highway Research, The University of Texas at Austin, May 1969.
21. Lacey, G. C., "The Design and Optimization of Long Span, Segmentally Precast, Box Girder Bridges," unpublished Ph.D. dissertation, The University of Texas at Austin, May 1969.
22. Lacey, G. C., Breen, J. E., and Burns, N. H., "Long Span Prestressed Concrete Bridges of Segmental Construction--State-of-the-Art," Journal of the Prestressed Concrete Institute, Vol. 16, No. 5, October 1971.
23. Lacey, G. C., and Breen, J. E., "The Design and Optimization of Segmentally Precast Prestressed Box Girder Bridges," Research Report 121-3, Center for Highway Research, The University of Texas at Austin, July 1975.

24. Leyendecker, E. V., and Breen, J. E., "Structural Modeling Techniques for Concrete Slab and Girder Bridges," Research Report 94-1, Center for Highway Research, The University of Texas at Austin, August 1968, pp. 26-28.
25. Leyendecker, E. V., "Behavior of Pan Formed Concrete Slab and Girder Bridges," unpublished Ph.D. dissertation, The University of Texas at Austin, 1969.
26. Lin, T. Y., Design of Prestressed Concrete Structures, Second Edition, John Wiley & Sons, Inc., New York, 1963.
27. Litle, W. A., Cohen, E., and Somerville, G., "Accuracy of Structural Models," Models for Concrete Structures, ACI Publication SP-24, 1970, pp. 65-124.
28. Matlock, H., and Haliburton, T. A., "A Program for Finite Element Solution of Beam-Columns on Nonlinear Supports," unpublished report, The University of Texas at Austin, June 1964.
29. Mattock, A. H., "Structural Model Testing--Theory and Applications," Journal of the PCA Research and Development Laboratories, Vol. 4, No. 3, September 1962, pp. 12-22.
30. Muller, J., "Long Span Precast Prestressed Concrete Bridge Built in Cantilever," Concrete Bridge Design, ACI Publication SP-23, 1969, pp. 705-740.
31. Neville, A. M., Properties of Concrete, John Wiley & Sons, Inc., New York, 1963.
32. Prestressed Concrete Institute (Japan), Construction Manual for Precast Concrete Segmental Construction, December 1968.
33. Prestressed Concrete Institute Post-Tensioning Committee, Recommended Practice for Grouting of Post-Tensioned Prestressed Concrete, PCI Specification Draft, 1970.
34. Scordelis, A. C., "Analysis of Simply Supported Box Girder Bridges," Report No. SESM 66-17, Department of Civil Engineering, University of California, Berkeley, October 1966.
35. Scordelis, A. C., Bouwkamp, J. G., and Wasti, S. T., "Structural Behavior of a Two-Span Reinforced Concrete Box Girder Bridge Model, Vol. II," Report No. US SESM 71-16, Department of Civil Engineering, University of California, Berkeley, October 1971.
36. Swann, R. A., "The Construction and Testing of a One-Sixteenth Scale Model for the Prestressed Concrete Superstructure of Section 5, Western Avenue Extension," Technical Report, Cement and Concrete Association, London, 1970.

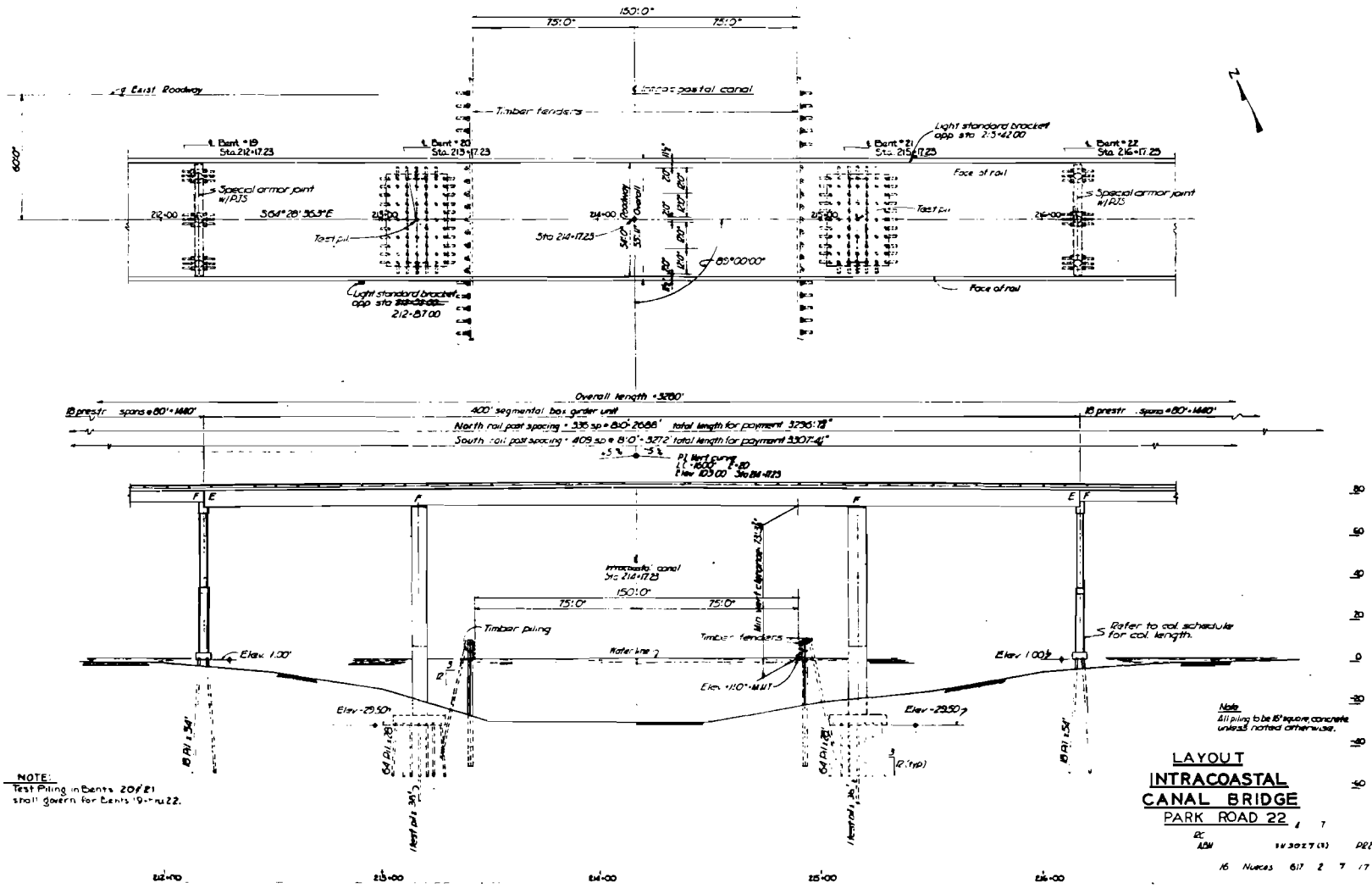
37. VIDAR Corporation, "VIDAR 5404 D-Das System Information,"
Technical Manual, California, May 1971.

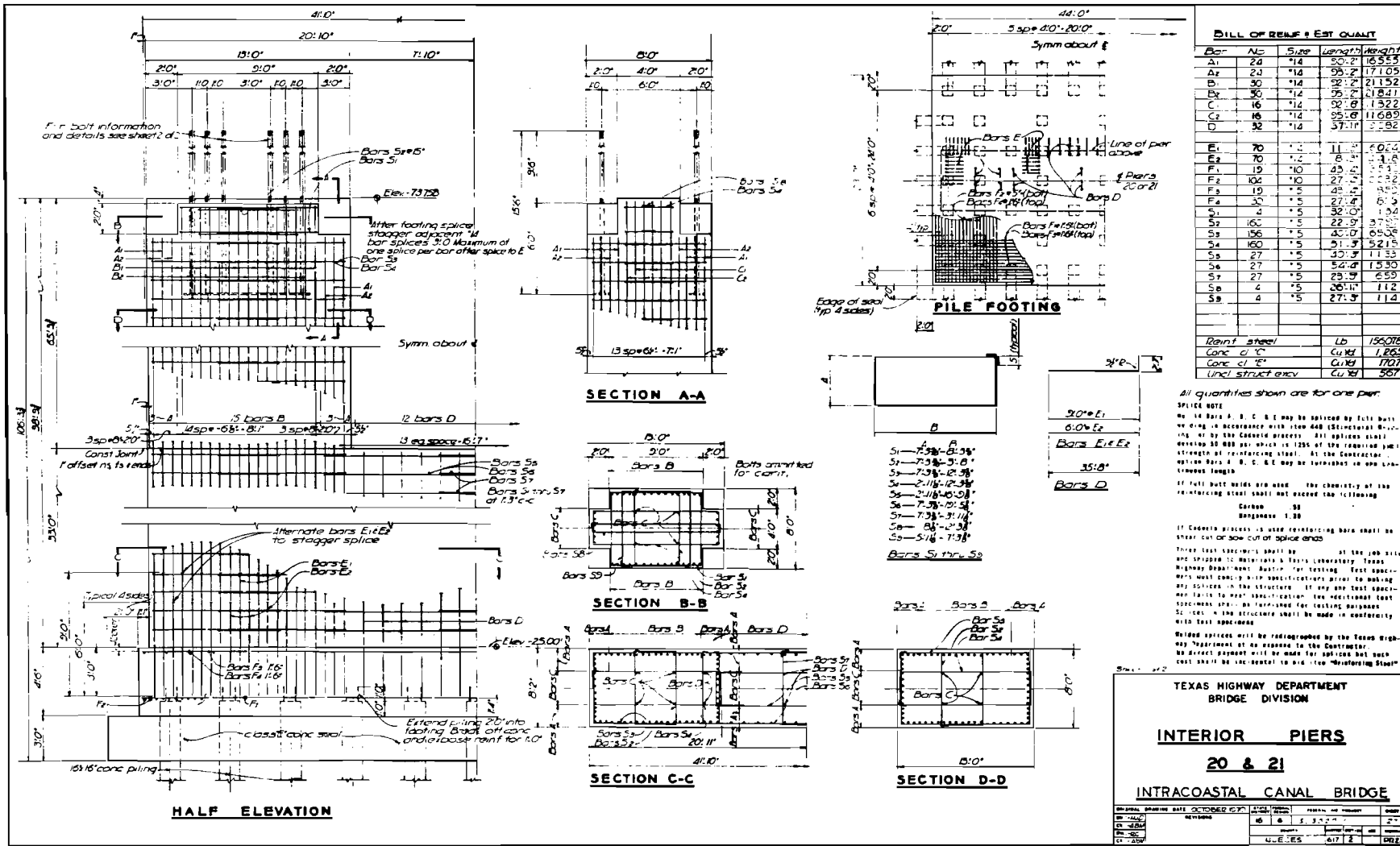
A P P E N D I X A

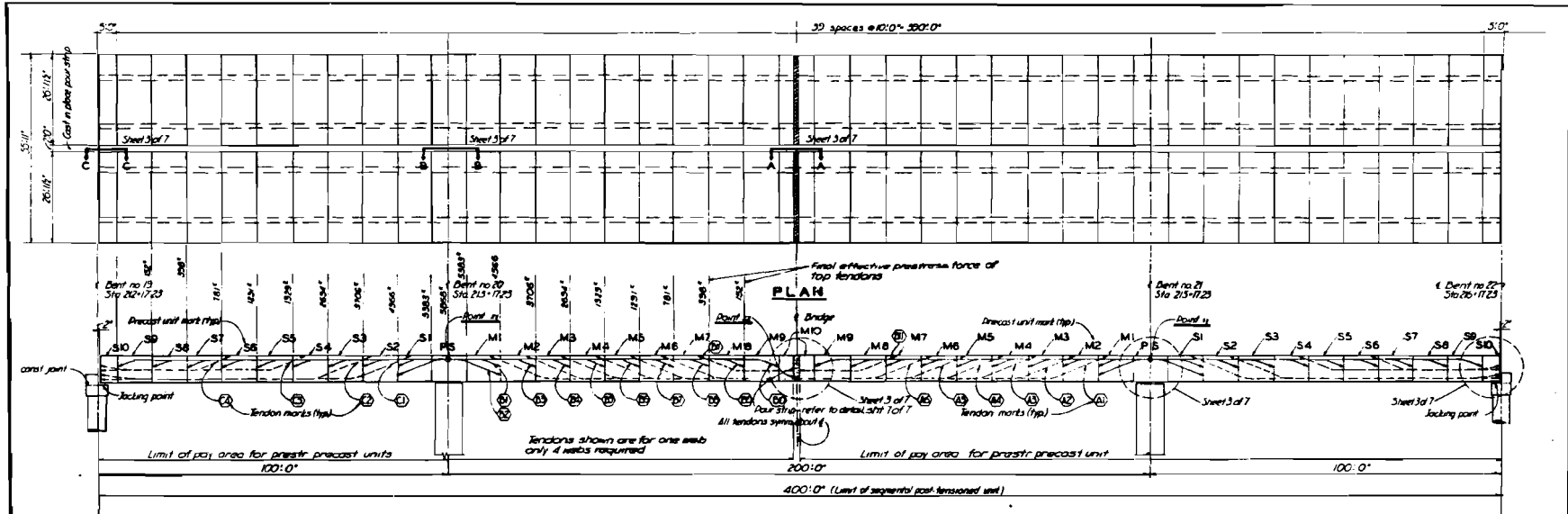
PROTOTYPE BRIDGE PLANS

This page replaces an intentionally blank page in the original.

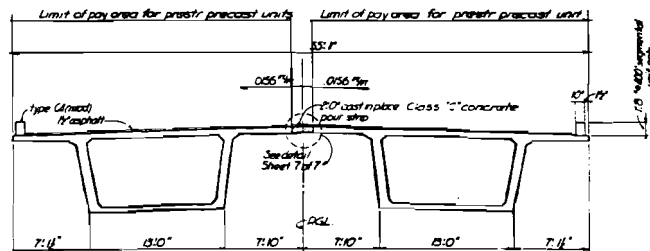
-- CTR Library Digitization Team







ELEVATION



TYPICAL SECTION

Apply epoxy joint sealer to all mating surfaces of precast units in accordance with specifications

Grout all anchorage blockouts & match exposed surfaces to precast units

The design will accommodate a 25% load on the end of the cantilever, in addition to the weight of a segment. This value will be used as a guide in evaluating the effects of any reaction or working apparatus attached to the cantilever.

Other tendon forces to be considered provided the minimum design forces, shown in the elevation are provided

Friction factors for calculating effective prestress will be as follows:
 Rigid Conduit - $k = .0002$ $\mu = .25$
 Flexible Conduit - $k = .0015$ $\mu = .25$

Suggested Tendon Schedule

all forces shown are final effective prestress force after losses

| Tendon Mark | Min. Force (k) | Tendon Mark | Min. Force (k) |
|-------------|----------------|-------------|----------------|
| B1 | 322.4* | A1 | 128.4* |
| B2 | 322.4* | A2 | 128.4* |
| B3 | 426.0** | A3 | 128.4* |
| B4 | 426.0** | A4 | 128.4* |
| B5 | 322.4* | A5 | 128.4* |
| B6 | 322.4* | A6 | 128.4* |
| B7 | 322.4* | Tendon Mark | Min. Force |
| B8 | 148.8* | C1 | 148.8* |
| B9 | 148.8* | C2 | 148.8* |
| B10 | 148.8* | C3 | 148.8* |
| B11 | 148.8** | C4 | 148.8* |

* Minimum force read in tendon
 ** Optional 2 tendons @ 205*

Sheet 1 of 7

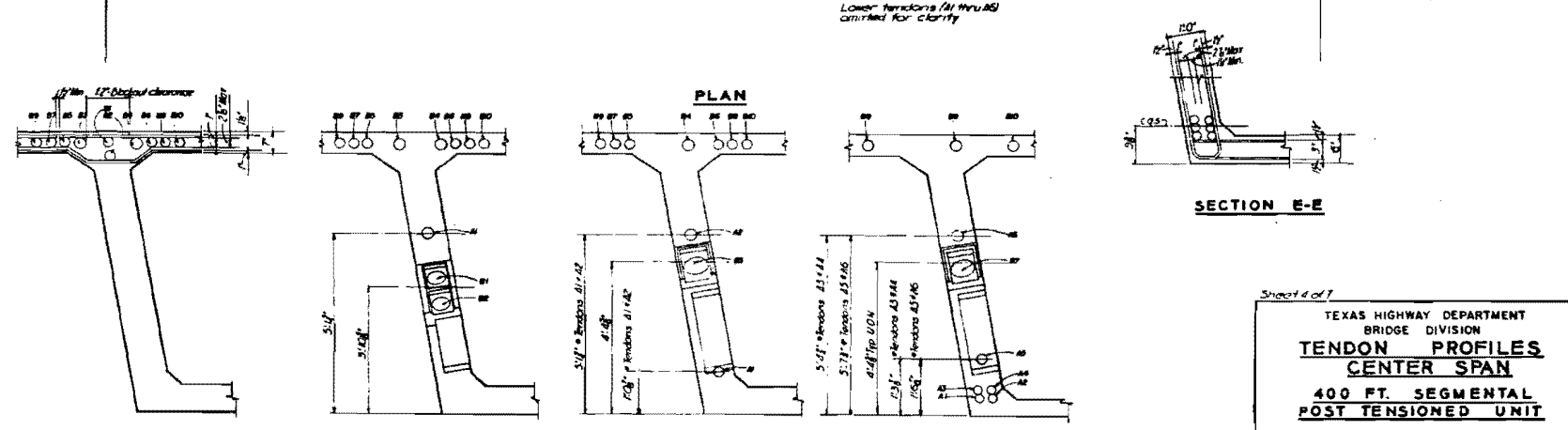
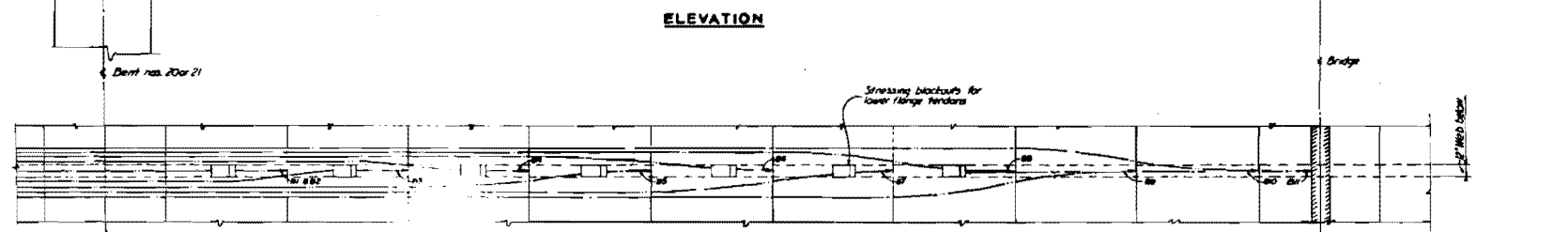
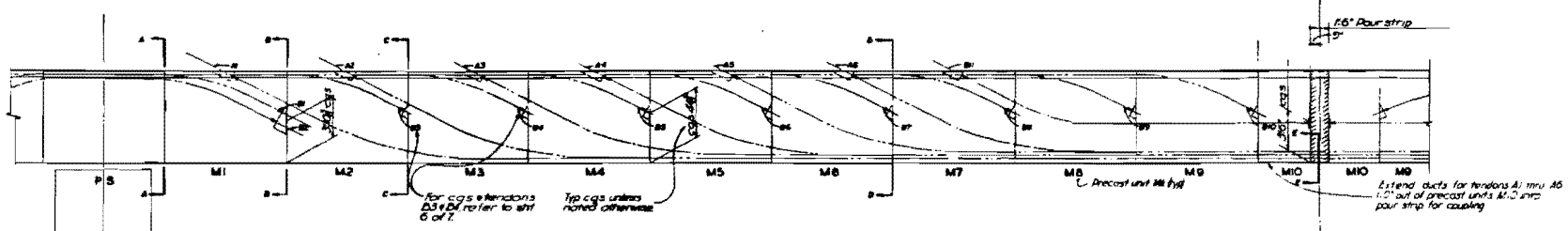
TEXAS HIGHWAY DEPARTMENT
 BRIDGE DIVISION

PLAN AND ELEVATION

**400 FT. SEGMENTAL
 POST TENSIONED UNIT**

INTRACOASTAL CANAL BRIDGE

| | | | |
|--------------------------|------------------------------------|---------------------|---------------|
| DESIGNED BY: LUT | DATE: OCTOBER 1970 | CHECKED BY: LUT | DATE: 10/1/70 |
| SCALE: 1/8" = 1'-0" | PROJECT: INTRACOASTAL CANAL BRIDGE | CONTRACT NO.: 017-2 | SECTION: 25 |
| APPROVED BY: [Signature] | | DATE: 10/1/70 | |



Sheet 6 of 7

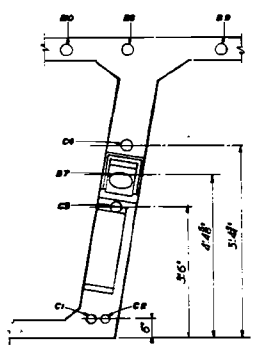
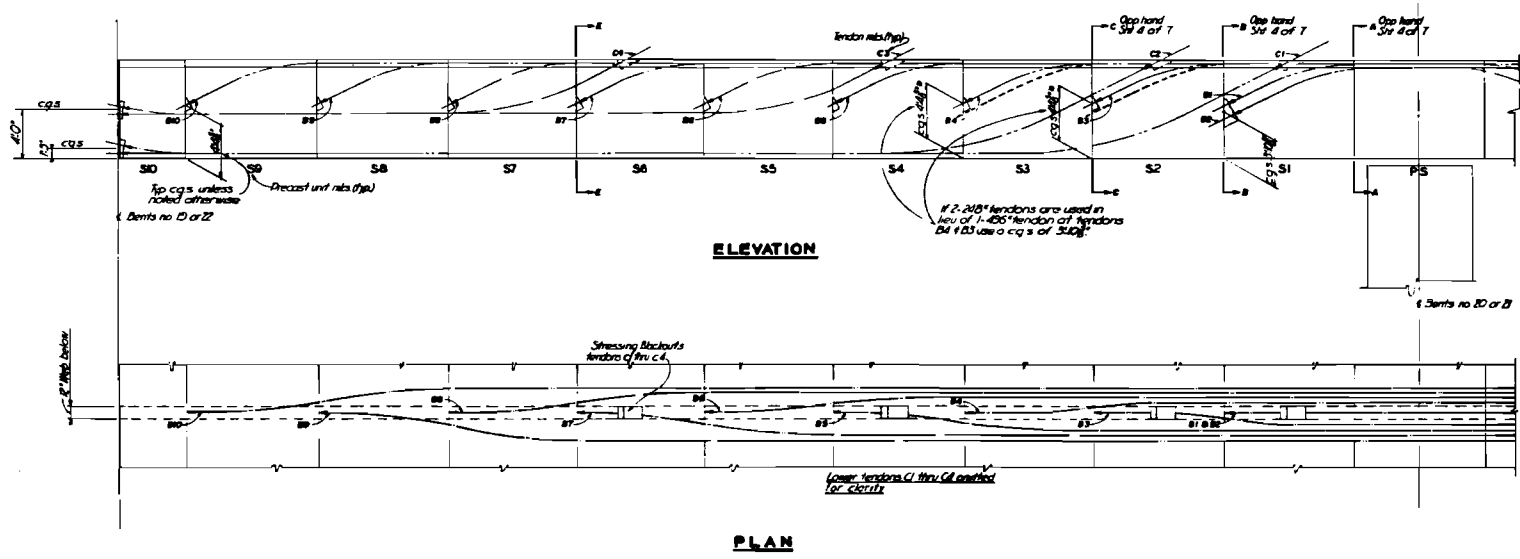
TEXAS HIGHWAY DEPARTMENT
BRIDGE DIVISION

TENDON PROFILES
CENTER SPAN

400 FT. SEGMENTAL
POST TENSIONED UNIT

INTRACOASTAL CANAL BRIDGE

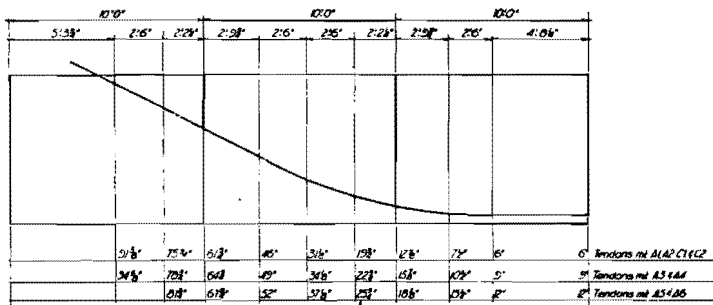
| | | | |
|-----------------------------|-------------------|------------------|---------------|
| ORIGINAL DATE: OCTOBER 1970 | DESIGNER: [blank] | CHECKED: [blank] | DATE: [blank] |
| BY: [blank] | BY: [blank] | BY: [blank] | BY: [blank] |
| BY: [blank] | BY: [blank] | BY: [blank] | BY: [blank] |
| BY: [blank] | BY: [blank] | BY: [blank] | BY: [blank] |



Sheet 5 of 7

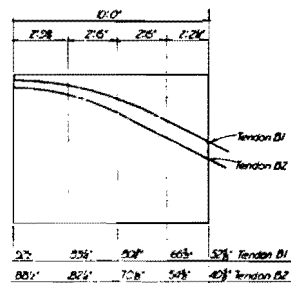
TEXAS HIGHWAY DEPARTMENT
 BRIDGE DIVISION
TENDON PROFILES
SIDE SPANS
 400 FT. SEGMENTAL
 POST TENSIONED UNIT
 INTRACOASTAL CANAL BRIDGE

| | | | | |
|-------------|---------|-------|-------------|-----------|
| DESIGNED BY | DATE | SCALE | PROJECT NO. | SHEET NO. |
| BY | REVISED | BY | NO. | DATE |
| BY | BY | BY | BY | BY |
| BY | BY | BY | BY | BY |

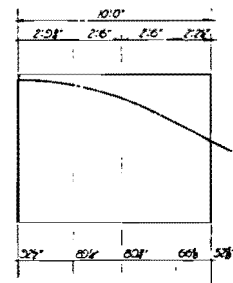


Dimensions indicate distance from bottom of precast unit to 6 of tendon (typ)

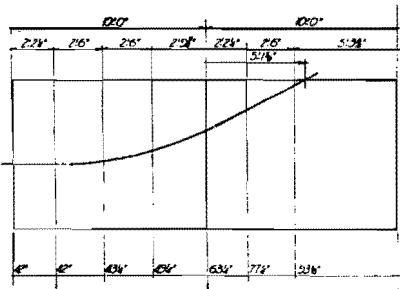
TENDON PROFILES
TENDONS MK. A1 THRU A6 - C1 & C2



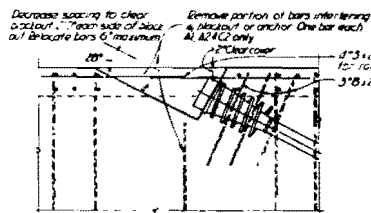
TENDON PROFILES
TENDON MK. B1 & B2



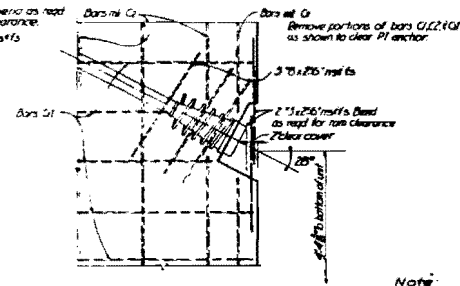
TENDON PROFILES
TENDONS MK. B3 THRU B4



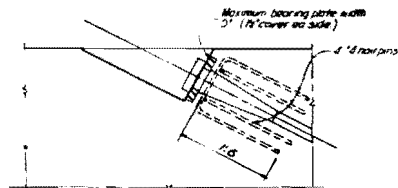
TENDON PROFILES
TENDONS - MK. C3 - C4 & B11



TENDON ANCHORAGE
WEDGE TYPE ANCHOR
TENDONS MK. A1 THRU A6 & C1 THRU C4



TENDON ANCHORAGE
WEDGE TYPE ANCHOR
TENDONS MK. B3 THRU B4



TENDON ANCHORAGE
BEARING PLATE TYPE ANCHOR
TYPICAL DETAIL

Note:
Tendon anchorage details are not intended to limit types of strand systems used.

Sheet 6 of 7

TEXAS HIGHWAY DEPARTMENT
BRIDGE DIVISION
**TENDON PROFILES
AND DETAILS**
400 FT. SEGMENTAL
POST TENSIONED UNIT
INTRACOASTAL CANAL BRIDGE

| | | | | | |
|-------------|---------------|------------|----------|-------------|----------|
| DESIGNED BY | DATE | CHECKED BY | DATE | PROJECT NO. | SCALE |
| BY: JLD | OCTOBER, 2000 | BY: JLD | 10/20/00 | 440 | AS SHOWN |
| BY: JLD | | BY: JLD | | | |
| BY: JLD | | BY: JLD | | | |

A P P E N D I X B

SPECIFICATION FOR EPOXY BONDING AGENT

This page replaces an intentionally blank page in the original.

-- CTR Library Digitization Team

TEXAS HIGHWAY DEPARTMENT

SPECIAL SPECIFICATION

ITEM 2131

EPOXY BONDING AGENT

1. DESCRIPTION. This item shall govern for the furnishing and application of epoxy material for use in the joint between precast concrete units, as required by the plans.

2. MATERIALS. The epoxy material shall be of two components, a resin and a hardener (1 to 1 ratio), meeting the following requirements:

- a. Pot Life Min. 90 minutes at 68 F (ASTM D1338)
- b. Compressive Strength 6,000 p.s.i. min.
- c. Tensile Strength (Direct or Bending) 2,000 p.s.i. min.
- d. Specific Gravity 70 to 120 lbs./cu.ft.
- e. Viscosity at 68 F 10,000 to 50,000 cps
- f. Coefficient of Thermal Expansion Within 10% of that for concrete

The material shall have a rate of absorption, rate of shrinkage, chemical resistance and weather resistance compatible with concrete and a consistency such that it will not flow appreciably when applied to a vertical concrete surface. The color shall be concrete gray.

The Contractor shall furnish the Engineer a sample of the material for testing, and a certification from a reputable laboratory indicating that the material complies with the above requirements.

The sample of the material submitted will be tested additionally for the following:

- a. Ability to join test specimen under the following conditions:

Temperature Range 50 F to 100 F
Surface Conditions Dry to Moist
(Moist is defined as 'one hour drying after complete saturation'.)

- b. The joint material shall be able to develop 95 percent of the flexural tensile strength and 70 percent of the shear strength of a monolithic test specimen.

The test specimen shall be made of concrete having a minimum compressive strength of 6,000 p.s.i. The specimen will be tested with both dry and moist surface conditions.

3. CONSTRUCTION METHODS. Surfaces to which the epoxy material is to be applied shall be free from all oil, laitance or any other material that would prevent the material from bonding to the concrete surface. All laitance shall be removed by sanding or by washing and wire brushing.

Mixing of the resin and hardener components shall be in accordance with the manufacturer's instruction. Use of a proper sized mechanical mixer will be required.

The epoxy material shall be applied to all surfaces to be joined within the first half of the pot life as shown on the containers.

The coating shall be smooth and uniform and shall cover the entire surfaces to be joined with a maximum thickness of 1/16 inch. The units shall be joined within 45 minutes after application of the epoxy material.

No jointing operations shall be performed when the ambient temperature is below 50 F or above 100 F. When the temperature is above 85 F the epoxy coated surfaces shall be shaded from direct sunlight.

If the jointing is not completed within 45 minutes after application of the epoxy material the operation shall be stopped and the epoxy material shall be completely removed from the surfaces. Fresh material shall be applied to the surfaces before resuming jointing operations.

4. MEASUREMENT AND PAYMENT. No direct measurement or payment will be made for the materials, work to be done or equipment to be furnished under this item, but it shall be considered subsidiary to the particular items required by the plans and the contract.

This page replaces an intentionally blank page in the original.

-- CTR Library Digitization Team

A P P E N D I X C

NOTATION

This page replaces an intentionally blank page in the original.

-- CTR Library Digitization Team

- A = average area of cross sections of specimens [Chapter 3];
area of bolt [Chapter 6]
- A_p = area of prestressing cable
- A_v = area of web reinforcement placed perpendicular to the axis
of the member
- a = depth of equivalent rectangular stress block
- b = average width of specimen [Chapter 3]; width of compression face
of flexural member [Chapter 8]
- b' = minimum width of a flanged member
- C = ultimate compressive force
- c = distance from extreme compression fiber to neutral axis
- d = average depth of specimen [Chapter 3]; distance from extreme
compression fiber to centroid of prestressing force [Chapter 8]
- d_c = distance from plastic center to centroid of compressive force
- d_p = distance from plastic center to centroid of negative tendon
- d_{t1}, d_{t2}, d_{t3} = distance from plastic center to centroid of each positive tendon
- DL_1 = dead load of the cantilevered section
- DL_3 = dead load added after completion of closure
- E_c = modulus of elasticity of concrete
- E_s = modulus of elasticity of steel
- E_1 = thickness of error in joint at bottom
- E_2 = accumulated error in height at the distance l_E
- e = distance from centroid of prestressing cable to C.G.
- e_1, e_2 = distance from centroid of each prestressing cable to C.G.
- f'_c = compressive strength of concrete
- F_{sp} = ratio of splitting tensile strength to the square root of
compressive strength

| | |
|------------------|---|
| F_s | = ultimate load of steel |
| f'_s | = ultimate strength of steel |
| f_y | = yield strength of reinforcement |
| f_{cp} | = permissible compressive concrete stress on bearing area under anchor plate of post-tensioning steel |
| F | = internal force |
| F_I, F_{I1} | = internal force due to prestressing cable |
| F_{I2}, F_{I3} | |
| $^{\circ}F$ | = fahrenheit degree |
| f_{sp} | = splitting tensile strength of concrete |
| f_{pe} | = compressive stress of concrete due to prestressing only at bottom fiber |
| f_d | = stress due to dead load at the extreme fiber of a section at which tensile stress is caused by applied load |
| f_{pc} | = compressive stress in concrete, after all prestress losses have occurred, at the centroid of the cross section resisting the applied load |
| h | = depth of segment |
| h_p | = height of pier |
| I | = moment of inertia [Chapter 6]; impact factor [Chapter 7] |
| IL | = impact load |
| jd | = distance between ultimate compressive force (C) and ultimate tensile force (T) |
| l | = span length |
| l_E | = distance from the joint with the erection errors |
| l_c | = length of bolt in compression side |
| l_t | = length of bolt in tension side |
| l_p | = length of prestressing cable |

| | |
|------------------|--|
| LL | = live load |
| LF | = load factor |
| M | = moment due to externally applied load |
| M_p | = moment due to prestressing force |
| M_{cr} | = net flexural cracking moment |
| M_s | = moment due to end reaction caused by prestressing of positive tendons and seating forces at outer supports |
| M_{s1} | = secondary moment due to prestressing of negative tendons |
| M_{s2} | = secondary moment due to prestressing positive tendons in main span |
| M_{s3} | = secondary moment due to prestressing of positive tendons in side span |
| M_u | = ultimate external moment |
| M_{DL} | = moment due to dead load |
| $M_{(LL+IL)}$ | = moment due to (live + impact) load |
| M_x | = longitudinal slab moment per unit width |
| M_y | = transverse slab moment per unit width |
| M_{01}, M_{02} | = plastic moment |
| M_E | = external moment |
| M_I | = internal moment |
| M_{E1} | = moments due to weight of segment (1.0 DL) |
| M_{E2} | = moments due to resultant force of prestressing in main span and jacking force at outer supports (= M_s) |
| M_{E3} | = moments due to 0.35 DL |
| M_{E4} | = moment due to live load |
| M_{UI} | = ultimate internal moment |
| M_{I1} | = moments due to negative tendons |
| M_{I2} | = moments due to positive tendons in side span |

| | |
|-----------------|--|
| M_{13} | = moments due to positive tendons in main span |
| P | = applied load [Chapters 3, 6, 7]; prestressing force [Chapters 6, 8] |
| P_u | = ultimate applied load |
| P_{ij} | = prestressing force at a certain point |
| P_{io} | = prestressing force applied at the end |
| P_1, P_2 | = prestressing force of each tendon |
| RH | = relative humidity |
| \bar{s} | = standard deviation |
| S_1, S_2 | = force on the bolt |
| SL | = resultant reactions due to prestressing of tendons and seating forces at outer supports |
| s | = longitudinal spacing of web reinforcement |
| T | = ultimate tensile force |
| T_1, T_2, T_3 | = tensile force of each prestressing cable |
| U | = ultimate design load |
| V | = shear force due to externally applied load |
| V_p | = equivalent vertical load of prestressing force |
| V_c | = shear carried by concrete |
| V_{ci} | = shear at diagonal cracking due to all loads, when such cracking is the result of combined shear and moment |
| V_{cw} | = shear force at diagonal cracking due to all loads, when such cracking is the result of excessive principal tensile stress in the web |
| V_d | = shear due to dead load |
| V_u | = shear due to specified ultimate load |
| w | = unit weight of concrete |
| W | = weight of truck |
| W_b | = section modulus at bottom |

| | |
|--------------------------------|---|
| W_T | = section modulus at top |
| X | = load factor of (LL + IL) |
| Y | = reaction at support at complete collapse of the structure |
| α | = angle change of tendon |
| ϕ | = diameter [Chapter 2]; capacity reduction factor [Chapter 8] |
| τ_u | = ultimate shear strength |
| σ_u | = ultimate flexural strength |
| σ_s | = stress of prestressing cable |
| ϵ'_s | = ultimate steel strain |
| ϵ_c | = concrete strain |
| $\epsilon_{s1}, \epsilon_{s2}$ | = strain of each prestressing cable (positive tendon) |
| ϵ_{s3} | = strain at level of prestressing cable (negative tendon) |
| ϵ_p | = strain at level of prestressing cable (negative tendon) |
| ϵ_s | = steel strain |
| ϵ_{sp} | = steel strain due to prestressing |
| ϵ_{sl} | = steel strain due to external load |
| δ_1 | = cantilever tip deflection to to segment flexure |
| δ_2 | = cantilever tip deflection due to elongation of bolts |
| δ_3 | = cantilever tip deflection due to bending of pier |
| Δ_1, Δ_2 | = elongation of bolts |
| θ_2 | = angle change due to elongation of bolts |
| θ_3 | = angle change of pier at the top due to bending of pier |
| μ | = Poisson's ratio [Chapter 4]; friction coefficient [Chapter 6] |
| λ | = wobble coefficient |